

N° d'ordre : 41551



**Ecole Doctorale**

Sciences de la Matière, du Rayonnement et de l'Environnement

Thèse pour obtenir le grade de

**Docteur de l'Université Lille1 Sciences et Technologies**

Sciences de la Matière

**Bing HONG**

**Multiphase Microemulsion Systems Based on Catalytic Surfactants:  
Physicochemical Investigation and Application to Fine Chemistry**

Thèse dirigée par :

Véronique RATAJ, Professeur à l'Université Lille1

Jean-Marie AUBRY, Professeur à l'ENSCL

Soutenue le 7 Novembre 2014

**Membres du Jury :**

<b>Pr. Aristotelis XENAKIS</b>	Institute Biologique du National Hellenic Research Foundation	<b>Rapporteurs</b>
<b>Pr. Pierre BAUDUIN</b>	Institut de Chimie Séparative de Marcoule	
<b>Pr. Giorgio STRUKUL</b>	Université de Venise	<b>Examineurs</b>
<b>Pr. Veronique RATAJ</b>	Université de Lille 1	
<b>Pr. Jean-Marie AUBRY</b>	ENSCL	



---

## Acknowledgements

---

This research work was fulfilled in the group of “Oxidation and Physicochemistry of the Formulation” in the University of Lille 1, Science and Technology. Before beginning my thesis, I would like to express my deepest gratitude to all those people who made it possible through their generous support in many different ways.

First and foremost, I would like to express my most sincere gratitude to my supervisors, **Prof. Véronique RATAJ** and **Prof. Jean-Marie AUBRY**, for giving me the opportunity to work with them on this interesting subject and for their guidance, constant support and encouragement throughout the work of my thesis. Their enormous helps and suggestions not only enriched my scientific knowledge, but also are precious treasures in my future life.

I would like also express my sincere gratitude to **Prof. Aristotelis XENAKIS**, from Institute Biologique du National Hellenic Research Foundation, and **Prof. Giorgio STRUKUL**, from Ca’Foscari University of Venice, for their acceptance to be members of the thesis committee, for their precious time to read my manuscript and their helpful comments.

My special thanks to **Dr. Pierre BAUDUIN**, from Institute of Separation Chemistry in Marcoule, for his acceptance to judge my thesis and his kind reception during my stay in Marcoule for the manipulation of SAXS. I would like also thank **Dr. Olivier Diat** and **Dr. Jonathan LAI**, for their invaluable assistance for the SAXS analyses and data treatment.

I also convey my special acknowledge to **Prof. Éric Monflier**, **Prof. Sébastien Tilloy** and **Théodore Vanbesien** for their generous help and advices during my stay in Lens for hydroformylation.

I would like to thank the assistant professors in our group: **Christel Pierlot**, **Loïc Leclercq**, **Raphael Lebeuf**, and **Valérie Molinier**, for their generous cooperation, kind help and valuable discussions.

My appreciation is also extended to my colleagues: **Andrea**, **Roberto**, **Adrien B**, **Adrien M**, **Delphine**, **Laurianne**, **Thomas**, **Aurélie**, **Christophe**, **Romain**, **Maxime R**, **Maxime N**, **Laura**, and **Benjmin**. It is truly my honor to cooperate and share the joy with them.

I would also like to thank my Chinese friends in Lille, **Yao Z**, **Kui L**, **Qi W**, for their support during these three years.

At last, I would like to express my great gratitude to **my parents**, **my sister** and my girlfriend, **Jing**, for their support and unconditional love. They always had trust and confidence on my decision and encouraged me during my study.

---



---

## Abstract

---

Balanced Catalytic Surfactants (abbreviated as “Catasurfs”) allow the design multiphase microemulsion systems used as reaction media. In this context, the double tailed alkylammonium and alkylsulphonate amphiphiles have been developed. Their behavior in aqueous system (solubility, critical micellar concentration, binary diagram, lyotropic liquid crystal) as well as biphasic oil/water system (Fish diagram, forming microemulsions systems Winsor Type I, II, III and IV) were studied based on the nature of counter ions (Br, Cl,  $\text{WO}_4^{2-}$ ,  $\text{MoO}_4^{2-}$ ,  $\text{SO}_4^{2-}$  for anionic and  $\text{H}^+$ ,  $\text{Li}^+$ ,  $\text{Na}^+$ ,  $\text{K}^+$ ,  $\text{Cu}^{2+}$ ,  $\text{Zn}^{2+}$ ,  $\text{Ca}^{2+}$ ,  $\text{Sc}^{3+}$  for cationic). Lyotropic crystal phases were identified by polarization optical microscopy and small angle X-ray scattering diffusion (SAXS). A classification of surfactants according to their amphiphilicity was established from the Fish diagrams constructed by scanning oil polarities. The phase behavior of these surfactants in water (micelles) and biphasic oil / water system (microemulsion) does not only depend on the alkyl chain length but also the hydration degree of counter ions, in agreement with the Hofmeister series. The advantages of multiphase microemulsions based on “Catasurfs” were on one hand demonstrated through the epoxidation of olefins and oxidation of sulfides in a Winsor III microemulsion based on  $[\text{DiC}_{10}]_2\text{WO}_4$  in the presence of  $\text{H}_2\text{O}_2$  and, on the other hand, by the development of a thermosensitive Winsor IV microemulsions using synergy between  $\text{C}_8\text{E}_4$  and  $[\text{DiC}_8]_2\text{MoO}_4$  for “Dark Singlet Oxygenation”. In addition, a new “one-pot” synthetic route of the (+)- nootkatone, a high value-added fragrance, from the (+)-valencene was developed under solvent-free conditions. The advantages of multiphase microemulsions based on Catasurfs (increased reactivity, better selectivity, easy product recovery and catalyst recycle) make these nanostructured reaction media alternatives to the phase transfer catalysis (PTC).

Keywords: *Catalytic Surfactant; Catasurf; Quaternary dialkylammonium; Dialkylsulphonate; Microemulsions; Winsor; Physicochemical properties; Binary diagram; liquid crystal; Fish diagrams; Oxidation; Hydroformylation; Synergy; Molybdate; Tungstate; Hydrogen peroxide; (+)-Nootkatone*

---

## Résumé

---

Les surfactifs catalytiques équilibrés (baptisés "Catasurfs") permettent d'élaborer des systèmes de microémulsions polyphasiques utilisés comme milieux réactionnels. Dans ce contexte, des alkylammonium et des alkylsulphonates amphiphiles bicaténaires ont été développés. Leurs comportements en système aqueux (solubilité, concentration micellaire critique, diagramme binaire, cristaux liquides) ainsi qu'en système biphasique eau/huile (diagramme de Fish, formation de systèmes de microémulsions de type Winsor I, II, III et IV) ont été étudiés en fonction de la nature des contre-ions ( $\text{Br}^-$ ,  $\text{Cl}^-$ ,  $\text{WO}_4^{2-}$ ,  $\text{MoO}_4^{2-}$ ,  $\text{SO}_4^{2-}$  pour les anioniques et  $\text{H}^+$ ,  $\text{Li}^+$ ,  $\text{Na}^+$ ,  $\text{K}^+$ ,  $\text{Cu}^{2+}$ ,  $\text{Zn}^{2+}$ ,  $\text{Ca}^{2+}$ ,  $\text{Sc}^{3+}$  pour les cationiques). Les phases cristallines lyotropes ont été identifiées par microscopie optique à polarisation et par diffusion des rayons X aux petits angles (SAXS). Une classification des surfactifs selon leur amphiphilicité a été établie à partir des diagrammes de Fish construits selon un balayage en huiles. Le comportement de phases de ces surfactifs dans l'eau (micelles) et en système biphasique eau/huile (microémulsion) dépend non seulement de la longueur de la chaîne mais aussi du degré d'hydratation des contre-ions, en accord avec la série d'Hofmeister. L'intérêt des microémulsions polyphasiques à base de Catasurfs a été démontré d'une part en microémulsion Winsor III à base de  $[\text{DiC}_{10}]_2\text{WO}_4$  appliquée à l'époxydation des oléfines et à l'oxydation de sulfures en présence de  $\text{H}_2\text{O}_2$  et d'autre part, *via* l'élaboration de microémulsions Winsor IV thermosensible utilisant la synergie entre les  $\text{C}_8\text{E}_4$  et  $[\text{DiC}_8]_2\text{MoO}_4$  pour la "Dark Singlet Oxygenation". Par ailleurs, une nouvelle voie de synthèse « one-pot » de la (+)-nootkatone, fragrance à haute valeur ajoutée, à partir du(+)-valencène a été mise au point dans des conditions sans solvant. Les avantages des microémulsions polyphasiques à base de Catasurfs (réactivité accrue, meilleure sélectivité, récupération du produit et recyclage du catalyseur facilités) font de ces milieux réactionnels nanostructurés des alternatives pertinentes à la catalyse par transfert de phases (PTC).

**Mots-clés :** *Surfactif catalytique ; Catasurf ; Dialkylammonium quaternaire ; Dialkylsulphonate ; Microémulsions ; Winsor ; Propriétés physicochimiques ; Diagramme binaire ; Cristaux liquides ; Diagrammes de Fish ; Oxydation ; Hydroformylation ; Synergie ; Molybdate ; Tungstate ; Eau oxygénée ; (+)-Nootkatone*

---

# TABLE OF CONTENTS

Acknowledgements.....	1
Abstract.....	3
Résumé.....	4
List of the abbreviations.....	9
General introduction .....	11
<b>CHAPTER 1: State of The Art: New Strategy of Green Chemistry, The Role of Surfactant-Combined Catalysts .....</b>	<b>19</b>
<b>1.1 Introduction.....</b>	<b>21</b>
<b>1.2 Surfactant-combined catalysts and their catalytic applications .....</b>	<b>24</b>
1.2.1 Anionic surfactant-combined Lewis acid and Brönsted acid catalysts .....	24
1.2.1.1 Sc <sup>III</sup> as catalytic part of LASCs .....	25
1.2.1.2 Cu <sup>II</sup> , Zn <sup>II</sup> and miscellaneous Lewis acids as catalytic part of LASCs.....	30
1.2.1.3 Brönsted acid-surfactant combined catalysts and their application .....	32
1.2.1.4 The physicochemical properties of the anionic surfactant-combined catalysts .....	35
1.2.2 Cationic surfactant-combined polyoxometalate and peroxometalate catalysts.....	38
1.2.2.1 Cationic surfactant-combined polyoxometalates (POMs) in catalytic reactions .....	40
1.2.2.2 Cationic surfactant-combined peroxometalates in catalytic reactions .....	44
1.2.2.3 The physicochemical properties of the cationic surfactant-combined catalysts .....	49
<b>1.3 Conclusion .....</b>	<b>52</b>
<b>Appendix A: Structures of the abbreviations.....</b>	<b>54</b>
<b>Appendix B: Application of Lewis acids and Brönsted acid-combined surfactant catalysts...55</b>	
<b>Appendix C: Cationic surfactant-combined polyoxometalate and peroxometalate catalysts..58</b>	
<b>CHAPTER 2: Preparation and Physicochemical Properties of Cationic and Anionic Catalytic Surfactants (Catasurfs) .....</b>	<b>61</b>
<b>2.1 Double-chain alkylammonium catalytic surfactants .....</b>	<b>63</b>

---

2.1.1 Cationic surfactant applications and recent investigations on double-chain quaternary ammonium amphiphiles for “Catasurf” design.....	63
2.1.2 Synthesis and CACs of the dialkyldimethylammonium surfactants.....	67
2.1.3 Aqueous phase behavior of dialkyldimethylammonium catasurfs in concentrated solution: lyotropic liquid crystal formation .....	71
2.1.4 Microemulsion phase diagrams and amphiphile classification.....	79
2.1.5 Conclusion .....	94
<b>2.2 Double-chain sulphonate catalytic surfactants.....</b>	<b>95</b>
2.2.1 Applications of ionic surfactants and synthesis of double-chain sulphonate surfactants.....	95
2.2.2 CMCs of the $\text{DiC}_n\text{CHSO}_3\text{M}$ ( $\text{M}=\text{H, Li, Na, K, [DiC}_n\text{CHSO}_3\text{]}_2\text{M}$ ( $\text{M} = \text{Cu, Zn, Ca}$ ) and $[\text{DiC}_n\text{CHSO}_3\text{]}_3\text{Sc}$ .....	99
2.2.3 Water/surfactant binary diagrams .....	104
2.2.4 Conclusion .....	108
<b>2.3 Experiment section.....</b>	<b>109</b>
2.3.1 Experimental section for Double-chain alkylammonium catalytic surfactants.....	111
2.3.2 Double-chain sulphonate catalytic surfactants.....	113
2.3.3 The physicochemical investigation of surfactants .....	116
<b>CHAPTER 3: Reactions in Multiphase Microemulsions Elaborated with Catalytic Surfactants</b> .....	<b>119</b>
<b>3.1 Introduction.....</b>	<b>121</b>
<b>3.2 Catalytic oxidation reactions in acidic three-phase <math>\mu\text{em}</math> .....</b>	<b>122</b>
3.2.1 The design of acidic $\mu\text{em}$ systems .....	122
3.2.2 Optimization of conditions and epoxidation of various olefins in Winsor III system .....	125
3.2.3 Oxidation of sulfides and thiophenes.....	130
3.2.4 Conclusion .....	131
<b>3.3 Temperature–switch <math>\mu\text{ems}</math> for dark singlet oxygenation.....</b>	<b>132</b>
3.3.1 Description of the synergism between ionic and nonionic surfactants .....	132

---

---

3.3.2 The synergism between nonionic C <sub>8</sub> E <sub>4</sub> and cationic [DiC <sub>8</sub> ] <sub>2</sub> [MoO <sub>4</sub> ]	133
3.3.3 Dark singlet oxygenation in temperature-switch C <sub>8</sub> E <sub>4</sub> -[DiC <sub>8</sub> ] <sub>2</sub> [MoO <sub>4</sub> ]/cyclohexane/H <sub>2</sub> O μems	142
3.3.4 Conclusion	146
<b>3.4 Photochemical and chemical singlet oxygenation of valencene: (+)-Nootkatone</b>	<b>147</b>
3.4.1 Photooxidation of valencene	149
3.4.2 Dark singlet oxygenation of (+)-Valencene with a catalytic surfactant based on molybdate .....	153
3.4.3 Conclusion	154
<b>3.5 Hydroformylation of hydrophobic terminal alkenes in three-phase μem</b>	<b>155</b>
<b>3.6 Experimental section</b>	<b>161</b>
3.6.1 Catalytic oxidation reactions in acidic three-phase μem	163
3.6.2 Dark singlet oxygen oxygenation in temperature-switch μems	165
3.6.3 Photochemical and chemical singlet oxygenation of (+)-Valencene	167
3.6.4 Typical procedure of hydroformylation	168
General Conclusion	169
References	176
Appendix	<b>Error! Bookmark not defined.</b>

---

---

## List of the abbreviations

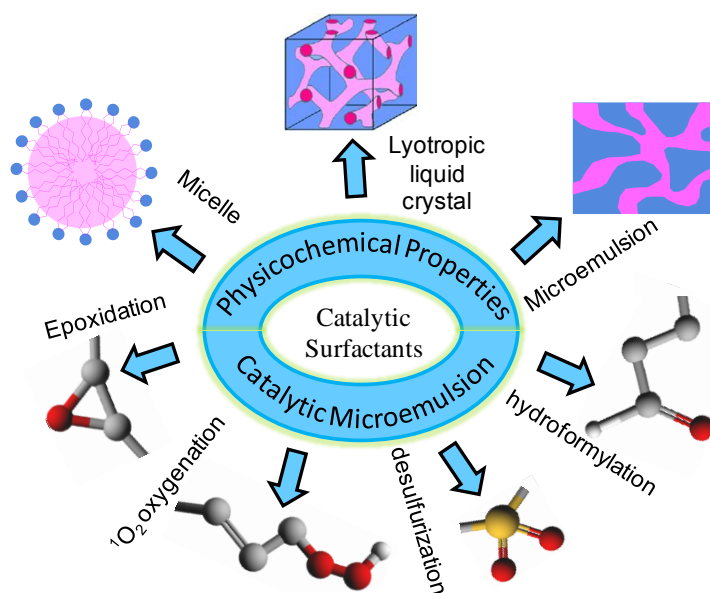
---

NMR	Nuclear Magnetic Resonance
$\mu\text{em}$	Microemulsion
Catasurf	Catalytic surfactant
CMC	Critical micelle concentration
DiC <sub>n</sub>	Dialkyldimethylammonium salt
P <sub>eff</sub>	Effective packing parameter
C <sub>i</sub> Cl	1-Chloroalkane
C <sub>i</sub> Cl <sub>2</sub>	$\alpha,\omega$ -Dichloro- <i>n</i> -alkanes
AOT	Sodium bis(2-ethylhexyl) sulfosuccinate
POM	Polarized optical microscopy
SAXS	Small angle X-ray scattering
LASC	Lewis-Acid-Surfactant-Combined catalyst
SATO	Surfactant-type Asymmetric Organocatalyst
BASC	Brønsted Acid-Surfactant-Combined catalyst
WERC	Water Exchange Rate Constant
DS	Dodecylsulfate
DSA	Dodecylsulfonic acid
C <sub>8</sub> E <sub>4</sub>	Tetraethylene glycol monoethyl ether
HLB	Hydrophilic-Lipophilic Balance
PACN	Preferred alkyl chain number
EACN	Equivalent alkyl chain number
DBT	Dibenzothiophene
DiC <sub>n</sub> CHSO <sub>3</sub>	Dialkylmethane sulphonate
DBSA	Dodecylbenzene sulfonic acid
HLD	Hydrophilic-lipophilic deviation
TPPTS	Sodium triphenylphosphine-3, 3', 3''-trisulphonate
DPPBS	Sodium 4'-(diphenylphosphino)-[1,1'-biphenyl]-4-sulphonate





General introduction





Green chemistry, also called sustainable chemistry, is focused on the chemical process that avoids the use of hazardous substances and the generation of toxic wastes. Since the concept was proposed by Paul Anastas in 1991, the principles of green chemistry were developed by Paul Anastas and John C. Warner (**Figure I1**).<sup>1</sup> In the last 3 decades, various strategies have been developed to answer the principles of green chemistry including: 1) the use of renewable substrates, for example, the conversion of glucose, fructose or polysaccharides to hydroxymethylfurfural (an petrol alternative);<sup>2</sup> 2) the use of green reaction media, such as ionic liquids, fluoruous solvents, and supercritical carbon dioxide;<sup>3</sup> 3) the use of green reagents, like oxygen or H<sub>2</sub>O<sub>2</sub>;<sup>4,5</sup> and 4) reactions in aqueous condition.<sup>6-8</sup> Besides, the bioengineering is also considered as a promising technique to achieve “green” chemistry goals as its high selectivity affording the higher atom economy and lower E-factor (environmental factor).<sup>9</sup> Among them, catalytic oxidation in aqueous phase or without solvent with O<sub>2</sub> and H<sub>2</sub>O<sub>2</sub> received great attention as conventional oxidants have been comprised of toxic reagents like heavy metal ions.<sup>10</sup> The clean oxidation with H<sub>2</sub>O<sub>2</sub> was even considered as one of the three key developments in green chemistry in 2005 due to its low price, easy and safe for manipulation, and harmless to the environment.<sup>11</sup>

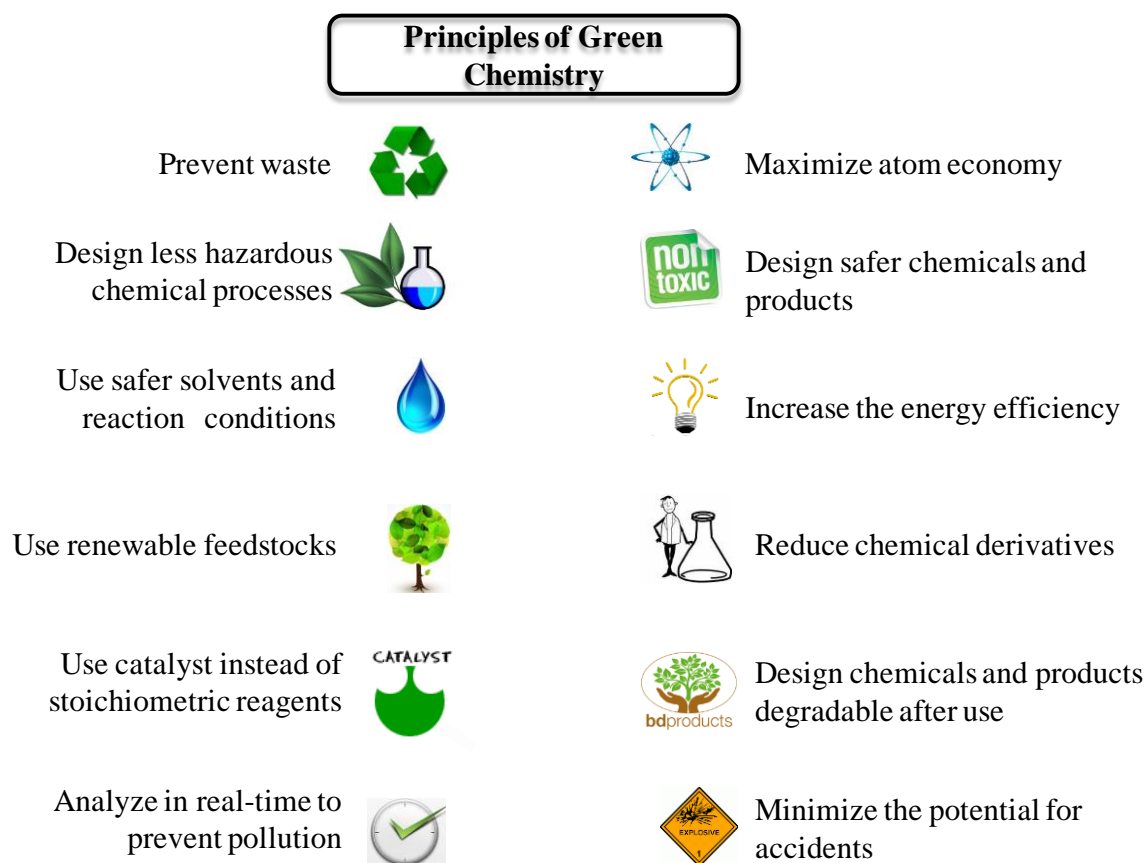
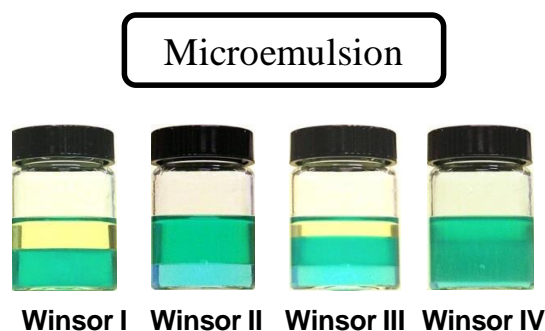


**Figure I1** Principles of Green Chemistry.<sup>1</sup>

Organic reactions in aqueous phase require the additives such as phase transfer catalysts (PTCs), cosolvent, or surfactant, *etc.* since most of substrates are immiscible with aqueous phase. Especially, the surfactants have been more and more used to prompt the reactions in water *via* the formation of

micelles.<sup>7,12</sup> Compared with phase transfer catalyst and cosolvent, the reactions in micellar solution presents various advantages: 1) without the use of organic solvent as the hydrophobic core of nanodroplets in aqueous phase solubilizes the organic substrate in aqueous solution; 2) greatly accelerated reaction rate due to the large specific membrane area; 3) the improved product selectivity as the nanodroplets can prevent the water sensible substrates or products from hydrolysis and the micelle membrane also exhibits steric effect. However, the limit of substrate concentration and the difficult catalyst separation limit the industrial application of reactions in micellar solution. Emulsion as reaction medium is an alternative for various reactions in the presence of appropriate organic solvents,<sup>13,14</sup> which overcomes the low concentration in micellar solution. For example, our group has reported the successful epoxidation of olefins with H<sub>2</sub>O<sub>2</sub> as an oxidant in the Pickering emulsion elaborated with only 1 wt% [C<sub>12</sub>H<sub>25</sub>N(CH<sub>3</sub>)<sub>3</sub>]<sub>3</sub>PW<sub>12</sub>O<sub>40</sub> as both surfactant and catalyst and the oil phase containing product was easily separated by centrifugation at the end of reaction.<sup>15</sup> While in many cases, stable emulsions are encountered and cause the difficult separation of product and catalyst. On the other hand, microemulsion ( $\mu$ em), a thermodynamic stable, transparent and isotropic mixture of water, surfactant (including co-surfactant) and oil, is another type of reaction medium elaborated with surfactant. Depending on the curvature of the interface film, the  $\mu$ ems can be divided into three types: O/W (Winsor I), W/O (Winsor II) and bicontinuous (Winsor III)  $\mu$ ems, and one phase  $\mu$ em (Winsor IV) is formed upon the addition of sufficient quantity of surfactant.<sup>16</sup> Several highlighted advantages and disadvantages of  $\mu$ em catalytic medium are shown in **Figure I2**. Although the  $\mu$ em has been used for several organic reactions,<sup>17,18</sup> the oxidations in  $\mu$ em were rarely reported.<sup>19</sup>



- Advantages:
- Small quantity of surfactant in multi-phase microemulsion
  - Large amount solubilization of organic substrates
  - High reaction activity
  - Easy separation of product for Winsor I and Winsor III

- Disadvantages:
- Organic solvent
  - Large amount of surfactant requirement for Winsor IV
  - Strict formulation condition requirement for Winsor III

**Figure I2** The advantages and disadvantages of  $\mu$ em media for catalytic reaction.

In the 1980s, Aubry *et al.* have systematically investigated the mineral compounds catalyzed disproportionation of  $\text{H}_2\text{O}_2$  into water and singlet oxygen ( $^1\text{O}_2$ )<sup>20</sup>, especially the molybdate, which was found catalyze the  $^1\text{O}_2$  generation quantitatively.<sup>21,22</sup> Compared with photosensitization of oxygen, which requires special equipment for gas manipulation and light irradiation, the chemical generation of  $^1\text{O}_2$  is preferable as  $\text{H}_2\text{O}_2$  is a cheap, safe and easy operating oxidant. Different from triplet state ( $^3\Sigma_g^-$ ), the oxygen in the singlet state ( $^1\Delta_g$ ) is a high reactive oxidant and could react with electron-rich compounds, such as olefin, sulfide, amine, *etc.*<sup>23</sup> While in aqueous phase, most of  $^1\text{O}_2$  is deactivated as its lifetime in water is extremely short ( $\approx 3 \mu\text{s}$ ) and its mean travel distance in water is only about 200 nm.<sup>24</sup> Since 1997, several  $\mu\text{em}$  systems were elaborated for the singlet oxygenation of various organic compounds to improve the efficiency  $^1\text{O}_2$ .<sup>25-30</sup> The earlier  $\mu\text{em}$  for oxidation of organic compounds was a Winsor IV W/O  $\mu\text{em}$  consisting of  $\text{Na}_2\text{MoO}_4$  (catalyst), water, SDS (surfactant), butanol (co-surfactant), and  $\text{CH}_2\text{Cl}_2$  (organic solvent).<sup>25</sup> Although the small size of aqueous droplets ( $\approx 10 \text{ nm}$ ) facilitated the transfer of  $^1\text{O}_2$  to organic phase before deactivation, the chlorinated solvent was unacceptable from the ecologic point of view. Besides, the large amount of SDS and butanol and the tedious workup also hindered its further industrial application. In contrast, less surfactant was required for elaboration of multiphase microemulsions. For example, a Winsor I microemulsion was elaborated with only about 5 wt% of SDS and applied in the singlet oxygenation in the presense of  $\text{Na}_2\text{MoO}_4$ .<sup>30</sup> Although the product separation was easily achieved in Winsor I  $\mu\text{em}$ , its sensitivity towards dilution was still unfavorable. In 2008, the concept of “Balanced Catalytic Surfactants” (Balanced Catasurfs) was proposed to overcome all the drawbacks of Winsor IV and Winsor I  $\mu\text{ems}$  previously described.<sup>29</sup> The balanced three-phase  $\mu\text{em}$  could be formed without additional co-surfactant and salts when appropriate chain length and solvent were chosen. The catalyst ( $\text{MoO}_4^{2-}$ ) is electrostatically bound to the interfacial film at the aqueous side and the catalytic process is represented by **Figure I3**.

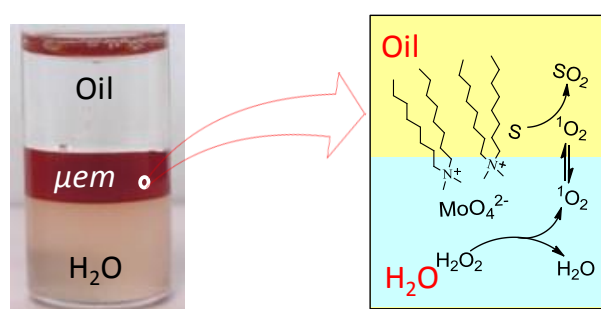


**Figure I3** Dark singlet oxygenation of substrate *S* in a three-phase  $\mu\text{em}$  system.<sup>29</sup>

The balanced three-phase  $\mu\text{em}$  based on the “Catasurf” presented various advantages including: 1) Co-solubilization of organic substrates and hydrophilic  $\text{H}_2\text{O}_2$  in the bicontinuous  $\mu\text{em}$  domain (10 – 100 nm); 2) Low amount of “Catasurf” without addition of co-surfactant and salts; 3) Complete location of the catalyst anion at  $\mu\text{em}$  interface film without leaching in aqueous phase and oil phase; 3) Large interface area; 4) The hydrophobic domain protect the water sensitive substrates and products; 5) The easy phase

separation at the end of reaction facilitates the product purification and catalyst recovering, *etc.* This thesis is focused on the further development of the “Catasurf” concept and consists of three chapters.

The first chapter reviewed the state of the art of surfactant combined catalysts and their applications in catalytic reactions. According to the surfactant part of the catalyst, this chapter containing two main parts. The first part talked about the recent development of anionic surfactant combined Lewis acids and Brønsted acids catalysts and their applications in various carbon-carbon bond formation reactions such as aldol reaction, Mannich reaction, Friedel-Crafts reaction, *etc.* and the dehydration reactions such as esterification, etherification, *etc.* The second part presented the development of cationic surfactant combined polyoxometalate and peroxometalate catalysts and their application in oxidative reactions such as the epoxidation, oxidative desulfurization, oxidative cleavage of olefins, *etc.* Most of the reactions were carried out in micellar or emulsion media and reactions in microemulsions were rarely reported. On the other hand, the physicochemical properties of the concerned amphiphilic surfactants were also presented in this chapter although they were rarely investigated and reported.

The second chapter focused on the syntheses of “Catasurfs” and their physico-chemical properties investigations. The CMCs, binary and ternary phase behaviors of various dialkyldimethylammonium salts (alkyl = hexyl, octyl and decyl) with different counter ions ( $\text{Cl}^-$ ,  $\text{Br}^-$ ,  $\text{SO}_4^{2-}$ ,  $\text{WO}_4^{2-}$ ,  $\text{MoO}_4^{2-}$ ) were investigated with the several technics including the tensiometer, Polarized Optical Microscope (POM) and Small Angle X-ray Scattering (SAXS) *etc.* The amphiphilicity of surfactants can be tuned not only by the chain length but also by the counter ions. The effect of counter ions ( $\text{F}^-$ ,  $\text{Cl}^-$ ,  $\text{Br}^-$ ,  $\Gamma$ ,  $\text{CH}_3\text{SO}_3^-$ ,  $\text{CH}_3\text{COO}^-$ ,  $\text{SO}_4^{2-}$ ,  $\text{WO}_4^{2-}$ ,  $\text{MoO}_4^{2-}$ ,  $\text{ReO}_4^-$ , *etc.*) on the CACs, and the aggregation behaviors of dioxydimethyl ammonium salts in dilute aqueous solution has been reported by our group.<sup>31</sup> Here the complete water/surfactant binary diagrams were investigated with Polarized Optical Microscope (POM) and Small Angle X-ray Scattering (SAXS). Furthermore, the surfactant amphiphilicity were evaluated by construction of the “Fish diagram” via the screening of the solvent polarity, which are crucial for the choice of appropriate solvent and surfactant to elaborate desired  $\mu\text{ems}$ . On the other hand, a series of double tailed sulphonate ( $[\text{DiC}_n\text{CHSO}_3]$ ,  $n = 6, 7, 8$ ) combined Lewis acid catalysts were also successfully synthesized, including the common used  $\text{Cu}^{2+}$ ,  $\text{Zn}^{2+}$ ,  $\text{Fe}^{2+}$  and  $\text{Sc}^{3+}$ , *etc.* in order to enlarge the application scope of the concept “Catasurfs”. The preliminary study of their physicochemical properties was carried out, such as the solubilities in water and the CMCs. The water/surfactant binary diagrams were also constructed with Polarized Optical Microscope (POM) for  $\text{DiC}_n\text{CHSO}_3\text{Na}$  and  $\text{DiC}_n\text{CHSO}_3\text{H}$ .

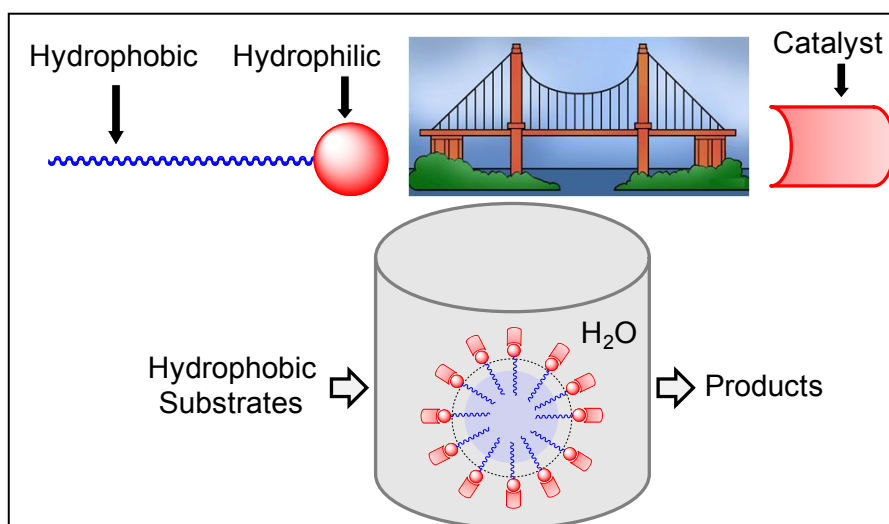
The third chapter mainly described the oxidation reactions in  $\mu\text{ems}$  elaborated with “Catasurfs”. As mentioned above, molybdate is ideal catalyst for the catalytic disproportionation of  $\text{H}_2\text{O}_2$  to generate  $^1\text{O}_2$  under weak basic condition and could be applied in the chemical singlet oxygenation reactions. In contrast, tungstate has been widely used as catalyst precursors under the acidic conditions for various

catalytic oxidations of organic substrates with  $\text{H}_2\text{O}_2$  as oxidant.<sup>4,32</sup> In the first part of chapter 3, an acidic catalytic three-phase  $\mu\text{em}$  was also elaborated based on  $([\text{DiC}_{10}]_2\text{WO}_4)$  and applied in the epoxidation of olefins and the oxidation of sulfides, which play important role in fine chemistry and desulfurization in petroleum industry. In the second part, the synergism between nonionic  $\text{C}_8\text{E}_4$  and ionic  $[\text{DiC}_8]_2\text{MoO}_4$  was investigated and a temperature-switch catalytic  $\mu\text{em}$  system was designed for singlet oxygenations. In the third part, the  $[\text{DiC}_8]_2\text{MoO}_4$  catalyzed “one pot, three steps” conversion of (+)-**Valencene** to (+)-**Nootkatone**, a high value-added product, was also investigated from two different processes, *i. e.* photooxygenation and chemical oxygenation. Finally, besides the oxidation reactions in  $\mu\text{ems}$ , hydroformylation of hydrophobic olefins were also carried out in catalytic  $\mu\text{ems}$  based on the “Fish diagram” of  $[\text{DiC}_8]\text{Br}$  and the metathesis between bromides and sulphonated phosphine ligands.





## CHAPTER 1: State of The Art: New Strategy of Green Chemistry- The Role of Surfactant-Combined Catalysts





## 1.1 Introduction

Green chemistry, also called sustainable chemistry, is a chemistry philosophy concept which focuses on minimizing the use and generation of hazardous products during a chemical process. The concept was firstly coined by Paul Anastas in 1991, and then the principles of green chemistry were developed by Paul Anastas and John C. Warner (**Figure 1.1**).<sup>1</sup> Performing the catalytic organic reactions in aqueous phase would be of interest from the point of green chemistry. Compared to the conventional harmful and expensive organic solvents, water is an economical and environmental benign solvent; furthermore, some organic substrates could be activated in aqueous phase giving significant acceleration of reaction rate and selectivity.<sup>33</sup> However, the organic reaction in aqueous phase is still one of the biggest challenges in modern organic chemistry due to the immiscibility of the hydrophobic organic substrates and water. Besides the problem of solubility, in many cases, water also decomposes the moisture sensitive compounds and deactivates the catalysts.

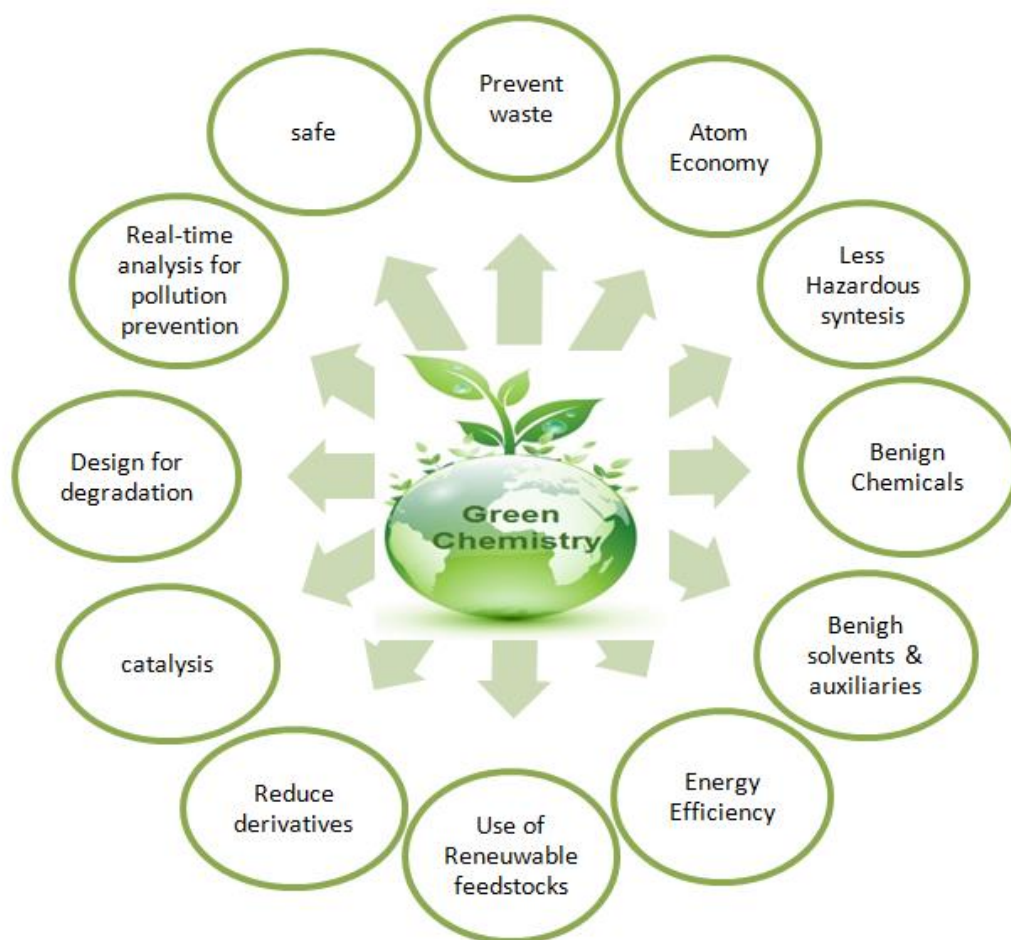


**Figure 1.1** *The twelve principles of Green Chemistry.*<sup>1</sup>

Besides avoiding the use of toxic organic solvents, easy procedures of recycling and reuse of expensive catalysts in catalytic reactions are also important aspects according to the principles of green chemistry.

The catalyst leaching is a commonly encountered problem in catalytic industry processes and the contamination of desired products by the catalyst, especially the transition metal catalysts, requires tedious purification processes. To facilitate the recycling of catalysts, several strategies have been reported, such as immobilizing the catalyst on inorganic porous solids or organic polymers.<sup>34,35</sup> Ionic liquids have also been widely used for carrying out organic reactions and facilitating the separation of the product and catalyst at the end of the reaction.<sup>36,37</sup> However, the immobilized catalysts generally result in a heterogeneous catalytic system and the decrease of the catalyst activity compared with homogeneous catalysts is inevitable, besides the catalyst leaching. Resorting to ionic liquids makes the recovery of product and reuse of the catalyst easier; however, the expensive cost and high purity requirement make this kind of reaction media not the best choice from the green chemistry view.

In the past few decades, amphiphilic catalysts combining surfactant and catalyst moieties, which could realize the organic reactions in aqueous phase, have attracted much attention.<sup>38,39</sup> Several highlighted advantages of the surfactant-type catalysts and disadvantages are shown in **Figure 1.2**.

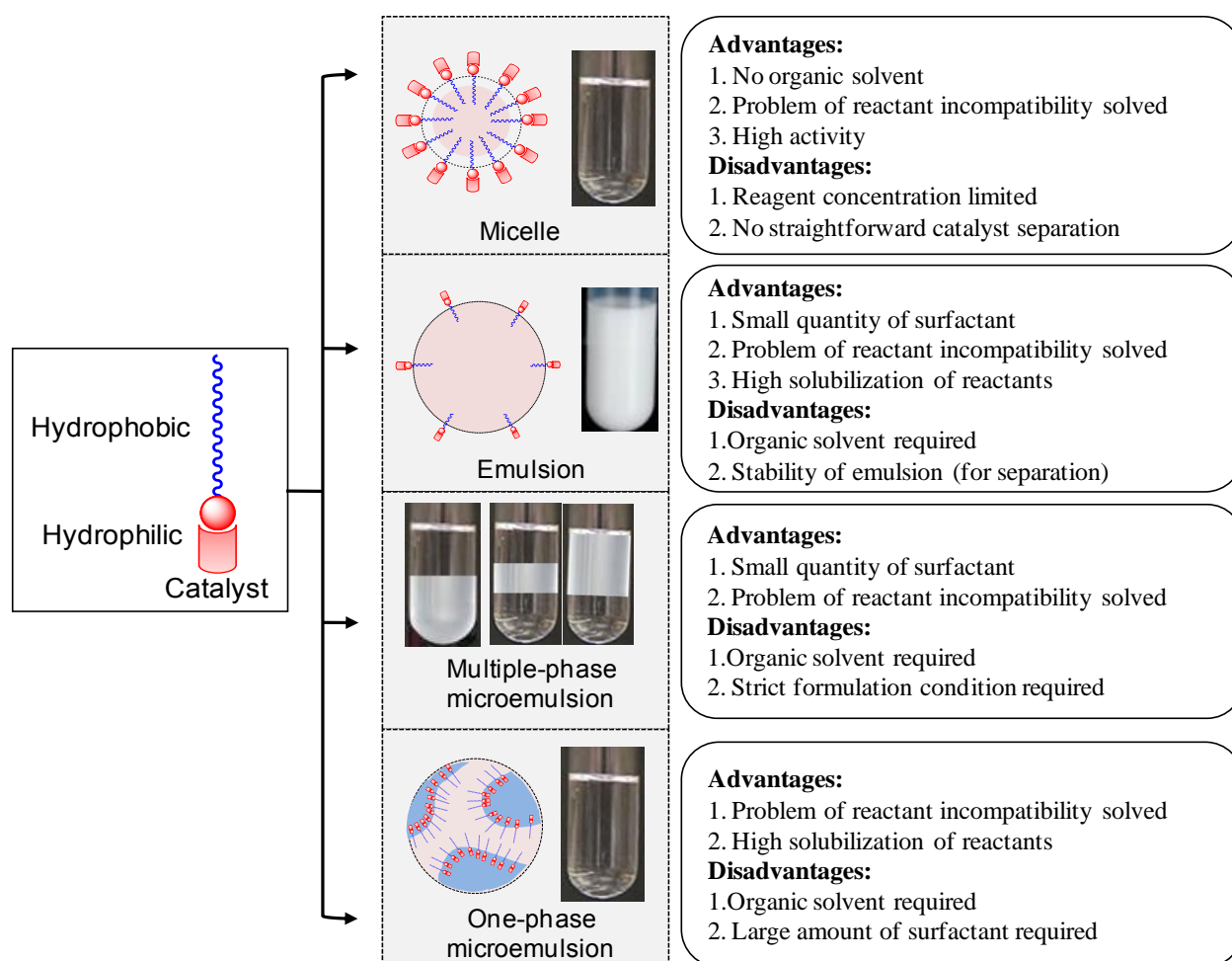


**Figure 1.2** The advantages /disadvantages of surfactant-type catalysts.

The micelles in the aqueous solution or the droplets in the (micro) emulsion can solubilize the organic substrates in the hydrophobic core and accumulate the concentration of reactants, which resolve the

immiscibility problem between organic hydrophobic reactants and aqueous phase. The large membrane, stabilized by the surfactant molecules, also increases the catalytic activity, whilst such nano- and microdispersed reaction media also inhibit the byproduct formation in some extent and enhance both the selectivity, for example due to compartmentalization of hydrophobic and hydrophilic regions, water-sensitive organic compounds are protected during the reaction.

After the initial work in the early 1990s, the surfactant-combined amphiphilic catalysts were applied to various important reactions and attracted more and more attention. This can be seen on **Figure 1.3** which represents the evolution of the number of publications in this area based on the database Scifinder® and using the keyword “amphiphilic catalyst”.

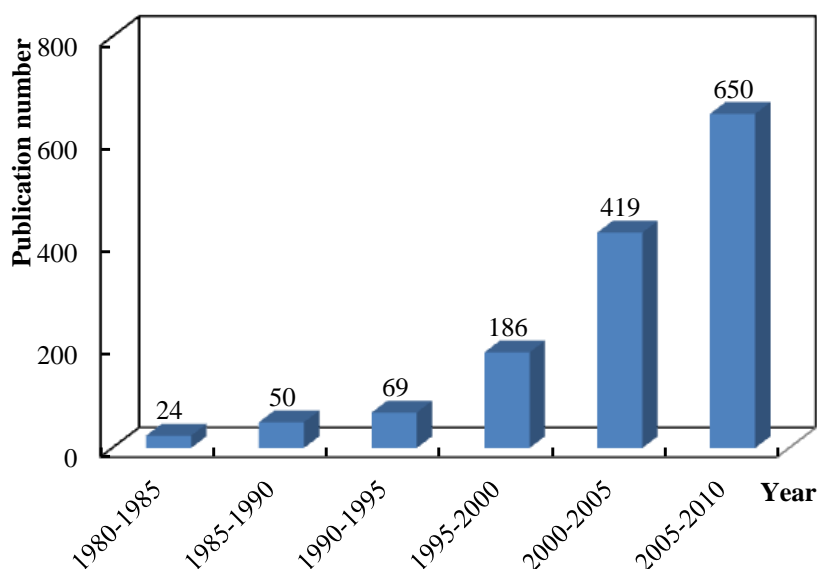


**Figure 1.3** Evolution of the number of publications related to “amphiphilic catalyst”.

Several types of amphiphilic catalysts have been reported in the literature and applied to various catalytic reactions. Different names have been proposed by different groups depending on the characteristics of the catalysts: the Lewis-Acid-Surfactant-Combined Catalysts (LASCs) and Brönsted Acid-Surfactant-Combined catalysts (BASC) proposed by Kobayashi et al.,<sup>40</sup> the Surfactant-type Asymmetric Organocatalysts (SATO) reported by Cheng et al.<sup>41</sup> and the Balanced Catalytic Surfactants (BCS) developed by our group.<sup>29</sup> Most of the surfactant-combined catalysts can be summarized into two main classes:

- the Lewis acid or Brönsted acid-anionic surfactant combined catalysts
- the polyoxometalate or peroxometalate-cationic surfactant combined catalysts

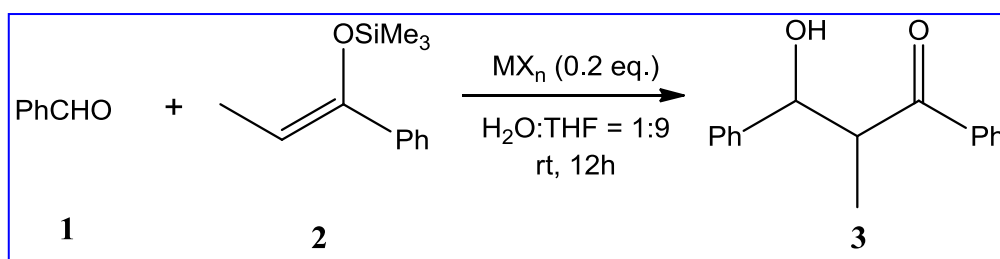
We will below introduce the recent developments in the surfactant-type catalyst field based on these two categories focusing on their catalytic activity and physicochemical properties.

## 1.2 Surfactant-combined catalysts and their catalytic applications

### 1.2.1 Anionic surfactant-combined Lewis acid and Brønsted acid catalysts

Lewis acid catalysts are of great interest in organic chemistry due to their unique activity and selectivity under mild reaction conditions.<sup>42,43</sup> A Lewis acid is defined as electron acceptor and a metal based Lewis acid acts as an electron pair acceptor to increase the reactivity of the substrates. While most of the Lewis acid catalyzed reactions involve the use of organic solvent, strict dry conditions and inert air protection, the purification procedure is tedious.<sup>44-46</sup> Performing the Lewis acid catalyzed organic reactions in aqueous phase is attractive but it also encounters great challenges which have been ascribed to the decomposition and deactivation of the Lewis acid in the presence of water. Initially, Kobayashi *et al.* reported that the lanthanide trifluoromethanesulphonates (*i.e.* triflates), water-stable Lewis acids, can catalyze the carbon-carbon formation reaction in aqueous phase.<sup>47,48</sup> In order to evaluate the possibility of Lewis acid catalyzed reactions in aqueous phase and the factors related to the catalyst activity, the authors found that the stability and activity of the catalyst are closely dependent on the hydrolysis constant ( $pK_h$  in Figure 1.4) and the inner sphere Water Exchange Rate Constant (**WERC**) (**Figure 1.4**).<sup>49-51</sup>

With the Mukaiyama aldol reaction in H<sub>2</sub>O-THF mixture solvent as a model reaction (**Scheme 1.1**),<sup>49</sup> the metal compounds, which provide high yields, have  $pK_h$  ranging from 4.3 to 10.08, and **WERC**s are greater than  $3 \times 10^6 \text{ M}^{-1} \text{ s}^{-1}$ . The cations are easily hydrolyzed when  $pK_h$  is lower than 4.3 while above 10.08 supported too low Lewis acidity to coordinate with substrates. As shown in **Figure 1.4**, Cu(ClO<sub>4</sub>)<sub>2</sub>, Fe(ClO<sub>4</sub>)<sub>2</sub>, Cd(ClO<sub>4</sub>)<sub>2</sub>, InCl<sub>3</sub> and Pb(ClO<sub>4</sub>)<sub>2</sub> as well as the rare earth metal salts (Sc(ClO<sub>4</sub>)<sub>3</sub>, Y(ClO<sub>4</sub>)<sub>3</sub>, Ln(OTf)<sub>3</sub>) afford promising yields while chloride salts of B(III), Ti(IV), V(III) cause the decomposition of silylenol ethers and no desired product is obtained.



**Scheme 1.1** Mukaiyama aldol reaction catalyzed by Lewis acids in H<sub>2</sub>O-THF mixture solvent.<sup>49</sup>

<b>Li<sup>+</sup></b> 13.64 4.7×10 <sup>7</sup>	<b>Be<sup>2+</sup></b>	<div style="display: flex; align-items: center;"> <div style="border: 1px solid black; padding: 5px; margin-right: 10px;"> <b>Sc<sup>3+</sup></b> 4.3 4.8×10<sup>7</sup> 82%         </div> <div>           Cation pK<sub>n</sub> WERC Yield of reaction         </div> </div> <div style="margin-left: 20px;"> <p>*Definition of pK<sub>n</sub> :</p> <math display="block">xM^{z+} + yH_2O \rightleftharpoons M_x(OH)_y^{(xz-y)+} + yH^+</math> <math display="block">K_{xy} = \frac{[M_x(OH)_y^{(xz-y)+}][H^+]^y}{[M^{z+}]^x}; pK_n = -\log(K_{xy})</math> </div>											<b>B<sup>3+</sup></b>	<b>C</b>	<b>N</b>
<b>Na<sup>+</sup></b> 14.18 1.9×10 <sup>8</sup>	<b>Mg<sup>2+</sup></b> 11.44 5.3×10 <sup>5</sup>												<b>Al<sup>3+</sup></b> 1.14 1.6×10 <sup>0</sup> Trace	<b>Si<sup>4+</sup></b> — —	<b>P<sup>5+</sup></b> — —
<b>K<sup>+</sup></b> 14.46 1.5×10 <sup>8</sup>	<b>Ca<sup>2+</sup></b> 12.85 5×10 <sup>7</sup>	<b>Sc<sup>3+</sup></b> 4.3 4.8×10 <sup>7</sup> 82%	<b>Ti<sup>4+</sup></b> <2.3 —	<b>V<sup>3+</sup></b> ≤2.26 —	<b>Cr<sup>3+</sup></b> 4.0 5.8×10 <sup>7</sup> Trace	<b>Mn<sup>2+</sup></b> 10.59 3.1×10 <sup>7</sup> 18%	<b>Fe<sup>2+</sup></b> 9.5 3.2×10 <sup>6</sup> 26%	<b>Co<sup>2+</sup></b> 9.65 2×10 <sup>5</sup> 17%	<b>Ni<sup>2+</sup></b> 9.86 2.7×10 <sup>4</sup> 17%	<b>Cu<sup>2+</sup></b> 7.53 2×10 <sup>8</sup> 47%	<b>Zn<sup>2+</sup></b> 8.96 5×10 <sup>8</sup> 46%	<b>Ga<sup>3+</sup></b> 2.6 7.6×10 <sup>2</sup> Trace	<b>Ge<sup>4+</sup></b> — —	<b>As</b>	
<b>Rb<sup>+</sup></b> — —	<b>Sr<sup>2+</sup></b>	<b>Y<sup>3+</sup></b> 7.7 1.3×10 <sup>7</sup> 90%	<b>Zr<sup>4+</sup></b> 0.22 —	<b>Nb<sup>5+</sup></b> (0.6) —	<b>Mo<sup>5+</sup></b> — —	<b>Tc</b>	<b>Ru<sup>3+</sup></b>	<b>Rh<sup>3+</sup></b> 3.4 3×10 <sup>8</sup> Trace	<b>Pd<sup>2+</sup></b> 2.3 — Trace	<b>Ag<sup>1+</sup></b> 12 >5×10 <sup>5</sup> Trace	<b>Cd<sup>2+</sup></b> 10.08 >1×10 <sup>9</sup> 49%	<b>In<sup>3+</sup></b> 4.00 4.0×10 <sup>4</sup> 68%	<b>Sn<sup>4+</sup></b> — —	<b>Sb<sup>5+</sup></b> — —	
<b>Cs<sup>+</sup></b> — —	<b>Ba<sup>2+</sup></b> 13.47 6×10 <sup>7</sup>	<b>Ln<sup>3+</sup></b>	<b>Hf<sup>4+</sup></b> 0.25 —	<b>Ta<sup>5+</sup></b> (-1) —	<b>W<sup>6+</sup></b> — —	<b>Re<sup>5+</sup></b>	<b>Os<sup>3+</sup></b>	<b>Ir<sup>3+</sup></b> — Trace	<b>Pt<sup>2+</sup></b> 4.8 — Trace	<b>Au<sup>1+</sup></b> — — Trace	<b>Hg<sup>2+</sup></b> 3.40 2×10 <sup>9</sup> Trace	<b>Tl<sup>3+</sup></b> 0.62 7×10 <sup>5</sup>	<b>Pb<sup>2+</sup></b> 7.71 7.5×10 <sup>9</sup> 59%	<b>Bi<sup>5+</sup></b> 1.09 Trace	

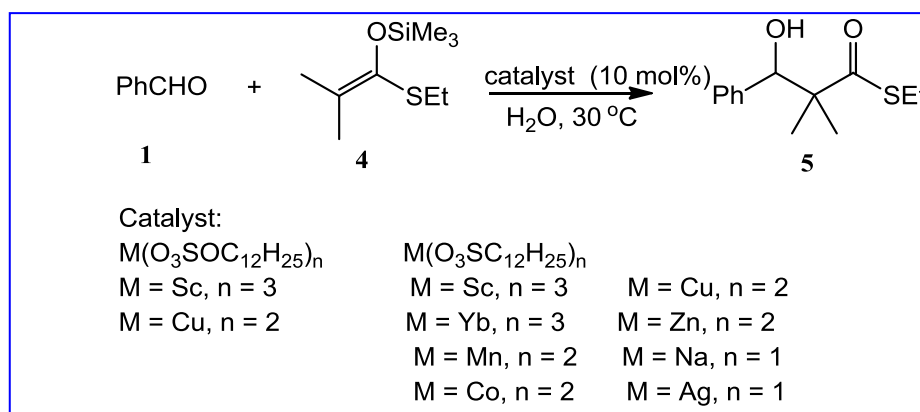
<b>La<sup>3+</sup></b> 8.5 2.1×10 <sup>8</sup> 80%	<b>Ce<sup>3+</sup></b> 8.3 2.7×10 <sup>8</sup> 81%	<b>Pr<sup>3+</sup></b> 8.1 3.1×10 <sup>8</sup> 83%	<b>Nd<sup>3+</sup></b> 8.0 3.9×10 <sup>8</sup> 78%	<b>Pm</b> — —	<b>Sm<sup>3+</sup></b> 7.9 5.9×10 <sup>8</sup> 85%	<b>Eu<sup>3+</sup></b> 7.8 6.5×10 <sup>8</sup> 88%	<b>Gd<sup>3+</sup></b> 8.0 6.3×10 <sup>7</sup> 90%	<b>Tb<sup>3+</sup></b> 7.9 7.8×10 <sup>7</sup> 81%	<b>Dy<sup>3+</sup></b> 8.0 6.1×10 <sup>7</sup> 85%	<b>Ho<sup>3+</sup></b> 8.0 6.1×10 <sup>7</sup> 89%	<b>Er<sup>3+</sup></b> 7.9 1.4×10 <sup>8</sup> 85%	<b>Tm<sup>3+</sup></b> 7.7 6.4×10 <sup>8</sup> 85%	<b>Yb<sup>3+</sup></b> 7.7 8×10 <sup>7</sup> 92%	<b>Lu<sup>3+</sup></b> 7.6 6×10 <sup>7</sup> 84%
---	---	---	---	---------------------	---	---	---	---	---	---	---	---	---	---

\* WERCs are measured by NMR, sound absorption or multidentate ligand method<sup>20</sup>

**Figure 1.4** Hydrolysis Constant and Exchange Rate Constants for Substitution of Inner-Sphere Water Ligands (WERC) and Lewis acid catalyzed Aldol Reaction.<sup>49,50</sup>

### 1.2.1.1 Sc<sup>III</sup> as catalytic part of LASCs

In order to completely avoid the use of toxic organic solvents and circumvent the immiscibility problem of organic compounds and water, various **Lewis acid-surfactant combined catalysts** have been synthesized and employed for organic reactions in aqueous phase. The **dodecanesulphonate** and **dodecylsulfate (DS) salts** of several water-stable Lewis acids were prepared by Kobayashi et al.<sup>49,52</sup> The catalytic activities and conversions of different metal cations were evaluated with the Mukaiyama aldol addition between benzaldehyde **1** and thioketene silyl acetal **4** as model substrates (**Scheme 1.2**). The formation of an emulsion thanks to the presence of the surfactant moiety not only overcome the immiscibility of organic substrates in water but also prevent the dramatic hydrolysis of water-labile silyl enol ether. Except the sodium, manganese and cobalt salts, the dedecanesulphonate salts of the other metal salts afford moderate to good conversions. Although the Cu salts give the highest activity at the initial stage, at the end of the reaction, Sc and Yb salts exhibit the most effective results. This has been likely ascribed to the dramatically hydrolysis of thioketene silyl acetal catalyzed by the Cu salts besides the high efficiency.



**Scheme 1.2** Mukaiyama aldol reaction catalyzed by various Lewis acid-surfactant combined catalysts.<sup>52</sup>

Since  $\text{Sc}(\text{DS})_3$  shows good stability and activity in aqueous phase, several similar condensation reactions and other types of reactions were also tested by Kobayashi *et al.*, such as aldol reaction, Mannich-type reaction,<sup>53</sup> hydroxymethylation reaction<sup>54</sup> and allylation. The products are shown in **Figure 1.5**. Generally, not only the activities are enhanced dramatically compared to classical water soluble Lewis acid salts, but also the selectivity to the desired product is improved to a great extent with the amphiphilic LASCs. At the end of the reactions, a simple phase separation or centrifugation are sufficient to recycle the catalyst and to recover the crude product. These advantages make the  $\text{Sc}(\text{DS})_3$  one of the best LASCs for catalytic reactions in aqueous phase.

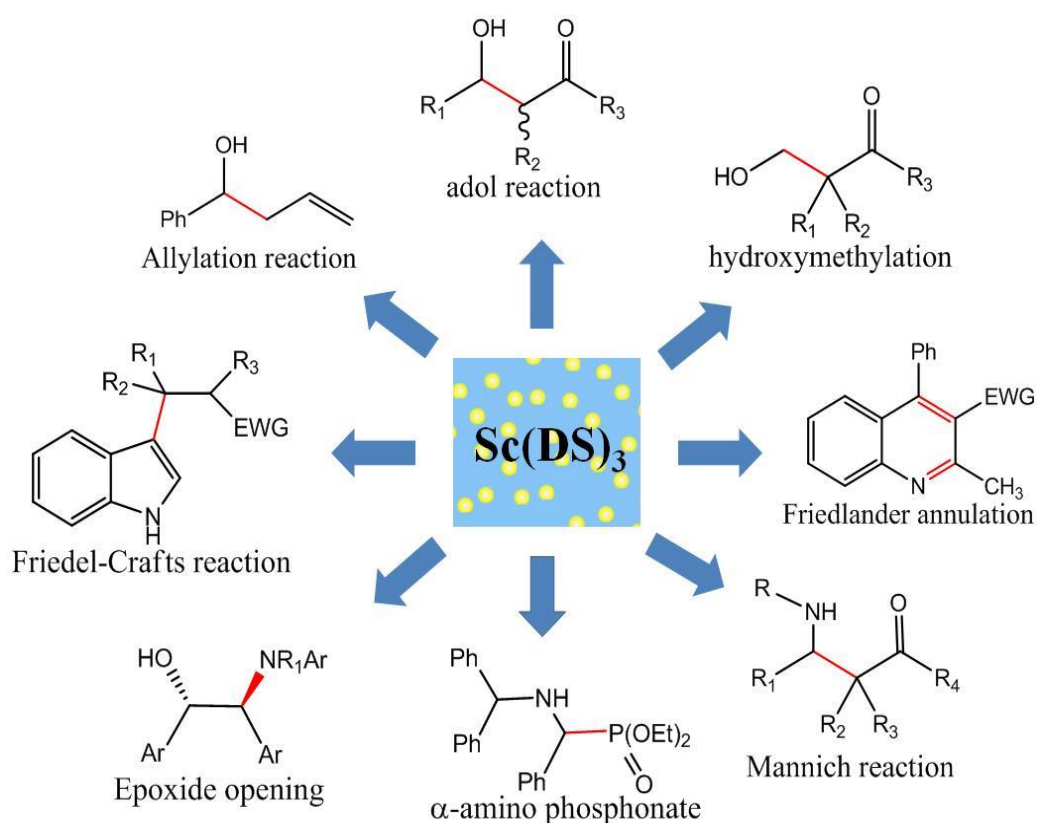
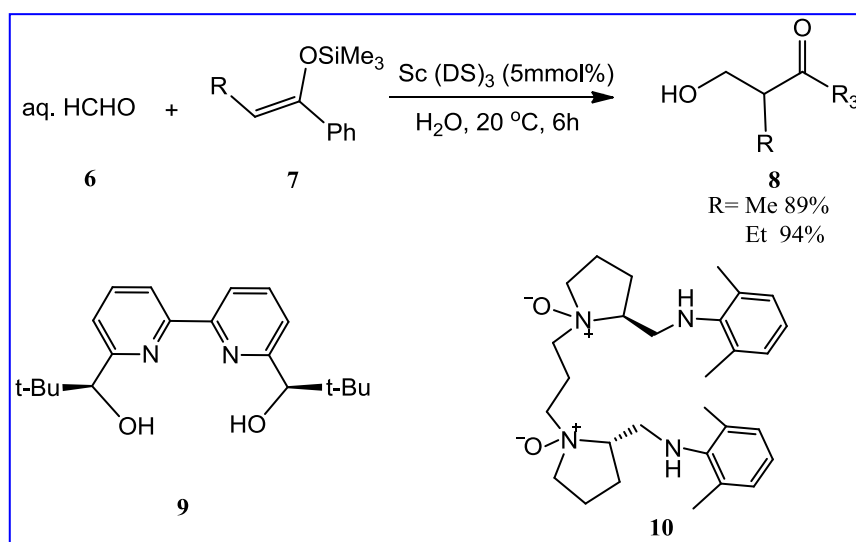


**Figure 1.5** Products of some  $\text{Sc}(\text{DS})_3$  catalyzed reactions in aqueous phase.<sup>53-58</sup>



With **Sc(DS)<sub>3</sub>** as catalyst, the initial rate of the aldol reaction is 1300 times higher in water than in CH<sub>2</sub>Cl<sub>2</sub>. Water is the solvent of choice compared to the other organic solvents. The separation of the product and catalyst involves the extraction by ethyl acetate or more conveniently by centrifugation.<sup>53</sup> Among the electrophiles in the aldol reactions, formaldehyde, a representative hydrophilic substrate, is one of the most important single carbon electrophiles.<sup>59,60</sup> Catalytic hydroxymethylation of silylenol ether with formaldehyde is also catalyzed effectively with **Sc(DS)<sub>3</sub>** as a Lewis acid-surfactant combined catalyst.<sup>54</sup> The **Sc(DS)<sub>3</sub>** micelles containing organic substrates not only protects the water sensitive substrates but also increases the solubility of the hydrophilic HCHO in a hydrophobic environment resulting in the reaction in water (**Scheme 1.3**). Furthermore, the asymmetric catalytic hydroxymethylation reaction can be achieved by addition of chiral ligands **9** and **10**. However, due to the decrease of the reaction rate, an additional surfactant is required to suppress the hydrolysis of the silylenol ether. By combining **9** with Triton X705 or ligand **10** with CH<sub>3</sub>(CH<sub>2</sub>)<sub>10</sub>SO<sub>3</sub>Na, different kinds of substrates can be converted to the corresponding hydroxymethylation product in good yield and selectivity (> 80% yield and > 90% ee).<sup>54</sup>



**Scheme 1.3** *Sc(DS)<sub>3</sub> catalyzed hydroxymethylation in water and ligand for asymmetric hydroxymethylation.*<sup>54</sup>

Besides the aldol reaction, Sc<sup>III</sup> combined with an amphiphilic moiety also presents much better results than either surfactant SDS or Lewis acid Sc(OTf)<sub>3</sub> in the Michael reaction, asymmetric ring-opening reaction and Friedel-Craft reaction *etc.*<sup>53,55-58</sup> Under the same conditions, the yields of the desired products with **Sc(DS)<sub>3</sub>** as catalyst are much better than with **Sc(OTf)<sub>3</sub>** and **SDS** (**Figure 1.6**). The chemoselectivity and the reaction rate improvement have been ascribed to the micro-hydrophobic compartments in the aqueous phase, which could not only overcome the miscibility problem between organic reactants and catalyst-containing aqueous phase, but also accumulate the reactants in the micelles, emulsion or  $\mu\text{em}$  droplets. Indeed, the emulsion droplets of **Sc(DS)<sub>3</sub>** in the presence of benzaldehyde in aqueous phase were

confirmed by light microscopy (**Figure 1.7**). For epoxide-ring opening reaction, the membrane of emulsion droplets presented the steric effect and increased enantioselectivity.

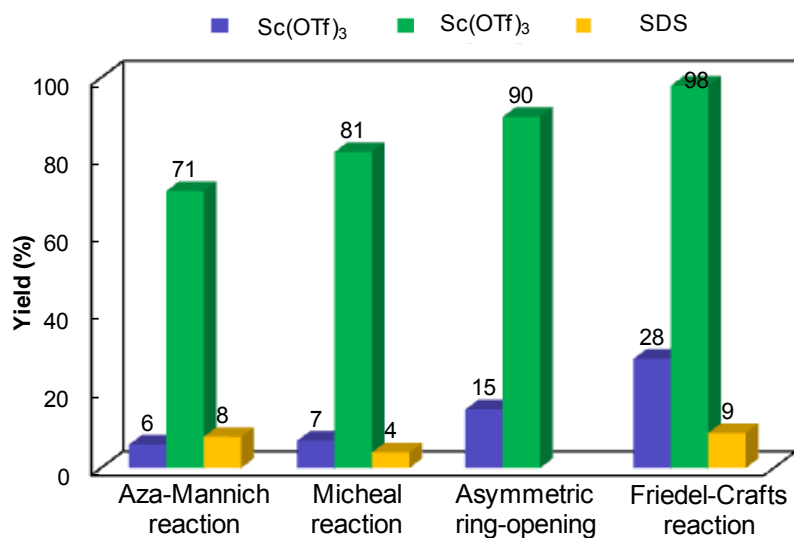


**Figure 1.6** Results of several reactions catalyzed by  $Sc(DS)_3$ , SDS and  $Sc(OTf)_3$ .<sup>55-58</sup>

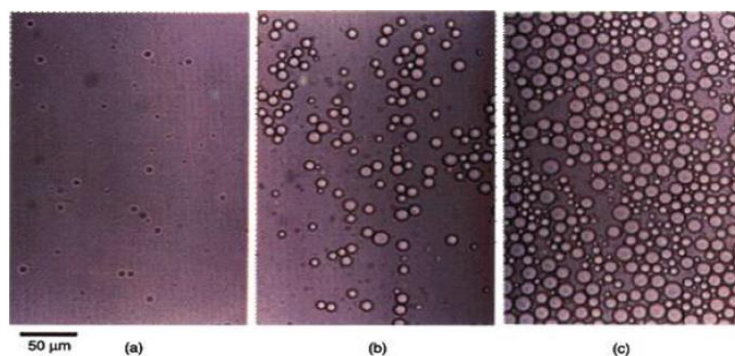
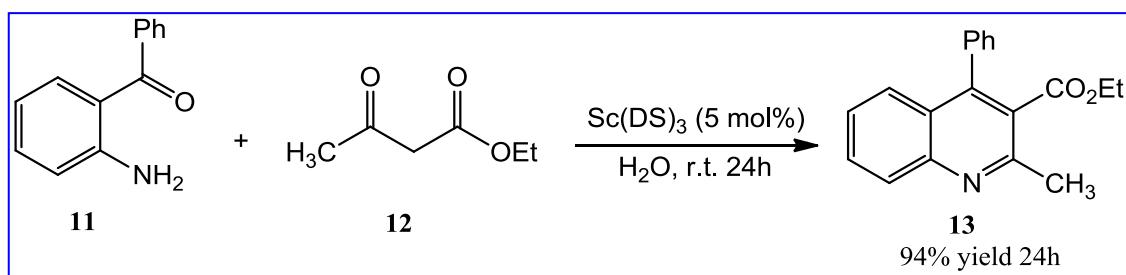


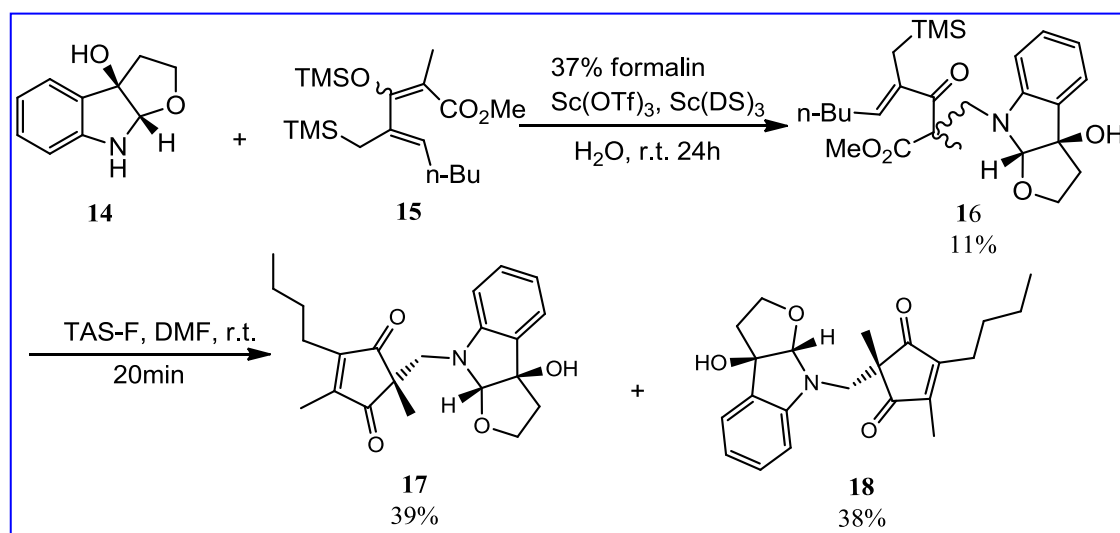
**Figure 1.7** Mixtures of  $Sc(DS)_3$  and benzaldehyde as detected by optical microscopy. (a)  $Sc(DS)_3$ :benzaldehyde = 1:10; (b)  $Sc(DS)_3$ :benzaldehyde = 1:20; (c)  $Sc(DS)_3$ :benzaldehyde = 1:100.<sup>53</sup>

The products of aldol reaction, Mannich reaction and Friedel-Crafts reaction are important synthetic intermediates in pharmaceuticals and in the synthesis of natural products. Besides the research of catalytic fundamental organic reactions, the Lewis acid-surfactant combined catalysts catalyze the reactions leading to various heterocyclic compounds allowing the synthesis of natural molecules in water. For example, in the presence of 10 mol%  $Sc(DS)_3$ , the formation of 2-methyl-4-phenylquinoline-3-carboxylate **13** via the Friedländer annulation was obtained in 90% yield in 12h (5 mol% catalyst: 94% yield in 24h) (**Scheme 1.4**).<sup>61</sup>



**Scheme 1.4**  $\text{Sc}(\text{DS})_3$  catalyzed Friedländer annulation in water.<sup>61</sup>

Another example is the total synthesis of IL-6 inhibitor (+)-madindoline A (**17**) and (+)-madindoline B (**18**) reported by Omura *et al.* The key step in the reaction is a three-component one step process catalyzed by  $\text{Sc}(\text{DS})_3$  combined with  $\text{Sc}(\text{OTf})_3$  (**Scheme 1.5**).<sup>62</sup>



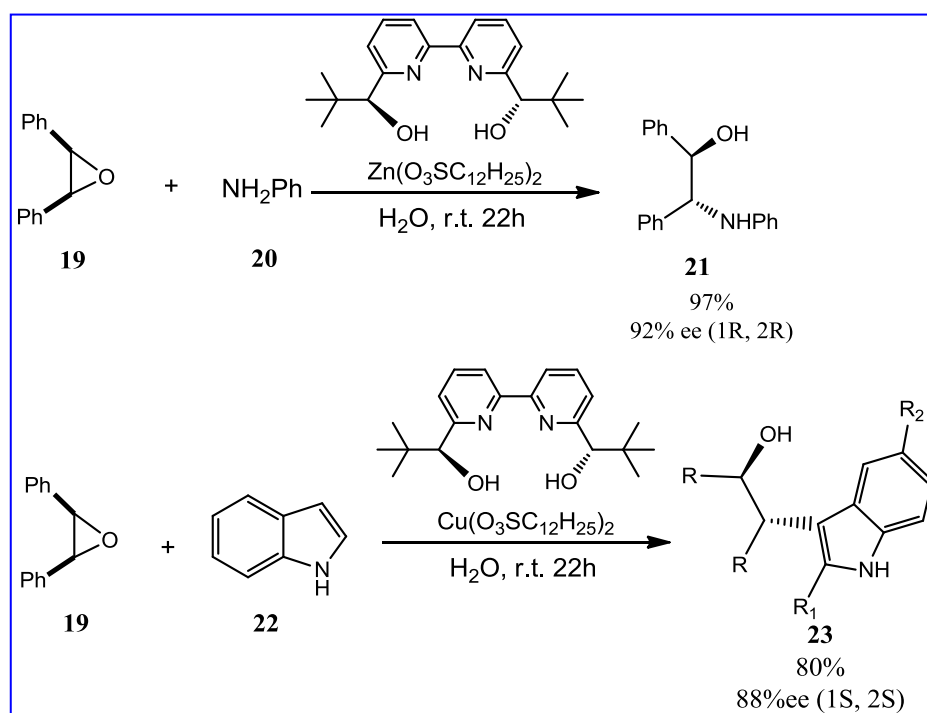
**Scheme 1.5** Total synthesis of (+)-madindoline A and B.<sup>62</sup>

$\text{Sc}^{\text{III}}$  has been combined with other amphiphilic moieties and applied to the same reactions as mentioned above, *i.e.* aldol reaction, Mannich-type reaction, dehydration reaction, etc. For example, scandium dodecanesulphonate  $\text{Sc}(\text{C}_{12}\text{SO}_3)_3$  has also been widely used but in most cases, the results were inferior to those obtained with  $\text{Sc}(\text{DS})_3$ , probably due to a difference in the water solubility of the two surfactant-combined surfactants.<sup>52,63</sup> Compared with the normal carbon-hydrogen alkyl chain, fluoro-surfactants generally afford some special properties, *e.g.* lower surface tensions, higher stability, etc. On account of these advantages, **Sc-perfluorosurfactant combined catalysts** have also been reported but the price of the surfactant and sometimes the requirement of the presence of an expensive fluoro solvent made this type of catalyst not acceptable from the view of green chemistry.<sup>64,65</sup> The detailed applications of different types of Sc-surfactant combined catalysts were listed in **Appendix A**.

### 1.2.1.2 Cu<sup>II</sup>, Zn<sup>II</sup> and miscellaneous Lewis acids as catalytic part of LASCs

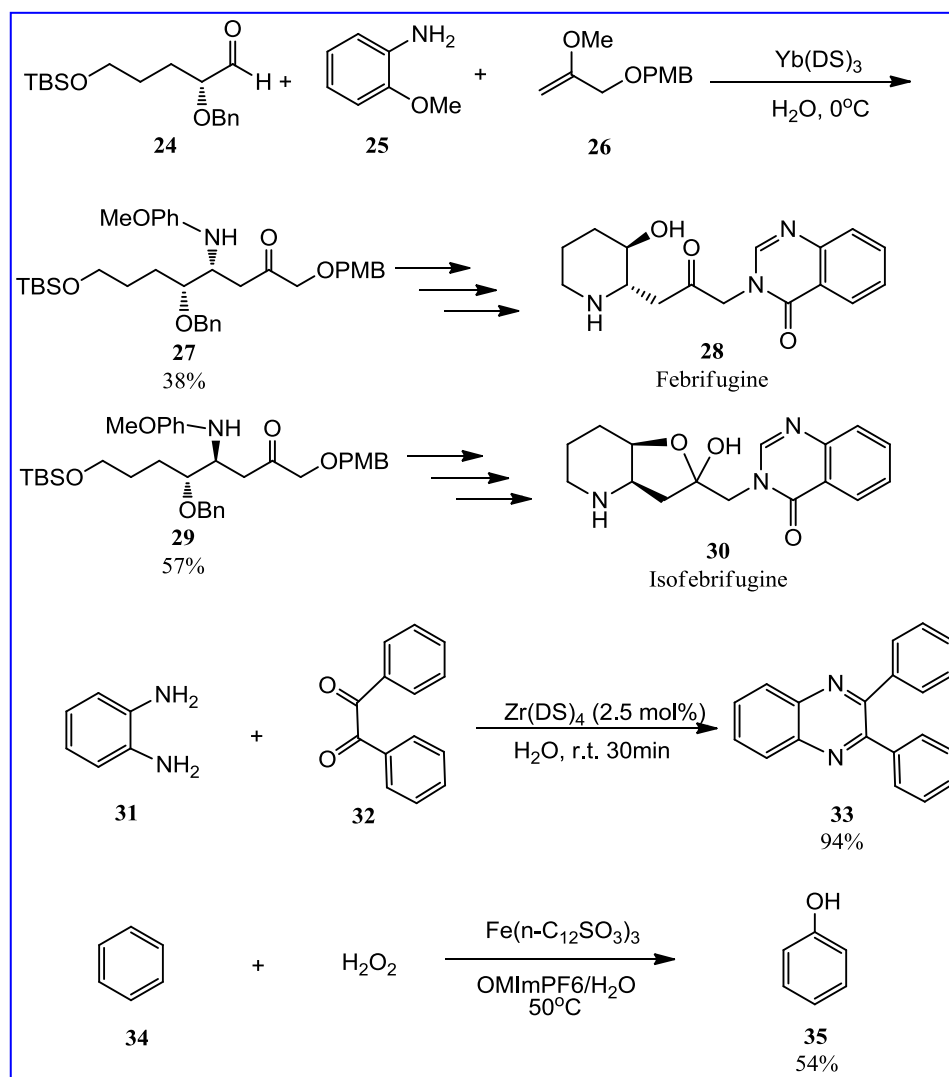
Although Cu<sup>II</sup> and Zn<sup>II</sup> give lower yields than Sc<sup>III</sup> and rare earth metal salts during the catalyzed Mukaiyama-aldol reaction reported by Kobayashi due to their lower Lewis acidity.<sup>49</sup> The surfactant combined Cu<sup>II</sup> and Zn<sup>II</sup> salts are however still widely used in catalytic reactions in water with appropriate substrates or co-catalysts. For example, the asymmetric aldol reaction in aqueous phase can be achieved by introducing the **Cu(DS)<sub>2</sub>** catalyst and bis(oxaline) ligand.<sup>66</sup> Compared to **Sc(DS)<sub>3</sub>**, **Cu(DS)<sub>2</sub>** provides better results for the catalytic Mannich reaction which proceeds *via* a dehydration process giving water labile imines and further addition with silylenol ether or enolate. Besides benzaldehyde, heteroaromatic,  $\alpha,\beta$ -unsaturated and aliphatic aldehydes also react smoothly to afford the desired adducts in high yields.<sup>53</sup>

As mentioned above, **Sc(DS)<sub>3</sub>** catalyzes the asymmetric ring-opening of meso-epoxide,<sup>57</sup> while other Lewis acids have also been evaluated with *cis*-stilbene epoxide and aniline as model substrates<sup>67</sup> and among them, Cu and Zn lead to considerable conversions and enantioselectivities in water, **Zn(DS)<sub>2</sub>** affording the best results. When indole is used as a ring-opening agent, the best result is obtained with **Cu(DS)<sub>2</sub>** as a catalyst (**Scheme 1.6**). The opposite enantiomers obtained from **Sc(DS)<sub>3</sub>** and **Cu(DS)<sub>2</sub>** under the same conditions can be rationalized by the structure of the Lewis acid ligand complex. The Cu-ligand complex adopts square pyramidal structure with two pyridines and one hydroxyl groups coordinated in a tridentate manner, while Sc-complex adopts a pentagonal bipyramidal structure in a tetradentate form.<sup>59,67</sup>



**Scheme 1.6** Asymmetric ring-opening of meso-epoxide with Cu and Zn surfactant salts.<sup>67</sup>

According to the data of  $pK_h$  values (hydrolysis constant of metal cations) and WERCs (inner sphere Water Exchange Rate Constant) reported by Kobayashi, besides the most common used  $\text{Sc}^{\text{III}}$ ,  $\text{Cu}^{\text{II}}$ ,  $\text{Zn}^{\text{II}}$  surfactant-combined catalysts, there are many other Lewis acids that can be used as catalysts in aqueous phase for organic reactions,<sup>49</sup> especially in synthesis of special products. For example,  $\text{Yb}(\text{DS})_3$  is used to catalyze an important Mannich-type reaction step in the total synthesis of antimalarial alkaloids Febrifugine and Isofebrifugine.<sup>68</sup> The *cis*-product of **27** can be converted into iso-febrifugine by multistep reactions while the *trans* product of **29** is converted into febrifugine. Another example is the quinoxaline derivatives, which are important heterocyclic compounds easily synthesized in water with  $\text{Zr}(\text{DS})_4$ , another kind of catalytic surfactant combined Lewis acid. Several substituted 1,2-benzene diamines or even aliphatic 1,2-diamine can condense with benzyl or its analogues affording good conversion.<sup>69</sup> Different from the condensation reaction, the Lewis acid-surfactant combined catalyst  $\text{Fe}(\text{C}_{12}\text{SO}_3)_3$  based on the Fenton's reactant can be applied to the catalytic oxidation of benzene to phenol with  $\text{H}_2\text{O}_2$  as an oxidant in aqueous/ionic liquid biphasic system (**Scheme 1.7**).<sup>70</sup>

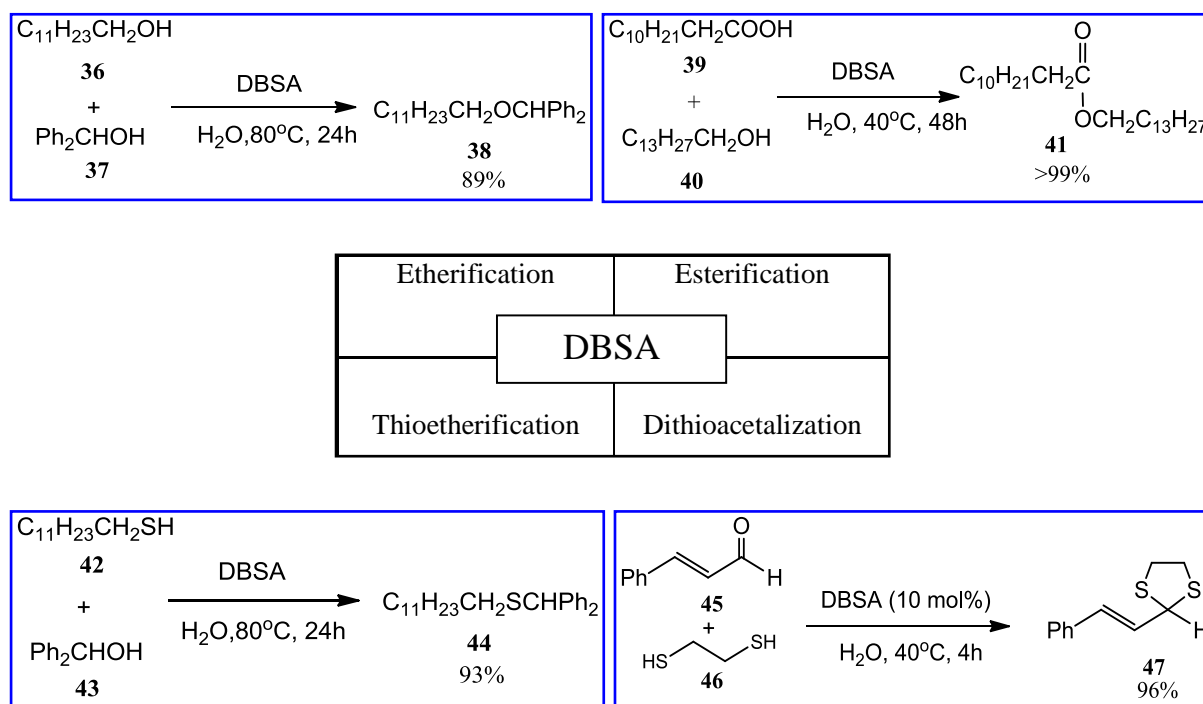


**Scheme 1.7** Reactions catalyzed by miscellaneous Lewis acids surfactant-combined catalysts.<sup>68-70</sup>

Besides the Lewis acid-surfactant combined catalysts mentioned above, other amphiphilic catalysts based on different kinds of metallic counterions have also been investigated. In some cases, due to their low catalytic activity or their high price, they are not the best choice but most of them afford good results for specific catalytic reactions. Detailed information is given in **Appendix A**.

### 1.2.1.3 Brönsted acid-surfactant combined catalysts and their application

Brönsted acid-surfactant combined catalysts have been widely used to perform catalytic reactions in water. The typical reactions catalyzed by the Lewis acid-surfactant-combined catalysts can also be catalyzed by the Brönsted acids and in some cases, better results are obtained. Some examples of reactions are esterification,<sup>71</sup> Mannich-type condensation<sup>72</sup> and some azocyclic compound synthesis.<sup>73-75</sup> The most common catalytic surfactant is the **dodecylbenzenesulfonic acid (DBSA)**. Kobayashi *et al.* have systematically investigated the dehydration reactions in water including esterification, etherification, thioetherification and dithioacetalization (**Scheme 1.8**).<sup>71,76</sup>



**Scheme 1.8** DBSA catalyzed esterification, etherification, thioetherification and dithioacetalization in aqueous solution.<sup>71,76</sup>

In such reaction media, the hydrophobic substrates constitute the core of the micelles formed by the catalytic surfactant and dispersed into the aqueous phase (**Figure 1.8**).

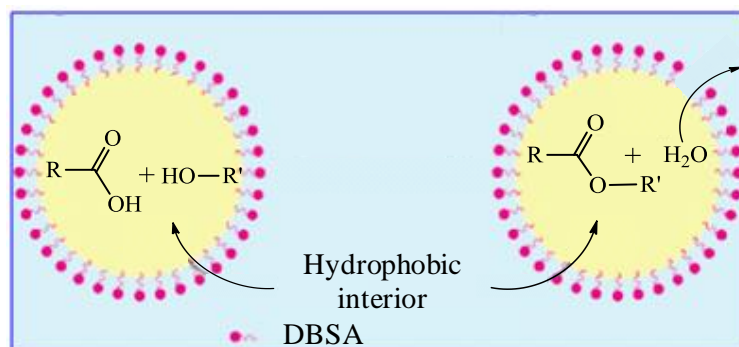


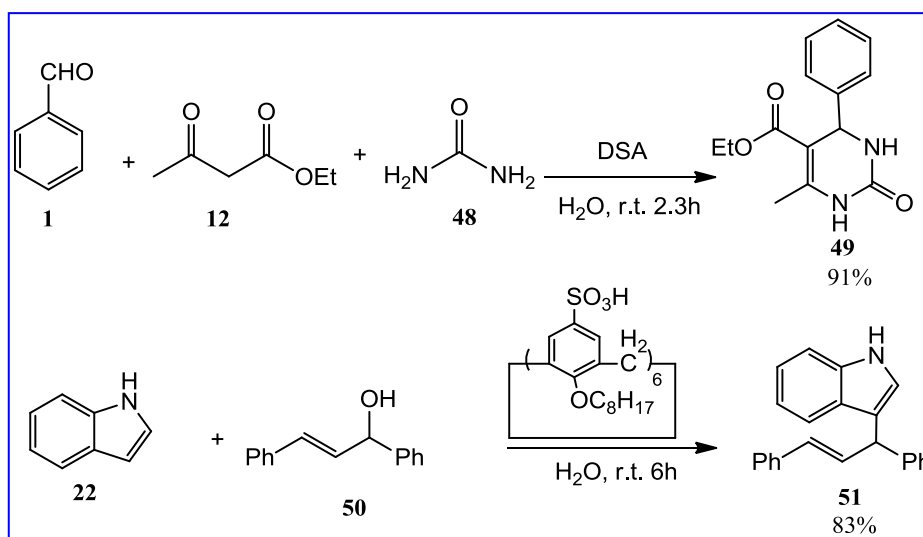
**Figure 1.8** Direct esterification by dehydration in the presence of DBSA catalyst in water.<sup>71</sup>

For esterification reactions, as indicated in **Scheme 1.8**, the equilibrium position of lauric acid with myristyl alcohol lies almost absolutely at the ester side while the less hydrophobic alcohol, like benzylalcohol and ethanol, gave 82 and 15% yield respectively. The different results from substrates of different hydrophobicity can also be applied to transesterification reactions.

With **DBSA** (10 mol %), the symmetric ether synthesis between two benzylic alcohols or asymmetric ether synthesis between a hydrophobic alcohol and benzylic alcohol gives the desired product in good conversion. The reaction between two alkyl alcohols affords very low yield. The same condition can also be applied to the thioether synthesis and acetalization reaction. The hydrophobic thiols react with activated alcohol under the **DBSA** catalytic condition affording even better yield than etherification (> 90% yield in 24h).

Several useful heterocyclic compounds can be prepared in aqueous condition with **DBSA** as a catalyst. For example, pyridone can be prepared by aza Diels-Alder reaction between the *in situ* generated imines and Danishefsky's diene with **DBSA** as a catalyst in water.<sup>77</sup> 4-Thiazolidinones, which have been widely used in pharmaceuticals,<sup>78,79</sup> are synthesized by condensation of a three-component-tandem reaction including a primary amine, a carbonyl compound and a mercapto-carboxylic acid with **DBSA** in water.<sup>74</sup> The formation of micelles is crucial to the reaction because the last step of condensation between amino and carboxylic groups proceeds by the removal of water from the hydrophobic micelle core.

Besides **DBSA**, some other Brønsted acids are also suitable for catalytic reactions in aqueous phase. Recently, Konwar et al. reported that **dodecylsulfonic acid (DSA)** catalyzes the three components and one-step synthesis of 3, 4-dihydropyrimidin-2-ones in water.<sup>73</sup> Wang et al. reported the synthesis and application of **calix[n]arene sulfonic acid** bearing pendant aliphatic chains in the allylation of indoles and other aromatic compounds with allyl alcohol directly.<sup>80</sup> Various calix[n]arene sulfonic acid derivatives with different n and hydrophobic chain length have been examined and among them, **calix[6]arene sulfonic acids** with **octyl chain** gives the best result with indole **22** and (E)-1,3-diphenylpropenol **50** as model substrates (**Scheme 1.9**).



**Scheme 1.9** DSA and octylcalix[6]arene sulfonic acids catalyzed reactions in water.<sup>73,80</sup>

The **perfluorooctylsulfonic acid (PFOSA)** is another example of Brønsted acid catalytic surfactant which is used to catalyze the Pictet–Spengler reactions,<sup>81</sup> for the synthesis of tetrahydroisoquinoline and isochroman derivatives.<sup>75</sup> **Polystyrene sulfonic acid** can also catalyze the hydrolysis of thioesters and transprotection of thiols.<sup>82</sup> In **Appendix A**, the different types of Brønsted acid-surfactant combined catalysts and their applications are listed in detail.

As mentioned above in **Figure 1.2**, introduction of a surfactant moiety in the catalyst not only overcome the immiscibility problem between the organic and aqueous phases, enhances the reaction rate and selectivity, but also facilitates the work-up and the recycling of the catalyst after the reaction. Indeed, several different simple procedures allow to recover the desired product and to separate the catalyst in the aqueous phase. As shown in **Figure 1.9**, after the **Sc(DS)<sub>3</sub>** catalyzed hydroxymethylation, a simple centrifugation separates the aqueous phase with the catalyst from the product.<sup>54</sup> **Cu(DS)<sub>2</sub>** catalyzed dithioacetalization gives insoluble product and simple filtration affords the pure product and the aqueous solution including a reuse of the catalyst for several times without loss of activity.

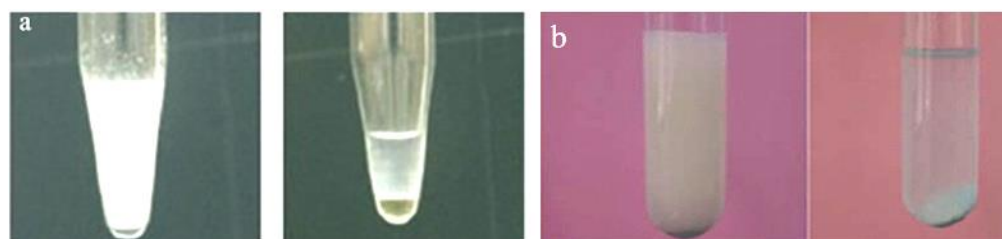


**Figure 1.9** Separation of the products after aqueous phase reaction catalyzed by the surfactant-combined catalyst. (a) hydroxymethylation: before centrifugation (left) and the separated phases after centrifugation (right);<sup>54</sup> (b) dithioacetalization: colloid dispersion during the reaction under stirring (left) and the product deposit after reaction without stirring (right).<sup>76</sup>



### 1.2.1.4 The physicochemical properties of the anionic surfactant-combined catalysts

The physicochemical properties of surfactant combined catalysts are rarely reported.<sup>83-85</sup> With the most widely used **Sc(DS)<sub>3</sub>** as an example, there is almost no physicochemical properties reported except the formation of emulsion drops in the reaction mixture observed by microscopy and AFM.<sup>53</sup> As we know, the amphiphilic properties of surfactant-combined catalysts play an important role in the activity and selectivity of the catalytic reactions. On the other side, combination of the above-mentioned Lewis acid with other types of anionic surfactant counterparts and their physical properties investigation are sparsely reported.<sup>86-90</sup>

The critical micelle concentrations (CMC) and Krafft points of **Cu(DS)<sub>2</sub>**, **Zn(DS)<sub>2</sub>** and some other catalytic surfactants have been reported by Moroi *et al.* during the investigation of the phase equilibrium of anionic surfactant mixtures (**Table 1.1**).<sup>83</sup> Obviously, the CMCs and Krafft points are closely related with not only the chain length of the hydrophobic part but also with the metallic counterions types. From dodecylsulfate to tetradecylsulfate, the Krafft point of a same metallic ion increases dozens of degrees Celsius and the CMCs decreases about four times. On the other side, the increment of Krafft points and decrease of CMC from the monovalent sodium to the divalent metallic ions are also dramatic when the hydrophobic part is constant. This indicates that the widely used Lewis acid surfactant combined catalysts can be prepared by precipitation from the mixture solution of SDS with the corresponding metallic salts when the appropriate temperature is controlled.<sup>52</sup> Furthermore, the catalytic activity and recycling of the surfactant catalyst can also be controlled by the temperature with appropriate hydrophobic counterpart.

**Table 1.1** CMCs at 30 °C and Krafft points of several surfactants based on dodecylsulfate (DS) and tetradecylsulfate (TS) combined with metallic salts.<sup>83</sup>

Surfactants	CMC (mM)	Krafft points (°C)
SDS	8.4	9
STS	2.1	21
Mn(DS) <sub>2</sub>	1.20	16
Mn(TS) <sub>2</sub>	-	29
Zn(DS) <sub>2</sub>	1.20	11
Zn(TS) <sub>2</sub>	-	32
Cu(DS) <sub>2</sub>	1.18	19
Cu(TS) <sub>2</sub>	-	40

The CMCs of these Lewis-acid surfactant combined catalyst have also been confirmed by Jain *et al.* during their search for synergic effects between the nonionic surfactant Triton X-100 and the metal dodecyl sulfates.<sup>84</sup> The interactions between nonionic and ionic surfactants often result in an increase of the clouding point of the nonionic surfactant, the decrease of the Krafft point of the ionic surfactant, the

increase of the surfactant efficiency and the decrease of the CMC. To describe the extent of this interaction, the  $\beta$  parameter estimated from the Rubingh's regular solution theory has been introduced (Eqs 1.1 and 1.2).<sup>91</sup>

$$\frac{(X_1)^2 \ln(\alpha_1 C^* / X_1 C_1)}{(1 - X_1)^2 \ln[(1 - \alpha_1) C^* / (1 - X_1) C_2]} = 1 \quad (\text{Eq. 1.1})$$

$$\beta = \frac{\ln(\alpha_1 C^* / X_1 C_1)}{(1 - X_1)^2} \quad (\text{Eq. 1.2})$$

Where  $X_1$  is the mole fraction of surfactant 1 in the mixed micelle,  $\alpha_1$  is the mole fraction of surfactant 1 in the mixture,  $C^*$  is the CMC of the surfactant mixture,  $C_1$ ,  $C_2$  are the CMC of pure surfactants 1 and 2. The deviation of  $C^*$ - $\alpha_1$  curve and  $X_1$ - $\alpha_1$  from the ideal values gives the intuitive perception of the nonionic-ionic surfactant interaction (Figure 1.10). The  $\beta$  values of various metal dodecyl sulfates with Triton X-100 (LiDS: -4.06, SDS: -3.08, **Cu(DS)<sub>2</sub>**: -1.6, **Co(DS)<sub>2</sub>**: -1.2) indicates that the synergic effects of divalent counter-ions are much weaker than monovalent counterparts due to their higher degrees of counter-ion binding. On the other side, the addition of salt also weakens the synergic nonionic-ionic surfactant interaction. The modification of the surfactant properties by addition of another type of surfactant can also be applied to the catalytic systems. For example, the interface between water and oil is greatly enlarged with surfactant mixture, which can results in an enhancement of the catalytic activity. Also, room temperature reactions catalyzed by catalytic surfactants with Krafft point above room temperature can be realized by addition of a nonionic surfactant, *etc.*

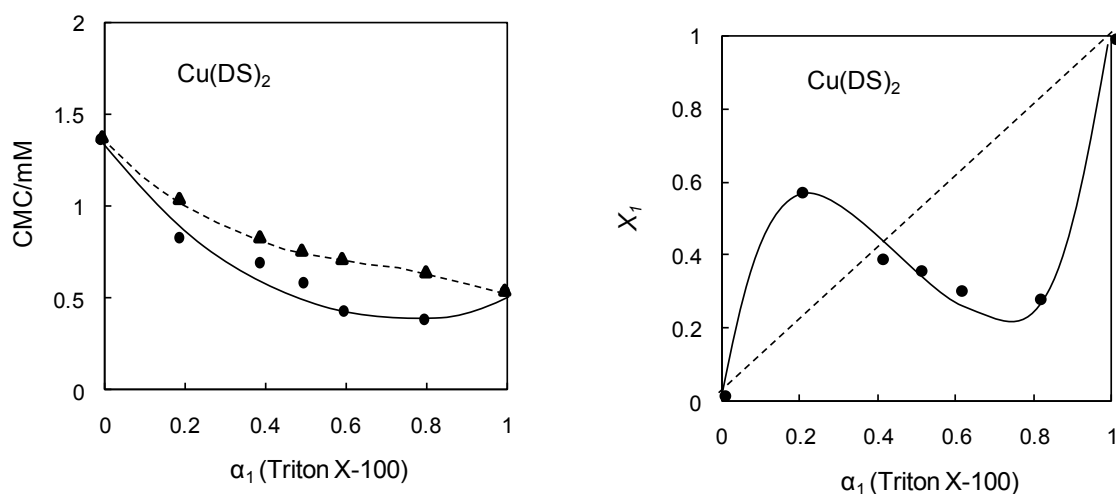
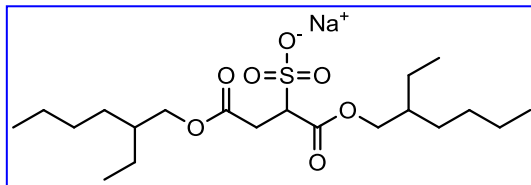


**Figure 1.10** Variation of CMC with mole fraction ( $\alpha_1$ ) of surfactant Triton X-100 at 30 °C (left) and corresponding mole fraction of Triton X-100 in the mixed micelle ( $X_1$ ).<sup>84</sup>

Although the investigation of the physicochemical properties of widely used surfactant combined catalysts is rarely reported, those of the Lewis acids combined with other types of surfactants have been

reported occasionally. The structures of aggregates of a series of metallic counter-ions from monovalent alkali ions to divalent alkaline and transition metal ions combined with sodium bis(2-ethylhexyl) sulfosuccinate (AOT) (Scheme 1.10) in cyclohexane with addition of small amounts of water have been investigated by Eastoe et al. by viscosity and SANS measurements.<sup>87</sup>



**Scheme 1.10** Structure of surfactant AOT.

The hydration radius ( $r_h$ ) of the metal counterions plays a crucial role in the structure of aggregates: for  $r_h < 3\text{\AA}$  (bulk aqueous solution value), spherical surfactant aggregates are present whereas, for  $r_h > 3\text{\AA}$ , cylinder shapes aggregates are favored. As we know, the solution viscosity reflects the structure of aggregates and their mutual interactions. At the infinite dilution, the viscosity indicates only the shape information and defines as shape-dependant intrinsic viscosity (Eq. 1.3):<sup>92</sup>

$$[\eta] = \{\eta_r\}_{\phi \rightarrow 0} \approx \left\{ \left[ (\eta_{solu} - \eta_{solv}) / \eta_{solv} \right] / c \right\}_{c \rightarrow 0} = 2.5 + 0.4075(J - 1)^{1.508} \quad (\text{Eq. 1.3})$$

Where  $[\eta]$ ,  $\eta_r$ ,  $\eta_{solu}$ ,  $\eta_{solv}$ ,  $\phi$  and  $c$  are the intrinsic viscosity, reduced viscosity, viscosity of solution, viscosity of solvent, volume fraction of surfactant and concentration of surfactant respectively.  $J = (r_1/r_2)$ ,  $r_1$  is the major axis;  $r_2$  is the minor axis of aggregate). The spherical aggregates generally give  $[\eta]$  close to 2.5 whereas non spherical particles give much higher values. The hydration radii of various metallic ions and aggregate characteristics of corresponding metallic AOT surfactants in cyclohexane in the presence of small amounts of water are given in Table 1.2.

**Table 1.2** Hydration radii, intrinsic viscosities  $[\eta]$ , and the axial ratios of the aggregates for  $M^{n+}(\text{AOT})_n/\text{cyclohexane}/\text{water}$  systems.<sup>a</sup>

$M^{n+}$	$r_h$ ( $\text{\AA}$ )	$[\eta]$	$J_{vis}$	$J_{sans}$
$\text{Na}^+$	1.8	2.7	–	–
$\text{K}^+$	1.1	2.6	–	–
$\text{Rb}^+$	1.0	2.9	–	–
$\text{Mg}^{2+}$	3.1	5.6	2.8	2.5
$\text{Ni}^{2+}$	3.7	20.8	11.1	22.6
$\text{Cu}^{2+}$	3.4	10.0	7.9	7.5
$\text{Zn}^{2+}$	3.5	11.6	8.8	23.8

<sup>a</sup> $m_{\text{H}_2\text{O}}/m_{M^{n+}(\text{AOT})_n} = 5$ ,  $[\text{AOT}] = 0.075 \text{ mol} \cdot \text{L}^{-1}$ , temperature = 25.0 °C.  $r_h$  is bulk aqueous solution value.

The evolution of aggregates in the  $\text{Cu(AOT)}_2$ /isooctane/water system by increasing the amount of water in the oil rich side has been reported by Pileni *et al.* The hydration radius is controlled by the hydration extent of the counter ions which has also a dramatic effect on the aggregation shape.<sup>88,93</sup> On the other side, the “Fish diagram” of the  $\text{M(AOT)}_2$ /isooctane/water ( $M = \text{Co}, \text{Ni}, \text{Cu}$ ) systems have been determined with the temperature as ordinate and mass fraction of surfactant  $\gamma$  as abscissa (**Figure 1.11**). The Winsor type of the  $\mu_{em}$  is controlled by the temperature; its effect is opposite to that of the nonionic surfactants. Indeed, the hydration of the counterions and headgroups increases with temperature while dehydration takes place for nonionic surfactants. The hydrophilic-lipophilic balance temperatures are around 36 °C for  $\text{Cu(AOT)}_2$ , 43 °C for  $\text{Co(AOT)}_2$  and 47 °C for  $\text{Ni(AOT)}_2$ .<sup>90</sup>

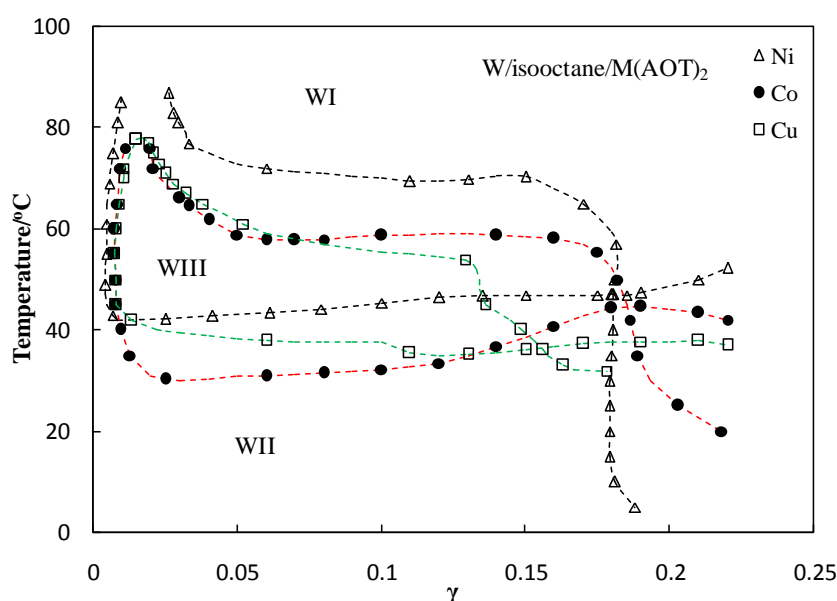


**Figure 1.11** “Fish diagrams” of  $\text{H}_2\text{O}/\text{iso-octane}/\text{M(AOT)}_2$  ternary mixture where  $M = \text{Co}, \text{Ni}, \text{and Cu}$ ;  $\alpha = O/(O + W)$ ;  $\gamma = S/(S + O + W)$ ; the oil rich  $\mu_{em}$ : Winsor II, the water rich  $\mu_{em}$ : Winsor I and intermediate-phase  $\mu_{em}$ : Winsor III.<sup>90</sup>

### 1.2.2 Cationic surfactant-combined polyoxometalate and peroxometalate catalysts

The applications of polyoxometalates (POMs) and peroxometalates in the catalytic oxidations and the relation between the structure and activity have been intensively investigated in the last three decades. POMs, the anionic clusters of early transition metal and oxygen with a general formula  $[\text{X}_x\text{TM}_n\text{M}_m\text{O}_y]^{q-}$  ( $X = \text{P}, \text{Si}$ ;  $M = \text{Mo}, \text{W}$ ;  $\text{TM} = \text{Co}, \text{Zn}, \text{Mn}, \text{V}, \text{Ti}, \text{etc.}$ ), show strong thermostability and intrinsic stability to oxidation. Furthermore, the versatility of their properties such as redox potential, acidity and stability *etc.* can be tuned for example by varying the counterions,<sup>94-96</sup> which leads to their wide application in catalysis, medicine and materials. Among the catalytic reactions with polyoxometalates or peroxometalates as catalysts,  $\text{H}_2\text{O}_2$  or  $\text{O}_2$  as oxidants received great attention due to their sustainability and environmental safety.<sup>32,97,98</sup> Compared with  $\text{O}_2$ , special installations for the gas-liquid reaction are not required for  $\text{H}_2\text{O}_2$  with which, manipulations are safe when the concentration is controlled. Besides, the

cheap price also makes  $\text{H}_2\text{O}_2$  the most popular green oxidant in recent decade. The common structures of POMs used in catalysis include Keggin-types, “sandwich” type (transition metals ring between two truncated Keggin ligands) and Wells-Dawson structure (**Figure 1.12**).<sup>99</sup> Depending on the composition, structure and redox potential, different POMs interact with oxidants in different ways and show different activities. The cationic counter-part also affects the solubility and other physicochemical properties in the catalytic systems also playing an important role in the reaction.

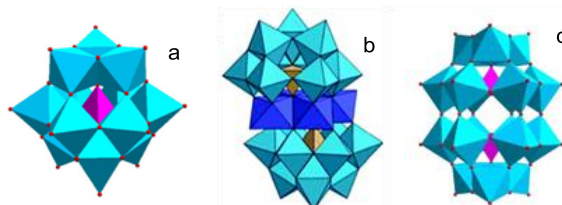


**Figure 1.12** Common POM structures: a) Keggin; b) Sandwich; c) Wells-Dawson.<sup>99</sup>

In previous research, it was demonstrated that peroxometalates derived from tungsten and molybdenum can catalyze various oxidations of organic substrates, especially after the initial work by Venturello and Ishii.<sup>100,101</sup> The reaction types with  $\text{H}_2\text{O}_2$  as an oxidant can be catalyzed by tungsten and molybdenum based peroxometalates as depicted in **Figure 1.13**. The active structures in the catalytic systems have been intensively studied by Venturello,<sup>100</sup> Bregeault,<sup>102</sup> Griffith<sup>103</sup> and Hill<sup>95</sup> by IR, Raman,  $^{31}\text{P}$  NMR,  $^{183}\text{W}$  NMR and dynamic studies. Actually, the different active species can be converted to each other and can even form Keggin structure again after decomposition in the presence of  $\text{H}_2\text{O}_2$  under special conditions of pH, concentration, species ratio, *etc.* The proposed structures of active species in the catalytic systems are shown in **Figure 1.14**.

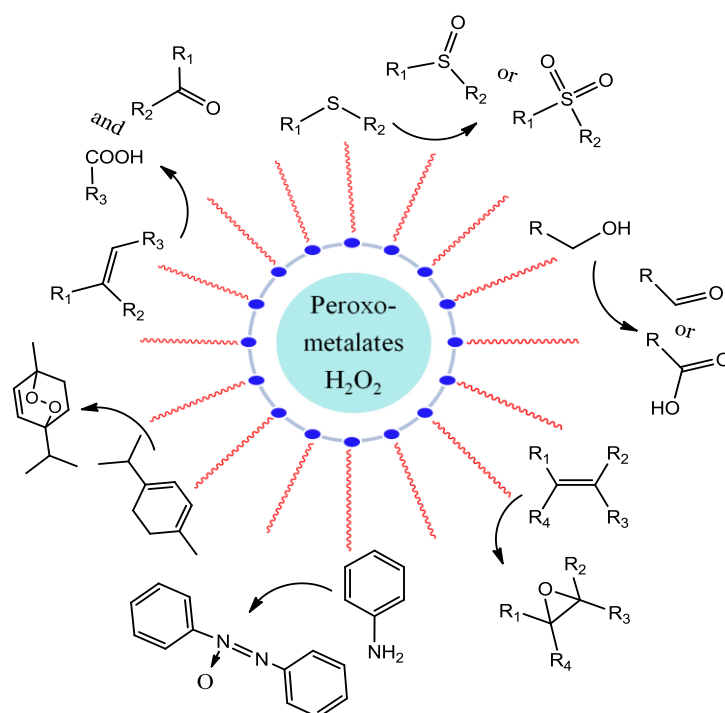


**Figure 1.13** Oxidations catalyzed by tungsten and molybdenum peroxometalates.

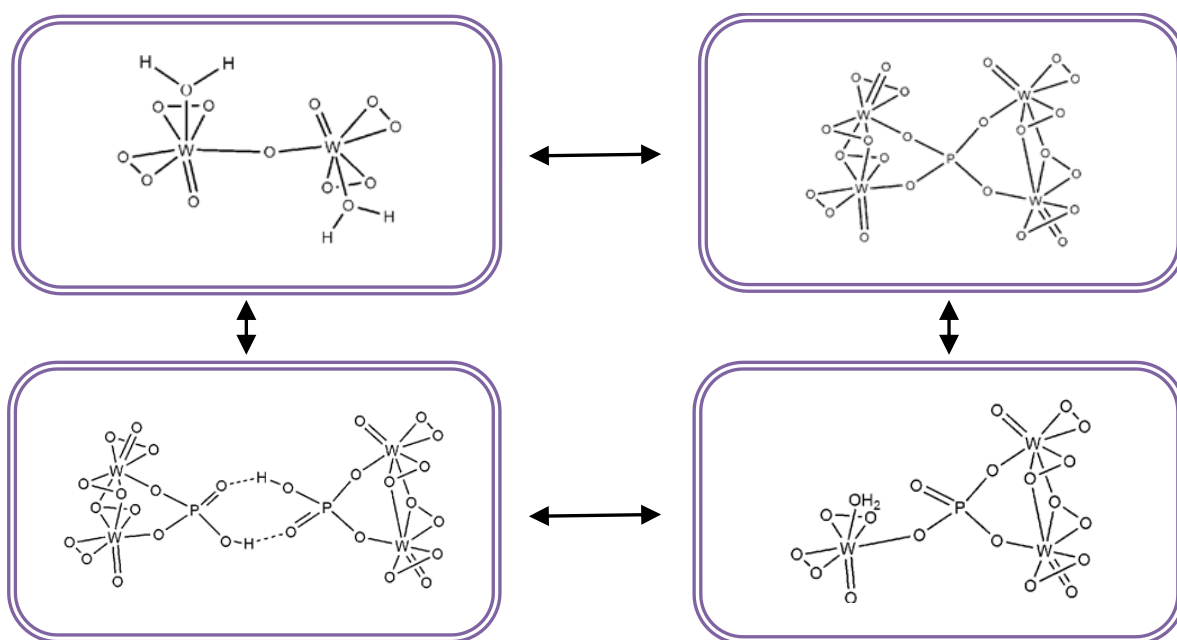


**Figure 1.14** Proposed active species in the peroxometalate catalytic reactions.<sup>100,102,103</sup>

### 1.2.2.1 Cationic surfactant-combined polyoxometalates (POMs) in catalytic reactions

The solubility of polyoxometalates (POMs) can be controlled by simply variation of their counter-cations, for example, the acid form and alkali salts are soluble in water while the ammonium salts are insoluble. On the other side, the alkyl substituted ammonium salts are soluble in apolar solvents and the perfluoroalkyl substituted ammonium salts are soluble in fluoruous solvents.<sup>99</sup> The combination of appropriate surfactant parts with POMs widely enlarges their application in oxidation while the micelle or  $\mu\text{em}$  formation also overcomes the immiscibility between organic substrates and hydrophilic  $\text{H}_2\text{O}_2$ . The catalytic activity and selectivity can also be improved by tuning the number and length of the alkyl groups in the ammonium counterpart.

The ultra-deep desulfurization is an environmental urgent subject due to strict emission control standards in the recent stringent regulation which limits the sulfur level in diesel to less than 15 ppm.<sup>99</sup> Besides the environmental consideration, the ultra-deep desulfurization is also important for producing sulfur free hydrogen from diesel for fuel cell system, in which the precious metal catalysts and electrodes can be irreversibly poisoned by sulfur.<sup>104</sup> The dibenzothiophene (**DBT**) and its derivatives are most refractory sulfur-containing molecules existing in diesel and cannot be removed by conventional hydrodesulfurization (**HDS**). On the contrary, the oxidative ultra-deep desulfurization is a powerful strategy. In this context, the oxidative desulfurization (**ODS**) catalyzed by several different surfactant-combined polyoxometalates has been reported by Li *et al.* (**Table 1.3**).<sup>105-108</sup> The alkyl chains of the ammonium counter cations not only affect the catalytic activity by forming hydrophobic droplets but also determinethe recycling of the catalyst and separation of the products.

**Table 1.3** Surfactant-combined polyoxometalate catalyzed oxidative desulfurization.<sup>105-108</sup>

Catalysts	Oil phase	Sulfur level (ppm)	Cat. (%)/Sulfur H <sub>2</sub> O <sub>2</sub> (equiv.)	Temp(°C)/Time (min)	Final Sulfur level (ppm)
[DiC <sub>18</sub> ] <sub>3</sub> PW <sub>12</sub> O <sub>40</sub>	Prehydrotreated diesel	500	0.3%/1 2.6	30/80	< 0.1
[DiC <sub>18</sub> ] <sub>4</sub> H <sub>2</sub> NaPW <sub>10</sub> O <sub>36</sub>	Prehydrotreated diesel	500	1.4%/1 3	r.t./60	<0.1
[C <sub>16</sub> ] <sub>4</sub> W <sub>10</sub> O <sub>32</sub>	Diesel	1078	1%/1 3	60/30	70.1
[C <sub>18</sub> ] <sub>5</sub> Na <sub>2</sub> [PW <sub>11</sub> O <sub>39</sub> ]	Decane	1000	2%/1 3	30/60	20
[C <sub>18</sub> ] <sub>7</sub> PW <sub>11</sub> O <sub>39</sub>	Gasoil	1236	0.6%/1 4	30/180	65

The combination of an appropriate hydrophobic surfactant part with a polyoxometalate anion such as PW<sub>12</sub>O<sub>40</sub><sup>3-</sup> is crucial to obtain a metastable emulsion, which directly determines the reaction rate and the recycling of the catalyst.<sup>105</sup> For example, [p-C<sub>5</sub>H<sub>5</sub>N(C<sub>16</sub>H<sub>33</sub>)<sub>3</sub>][PW<sub>12</sub>O<sub>40</sub>] generates a very stable W/O emulsion and demixion after the reaction is impossible and [(C<sub>8</sub>H<sub>17</sub>)<sub>4</sub>N]<sub>3</sub>[PW<sub>12</sub>O<sub>40</sub>] does not form an emulsion and gives a very low activity, while a metastable emulsion is formed with [(C<sub>18</sub>H<sub>37</sub>)<sub>2</sub>N(CH<sub>3</sub>)<sub>2</sub>]<sub>3</sub>[PW<sub>12</sub>O<sub>40</sub>] in the presence of H<sub>2</sub>O<sub>2</sub>. The emulsion is then readily demulsified after simple centrifugation, the catalyst precipitates and can be reused for the next cycle of ODS process, while the sulfone in the oil phase is removed by extraction with a polar solvent such as 1-methyl-2-pyrrolidinone. For the lacunary [H<sub>2</sub>NaPW<sub>10</sub>O<sub>36</sub>]<sup>4-</sup>, [(C<sub>18</sub>H<sub>37</sub>)N(CH<sub>3</sub>)<sub>3</sub>] gives a higher catalytic activity than [(C<sub>18</sub>H<sub>37</sub>)<sub>2</sub>N(CH<sub>3</sub>)<sub>2</sub>].

As mentioned previously, some polyoxometalates were easily degraded into peroxometalates, which were real active species in the catalytic system, in the presence of H<sub>2</sub>O<sub>2</sub>.<sup>102</sup> For [C<sub>18</sub>]<sub>5</sub>Na<sub>2</sub>PW<sub>11</sub>O<sub>39</sub>, H<sub>2</sub>O<sub>2</sub> degrades the lacunary Keggin anion PW<sub>11</sub>O<sub>39</sub><sup>7-</sup> much quickly than Keggin structure anion PW<sub>12</sub>O<sub>40</sub><sup>3-</sup> in decane and gives much better catalytic activity. On the other side, the coordination of several kinds of transition metal cations to the lacunary PW<sub>11</sub>O<sub>39</sub><sup>7-</sup> also obviously blocks the transformation to peroxometalate species due to the formation of more stable substituted intact Keggin structures.

An ionic liquid H<sub>2</sub>O<sub>2</sub>/[C<sub>18</sub>]<sub>7</sub>PW<sub>11</sub>O<sub>39</sub>/[Bmin]PF<sub>6</sub> ([Bmin]PF<sub>6</sub>: 1-Butyl-3-methylimidazolium hexafluorophosphate) emulsion system was used by Zhou *et al.*<sup>109</sup> The sulfur compounds in the oil phase, which is immiscible with the ionic liquid emulsion phase, are extracted into the emulsion phase where they are oxidized to sulfones at the H<sub>2</sub>O<sub>2</sub>/[Bmin]PF<sub>6</sub> interface with [C<sub>18</sub>]<sub>7</sub>PW<sub>11</sub>O<sub>39</sub> which acts both as a catalyst

and a surfactant. At the end of oxidation, the desulfurized oil phase is easily decanted and the emulsion phase is used for the next run and can be recycled for five times without losing activity (**Figure 1.15**).

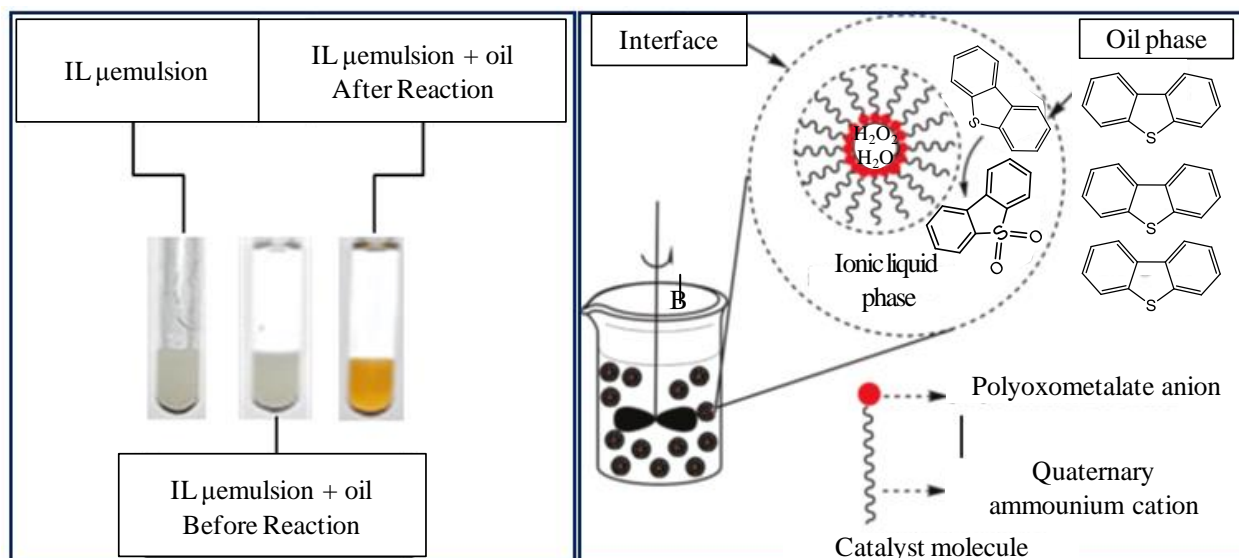
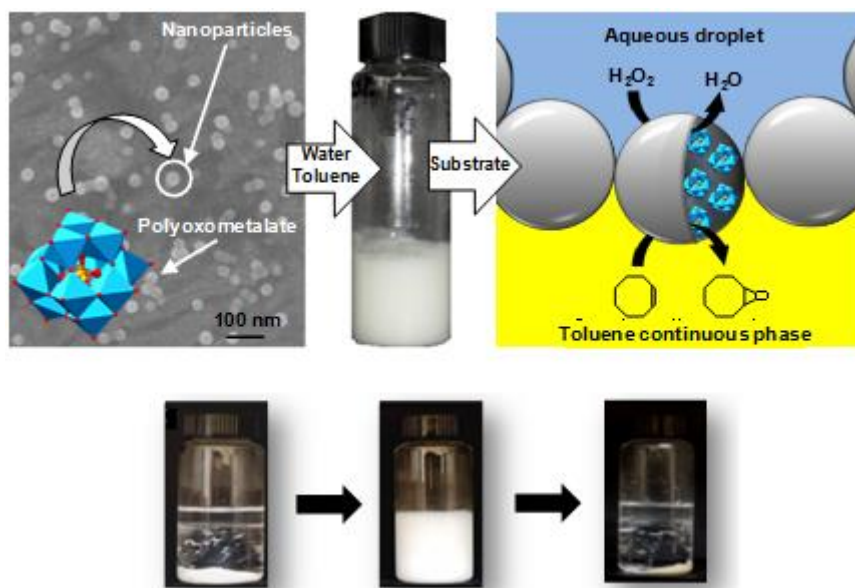


**Figure 1.15** Deep-desulfurization in the  $H_2O_2/[C_{18}]_7PW_{11}O_{39}/[Bmin]PF_6$  ionic liquid emulsion system: left) photos of the catalytic reactions right) model of the catalytic system.<sup>109</sup>

Several surfactant-combined polyoxometalates also catalyze the molecular oxygen oxidized desulfurization.<sup>110-112</sup> However, due to security reasons at high temperature,  $O_2$  is more rarely used in the ODS process. Li *et al.* reported the oxygen oxidation of refractory sulfur compounds at ambient temperature with the  $[(DiC_{18})_2]_5IMo_6O_{24}$  Anderson-type catalyst which contains an  $IO_6$  octahedron surrounded by six  $MoO_6$  groups.<sup>110</sup> The catalytic activity decreases when the hydrophobicity of the surfactant decreases. Although much longer time (12h) is required compared to  $H_2O_2$ , the DBT in decalin could be converted into the corresponding sulfone and completely precipitated.  $C_{18}PW_{10}Ti_2(O_2)_2$ <sup>111</sup> and  $[C_8]_3H_3V_{10}O_{28}$ <sup>112</sup> were also reported as catalysts for similar process requiring however high temperature (90 °C).

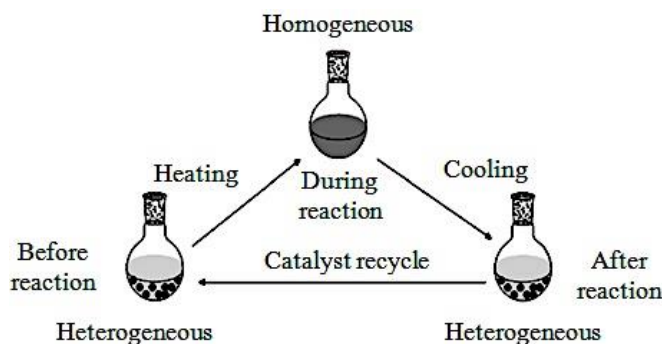
The surfactant combined POMs can also catalyze the oxidation of other types of substrates, such as alcohols, alkenes, amines, etc. besides refractory sulfides. Our group reported the epoxidation of several substrates in a Pickering emulsion system stabilized by  $[C_{12}]_3PW_{12}O_{40}$  nanoparticles.<sup>15</sup> By screening the biphasic water/aromatic system in the presence of  $[C_n]_3PW_{12}O_{40}$  ( $n = 6-16$ ), only  $C_{10}$ ,  $C_{12}$ ,  $C_{14}$  give stable emulsions. The  $[C_{12}]PW_{12}O_{40}$  nanoparticles are relevant regarding the physicochemical properties of the Pickering emulsion including the W/O interface, stability, potential catalytic activity and facile breaking after reaction by centrifugation. The system during the reaction and a schematic representation of the catalytic epoxidation are shown in **Figure 1.16**.





**Figure 1.16** Scheme of the water/toluene/ $[C_{12}]_3[PW_{12}O_{40}]$  system used as a catalytic Pickering emulsion for  $H_2O_2$ -based epoxidation - Pictures of the system before emulsification, during the reaction, and after centrifugation (from left to right).<sup>15</sup>

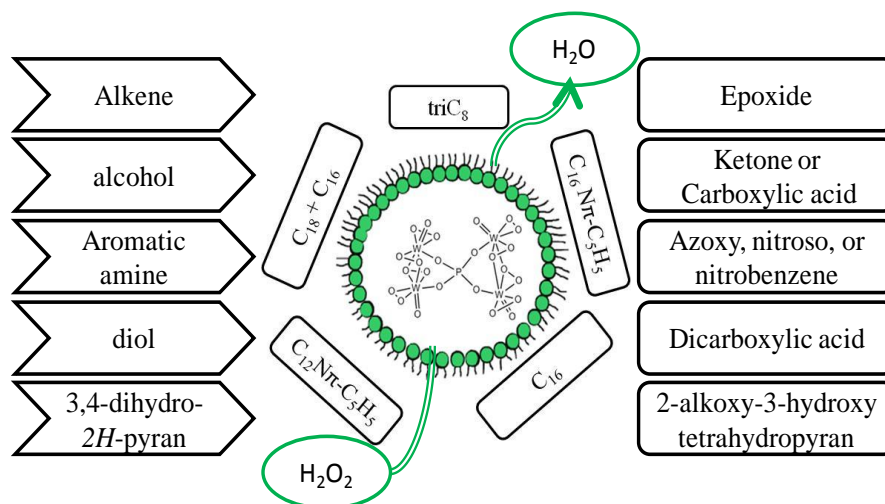
Additionally, some other examples are found in the literature, such as the oxidation of phenols with  $(C_{16}TA)_5PV_2Mo_9O_{40}$ ,<sup>113</sup> the oxidation of pyridine derivatives and alcohols with  $[(C_{18}H_{37})_2(CH_3)_2N]_7[PW_{11}O_{39}]$ ,<sup>114</sup> the epoxidation of alkenes with Ti-substituted  $[C_{12}mim]_5PTiW_{11}O_{40}$ <sup>115</sup> and the oxidation of  $SCN^-$  with  $[C_{16}]_7[PW_{10}Ti_2O_{38}(O_2)_2]$ .<sup>116</sup> Although the length of the alkyl tail of the surfactant counter-cation is crucial for the catalytic performances, the exact mechanism does not work in the same way in the different catalytic systems. In the case of phenol oxidation with  $(C_nTA)_5PV_2Mo_9O_{40}$  ( $n = 8-16$ ), the catalytic activity increases with an increase in length due to the phenol absorption increment in the micelles, while for the heterogeneous catalyst  $[C_{12}mim]_5PTiW_{11}O_{40}$ , the better catalytic activity has been ascribed to not only the hydrophobicity but also the largest BET surface area of  $[C_{12}mim]_5PTiW_{11}O_{40}$  particles compared to the  $C_{16}$  and tetra $C_4$  as counter-cations. Instead of recycling the catalyst by centrifugation,  $[(C_{18}H_{37})_2(CH_3)_2N]_7[PW_{11}O_{39}]$  can be precipitated, recycled and reused by cooling after the reaction when 1,4-dioxane is used as a solvent (**Figure 1.17**).



**Figure 1.17** Temperature-controlled  $[(C_{18}H_{37})_2(CH_3)_2N]_7[PW_{11}O_{39}]$  catalytic system.<sup>115</sup>

### 1.2.2.2 Cationic surfactant-combined peroxometalates in catalytic reactions

Since in the case of Keggin type or lacunary polyoxotungstate and molybdate, the active species are peroxometalates resulting from the degradation in the presence of  $\text{H}_2\text{O}_2$ , the combination of pre-prepared and isolated peroxometalates with surfactants directly has also been widely reported for the oxidation of various substrates. Tetrahexylammoniumtetrakis(diperoxotungsto)phosphate [ $\text{tetraC}_6$ ] $\{[\text{PO}_4[\text{WO}(\text{O}_2)_2]_4]\}^{3-}$  has been firstly well characterized and the high catalytic activity of  $\{[\text{PO}_4[\text{WO}(\text{O}_2)_2]_4]\}^{3-}$  was confirmed in several catalytic systems by combination with various surfactant parts as indicated in **Figure 1.18**.<sup>117-123</sup> The earlier reported biphasic catalytic system involves the use of toxic organic solvents such as chloroform, dichloroethane and benzene. Although the desired product can be obtained in considerable yields by controlling the amount of  $\text{H}_2\text{O}_2$ , pH, temperature *etc.*, the effect of the hydrophobic surfactant part on the reaction and the recycling of the catalyst are rarely reported.<sup>117-121</sup> With dodecylpyridinium as a counter-cation and ethyl acetate as a solvent, although the conversion of the epoxidation of alkene is slightly lower than with trioctylmethylammonium as a counter-cation and dichloroethane as a solvent, the former is a much environmentally-friendly system and furthermore, the catalyst can be recycled by cooling after the reaction and reused for several times.<sup>117,123</sup>

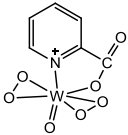
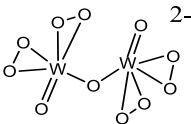
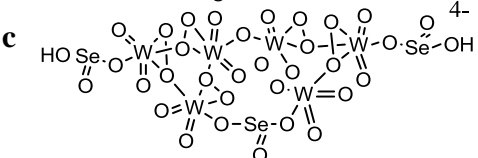


**Figure 1.18** Surfactant combined catalyst based on  $\{[\text{PO}_4[\text{WO}(\text{O}_2)_2]_4]\}^{3-}$  and their applications.<sup>117-123</sup>

Besides tetrakis(diperoxotungsto)phosphate ( $\{[\text{PO}_4[\text{WO}(\text{O}_2)_2]_4]\}^{3-}$ ), several surfactant-combined peroxometalates based on other types of active species have been prepared and applied to the emulsion or  $\mu\text{em}$  catalytic oxidative desulfurization processes (**Table 1.4**).<sup>124-126</sup> For the peroxometalate (**a**) in **Table 1.4**, the shorter length of alkyl group does not form a metastable emulsion. Although the desired metastable emulsion system is obtained with  $\text{C}_{18}$  as a counter-cation, the recovery yield of the catalyst is much lower than with  $\text{diC}_{18}$ .<sup>124</sup> When peroxotungstate (molybdate) (**b**) combined with trioctylmethyl ammonium, a new functionalized ionic liquid is obtained and in the presence of  $\text{H}_2\text{O}_2$ , the DBT derivatives in the model oil are oxidized in the ionic liquid/model oil/ $\text{H}_2\text{O}_2$  emulsion system. At the end

of the reaction, the ionic liquid is self-separated from the emulsion and can be reused.<sup>126</sup> For the  $[\text{C}_{18}]_4[\text{H}_2\text{Se}_3\text{W}_6\text{O}_{34}]$  (c), the addition of acetonitrile in the diesel gives better results than  $\text{H}_2\text{O}$  or without additional phase. The DBT is almost completely converted into  $\text{DBTO}_2$  and precipitates during the reaction.<sup>125</sup>

**Table 1.4** Several pre-prepared surfactant-combined peroxometalates in the ODS process.<sup>124-126</sup>

Surfactant	Peroxometalate counter-part	Removal of DBT (%)
$[\text{diC}_{18}]$	<b>a</b> 	98.0
$[\text{triC}_8]_2$	<b>b</b> 	96.2
$[\text{C}_{18}]_4$	<b>c</b> 	99.9

As shown in **Figure 1.14**, the different active species can transform to each other and generally several different peroxometalates coexist in the same catalytic system, the *in situ* generated peroxometalates are preferred than pre-prepared ones by mixing the amphiphilic tungstate (or molybdate),  $\text{H}_2\text{O}_2$  and appropriate additives. The most well-known environmentally-friendly systems are the combination of  $\text{Na}_2\text{WO}_4$  with  $[\text{triC}_8]\text{HSO}_4$  in the presence of  $\text{H}_2\text{O}_2$ . Different substrates can be oxidized into the desired product with or without co-catalyst (**Figure 1.19**).<sup>127-131</sup>

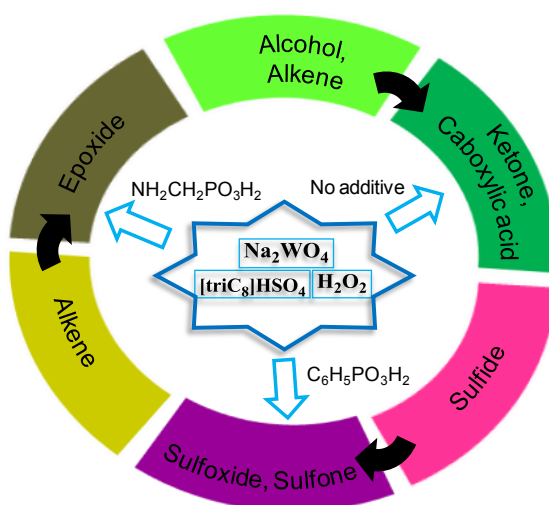


**Figure 1.19** The *in situ* generated peroxometalate systems proposed by Noyori *et al.* and their applications to oxidation reactions with different co-catalysts.<sup>127-131</sup>

All these reactions have been carried out without using toxic organic solvents. In the absence of co-catalyst, primary and secondary alcohols can be converted to the desired carboxylic acids and ketones in high yields; the former requires 3 equivalents  $\text{H}_2\text{O}_2$  and 2 mol% catalyst loading, while the latter only needs 1.1 equivalent  $\text{H}_2\text{O}_2$  and 0.2 mol% catalyst. Under suitable conditions, the benzylic alcohols can even be oxidized to the aldehyde stage.<sup>127</sup> Under similar condition with 4.4 equivalents  $\text{H}_2\text{O}_2$ , cyclohexene is converted directly to shiny, colorless, analytically pure crystalline adipic acid in 90% yield at 90 °C for 8h, the product is separated by filtration and the aqueous phase is reused with a renewed  $[\text{triC}_8]\text{HSO}_4$  and  $\text{H}_2\text{O}_2$  (**Figure 1.20**).<sup>128</sup>

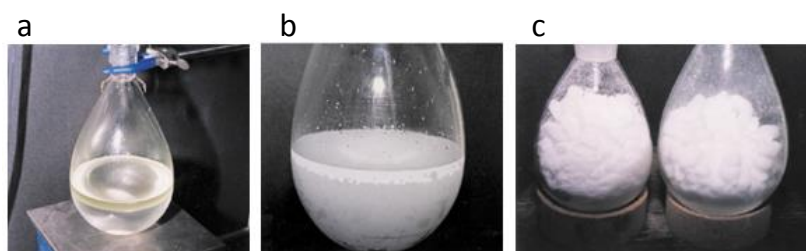


**Figure 1.20** Direct conversion of cyclohexene to adipic acid. (a) reaction mixture. (b) product. (c) adipic acid.<sup>128</sup>

Although the combination of  $\text{Na}_2\text{WO}_4$  and  $(\text{C}_8\text{H}_{17})_3\text{NCH}_3\text{HSO}_4$  is not effective for the epoxidation of alkenes, in the presence of aminomethylphosphonic acid, the reaction proceeds smoothly even with the poorly active terminal alkenes as substrates.<sup>129,130</sup> Various alkenes have thus been oxidized into epoxides in good yield with ratio of olefin:  $\text{H}_2\text{O}_2$  :  $\text{Na}_2\text{WO}_4$  :  $(\text{C}_8\text{H}_{17})_3\text{NCH}_3\text{HSO}_4$  :  $\text{NH}_2\text{CH}_2\text{PO}_3\text{H}_2$  = 100: 150: 2: 1: 1. For acid stable epoxides, the introduction of toluene improves the selectivity to epoxide. On the other side, the addition of phenylphosphonic acid is much more effective than  $\text{NH}_2\text{CH}_2\text{PO}_3\text{H}_2$  for the epoxidation of sulfides.<sup>131</sup>

In addition to the systems reported by Noyori et al., several other amphiphilic *in situ* generated peroxometalates have also been investigated. For example, the biphasic system based on  $\text{H}_2\text{WO}_4/\text{H}_2\text{O}_2\text{-H}_2\text{O}/[\text{triC}_8]\text{H}_2\text{PO}_4/\text{toluene}$  was applied to the epoxidation of various alkenes and the catalyst could be reused for 5 times without loss of activity. The acid-sensitive epoxide such as limonene epoxide could be also obtained in high yield and selectivity in the presence of  $\text{H}_2\text{PO}_4^-/\text{HPO}_4^{2-}$ .<sup>132</sup> A gemini surfactant, **diethyl-ether- $\alpha,\omega$ -bis-(dimethyldodecylammoniummolybdate)** abbreviated as **12-EO-12-Mo** (**Figure 1.21**), has also been prepared by our group.<sup>28</sup> After the detailed investigation of its physicochemical properties such as Krafft temperature, critical micelle concentration, surface activity and binary water-surfactant behavior, an efficient Winsor I dark singlet oxygen oxidation  $\mu\text{em}$  system was obtained.  $\alpha$ -Terpinene which reacts with  $^1\text{O}_2$  according to a [4 + 2] cycloaddition and  $\beta$ -citronellol which provides two hydroperoxides according to the ene-reaction are efficiently oxidized with this catalytic system which not only increases the efficiency of hydrogen peroxide but also provides a  $\mu\text{em}$  system which facilitates the separation of product and the recycling of the catalyst.

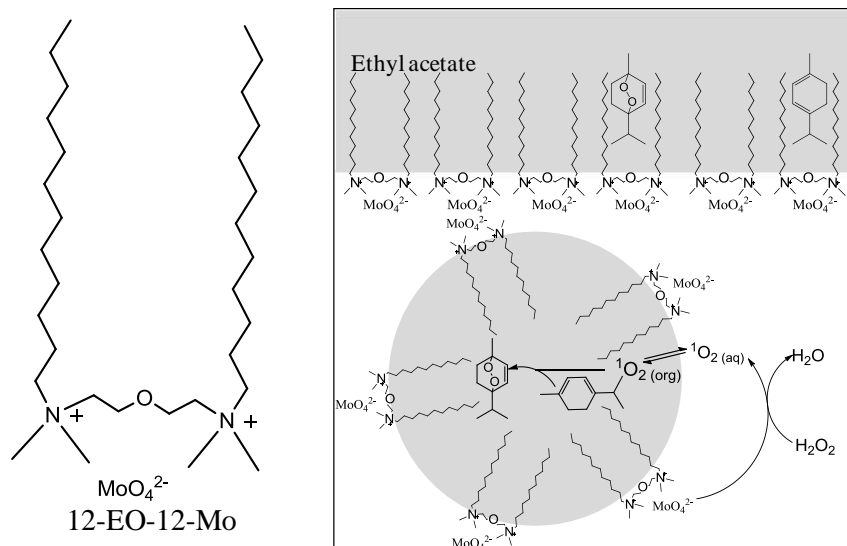


**Figure 1.21** 12-EO-12-Mo catalyzed dark  $^1\text{O}_2$  oxidation in a Winsor I  $\mu\text{em}$  system.<sup>28</sup>

Furthermore, a more elegant three-phase  $\mu\text{em}$  catalytic system based on amphiphilic molybdate has been developed by our group.<sup>29</sup> The triphasic  $\mu\text{em}$  (also called Winsor III system) catalytic system was also applied to the dark singlet oxygenation. It has been shown that if the conventional phase transfer reagent  $(\text{C}_4\text{H}_9)_4\text{NBr}/\text{NaMoO}_4$  system is used, most of the  $^1\text{O}_2$  is deactivated by water because of the large distance between the  $^1\text{O}_2$  generated and the substrate. The three-phase  $\mu\text{em}$  catalytic system overcomes this drawback with additional advantages compared to the traditional catalytic reactions (**Figure 1.22**). The presence of a double chain in the catalytic surfactant is a key parameter for the formation of a Winsor III  $\mu\text{em}$ , at room temperature, without addition of salts or cosurfactants due to its appropriate packing parameter ( $\approx 1$ ). By adjusting the chain length of the hydrophobic part of the surfactant moiety, a green solvent like *tert*-BuOAc can also be used as the oil phase. The catalytic species is located in the middle phase  $\mu\text{em}$  and the immiscibility problem of organic substrate with aqueous  $\text{H}_2\text{O}_2$  is thus resolved.

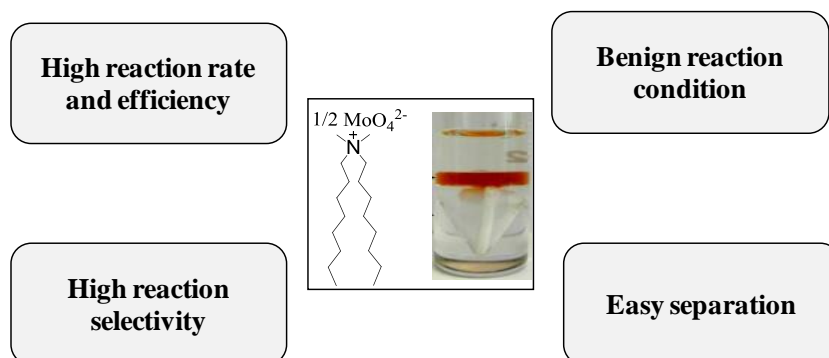


**Figure 1.22** Advantages of “optimal” three-liquid-phase  $\mu\text{em}$  system based on a “Balanced Catalytic Surfactant.”<sup>29</sup>

Besides the above mentioned surfactant combined polyoxometalates or peroxometalates as catalysts for various reactions, there are a lot of other cationic surfactant catalysts with various hydrophobic parts or different catalytic counterions such as the sandwich type polyoxometalate  $[\text{WZnMn}_2(\text{H}_2\text{O})_2(\text{ZnW}_9\text{O}_{34})_2]^{12-}$  combined with polyfluorinated alkylmethylammonium leading to a thermomorphic catalyst (phase behavior is controlled by temperature) with ethyl acetate and toluene as organic phases.<sup>133</sup> In such systems, polyfluorinated thermomorphic catalysts are soluble in hydrocarbons at elevated temperatures but are immiscible at lower temperatures, allowing the separation by precipitation of the catalyst from the product and solvent phase by cooling the reaction mixture. Other similar examples are listed in **Appendix B**.

Instead of combining a catalyst and an amphiphilic moiety through an ionic electrostatic interaction, catalytic surfactants can also be realized by directly covalent binding of a polyoxometalate with an organic hydrophobic part.<sup>134</sup> For example, one or two  $\text{C}_{18}$  chains have been grafted to the hexavanadate cluster by esterification reaction between stearic acid and  $[(\text{C}_4\text{H}_9)_4\text{N}]_2[\text{V}_6\text{O}_{13}\{(\text{OCH}_2)_3\text{CCH}_2\text{OH}\}_2]$  (**Figure 1.23**) The tetrabutylammonium counterions can be replaced by proton or sodium by ion exchange. Their amphiphilic properties were confirmed by observation of vesicles formation in aqueous solution by TEM and CMC measurements. The catalytic oxidation of thiophene was successfully carried out in the emulsion system with these hybrid hexavanadate cluster and hexane as model oil. The stability of the emulsion was controlled by the pH: very low pH neutralized the charge of cluster and caused the collapse of emulsion.

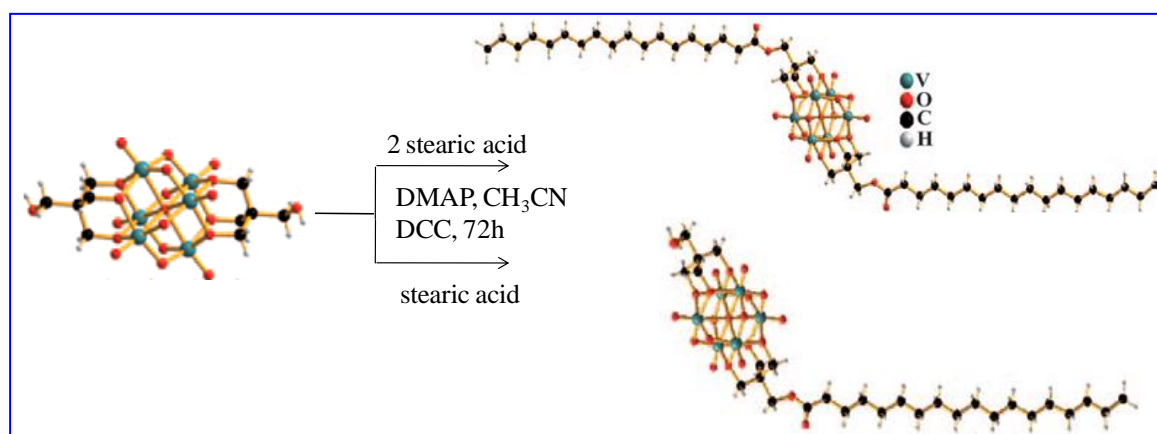


**Figure 1.23** Synthesis of stearic acid grafted hexavanadate; DCC = 1,3-dicyclohexylcarbodiimide, DMAP = 4-dimethylaminopyridine.<sup>134</sup>

Advantages of surfactant-combined catalysts in micellar solution has also been demonstrated through the sulfide oxidation using  $[\text{C}_{16}]\text{HCO}_3^-$  as a catalyst.<sup>135</sup> Indeed, in the presence of  $\text{H}_2\text{O}_2$ ,  $\text{HCO}_3^-$  is in equilibrium with the peroxy monocarbonate  $\text{HCO}_4^-$ , which oxidizes sulfides. Based on the pseudo-phase model (**Figure 1.24**), the second-order rate constants in the Stern layers for sulfide oxidation have been estimated to ~50-fold (for PhSEtOH) and ~180-fold (for PhSEt), higher than the reaction at the micelle



surface, while lower than the corresponding values in water by 20-70 times, but the high local concentration of active  $\text{HCO}_4^-$  and substrate in the micelle results in the net increase of the reaction rate.

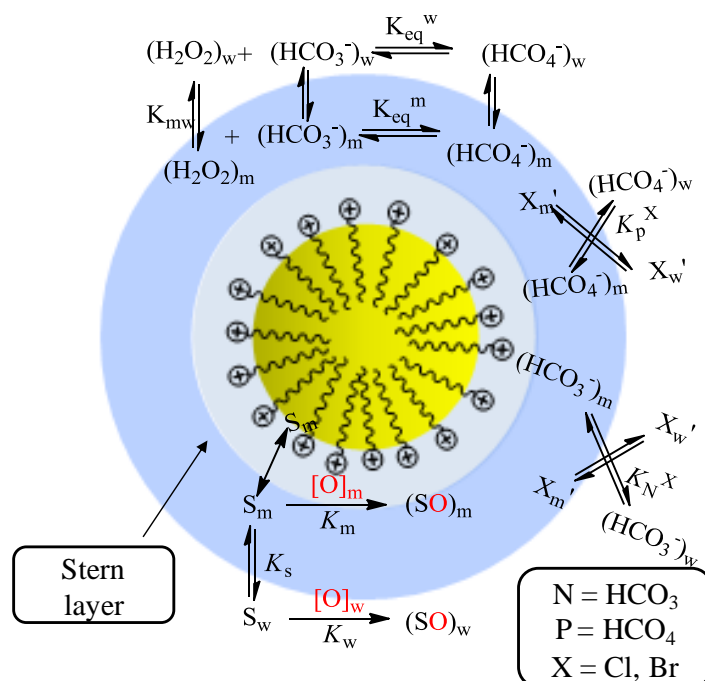


**Figure 1.24** Pseudo-phase model for bicarbonate-activated peroxide oxidations in aqueous cationic micelles; Reactants are distributed rapidly between water and micelles. Kinetic treatments are based on the assumption that reactions occur in both the Stern layer and the bulk aqueous medium.<sup>135</sup>

### 1.2.2.3 The physicochemical properties of the cationic surfactant-combined catalysts

Physicochemical properties of cationic surfactant-combined catalysts have been little investigated. They can be roughly summarized into pictures of emulsion droplets (or micelles) obtained by microscopy or TEM while other important properties like CMC, binary phase diagram and emulsion or  $\mu\text{em}$  phase behavior are rarely reported.<sup>15,28,113,136</sup>

We can however find a detailed study of a series of alkyltrimethylammonium dichromate, tungstate and molybdate, prepared from  $[\text{C}_n]\text{Br}$  ( $n = 10, 12, 14, 16, 18$ ), and their physicochemical properties have been investigated with different techniques, including XRD, TGA-DSC, surface pressure ( $\pi$ )-area (A) measurement, tensiometry, conductimetry and DLS.<sup>137</sup> The dichromate surfactants are poorly soluble in water and form Langmuir monolayer at the air-water surface. The  $\pi$ -A isotherms of dichromate surfactants are given in **Figure 1.25** and show a strong dependence on the hydrophobic chain length. The area lift-off  $A_0$ , which indicates the surface pressure, starts rising from zero, increases linearly with the chain length.

Surfactant	Solubility (mmol·L <sup>-1</sup> )	A <sub>0</sub> (A <sub>min</sub> ) (nm <sup>2</sup> ·mol <sup>-1</sup> )	Π <sub>c</sub> (mN·m <sup>-1</sup> )
[C <sub>10</sub> ] <sub>2</sub> Cr <sub>2</sub> O <sub>7</sub>	0.198	1.30 (0.98)	25
[C <sub>12</sub> ] <sub>2</sub> Cr <sub>2</sub> O <sub>7</sub>	0.144	1.50 (1.02)	30
[C <sub>14</sub> ] <sub>2</sub> Cr <sub>2</sub> O <sub>7</sub>	0.065	1.65 (1.06)	34
[C <sub>16</sub> ] <sub>2</sub> Cr <sub>2</sub> O <sub>7</sub>	0.023	1.80 (1.12)	37
[C <sub>18</sub> ] <sub>2</sub> Cr <sub>2</sub> O <sub>7</sub>	0.012	2.00 (1.21)	42

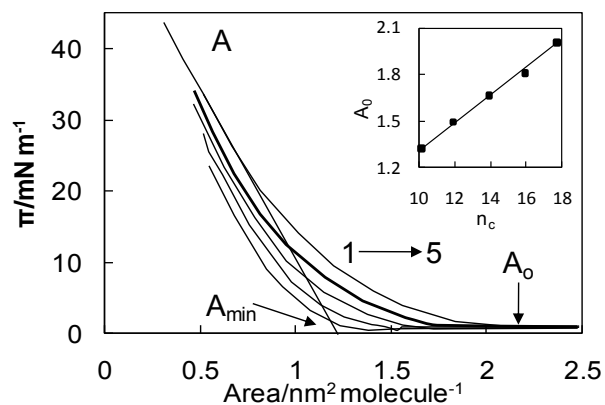


**Figure 1.25** Surface pressure ( $\pi$ )–area ( $A$ ) isotherm of solvent spread  $[C_n]_2Cr_2O_7$  monolayers at the air–water interface at 303 K.  $n = 10; 12; 14; 16, 18$ . Inset: Variation of lift-off area ( $A_0$ ) with the alkyl chain length of the complexes. Compression rate:  $4.36 \text{ \AA}^2 \cdot \text{molecule}^{-1} \cdot \text{min}^{-1}$ .<sup>137</sup>

On the other side, the CMC of water soluble  $[C_n]_2MoO_4$  and  $[C_n]_2WO_4$  ( $n = 12, 14, 16$ ) has been measured by tensiometry, conductimetry and microcalorimetry. Molybdate and tungstate surfactants have similar CMC values with the same chain length; this CMC decreases dramatically with the increase of chain length. The binding extent of counterions follows the order  $C_{12} > C_{14} > C_{16}$  for both tungstate and molybdate surfactants. The surface excess absorption  $\Gamma_{\max}$  and minimum area of headgroup  $A_{\min}^{Gibbs}$  can be deduced from the surface tension ( $\gamma$ )-concentration curve. All the results including the thermodynamic analysis of micelle formation and interfacial absorption, DLS and zeta potential are given in **Table 1.5**.

**Table 1.5** Micellar and energetic parameters of molybdate and tungstate complexes in water at 303K.<sup>137</sup>

CS <sup>a</sup>	CMC (mmol·L <sup>-1</sup> )			$10^{-6}\Gamma_{\max}$ (mol·m <sup>-2</sup> )	$A_{\min}^{Gibbs}$ (nm <sup>2</sup> ·mol <sup>-1</sup> )	$-\Delta G_m^{\ominus b}$ (kJ mol <sup>-1</sup> )	$-G_{ad}^{\ominus c}$ (kJ mol <sup>-1</sup> )	$\beta^d$	$d_h^e$ (nm) (PDI)	$\xi^f$ (mV)
	$\Gamma^g$	$\sigma^h$	$\mu cal^i$							
[C <sub>12</sub> ] <sub>2</sub> MoO <sub>4</sub>	7.32	7.58	7.25	1.50	1.10	38.7	62.7	0.72	3.1 (0.119)	20.7
[C <sub>14</sub> ] <sub>2</sub> MoO <sub>4</sub>	1.44	1.58	1.50	1.34	1.25	44.2	74.1	0.67	3.9 (0.354)	34.4
[C <sub>16</sub> ] <sub>2</sub> MoO <sub>4</sub>	0.24	0.25	–	1.18	1.41	48.2	86.3	0.55	5.7 (0.590)	50.0
[C <sub>12</sub> ] <sub>2</sub> WO <sub>4</sub>	7.04	7.10	7.01	1.48	1.12	40.0	68.3	0.77	2.9 (0.164)	15.8
[C <sub>14</sub> ] <sub>2</sub> WO <sub>4</sub>	1.15	1.23	–	1.35	1.23	46.6	77.8	0.72	5.9 (0.376)	25.2
[C <sub>16</sub> ] <sub>2</sub> WO <sub>4</sub>	0.21	0.20	–	1.14	1.45	52.9	90.9	0.68	9.1 (0.491)	37.7

<sup>a</sup> CS: Catalytic surfactant; <sup>b</sup>  $\Delta G_m^{\ominus}$ : standard Gibbs free energy change of micellization per mole of monomer unit; <sup>c</sup>  $\Delta G_{ad}^{\ominus}$ : standard Gibbs energy of absorption at the interface; <sup>d</sup>  $\beta$ : fraction of counter ions bound to the micelle; <sup>e</sup>  $d_h$  (PDI): mean diameter of micelles (polydispersity index); <sup>f</sup>  $\xi$ : Zeta potential values; CMC determined by <sup>g</sup>: conductimetry, <sup>h</sup>: tensiometry, <sup>i</sup>: microcalorimetry.



Understanding the physicochemical behavior of surfactant-combined catalyst is crucial to design the appropriate and efficient catalytic systems. As an example, with the amphiphilic polyoxometalate, stable Pickering emulsions could be elaborated and optimized based on the results obtained from SEM, TEM, DLS, SAXS analyses of the nanoparticles and on emulsion stability analysis by multiple light scattering coupled with vertical scanning.<sup>15</sup>

In the last decade, our group has focused on the application of  $\mu\text{em}$  systems based on double chain quaternary ammonium surfactant for oxidation reactions and the related surfactant-combined surfactants were also investigated from a physicochemical point of view. Packing parameter  $P = v/al$  (where  $v$ ,  $a$ ,  $l$  are alkyl chain volume swollen with oil, headgroup area, and alkyl chain length respectively), which reflects the geometry of the surfactant molecule, allows determining the aggregation types of the surfactants. For "Balanced Catalytic Surfactants (BCS)" leading to optimal three-phase  $\mu\text{em}$  systems,  $P$  equal to 1 is required to obtain the zero curvature of the interfacial film in the bicontinuous  $\mu\text{em}$ . The screening of different oils to elaborate  $[\text{DiC}_n]_2\text{MoO}_4/\text{H}_2\text{O}/\text{oil}$  ( $n = 8, 9, 10, 12$ )  $\mu\text{em}$  systems shows that the choice of the oil is also closely related to the length of the alkyl chain of the surfactant moiety.<sup>138</sup> The surfactant with longer alkyl chain required more hydrophobic oil which less penetrates in the surfactant aggregates to maintain  $P = 1$ . The results are shown in **Table 1.6**.

**Table 1.6** Microemulsion systems as a function of the chain length ( $n$ ) of the catalytic surfactant  $[\text{DiC}_n]_2\text{MoO}_4$  (5 wt%) and oil hydrophobicity at 25 °C (water-to-oil ratio = 1/1 (v/v)).<sup>138</sup>

n	C <sub>6</sub> H <sub>6</sub> or AcOPr	Xylene or AcOt-Bu	Pentene	Octane
8	Winsor III			
9		Winsor III		Winsor I
10		Winsor II	Winsor III	
12				Winsor III

The aggregation process of  $[\text{DiC}_8]\text{Cl}$  at the dilute aqueous solution was proposed based on the various experimental and theoretical techniques: zetametry, conductimetry, tensiometry, NMR, and molecular modeling.<sup>139</sup> Dimers form at very low concentration (below  $\text{CAC}_1 = 10\text{mM}$ ), then more complex bilayer structures by increasing the concentration and finally, after  $\text{CAC}_2$  (30mM), concentration of bilayers gives vesicles. Furthermore, the counterion effect of eight  $\text{DiC}_8$  salts including  $\text{DiC}_8\text{MoO}_4$  and  $\text{DiC}_8\text{MoO}_4$  on the phase behavior in dilution aqueous solutions was also investigated.<sup>31</sup> Three different behaviors were unveiled depending on the counter-anions by tensiometry, conductimetry,  $\text{DiC}_8$ -selective electrode measurement and confirmed by SANS and DLS analysis. For salting-out anions ( $\text{MoO}_4^{2-}$ ,  $\text{WO}_4^{2-}$ ,  $\text{F}^-$ ,  $\text{SO}_4^{2-}$ ), the micellization occurs at specific concentration, while for salt-in anions ( $\text{Br}^-$ ,  $\text{NO}_3^-$ ), dimers

are formed before micelles. For the anions between salting-in and salting-out anions ( $\text{Cl}^-$ ,  $\text{MeSO}_3^-$ ), two successive aggregations occur after dimers formation (**Figure 1.26**).

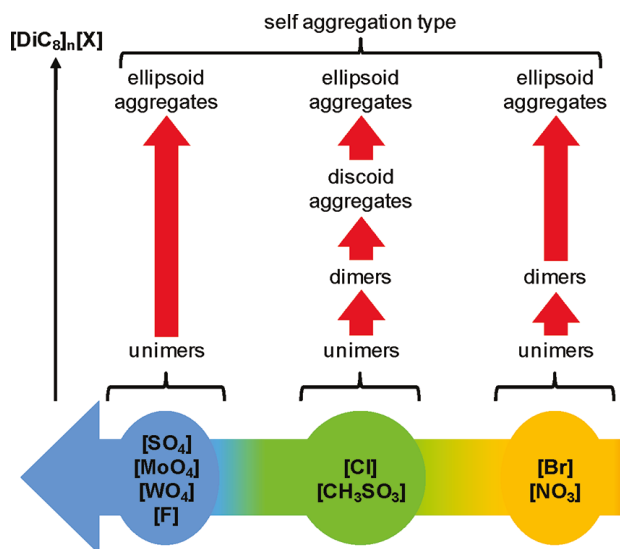


**Figure 1.26** Self-aggregations of  $[\text{DiC}_8]_n$  in water as a function of the  $[\text{DiC}_8]_n[\text{X}]$  concentration.<sup>31</sup>

### 1.3 Conclusion

Although various strategies have been reported to fulfill the principles of green chemistry in catalytic reactions, such as immobilization of catalyst on porous solids, usage of ionic liquid or other green solvents instead of common used organic solvent *etc.*, the disadvantages like low catalytic activity or high price of reagents still limit their widely application. The combination of surfactant and catalyst moieties incorporates the advantages of homogenous catalyst (high activity, high solubility, *etc*) and heterogeneous catalyst (easily separation of product, recycling of catalyst *etc.*). The water-solubilization of hydrophobic substrates by the aggregates and large interface area ensure the high catalytic activity; the separation of hydrophobic and hydrophilic part enhances the selectivity and the easily controlled phase behavior facilitates the separation of product and recovery of catalyst.

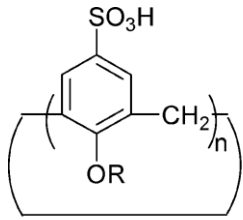
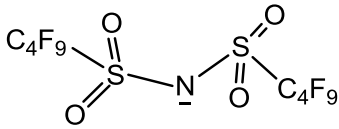
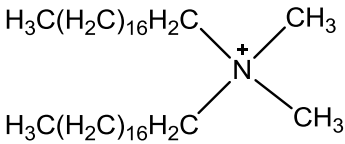
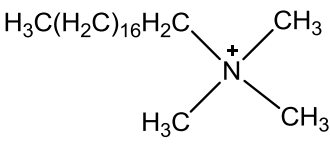
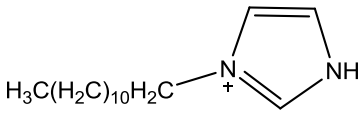
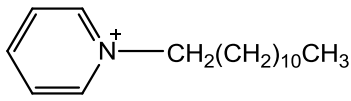
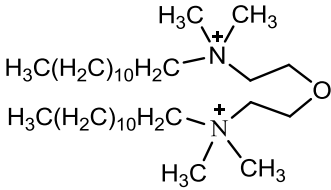
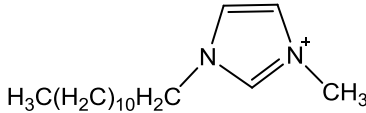
Most of the surfactant-combined catalysts belong to two groups: Lewis acid or Brønsted acid-anionic surfactant combined catalysts (LASCs or BASCs) and polyoxometalate or peroxometalate-cationic surfactant combined catalysts. Among the LASCs, the scandium dodecylsulfate ( $\text{Sc}(\text{DS})_3$ ) is the most widely used catalyst in catalytic reaction in aqueous media, although other types of amphiphilic catalysts such as  $\text{Cu}(\text{DS})_2$ ,  $\text{Zn}(\text{DS})_2$ , *etc.* can also be used and in some cases, better results are obtained. The reactions with LASCs as catalysts include the conventional Lewis acid catalyzed carbon-carbon formations reactions (*e.g.* Aldol reaction, Mannich reaction and Friedel-Craft reaction, *etc*) and with the BASCs as catalysts, the dehydration reactions including etherification, esterification, thioetherification and dithioacetalization proceed readily in aqueous phase. The reactions can be considered taking place in

the micelles which solubilize the hydrophobic substrates in the hydrophobic core in the absence of additional organic solvents.

The polyoxometalates and peroxometalates, especially derived from tungstate and molybdate, are widely applied to the oxidation of organic substrates with  $\text{H}_2\text{O}_2$  or  $\text{O}_2$  as oxidants. The active species in the presence of  $\text{H}_2\text{O}_2$  have been investigated by NMR, IR, and Raman analysis, *etc.* As shown in **Figure 1.14**, the different species can be converted to each other and even converted to polyoxometalates. Various surfactant-combined polyoxometalates are successfully applied to the oxidative desulfurization (ODS) process. The refractory sulfur compounds in model oil or real diesel can be removed at more than 99% and the catalysts can be recycled by simple centrifugation. The oxidation process occurs in the emulsion interface after the addition of  $\text{H}_2\text{O}_2$  in the oil in the presence of amphiphilic catalysts. Other oxidation reactions such as epoxidation, oxidation of alcohol, and oxidative cleavage of alkene *etc.* can be also catalyzed by polyoxometalates or pre-prepared peroxometalates, while the *in situ* generated peroxometalate mixtures are generally preferred. The *in situ* generated peroxometalates by combination of  $\text{triC}_8[\text{HSO}_4]$ ,  $\text{Na}_2\text{WO}_4$ , appropriate co-catalyst and  $\text{H}_2\text{O}_2$  are efficient catalysts for the oxidation of alcohols, epoxidation of alkenes, oxidative cleavage of alkenes to carboxylic acid and oxidation of sulfides in aqueous phase.

The physicochemical properties of the amphiphilic catalysts are rarely reported, although the phase behavior of amphiphilic catalysts in the catalytic systems is closely related to the activity, selectivity and work-up of the reactions. The early research gave the basic physicochemical properties (Krafft points and CMCs) of several LASCs mentioned in this chapter, the further investigation were not carried out. The alkyltrimethyl ammonium tungstate and molybdate physicochemical properties of cationic surfactant combined catalysts have been studied by several techniques. Dialkyldimethylammonium tungstate, molybdate and related bromide and chloride have been investigated by our group. Especially the properties of double chain ammonium salts in binary and ternary systems lead us successfully to elaborate the elegant three-liquid-phase  $\mu\text{em}$  systems stabilized with “Balanced Catalytic Surfactants”.

## Appendix A: Structures of the abbreviations.

Abbreviation	Structure	Abbreviation	Structure
<b>DS</b>	$\text{CH}_3(\text{CH}_2)_{10}\text{CH}_2\text{OSO}_3$	<b>n-C<sub>12</sub>SO<sub>3</sub></b>	$\text{CH}_3(\text{CH}_2)_{10}\text{CH}_2\text{SO}_3$
<b>OPf</b>	$\text{CF}_3(\text{CF}_2)_6\text{CF}_2\text{SO}_3$	<b>PFOSA</b>	$\text{CF}_3(\text{CF}_2)_2\text{CF}_2\text{SO}_3$
<b>Calix[n]arene sulfonic acid</b>		<b>NNf<sub>2</sub></b>	
<b>DiC<sub>18</sub></b>		<b>C<sub>18</sub></b>	
<b>N-C<sub>12</sub>imidazolium</b>		<b>C<sub>5</sub>H<sub>5</sub>NC<sub>12</sub></b>	
<b>C<sub>12</sub>(EO)<sub>2</sub>C<sub>12</sub></b>		<b>C<sub>12</sub>mim</b>	

**Appendix B: Application of Lewis acids and Brønsted acid-combined surfactant catalysts**

Catalytic surfactants	Reactions	References
<b>Sc(DS)<sub>3</sub></b>	Aldol reaction	40,52,53,63,140,141
	Mannich reaction	53
	Synthesis of β-amino phosphonate	55
	Michael reaction	53,56
	Friedel-Crafts reaction	58
	Asymmetric ring-opening of epoxide	57,142,143
	Allylation reaction	63
	Diels-Alder reaction	52
	Hydroxymethylation	54,144
	Nazarov-type reaction	145
	Friedländer annulations	61
	Synthesis of β-amino amides	146
	Synthesis of (+)-madindoline A and B	62
	Polyester synthesis	147
<b>Sc(<i>n</i>-C<sub>11</sub>SO<sub>3</sub>)<sub>3</sub></b>	Asymmetric ring-opening of epoxide	148
	Hydroxymethylation	54
<b>Sc(<i>n</i>-C<sub>12</sub>SO<sub>3</sub>)<sub>3</sub></b>	Aldol reaction	63
	Allylation reaction	63
	Aldol reaction	52,149
	Asymmetric ring-opening of epoxide	67
<b>Sc(C<sub>4</sub>F<sub>9</sub>OSO<sub>3</sub>)<sub>3</sub></b>	Diels-Alder reaction	150
<b>Sc(OPf)<sub>3</sub></b>	Baylis-Hillman reaction	151
	Mannich reaction	65,152
	Ring-opening of epoxide	153

	Aldol reaction	154
	Friedel-Crafts reaction	64,155
	Diels-Alder reaction	150,156,157
	Nitration of aromatic compounds	158
	Synthesis of 3-oxabicyclo[3.1.0]hexanederivatives	159,160
<b>Sc(NNf<sub>2</sub>)<sub>3</sub></b>	Ring-Opening Polymerization of ε-Caprolactone	161
	Polyester synthesis	162
<b>Cu(DS)<sub>2</sub></b>	Asymmetric Aldol reaction	52,63,66
	Asymmetric ring-opening of epoxide	67
	Mannich reaction	53
	Diels-Alder reaction	52,163
	Thioactalization	164
	Allylation	63,165
	Esterification	166
<b>Cu(n-C<sub>12</sub>SO<sub>3</sub>)<sub>3</sub></b>	Aldol reaction	52
	Benzaldehyde from Benzyl alcohol	167
	Synthesis of phenol from benzene	70
<b>Zn(DS)<sub>2</sub></b>	Asymmetric ring-opening of epoxide	67
	Esterification	166
	Diels-Alder reaction	163
<b>Zn(n-C<sub>12</sub>SO<sub>3</sub>)<sub>2</sub></b>	Aldol reaction	52
<b>Zr(DS)<sub>4</sub></b>	Epoxide ring-opening	168
	Michael reaction	169
	Preparation of bis-indolyl and tris-indolylmethanes	170
	Synthesis of quinolines	171
	Synthesis of quinoxalinederivatives	69
<b>Cr(DS)<sub>3</sub></b>	5-hydroxymethylfurfural formation from cellulose	172

<b>Fe(DS)<sub>3</sub></b>	Synthesis of chromeno[4,3-b]chromene derivatives	173
<b>Fe(n-C<sub>12</sub>SO<sub>3</sub>)<sub>3</sub></b>	Benzaldehyde from Benzyl alcohol	167
	Synthesis of 3-(9H-Xanthen-9-yl)-1H-indole Derivatives	174
	Synthesis of bis-indolyl methane	175
	Synthesis of phenol from benzene	70,176
<b>Ce(DS)<sub>3</sub></b>	Esterification	166
<b>Yb(DS)<sub>3</sub></b>	Synthesis of (+)-madindoline A and B	62
	Synthesis of febrifugine and isofebrifugine	68
<b>Yb(n-C<sub>12</sub>SO<sub>3</sub>)<sub>3</sub></b>	Aldol reaction	52
<b>Yb(OPf)<sub>3</sub></b>	Aldol reaction	154
	Friedel-Crafts reaction	177
<b>In(n-C<sub>12</sub>SO<sub>3</sub>)<sub>3</sub></b>	Synthesis of 3-(9H-Xanthen-9-yl)-1H-indole Derivatives	154
<b>DBSA</b>	Mannichreaction	72,77,178
	Dehydration (esterification, etherification, thioetherification, thioacetalization)	71,76,179-181
	Nucleophilic substitution of alcohol	182
	Pyridone synthesis (Diels-Alder reaction)	77
	Thiazolidinone synthesis	74
	3,4-dihydropyrimidin-2-ones synthesis	73
	Polyesterification	147
<b>Calix[n]arene sulfonic acid</b>	Substitution of allylic alcohol	80
<b>Cellulose-SO<sub>3</sub>H</b>	Synthesis of naphth[1,2-e][1,3] oxazin-3-one	183
<b>Polystyrene-SO<sub>3</sub>H</b>	Hydrolysis of thioesters and transprotection of thiols	82
	Mannich reaction	184
<b>PFOSA</b>	Pictet–Spengler reaction	75,81

## Appendix C: Cationic surfactant-combined polyoxometalate and peroxometalate catalysts

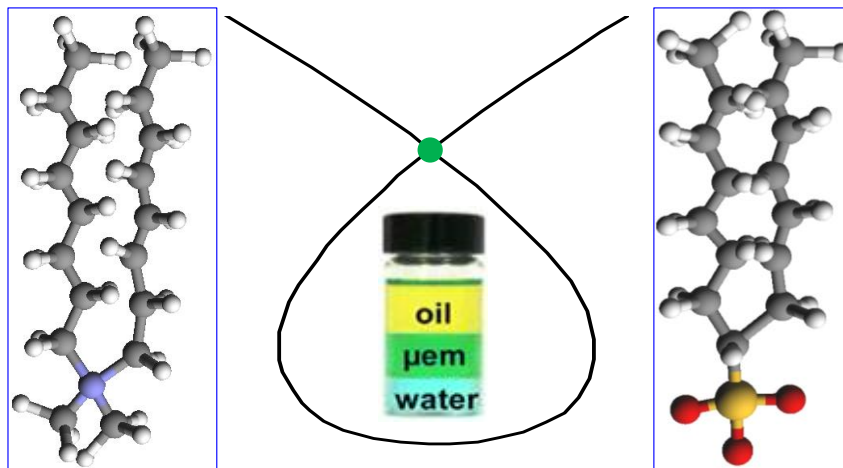
Catalyst	Reaction	References
[DiC <sub>18</sub> ] <sub>3</sub> [PW <sub>12</sub> O <sub>40</sub> ]	Oxidative desulfurization	105
[C <sub>18</sub> ] <sub>4</sub> [H <sub>2</sub> NaPW <sub>10</sub> O <sub>36</sub> ]		106
[DiC <sub>18</sub> ][W(O)(O <sub>2</sub> ) <sub>2</sub> (C <sub>5</sub> H <sub>4</sub> NCO <sub>2</sub> )]		124
[C <sub>18</sub> ] <sub>5</sub> [PV <sub>2</sub> Mo <sub>10</sub> O <sub>40</sub> ]		136
[C <sub>16</sub> ] <sub>4</sub> [W <sub>10</sub> O <sub>32</sub> ]		185
[DiC <sub>18</sub> ] <sub>5</sub> [IMo <sub>6</sub> O <sub>24</sub> ]		110
[C <sub>18</sub> ] <sub>5</sub> Na <sub>2</sub> [PW <sub>11</sub> O <sub>39</sub> ]		108
[C <sub>18</sub> ] <sub>7</sub> [PW <sub>11</sub> O <sub>39</sub> ]		109
[C <sub>18</sub> ] <sub>4</sub> [H <sub>2</sub> Se <sub>3</sub> W <sub>6</sub> O <sub>34</sub> ]		125
[C <sub>18</sub> ] <sub>7</sub> [PW <sub>10</sub> Ti <sub>2</sub> O <sub>38</sub> (O <sub>2</sub> ) <sub>2</sub> ]		111
[triC <sub>8</sub> ] <sub>2</sub> [Mo <sub>2</sub> O <sub>11</sub> ]		126
[C <sub>8</sub> ] <sub>3</sub> [H <sub>3</sub> V <sub>10</sub> O <sub>28</sub> ]		112
[DiC <sub>18</sub> ] <sub>7</sub> [PW <sub>11</sub> O <sub>39</sub> ]		186
Na <sub>2</sub> WO <sub>4</sub> + [triC <sub>8</sub> ]HSO <sub>4</sub> + C <sub>6</sub> H <sub>5</sub> PO <sub>3</sub> H <sub>2</sub>		131
[C <sub>16</sub> ] <sub>4</sub> [W <sub>10</sub> O <sub>32</sub> ]		185
[DiC <sub>18</sub> ] <sub>8</sub> [HBW <sub>11</sub> O <sub>39</sub> ]	Oxidation of pyridine	187
[DiC <sub>18</sub> ] <sub>7</sub> [PW <sub>11</sub> O <sub>39</sub> ]		114
[DiC <sub>18</sub> ] <sub>9</sub> [EuW <sub>10</sub> O <sub>36</sub> ]	Oxidation of alcohol	107
{Tri[C <sub>8</sub> F <sub>17</sub> (CH <sub>2</sub> ) <sub>3</sub> ]} [WZn <sub>3</sub> (H <sub>2</sub> O) <sub>2</sub> (ZnW <sub>9</sub> O <sub>34</sub> ) <sub>2</sub> ]		133
Na <sub>2</sub> WO <sub>4</sub> + [triC <sub>8</sub> ]HSO <sub>4</sub>		127
[C <sub>16</sub> ] <sub>3</sub> [PW <sub>12</sub> O <sub>40</sub> ]		188
[TriC <sub>8</sub> ] <sub>3</sub> [PW <sub>4</sub> O <sub>24</sub> ]		118
	Oxidation of aldehyde	118



	Oxidation cleavage of alkene	119
	Epoxidation–alcoholysis of cyclic enol ethers	122
	Epoxidation of alkene	117
$[\text{C}_{16}]_6[\text{PV}_3\text{Mo}_9\text{O}_{40}]$	Oxidation of phenol	113
$[\text{C}_{16}]_7[\text{PW}_{10}\text{Ti}_2\text{O}_{38}(\text{O}_2)_2]$	Oxidation of thiocyanate	116
$[\text{C}_{16}]\text{H}_2\text{PW}_{12}\text{O}_{40}$	Hydrolysis of polysaccharides	189
$[\text{C}_5\text{H}_5\text{N C}_{16}]_3[\text{PW}_{12}\text{O}_{40}]$	Oxidation 1, 2-vic diol	190
	Oxidation alcohol	101
		101,120
$\{\text{Tri}[\text{C}_8\text{F}_{17}(\text{CH}_2)_3]\}_{12}$ $[\text{WZnMn}_2(\text{H}_2\text{O})_2(\text{ZnW}_9\text{O}_{34})_2]$		133
$[\text{triC}_8]_{12}[\text{WZn}_3(\text{ZnW}_9\text{O}_{34})_2]$		191
$[\text{C}_5\text{H}_5\text{NC}_{12}]_3[\text{PW}_4\text{O}_{32}]$		123
$[\text{DiC}_{18}]_3\text{PW}_4\text{O}_{32}$		192
$\text{H}_2\text{WO}_4 + [\text{triC}_8]\text{H}_2\text{PO}_4$	Epoxidation of alkene	132
$[\text{C}_{12}\text{mim}]_5[\text{PTiW}_{11}\text{O}_{40}]$		115
$[\text{C}_{12}]_3[\text{PW}_{12}\text{O}_{40}]$		15
$[\text{C}_{10}]_{11}[\text{La}(\text{PW}_{11}\text{O}_{39})_2]$		193
$\text{Na}_2\text{WO}_4 + [\text{triC}_8]\text{HSO}_4 +$ $\text{NH}_2\text{CH}_2\text{PO}_3\text{H}_2$		129,130
$[\text{N-C}_{12}\text{imidazolium}][\text{W}_2\text{O}_{11}]$		194
$[\text{C}_{18}]_4[\text{PMo}_{11}\text{VO}_{40}]$	Oxidation of benzy alcohol to benzaldehyde	195
$[\text{C}_{12}(\text{EO})\text{C}_{12}]\text{MoO}_4$	Diels-Alder reaction and ene reaction with $^1\text{O}_2$	28
$[\text{DiC}_{18}]_6[\text{Mo}_7\text{O}_{24}]$	Oxidation of cyclohexane to adipic acid	196
$[\text{C}_5\text{H}_5\text{N C}_{16}]_3[\text{PW}_4\text{O}_{24}]$	Oxidation of aromatic amine	121
$[\text{C}_{16}][\text{H}_4\text{TiPW}_{11}\text{O}_{40}]$	Esterification	197
$\text{Na}_2\{\text{V}_6\text{O}_{13}$ $[(\text{OCH}_2)_3\text{CCH}_2\text{OCC}_{12}]_2\}$	Thiophene oxidation	134
$[\text{C}_{16}]\text{HCO}_3$	Sulfide oxidation	135



## CHAPTER 2: Preparation and Physicochemical Properties of Cationic and Anionic Catalytic Surfactants (Catasurfs)





## 2.1 Double-chain alkylammonium catalytic surfactants

### 2.1.1 Cationic surfactant applications and recent investigations on double-chain quaternary ammonium amphiphiles for “Catasurf” design

Surfactants are organic compounds with amphiphilic properties, due to their hydrophobic tail and hydrophilic head groups. They dramatically lower the surface tension of liquids or the interfacial tension between two immiscible liquids or at the liquid-solid interface. Depending on the hydrophilic head groups, the surfactants can be classified into four types, namely nonionic, anionic, cationic and zwitterionic surfactants. Nowadays, the global production of surfactants is estimated at 15 millions tons each year and the market share of different types of surfactants is shown in **Figure 2.1**.<sup>198</sup> The market share of cationic surfactants is only about ten percents. Cationic surfactant plays an important role in many industrial areas, especially in the formulation of disinfectants, fabric softeners and conditioners because of their ability to absorb onto to negatively charged surface.<sup>199-203</sup>

**Market Share of Different Types of Surfactants 2010**

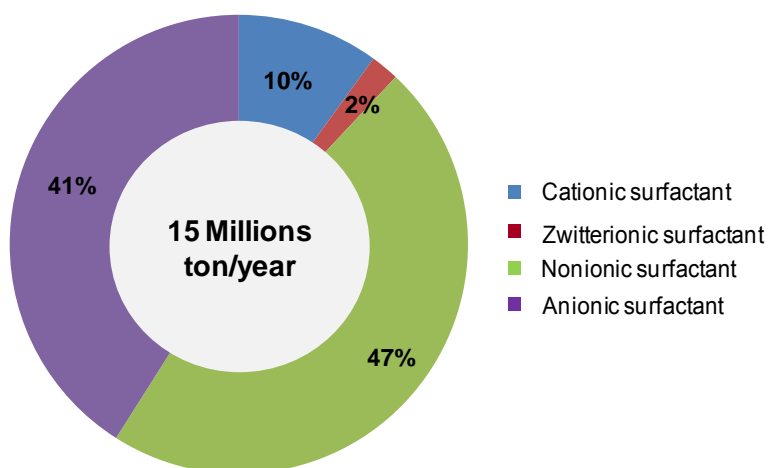


**Figure 2.1** The market share of different types of surfactants in 2010.<sup>198</sup>

The commonly used antiseptic benzalkonium chloride is generally available as a 50% solution of dodecyl and tetradecyl isomer mixture. The mechanism of its bactericidal/microbiocidal activity results from its adsorption onto the cell membrane (through electrostatic interactions) followed by the dissociation of the cellular membrane lipid bilayers, which compromises cellular permeability controls and induces leakage of cellular contents, resulted in the disruption of intermolecular interactions. Another important application involves the long-chain aliphatic amines (optionally ethoxylated) and amides, quaternary ammonium salts, which can absorb onto hydrophobic surface (through hydrophobic interactions) and reduce or eliminate static electricity generally caused by the triboelectric effect. Some selected commonly used cationic surfactants and their applications are listed in **Table 2.1**.

**Table 2.1** Selected commercial quaternary alkyl ammonium surfactants and their applications.<sup>204</sup>

Brand name	Alkyl chain	Aspect (25 °C)	Active (%)	Solvent	Main uses
<b>Monoalkyl ammonium chloride</b>					
			$\left[ \begin{array}{c} \text{CH}_3 \\   \\ \text{R}-\text{N}^+-\text{CH}_3 \\   \\ \text{CH}_3 \end{array} \right] \text{Cl}^-$		
<b>Arquad C-50</b>	Coconut	Liquid	50	IsoPrOH/water	
<b>Arquad T-28</b>	Stearyl	Liquid	28	Water	
<b>Arquad T-50</b>	Tallow	Liquid	50	IsoPrOH/water	• Fabric softeners
<b>Arquad T-800</b>	Stearyl	Liquid	50	EtOH/water	• Emulsifiers
<b>Arquad 16-29</b>	Cetyl	Liquid	29	Water	• Antistatics
<b>Arquad 18-63</b>	Stearyl	Viscous liquid	63	IsoPrOH/water	• Disinfectants
<b>Arquad 22-80</b>	Behenyl	Flake	80	EtOH/water	
<b>Dialkyl ammonium chloride</b>					
			$\left[ \begin{array}{c} \text{R} \quad \text{CH}_3 \\ \diagdown \quad / \\ \text{N}^+ \\ / \quad \diagdown \\ \text{R} \quad \text{CH}_3 \end{array} \right] \text{Cl}^-$		
<b>Arquad 210-80E</b>	Decyl	Liquid	80	EtOH/water	• Disinfectants
<b>Arquad 2C-75</b>	Coconut	Liquid			
<b>Arquad 2HP-75</b>	Vegetable Based stearyl	Paste	75	IsoPrOH/water	• Fabric softeners
<b>Arquad 2HT-75</b>	Hydrogenated tallow	Paste			• Emulsifiers
<b>Arquad 2O-75I</b>	Oleyl	Liquid			
<b>Ethoxylated ammonium chloride</b>					
			$\left[ \begin{array}{c} \text{R} \quad (\text{CH}_2\text{CH}_2\text{O})_m\text{H} \\ \diagdown \quad / \\ \text{N}^+ \\ / \quad \diagdown \\ \text{H}_3\text{C} \quad (\text{CH}_2\text{CH}_2\text{O})_n\text{H} \end{array} \right] \text{Cl}^-$		
<b>Ethoquad C/12</b>	Coconut	Liquid	75	IPA/water	• Fabric softeners
<b>Ethoquad O/12</b>	Oleyl				• Antistatic agents
					• Hair conditioners
<b>Other special quaternary salts</b>					
			$\left[ \begin{array}{c} \text{R}_4 \quad \text{R}_3 \\ \diagdown \quad / \\ \text{N}^+ \\ / \quad \diagdown \\ \text{R}_1 \quad \text{R}_2 \end{array} \right] \text{X}^-$		
<b>TBAB-50A</b>	Tetrabutyl bromide				
<b>BTMAC-50</b>	Benzyltrimethyl chloride				• Template and phase transfer catalyst
<b>BTEAC-50</b>	Benzyltriethyl chloride	Liquid	50	Water	
<b>BTBAC-50A</b>	Benzyltributyl chloride				
<b>Lanquat BC-50</b>	Benzalkonium chloride				• Disinfectant

The aggregation type of surfactants in aqueous solution and in water/solvent biphasic system is closely related to its molecular geometry which is rationalized by the packing parameter ( $P = v/a_0l_c$ ), where  $v$  and  $l_c$  are the volume and the chain length, respectively;  $a_0$  is the sectional area of the head group.<sup>205</sup> These parameters, especially  $a_0$ , depend not only on the geometry, given by the van der Waals radii of the atoms, but are sensitive to the experimental conditions (salts, electrostatic interactions, nature of the oil, temperature, pH, *etc.*). Spherical micelles are obtained when  $P \leq 1/3$ , whereas, for  $P$  values between  $1/3$  and  $1/2$ , cylindrical aggregates are formed; surfactants with  $P$  values in the range  $1/2$  to  $1$  always spontaneously form bilayer structures, such as vesicles, disk shape micelles, and liposomes. In the case of a water/surfactant/oil interface, the penetration of the oil into the interfacial layer should be considered and we must talk about the “effective packing parameter” ( $P_{\text{eff}}$ ).<sup>206</sup> When  $P_{\text{eff}} < 1$ , an oil-in-water  $\mu\text{em}$  (Winsor I) is formed and a water-in-oil  $\mu\text{em}$  (Winsor II) is formed for  $P_{\text{eff}} > 1$ , while if  $P_{\text{eff}} \approx 1$ , a balanced middle-phase  $\mu\text{em}$  balanced with excess oil and water phase (Winsor III) is the preferred (**Figure 2.2**).

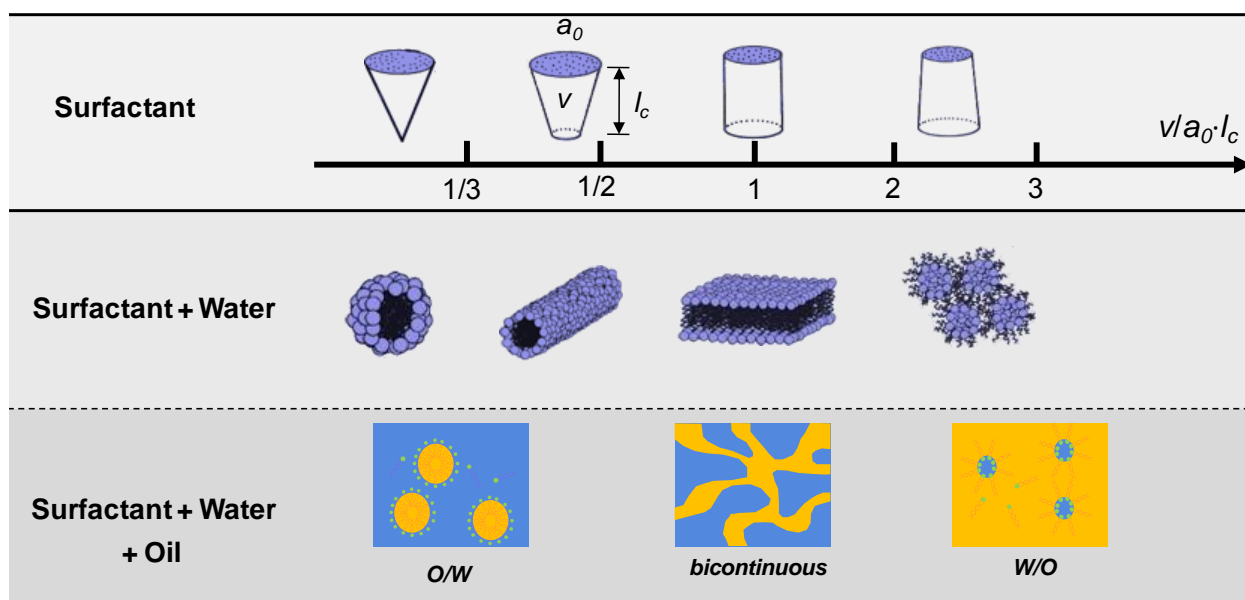


**Figure 2.2** The effect of the surfactant packing parameter on the aggregation and  $\mu\text{em}$  type.

In the last two decades, the dark singlet oxygen generation from hydrogen peroxide catalyzed by mineral compounds was investigated in details by our group.<sup>20,207,208</sup> Molybdate ions were shown to be the most efficient catalysts to induce the disproportionation of  $\text{H}_2\text{O}_2$  since, at appropriate  $\text{H}_2\text{O}_2$ /molybdate ratios and pH values, singlet oxygen,  $^1\text{O}_2$  ( $^1\Delta_g$ ), is quantitatively generated from this chemical source (**Figure 2.3**).<sup>209</sup>

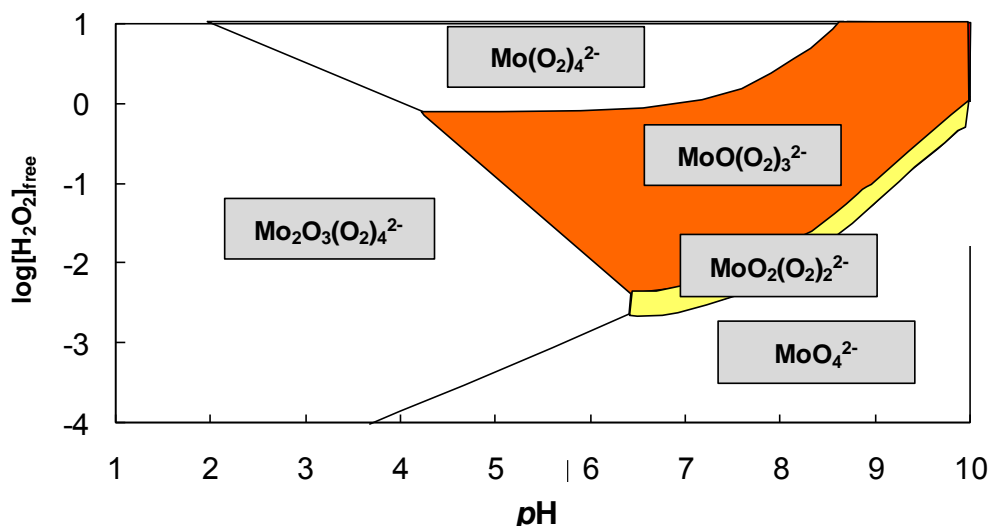


**Figure 2.3** Prevalent species formed by the interaction between  $H_2O_2$  and  $MoO_4^{2-}$  as a function of pH and free  $[H_2O_2]$  ( $T = 0\text{ }^\circ\text{C}$ ,  $[Na_2MoO_4] = 1\text{ M}$ ). The orange region corresponds to the prevalence region of the triperoxomolybdate which is the main precursor of  $^1O_2$ .<sup>209</sup>

The “Catasurf” concept has emerged in 2008 and was initially based on the combination of a dialkyldimethylammonium part with molybdate. When “Balanced”, the catasurf provides, without additional salts or co-surfactant, at room temperature, just in the presence of water and an appropriate solvent, an optimal three-liquid-phase  $\mu\text{em}$  system (Winsor III) which was successfully applied to the dark singlet oxygenation of various substrates.<sup>29</sup> Tungstate ions are also able to disproportionate hydrogen peroxide into singlet oxygen with a 100% yield under neutral or basic conditions, although 3.5 times slower than molybdate ions.<sup>208</sup> On the other side, tungstate was widely used in the catalytic oxidation of organic products (epoxidation, alcohol and sulfide oxidation, etc) with  $H_2O_2$  as an oxidant, as discussed in detail in the first chapter of the manuscript. Based on the above mentioned points, the “Catasurfs” dialkyldimethylammonium molybdate and tungstate, abbreviated as  $[diC_n]_2MoO_4$  and  $[diC_n]_2WO_4$ , respectively (where  $n = 6, 8, 10$ ), were prepared following the method previously reported by our group.<sup>139</sup> The  $[diC_n]_2SO_4$ ,  $[diC_n]Cl$  and  $[diC_n]Br$  homologous were also prepared to compare the effect of the counter ions on the surfactant properties (**Figure 2.4**).

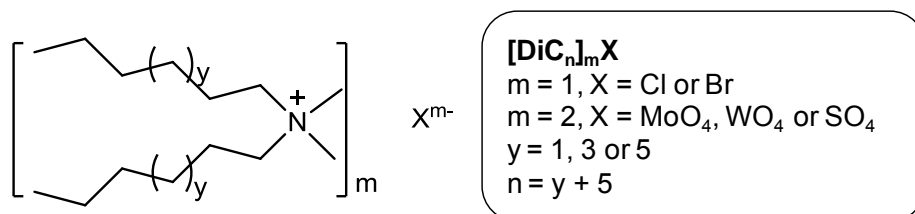


**Figure 2.4** Prepared dialkyldimethylammonium salts with different types of counter ions.

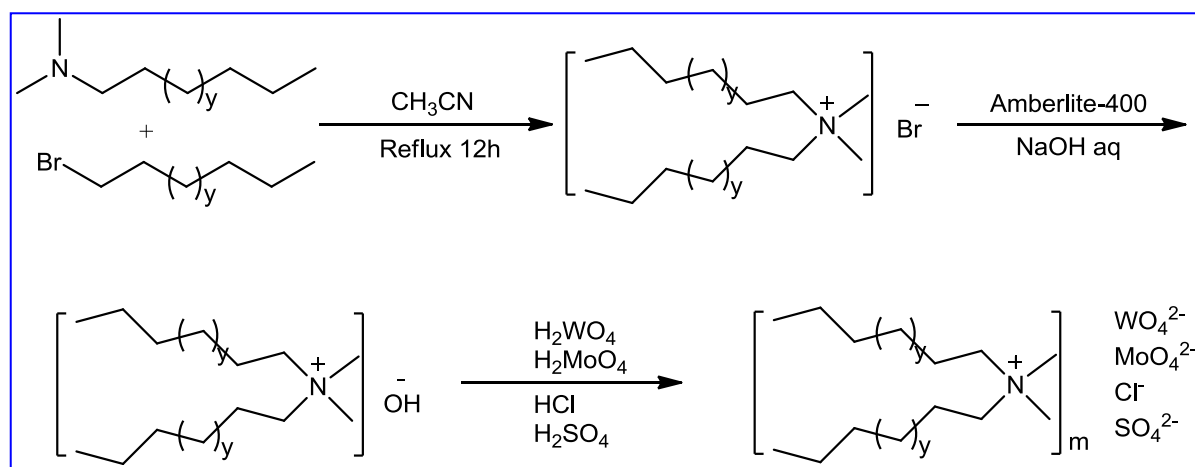
Before investigating the application of the Catasurfs to the oxidation of various organic substrates, the binary and ternary phase behaviors of the molybdate and tungstate based surfactants were studied in



comparison with the corresponding sulfate, chloride and bromide salts. The knowledge of their aggregation properties and the estimation of their amphiphilic character are necessary to predict their ability to form spontaneously three-liquid-phase  $\mu\text{em}$  systems in the presence of given oils. Such triphasic  $\mu\text{ems}$  have been proved to be of interest for hydrogen peroxide-based oxidations especially in terms of recycling and products/catalyst recovery. Developing such systems while extending them to other oxidation reactions and other catalysts was our main goal during these three years.<sup>29</sup> Herein, besides the critical aggregation concentrations (CACs) of surfactants, the aggregation behavior of the short chain dialkyldimethylammonium ( $\text{C}_6$ ,  $\text{C}_8$  and  $\text{C}_{10}$ ) with  $\text{Br}^-$ ,  $\text{Cl}^-$ ,  $\text{SO}_4^{2-}$ ,  $\text{MoO}_4^{2-}$  or  $\text{WO}_4^{2-}$  as counter anions in water from dilute isotropic solutions to high concentrated liquid crystal phases as a function of temperature has also been investigated by means of polarized optical microscopy (POM) and small angle X-ray scattering (SAXS). Furthermore, the phase behavior of the ternary dialkyldimethylammonium/water/solvent systems with terminal monochloroalkane or dichloroalkanes as oil phases has been examined through the construction of the so-called “Fish diagrams” which afforded a classification of the dialkyldimethylammonium amphiphiles according to their relative hydrophilic-lipophilic character, an useful information for the prediction of their ternary phase behavior.<sup>16</sup>

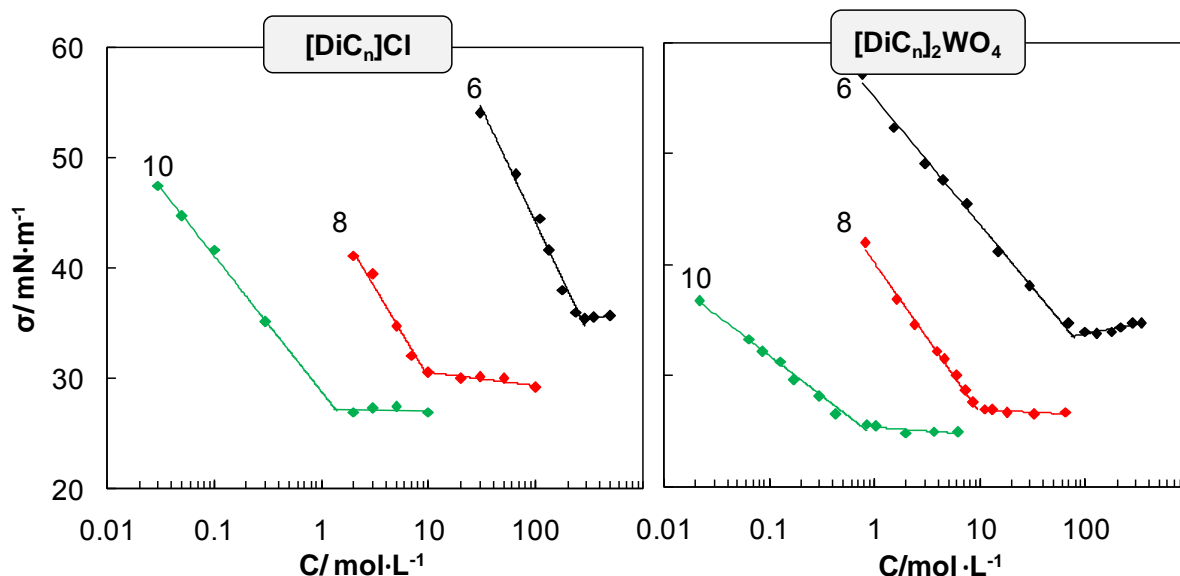
### 2.1.2 Synthesis and CACs of the dialkyldimethylammonium surfactants

All the syntheses were adapted from the methodology developed in our previous work.<sup>139</sup>  $[\text{DiC}_n][\text{Br}]$  was obtained by a  $\text{S}_{\text{N}}2$  reaction involving alkyldimethylamine and 1-alkylbromide ( $n = 6, 8$  and  $10$ ).  $[\text{DiC}_n]_m[\text{X}]^{m-}$  were obtained by two successive ion exchanges from  $[\text{DiC}_n][\text{Br}]$ : (i)  $\text{Br}^-$  was replaced by hydroxide by using the ion exchange resin Amberlite-400 providing the  $[\text{DiC}_n][\text{OH}]$ , and (ii)  $[\text{DiC}_n][\text{OH}]$  reacted with an aqueous solution of the acidic form of the desired counter ions. The aqueous solution of  $[\text{DiC}_n][\text{OH}]$  was neutralized with various acids ( $\text{HCl}$ ,  $\text{H}_2\text{SO}_4$ ,  $\text{MoO}_3$ ,  $\text{H}_2\text{WO}_4$ ) under the protection of argon atmosphere. The products were lyophilized and stocked under dry argon to avoid water absorption since the final compounds are very hygroscopic (**Scheme 2.1**).



**Scheme 2.1** Synthesis of dialkyldimethylammonium surfactants.

Critical aggregation concentration (CAC) is an important and fundamental characteristic of a surfactant, which is defined as the concentration above which the aggregates of the surfactant molecules formed. For a true surfactant, which forms well defined spherical aggregates (*i.e.* micelles) for example, we generally talk about the “critical micelle concentration” or CMC. However, in the present case, the hydrophobic tail of the surfactants are quite short and it is likely that they do not form well define aggregates. Hence, we prefer to talk about “CAC”. Before the CACs, the surface tension changed strongly with the concentration due to the absorption of surfactant molecules at the air-water interface, while reaching the CAC, the surface tension remains relatively constant or changes with a lower slope. The formation of the aggregates in aqueous solution also causes the transition of various solution properties such as conductivity, osmotic pressure, detergency *etc.* Correspondingly, the CAC values can be obtained by measuring these properties of surfactant solutions versus its concentration. Here, all the CACs of the surfactants were determined by measuring the surface tensions with the tensiometer K11 (Krüss) using the Wilhelmy plate method. Ultrapure water (Millipore water,  $\sigma = 72.0 \text{ mN}\cdot\text{m}^{-1}$  at  $25 \text{ }^\circ\text{C}$ ) was used to prepare all the solutions. Surface tension was recorded after equilibration for each mixture. All equilibrium surface tension values were mean quantities of at least three measurements. The standard deviation of the mean never deviated  $\pm 1.5\%$  of the mean. The precision of the force transducer of the surface tension apparatus was  $0.1 \text{ mN}\cdot\text{m}^{-1}$  and before each experiment, the platinum plate was cleaned in red/orange color flame. The temperature was stabilized at  $25 \pm 0.05 \text{ }^\circ\text{C}$  with a thermo-regulated bath Lauda RC6. The standard deviation was estimated at  $\pm 10\%$  for the CAC value. The results were shown in **Figure 2.5** and **Table 2.2**.



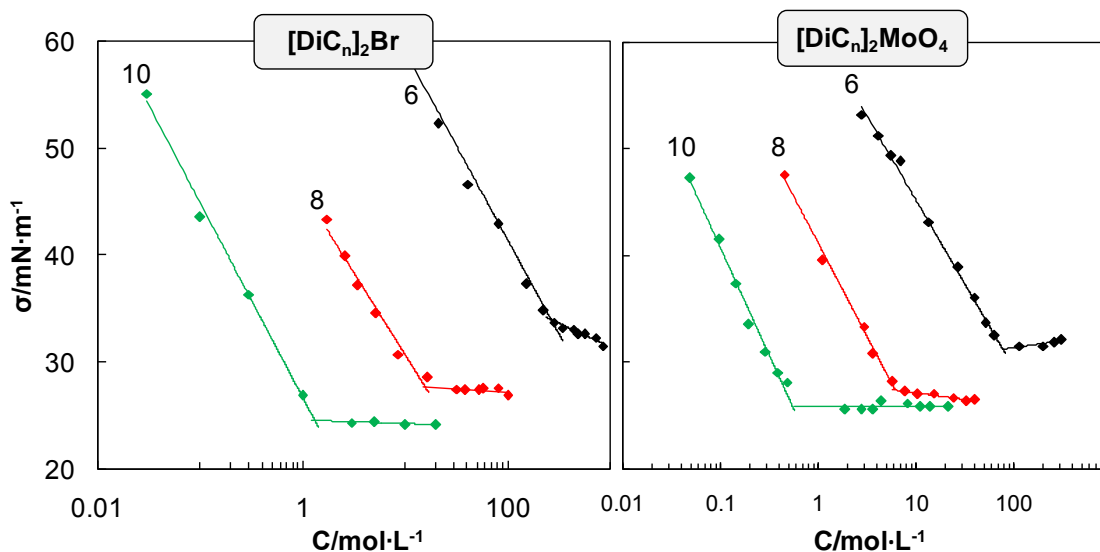


**Figure 2.5** Surface tension ( $\sigma$ ) plotted against surfactant concentration for  $[\text{DiC}_n][\text{X}]$  ( $\text{X} = \text{Cl}$  or  $\text{Br}$ ) and  $[\text{DiC}_n]_2[\text{MO}_4]$  ( $\text{M} = \text{Mo}$  or  $\text{W}$ ) at  $25.0\text{ }^\circ\text{C}$  ( $n = 6, 8$  or  $10$ ).

**Table 2.2** Critical aggregation concentration (CAC) values and surface tensions at CAC ( $\sigma_{\text{CAC}}$ ) at  $25\text{ }^\circ\text{C}$  for  $[\text{DiC}_n][\text{X}]$  ( $\text{X} = \text{Cl}$  or  $\text{Br}$ ) and  $[\text{DiC}_n]_2[\text{MO}_4]$  ( $\text{M} = \text{Mo}$  or  $\text{W}$ ) as a function of the alkyl chain carbon number ( $n$ ).

Dialkyldimethyl ammonium $[\text{DiC}_n]\text{X}$ or $[\text{DiC}_n]_2\text{X}$	CAC (mM)	$\sigma_{\text{CAC}}$ ( $\text{mN}\cdot\text{m}^{-1}$ )
<b>n = 6</b>		
Cl	320 <sup>210</sup>	35.5
Br	280	33.9
WO <sub>4</sub>	70	33.3
MoO <sub>4</sub>	80	31.2
<b>n = 8</b>		
Cl	10 (10) <sup>31</sup>	29.9
Br	13 (20) <sup>31</sup>	27.9
WO <sub>4</sub>	10 (9) <sup>31</sup>	27.5
MoO <sub>4</sub>	7 (8) <sup>31</sup>	27.2
<b>n = 10</b>		
Cl	1.1 (1.3) <sup>211</sup>	27.2
Br	1.3 (1.5) <sup>212</sup>	24.4
WO <sub>4</sub>	0.6	24.7
MoO <sub>4</sub>	0.7	25.7

From the general point of view, the aggregation behavior of surfactants in aqueous solution is closely related to their hydrophobic chain length. When the hydrophobic chain length decreases to some extent, the aggregate occurs in a stepwise self-aggregation process, gradually increasing aggregation size at relatively high concentrations, typically above 100 mM and the surfactant is converted to hydrotrope, which does not form well-defined aggregates unlike true surfactants forming micelles. The CAC is determined at the intersection of the two lines defined by the baseline of minimal surface tension ( $\sigma_{\text{CAC}}$ ) at high concentrations and the linear surface tension decrease just before reaching the plateau. It is noteworthy that the surface tension at CAC ( $\sigma_{\text{CAC}}$ ) is a measure of the surface efficiency in lowering the surface tension. CACs of some [DiC<sub>8</sub>] salts have already been investigated in detail previously for interpreting the aggregation mechanism in dilute solution.<sup>31</sup> However, some data are missing especially for [DiC<sub>6</sub>] cations and catalytic [DiC<sub>10</sub>]<sub>2</sub>[MO<sub>4</sub>] with M = MoO<sub>4</sub> or WO<sub>4</sub>.

The formation of aggregates in aqueous solution is driven by the so-called “**hydrophobic effect**”, which originates from the disruption of dynamic H-bonds of the water molecules around the hydrophobic alkyl chain of the surfactant and the increase of the entropy (water cage around non-polar chain).<sup>213,214</sup> The hydrophobic effect depends on the alkyl chain length and a longer hydrophobic chain results in a lower CAC. In contrast, the electrostatic interactions and hydration of the hydrophilic head group increase the affinity of the surfactant molecules for water, which increases the CAC. These results were also observed in our results. Indeed, for the [DiC<sub>n</sub>][Cl], the CAC decreases about 10 times when adding two carbons to each alkyl tail; *i.e.* there is no clear discontinuity in the aggregation process between [DiC<sub>6</sub>] and [DiC<sub>10</sub>] amphiphiles.

Generally, divalent anions are shown to efficiently screen the electrostatic interaction between the surfactant polar head, resulting in a decrease in the CAC compared to monovalent anions. While in our case the [DiC<sub>6</sub>] salts behave one way and the octyl [DiC<sub>8</sub>] and decyl [DiC<sub>10</sub>] salts behave the other way, which was ascribed to the nature of the aggregation processes for different surfactants, for example, for [DiC<sub>8</sub>][Cl], dimers were formed at the beginning, followed by ellipsoid aggregates, whereas, for [DiC<sub>8</sub>][Br], discoid aggregation was observed between the dimer and the ellipsoid aggregation. On the other hand, for [DiC<sub>8</sub>]<sub>2</sub>[WO<sub>4</sub>] and [DiC<sub>8</sub>]<sub>2</sub>[MoO<sub>4</sub>], the ellipsoid aggregation directly occurred when the CAC was reached.<sup>31</sup> The relatively high  $\sigma_{\text{CAC}}$  and CAC values observed for the [DiC<sub>6</sub>] series indicate that it does not behave as a true surfactant and exhibits hydrotropic behavior. The [DiC<sub>6</sub>] cation does not form well-defined aggregates in water, such as spherical or elongated micelles. Indeed, SAXS results (discussed later in this chapter) in the dilute regime (concentration <10% w/w, *i.e.* at concentrations around twice the CAC values,  $\approx 0.2$  M) confirmed the absence of well-defined aggregates for [DiC<sub>6</sub>]<sub>2</sub>[WO<sub>4</sub>] and [DiC<sub>6</sub>]<sub>2</sub>[MoO<sub>4</sub>].

### 2.1.3 Aqueous phase behavior of dialkyldimethylammonium catarurfs in concentrated solution: lyotropic liquid crystal formation

At low concentration range above the CAC, the interaction between the aggregates is negligible and the aggregates exist as independent entities without long ranged orientational order. These isotropic dispersions are generally referred as micellar solutions ( $L_1$ ). As the concentration of amphiphilic molecules increases, the interaction between the aggregates increases and the micelles are forced to be disposed regularly in space, where the lyotropic liquid crystals appear. Generally, the first type of lyotropic liquid crystal by sphere micelles is hexagonal phase ( $H_1$ ), which is formed by the fusion of micelles to form cylindrical aggregates of indefinite length, and these cylinders are arranged on a long-ranged hexagonal lattice. Further increase of the concentration resulted in the formation of lamellar phase ( $L_a$ ), which consists of amphiphilic molecules arranged in bilayer sheets separated by layers of water. While for most of the amphiphiles, one or more phases with complex architectures are formed between hexagonal and lamellar phases, often this intermediate phase is bicontinuous cubic phase ( $V_1$ ). At very high concentration region, the reverse cubic ( $V_2$ ), reverse hexagonal ( $H_2$ ) and reverse micellar phases ( $L_2$ ) are possibly present consecutively as the concentration increases (Figure 2.6).<sup>215</sup>

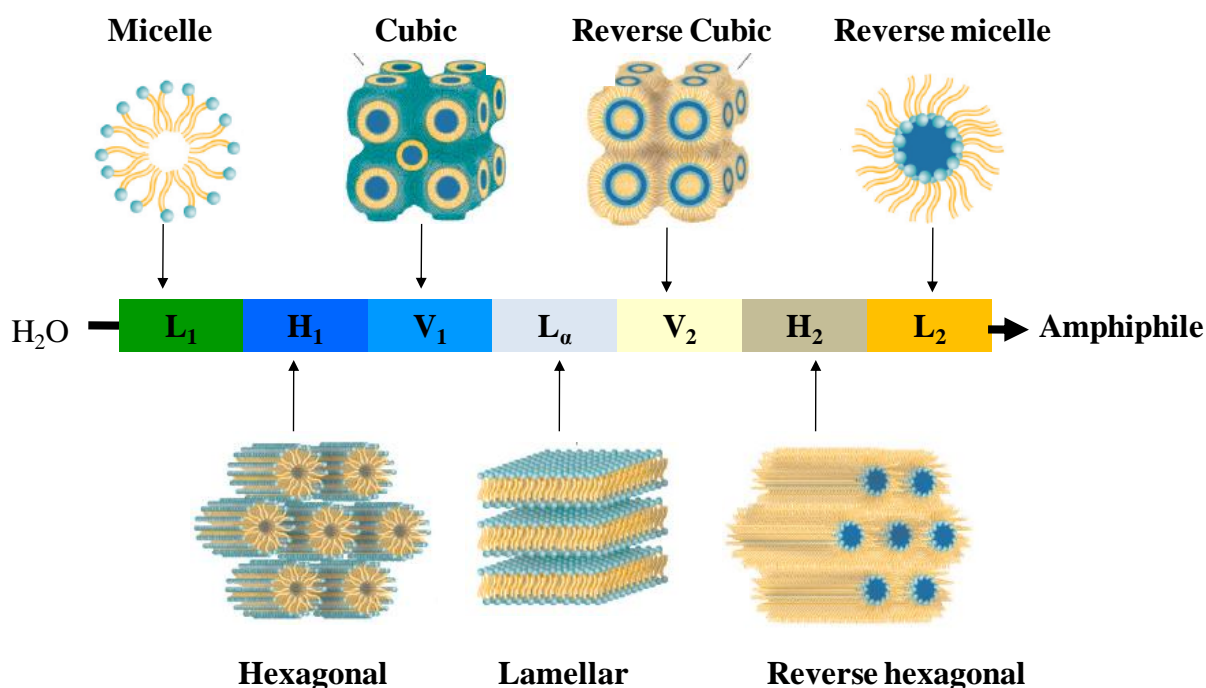


**Figure 2.6** The aggregation structures of amphiphiles in water as a function of concentration.<sup>215</sup>

The different types of lyotropic liquid crystals can be preliminary distinguished by their aspect (*e.g.* viscous, rigid gels, *etc.*) and by their different optical properties (such as birefringence). Different liquid crystal phases will have distinct textures under the optical polarizing light microscope (POM). The micellar solution is not birefringent and of low viscosity, while the hexagonal phase shows a “fan-like”

texture. Although the cubic phase is also not birefringent, the highly viscous appearance and the inside trapped distorted bubbles are the distinct properties to differentiate the cubic phase from others. On the other side, lamellar liquid crystal exhibits mosaic or “Maltese cross” textures<sup>216</sup> (**Figure 2.7**).

For single-chain surfactants, due to the packing parameter ranging from  $1/3$  to  $1/2$ , the binary phase diagram has a classical phase behavior pattern. In the dilute regime, micelles are formed, followed by an increase in the micelle size or a change in the micelle shape by increasing concentration. In the high concentration regime, lyotropic liquid crystals may form, with the classical evolution from hexagonal to cubic to lamellar phases.<sup>217</sup> On the other hand, the double-chain surfactants also exhibit a general sequence; the phase behavior evolves from an isotropic solution (vesicle, disk like micelle, oblate micelle, etc) and two phases (dispersed lamellae) to lamellar liquid crystals by increasing the concentration of surfactant in water.<sup>218-221</sup> Although sometimes the CMCs of two different surfactants are similar, such as in the case of sodium dodecyl sulfate (SDS) and  $[\text{DiC}_8]_2[\text{MoO}_4]$ , their respective binary phase behavior exhibits a great difference due to different packing parameters. Here, the binary quaternary ammonium amphiphile/water diagrams of  $[\text{DiC}_n][\text{X}]$  and  $[\text{DiC}_n]_2[\text{MO}_4]$  (with  $\text{X} = \text{Cl}, \text{Br}$ ;  $\text{M} = \text{Mo}, \text{W}$  or  $\text{S}$  and  $n = 6, 8,$  and  $10$ ) have been investigated. The phase diagrams were preliminarily studied by polarized optical microscopy (POM) by gradually increasing the concentration of the surfactants which allows discriminating the isotropic phases from the anisotropic ones. Then, the type of liquid crystals was distinguished by different textures and confirmed by SAXS experiments.<sup>222-225</sup>

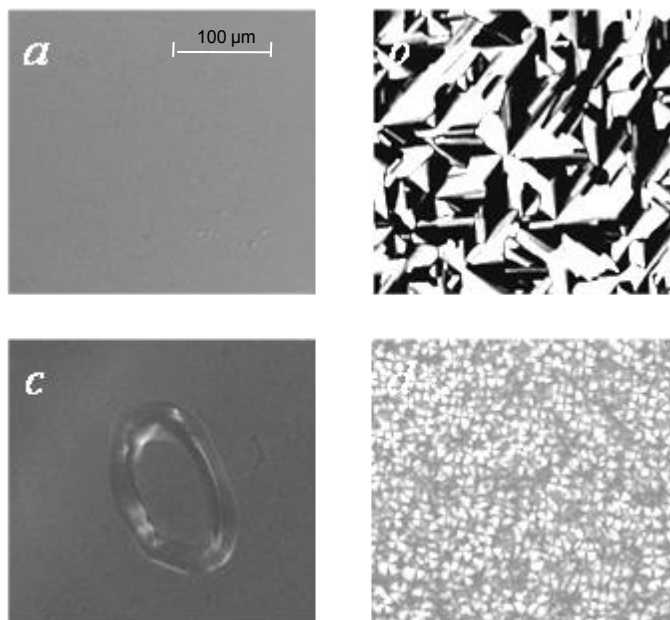


**Figure 2.7** Textures observed under polarized light microscope (POM): micellar solution (a), hexagonal liquid crystal (b), cubic liquid crystal (c) and lamellar liquid crystal phase (d).<sup>216</sup>

The phase penetration technique at room temperature was firstly used for a rough estimate of the sequence of mesophases occurring. A few milligrams of the surfactant powder (usually around 20 mg)

were placed between a glass slide and a cover slip. When the powder could not be made sufficiently compact to obtain a well-defined interface, the sample might be heated until softening for homogenization and then cooled down to room temperature, in order to obtain a well-defined interface. The sample was then contacted with a distilled water drop and diffusion of water by capillarity into the surfactant sample took place so that a concentration gradient from extremely dilute aqueous solution to pure surfactant was more or less quickly established. Identification of the different phases was based on visual observation through an optical polarizing microscope Olympus BX60 ( $100\times$  magnification) equipped with a LTS120 Analysa Peltier temperature stage capable of controlling to  $\pm 0.1\text{ }^\circ\text{C}$  the temperature (**Figure 2.8**).

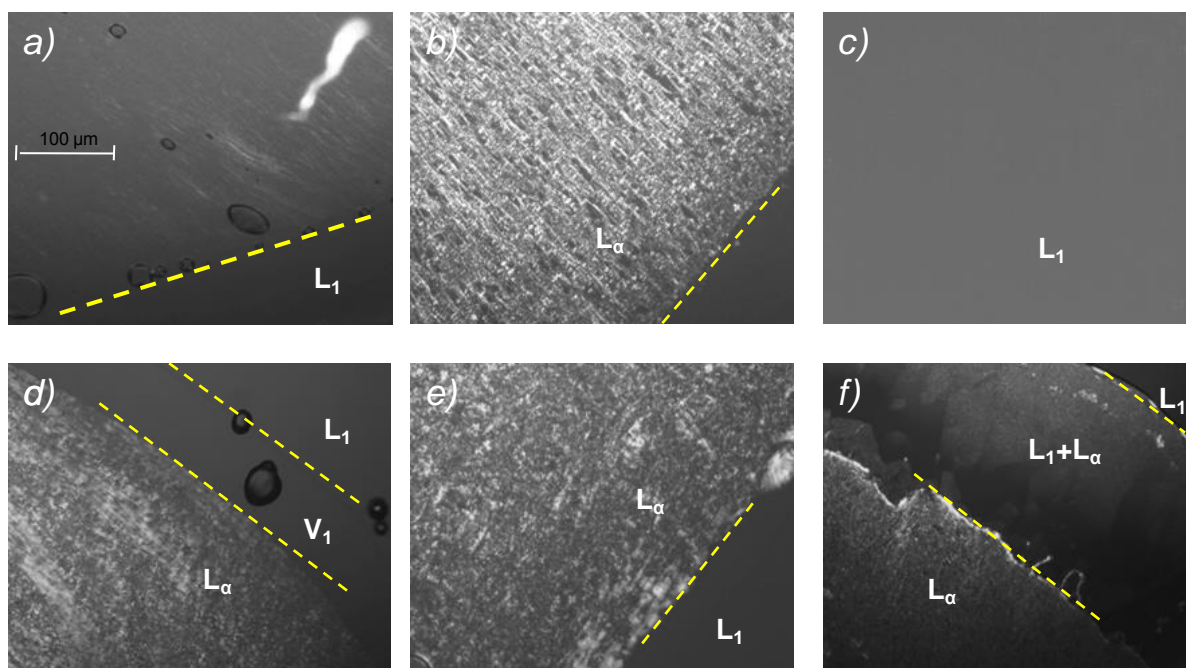
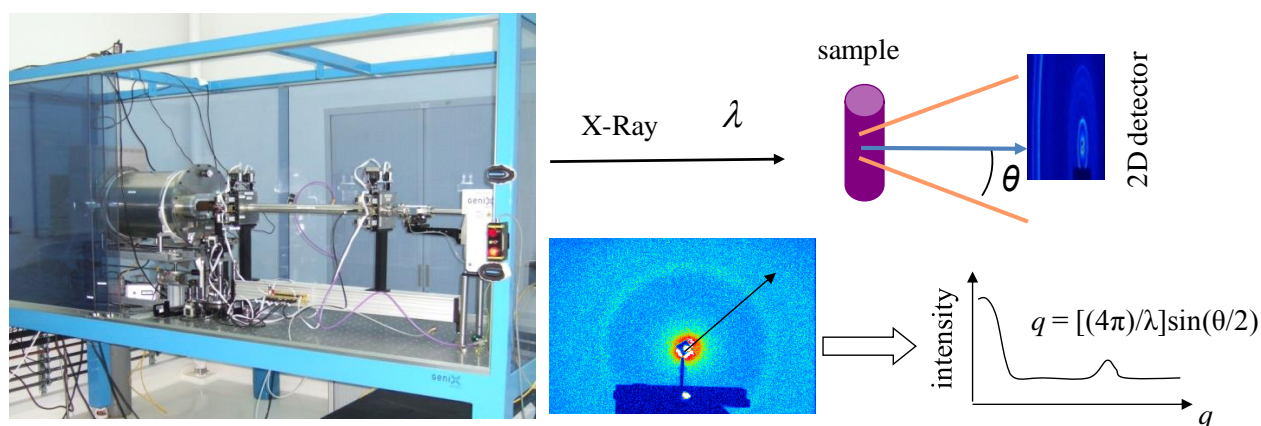


**Figure 2.8** Liquid crystal textures observed by POM during penetration scan experiment at  $25\text{ }^\circ\text{C}$  for  $[\text{DiC}_6]_2\text{MoO}_4$  (a),  $[\text{DiC}_8]\text{Cl}$  (b),  $[\text{DiC}_8]\text{Br}$  (c),  $[\text{DiC}_8]_2\text{MoO}_4$  (d),  $[\text{DiC}_{10}]\text{Cl}$  (e) and  $[\text{DiC}_{10}]_2\text{MoO}_4$  (f).

$[\text{DiC}_6]\text{Cl}$  is liquid and showed no liquid crystal phase. Although  $[\text{DiC}_8]\text{Br}$  is a white solid at room temperature, the birefringent phase disappeared rapidly due to its highly hygroscopic property and the liquid crystal phase region at very high concentration ( $> 90\text{ wt}\%$ ) (**Figure 2.8c**).  $[\text{DiC}_6]_2\text{WO}_4$  and  $[\text{DiC}_6]_2\text{MoO}_4$  showed the same sequence from micellar solution to a liquid crystal phase (unidentified at this stage) (**Figure 2.8a**). However, the textures of liquid crystal phases from  $[\text{DiC}_8]\text{Cl}$  (**Figure 2.8b**) and  $[\text{DiC}_{10}]\text{Cl}$  (**Figure 2.8e**) indicated that the lamellar phase formed. On the other side, for  $[\text{DiC}_8]_2\text{WO}_4$ ,  $[\text{DiC}_8]_2\text{MoO}_4$ , and  $[\text{DiC}_8]_2\text{SO}_4$ , the trapped distorted air bubble indicated the presence of a cubic phase between the micellar solution and the lamellar phase (**Figure 2.8d**). It is noteworthy that addition of two carbons in each of the two hydrophobic chains caused the disappearance of the cubic phase for  $[\text{DiC}_{10}]_2\text{WO}_4$  and  $[\text{DiC}_{10}]_2\text{MoO}_4$ , in favor of a phase mixture between the micellar and the lamellar phases (**Figure 2.8f**).

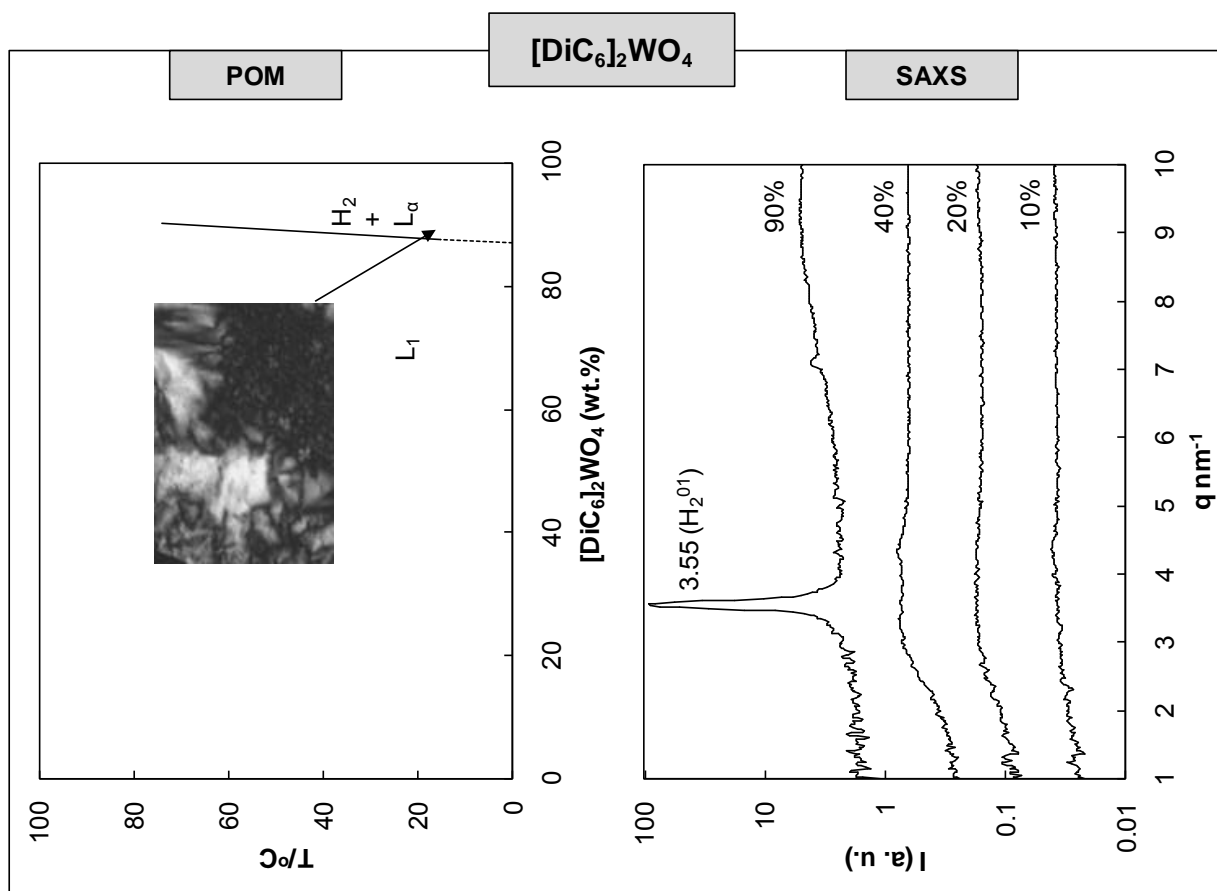
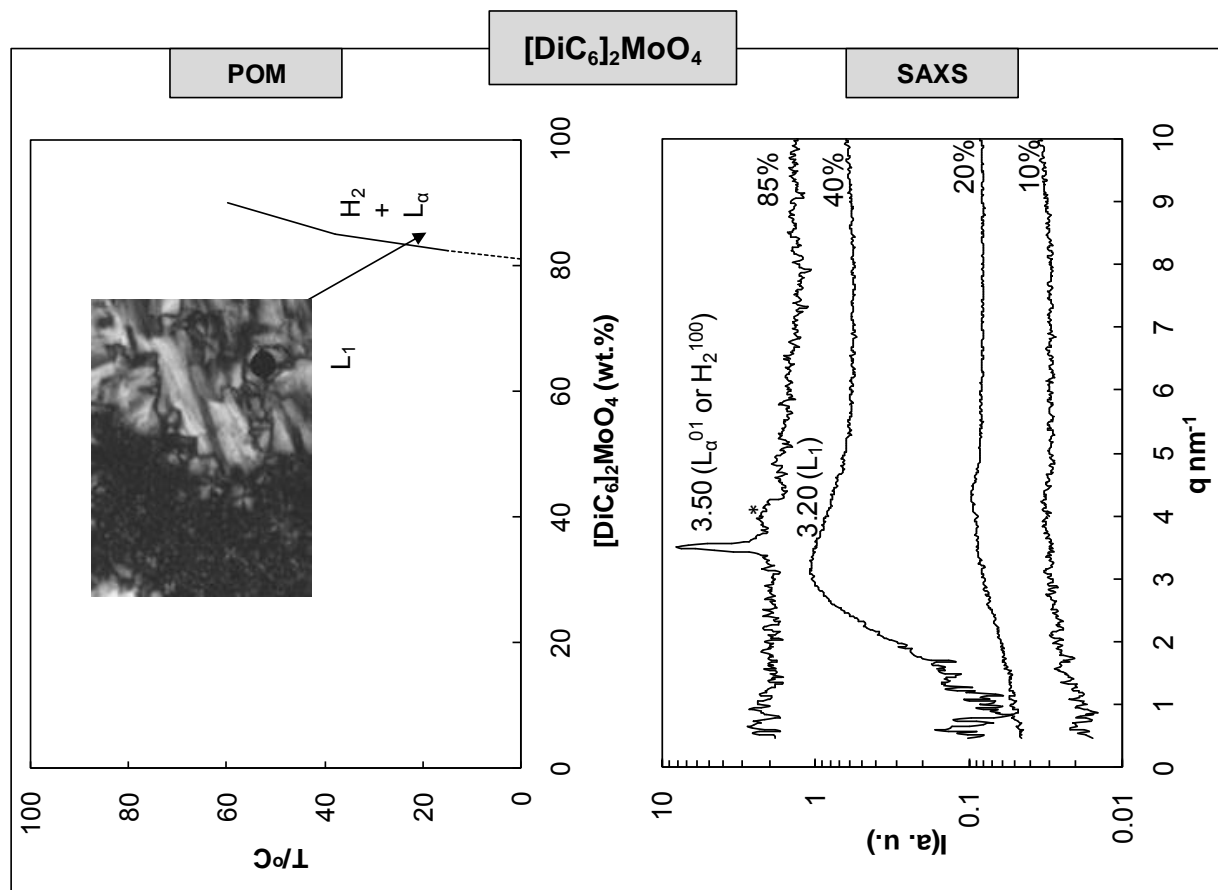


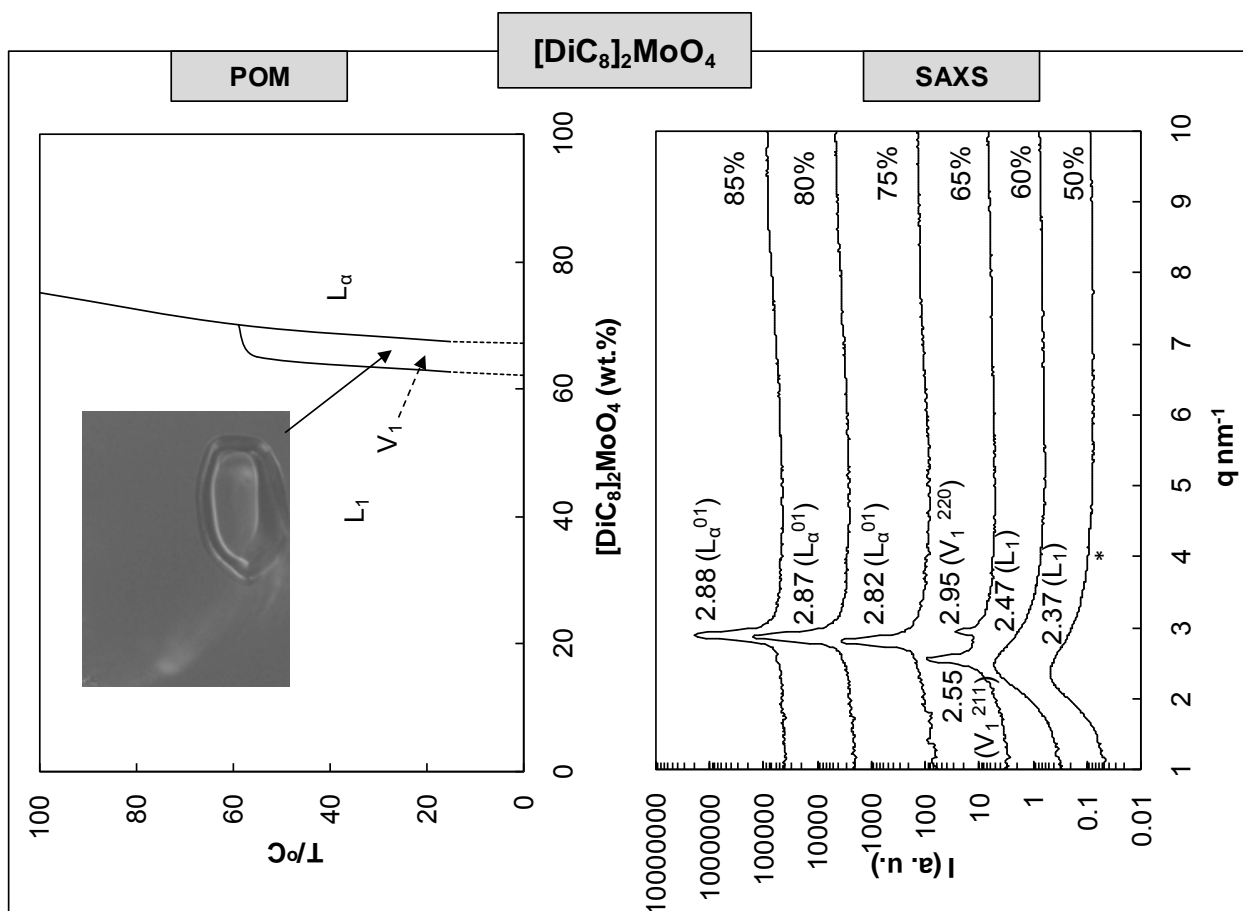
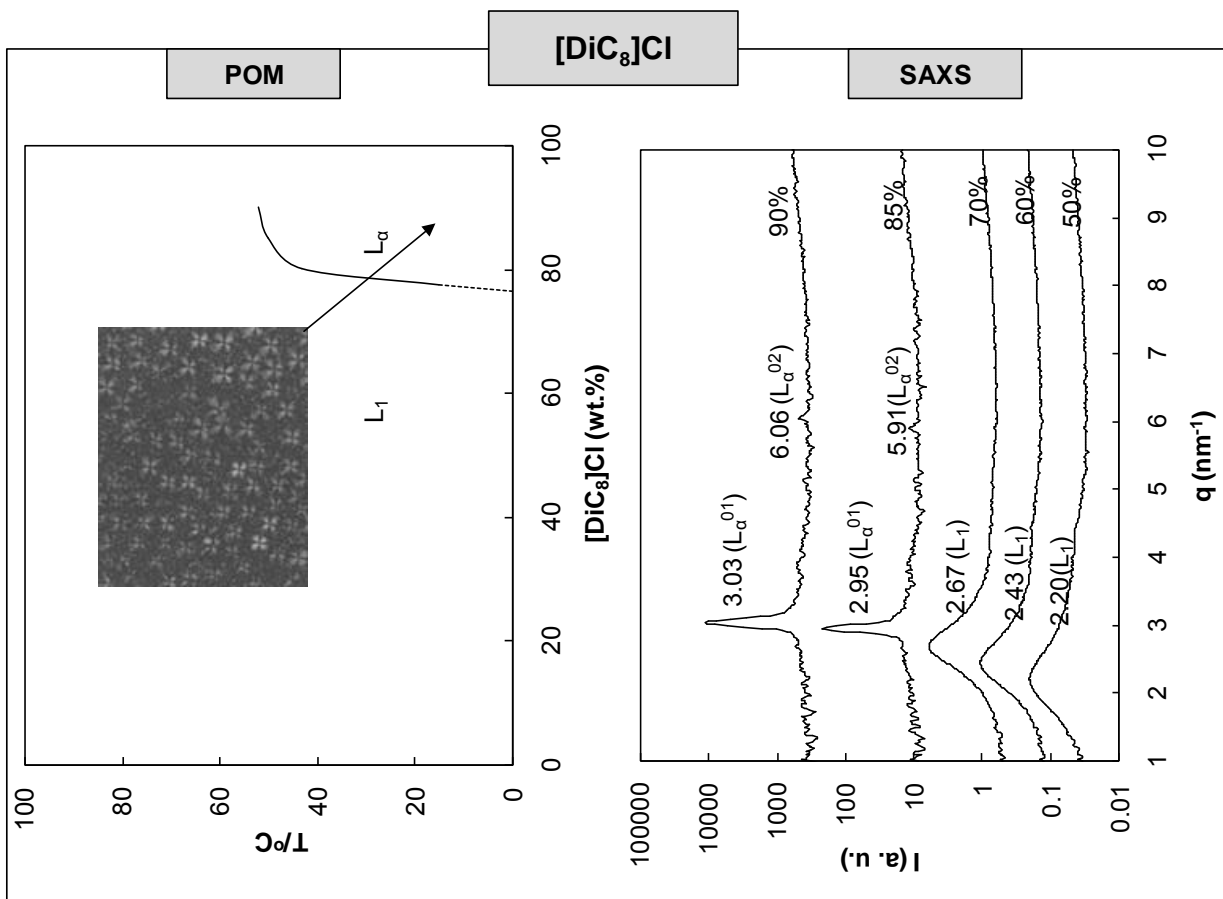
After having established roughly the succession of liquid crystalline phases from the penetration scan, the transition compositions were determined by preparing samples of given concentrations (from 5-95 wt% with 5 wt% intervals, so that the accuracy of the resulting diagrams was of about  $\pm 2.5\%$ ). Samples of 100 mg or more were prepared in glass tubes which were then sealed with a gas burner placed in water bath at 80 °C for 2h and were then centrifuged at 2500 rpm for one hour at room temperature for homogenization. The type of the phase was investigated by the birefringence of the mixture and the texture was given by the liquid crystal type. The rate used during the heating sequence was typically 5 °C.min<sup>-1</sup> and the temperature range was set from 15 to 100°C. To confirm the nature of the phases observed by POM, SAXS experiments were also carried out using Mo-radiation ( $\lambda = 0.71 \text{ \AA}$ ) on a bench built by XENOCSS. The SAXS experiments were carried at ICSM in Marcoule, in the group of Dr P. Bauduin. The scattered beam was recorded using a large online scanner detector (diameter: 345 mm, from MAR Research). A large  $q$  range ( $2.10 \cdot 10^{-2} - 2.5 \text{ \AA}^{-1}$ ) was covered with an off center detection. Pre-analysis of data was performed using FIT2D software. The scattered intensities were expressed *versus* the magnitude of the scattering vector  $q = [(4\pi)/\lambda]\sin(\theta/2)$ , where  $\lambda$  is the wavelength of incident radiation and  $\theta$  the scattering angle. 2 mm quartz capillaries were used as sample containers for dilute and fluid solutions, *i.e.* isotropic micellar solutions. Usual corrections for background (empty cell and detector noise) subtractions and intensity normalization using Lupolen<sup>TM</sup> as standard were applied. For the study of highly viscous lyotropic phases, a special home designed cell was used (**Figure 2.9**). L<sub>1</sub> isotropic solution exhibited a broad peak due to the low level of organization between surfactant aggregates. On the other hand, for well organized surfactant liquid crystal structures, *i.e.* cubic, hexagonal, or lamellar phases, Bragg peaks were generally obtained and indicated the types and parameters of liquid crystals. By combining POM and SAXS experiments, the complete binary diagrams of the prepared amphiphiles in water were thus determined (**Figure 2.10**).

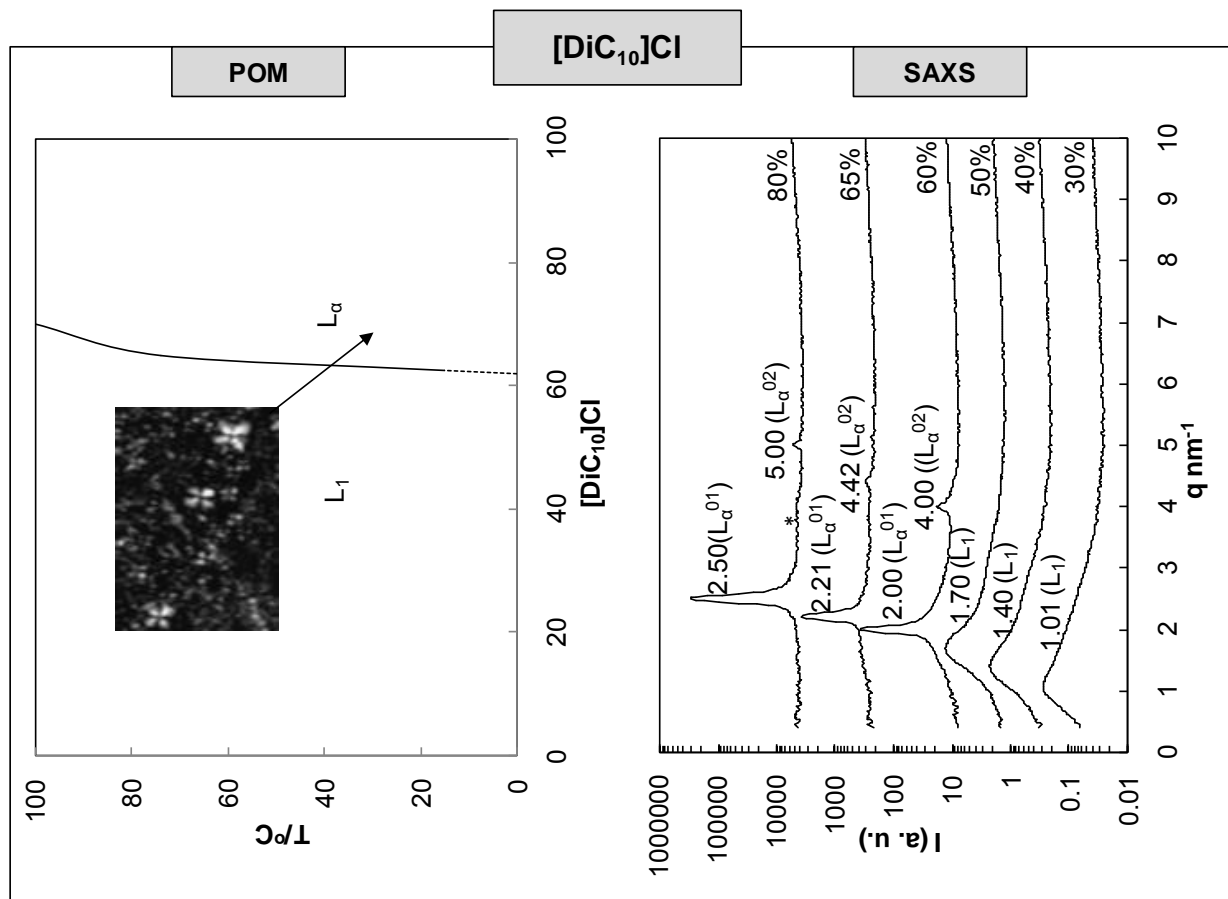
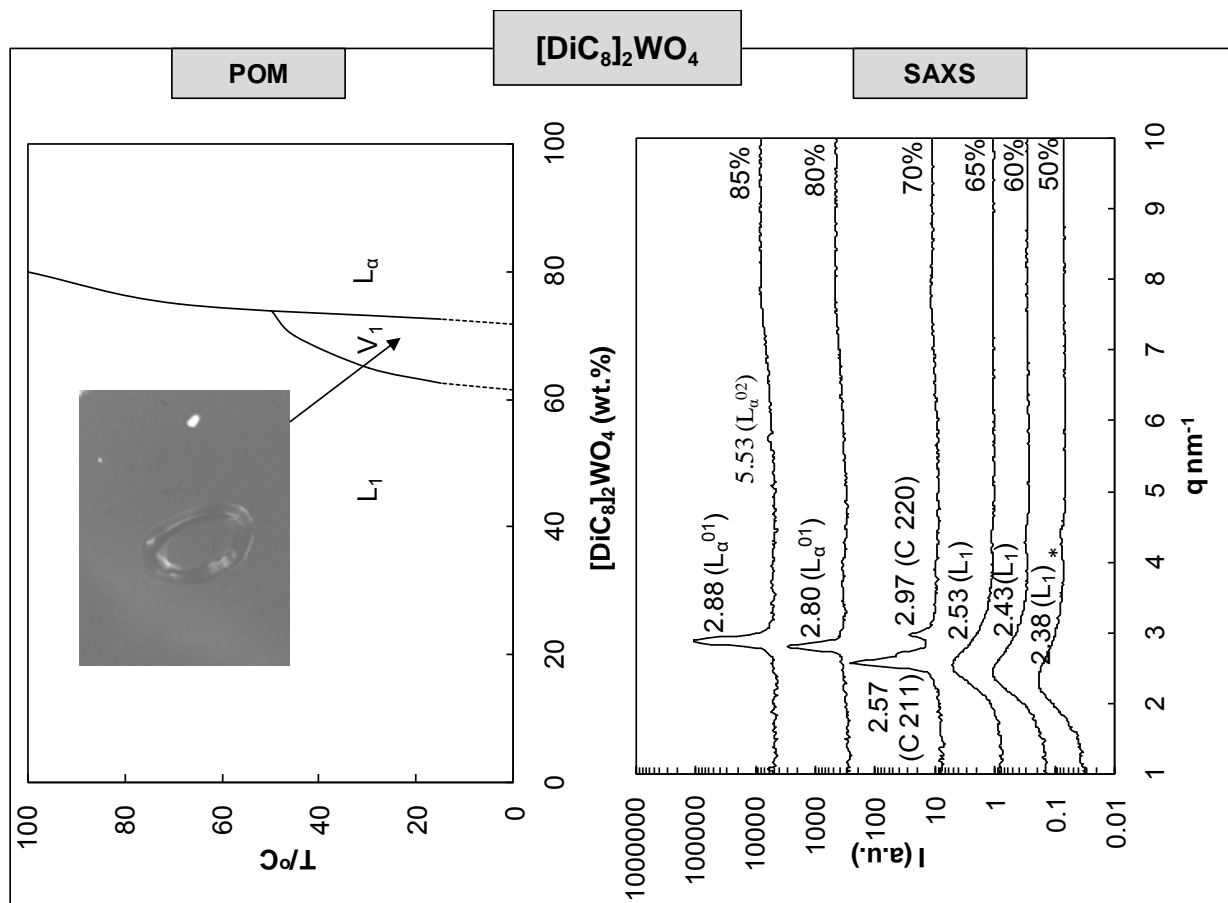


**Figure 2.9** SAXS apparatus (Institut de Chimie Séparative de Marcoule) and process of data collection.









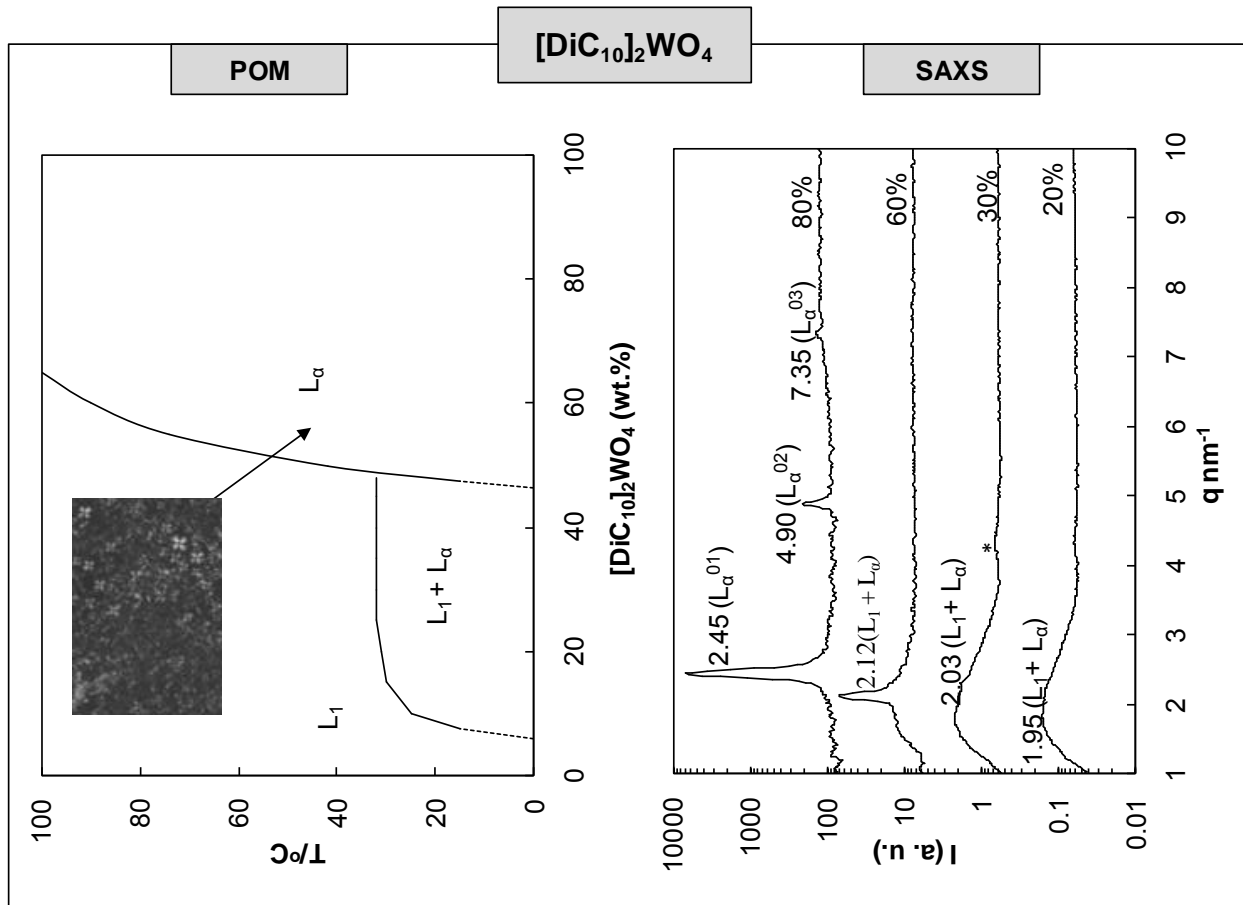
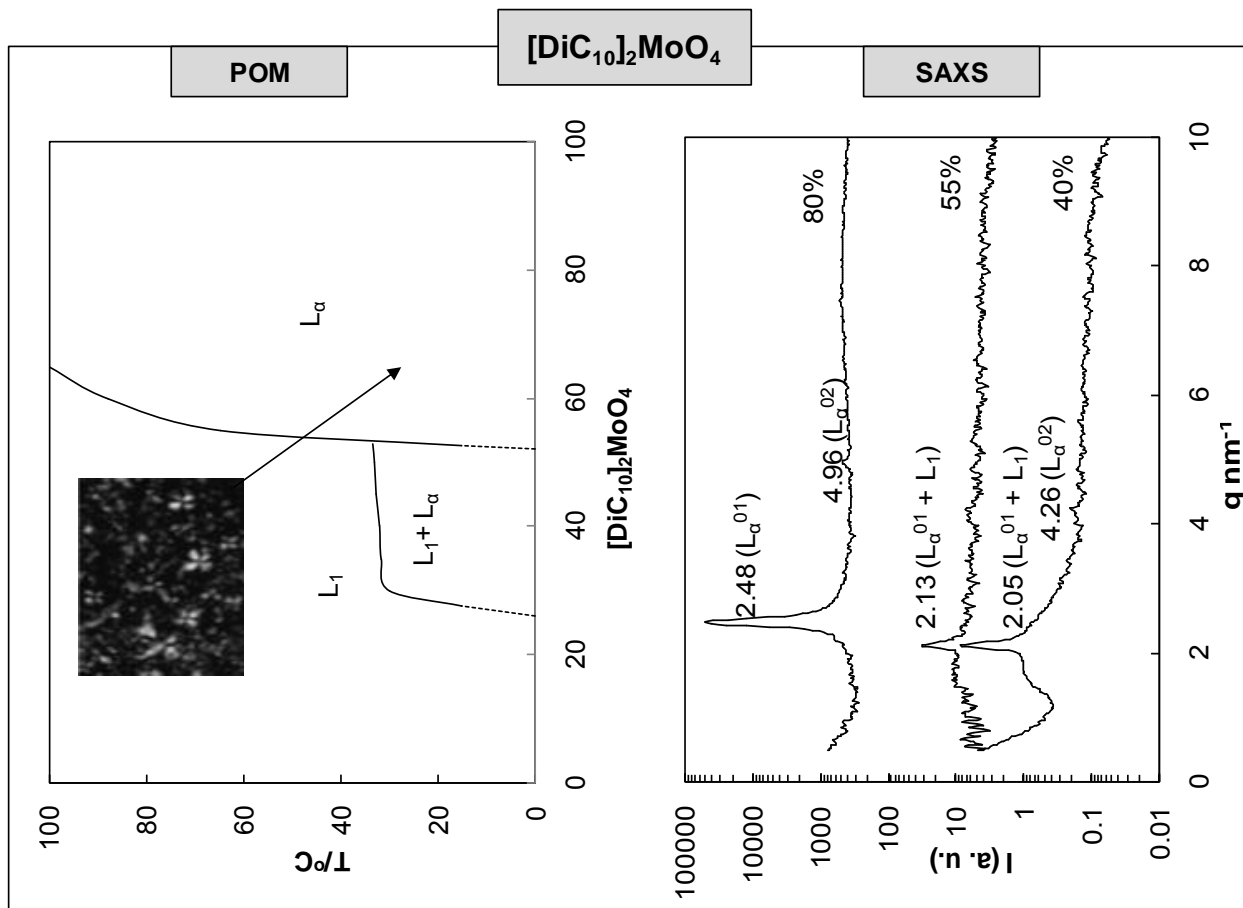


**Figure 2.10** Schematic partial binary phase diagrams determined by polarized light optical microscopy (POM) of  $[\text{DiC}_n]_m\text{X}$  ( $n = 6, 8, \text{ or } 10, m = 1, X = \text{Cl}; m = 2, X = \text{WO}_4 \text{ or } \text{MoO}_4$ ).  $L_1$  = isotropic solution,  $V_1$  = cubic phase,  $L_\alpha$  = lamellar phase, and  $H_2$  = reverse hexagonal phase. Photomicrographs show the optical textures of the lamellar phase (with Maltese cross patterns), the reverse hexagonal phase (“fan-like” texture), and faceted air bubbles in the cubic phase. Typical SAXS curves obtained at 25 °C for various concentrations were also given. The broad peak marked with a star symbol (\*) at  $q \approx 4 \text{ nm}^{-1}$  corresponds to the scattering of the “Kapton” plastic film used as a container in the experiment.

It is noteworthy that  $[\text{DiC}_6][\text{Cl}]$  does not present birefringent phases whatever its concentration or temperature. The SAXS experiment gave a broad peak which is typical for isotropic solution due to the low level of organization between surfactant aggregate. While increasing the chain length or substitution of the anion results in the appearance of various phases, *i.e.* cubic, hexagonal and lamellar phases. The nature of the liquid crystal phase follows the global curvature of the surfactant film which decreases by increasing surfactant concentration due to the hydration decrease of the polar head. Different from  $[\text{DiC}_6][\text{Cl}]$ , a biphasic region with lamellar  $L_\alpha$  and reverse hexagonal  $H_2$  phases was clearly observed in POM experiments for  $[\text{DiC}_6]_2[\text{MoO}_4]$  and  $[\text{DiC}_6]_2[\text{WO}_4]$  at very high concentrations,  $> 82$  and  $> 88\%$ , respectively (**Figure 2.10**).<sup>226</sup> From the SAXS spectra, lamellar and reverse hexagonal phases were characterized by sharp Bragg reflections with  $q$  ratios respectively of 1:2:3 and  $1:\sqrt{3}:2$  (**Figure 2.11a, 2.11b**). For  $[\text{DiC}_6]_2[\text{MoO}_4]$ , only one sharp reflection was observed which was attributed to either lamellar or reverse hexagonal phases, as suggested by the POM pictures (presence of “fan-like” texture). On the other hand,  $[\text{DiC}_6]_2[\text{WO}_4]$  shows a “fan-like” texture in POM pictures as well as a second reflection  $L_\alpha$ <sup>02</sup> that confirms the presence of a lamellar phase and suggests an equilibrium between a lamellar phase and a reverse hexagonal phase. The absence of  $H_2$ <sup>110</sup> reflection can be explained by a rather low proportion of reverse hexagonal phase *vs* lamellar phase. A reverse hexagonal phase is common for double-chained surfactant like AOT<sup>227</sup> or lecithin<sup>228</sup> in water at high concentrations ( $> 80$  wt %) and/or at high temperature ( $> 100^\circ\text{C}$ ).

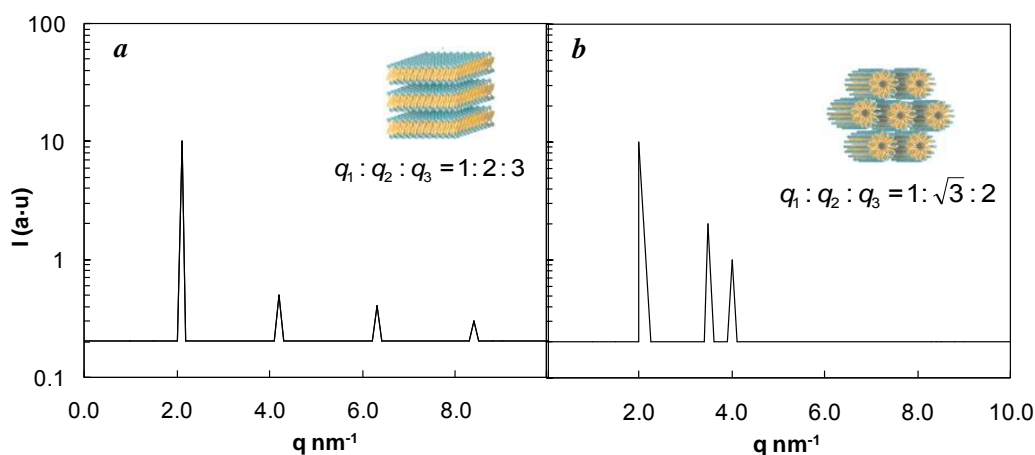


**Figure 2.11** Spectra patterns of SAXS given by lamellar phase (a) and hexagonal phase (b).

The diagrams of  $[\text{DiC}_8][\text{Cl}]$  and  $[\text{DiC}_{10}][\text{Cl}]$  have similar patterns, but the  $[\text{DiC}_{10}][\text{Cl}]/\text{water}$  system has a larger and more stable lamellar liquid crystal region (**Figure 2.10**). This is due to the longer chain and larger size of aggregates formed by  $[\text{DiC}_{10}][\text{Cl}]$  than  $[\text{DiC}_8][\text{Cl}]$ , which means the interactions between aggregates are stronger for the former.<sup>31,219</sup> These results also follow the trend already observed by Shinoda who reported the phase diagrams of dialkyl ( $\text{DiC}_{12}$ ,  $\text{DiC}_{14}$ , and  $\text{DiC}_{18}$ ) dimethylammonium chloride/water binary systems. The boundary temperature between micellar solution region and micellar/lamellar mixture phase region decreases from 190 °C for  $[\text{DiC}_{16}][\text{Cl}]$  to 60 °C for  $[\text{DiC}_{12}][\text{Cl}]$  at 5 wt% surfactant concentration, which anticipated that  $[\text{DiC}_{10}][\text{Cl}]$  and  $[\text{DiC}_8][\text{Cl}]$  do not have biphasic mixture regions at room temperature.<sup>219</sup>  $[\text{DiC}_8]_2[\text{MoO}_4]$  and  $[\text{DiC}_8]_2[\text{WO}_4]$  showed similar binary phase behavior with, for both of them, a narrow bicontinuous cubic region between the isotropic solution and the lamellar phase.<sup>229</sup> Different SAXS spectra patterns could be obtained from different types of cubic phases with different space symmetry, *i.e.*  $Ia3d$ ,  $Pn3m$  and  $Im3m$  (**Figure 2.12**).<sup>230</sup> The bicontinuous structures formed are well described by Infinite Periodic Minimal Surfaces (IPMS), *i.e.* surfaces whose mean curvature is zero at all points. Three types of IPMS surfaces have been discovered in amphiphile–water systems, namely the gyroid, diamond, and primitive surfaces, which correspond to space groups  $Ia3d$ ,  $Pn3m$ , and  $Im3m$ , respectively.<sup>231,232</sup> SAXS spectra of the cubic phase observed with  $[\text{DiC}_8]_2[\text{MoO}_4]$  and  $[\text{DiC}_8]_2[\text{WO}_4]$  show a main peak and a second order whose positions (the ratio of the peak position is  $\sqrt{6} : \sqrt{8}$ ) can be described by the two reflection peaks (211 and 220) of bicontinuous cubic phase of the symmetry group  $Ia3d$ , which is most commonly obtained in cubic phases.<sup>232</sup> In some of the SAXS 2D images, a 4-fold symmetry was observed, which is also typical of an  $Ia3d$  phase (**Figure 2.13**).<sup>233</sup>

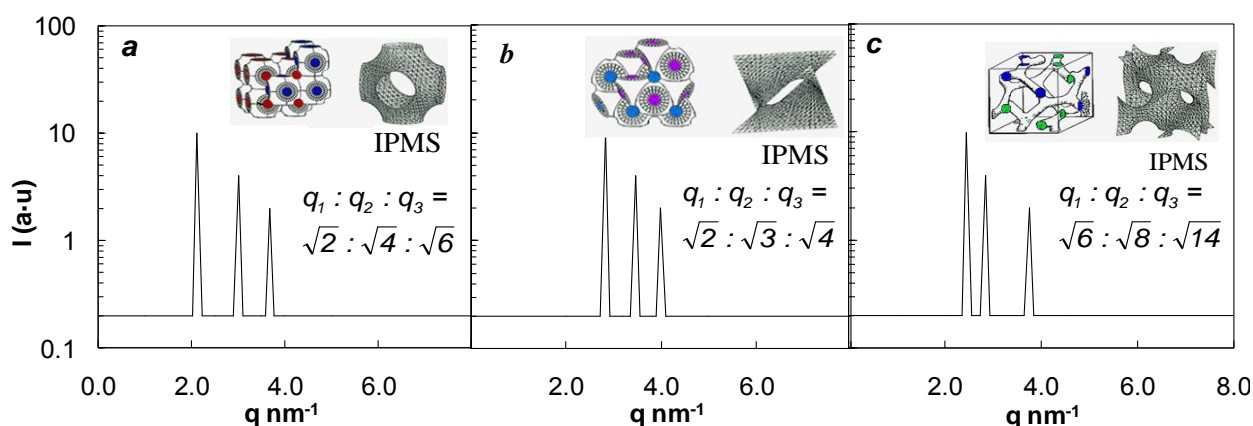


**Figure 2.12** SAXS patterns given by three types of cubic phases and their microstructures with corresponding IPMS surfaces: a)  $Im3m$ ; b)  $Pn3m$ ; c)  $Ia3d$ . Two networks of non-intersecting channels in microstructures are shown in different colors.<sup>230</sup>

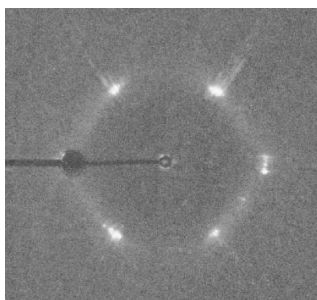


**Figure 2.13** SAXS pattern of the cubic phase  $V_1$  on the 2D detector. The dark rod on the picture corresponds to the “beam stop”.

Unlike  $[\text{DiC}_{10}][\text{Cl}]$ , the  $[\text{DiC}_{10}]_2[\text{MoO}_4]$  and  $[\text{DiC}_{10}]_2[\text{WO}_4]$  binary systems display in addition a large range of biphasic region before the formation of liquid crystal phases. According to a Monte Carlo simulation, there is a significant attraction between the lamellae derived from the charge fluctuation for divalent counter ions which cause lower swelling ability of this kind of amphiphile. This can lead to the phase demixing between  $L_\alpha$  and  $L_1$  phases.<sup>234</sup>

In the SAXS spectra, the position of the first reflection  $L_\alpha^{01}$ , here called  $q^*$ , can be correlated to the interlamellar spacing  $d^*$  with the relation  $d^* = 2\pi/q^*$ . For a homogeneous lamellar phase, the thickness of the lamella  $\delta$  can be calculated with  $\Phi = \delta/d^*$ , where  $\Phi$  is the surfactant volume fraction and  $\delta = 2l_c^n$ , with  $l_c^n$  being the lamella half-thickness for a given surfactant containing an alkyl chain with  $n$  carbons. For linear surfactant, the fully extended chain length can be estimated by Tanford’s relation ( $l_t^n = 1.5 + 1.265n$  in Å).<sup>214</sup> All the surfactants in this study, except  $[\text{DiC}_6][\text{Cl}]$ , form a lamellar liquid crystal at  $\Phi = 0.9$  with  $l_c^n \approx l_t^n$  which is typical for fluid bilayers (Table 2.3).

**Table 2.3** Chain length value  $l_c^n$  calculated from the first lamellar bragg reflection  $L_\alpha^{01}$  and comparison with Tanford’s length  $l_t^n$  at  $\Phi = 0.9$ .

Surfactant	$q^* / \text{nm}^{-1}$	$d^* / \text{nm}$	$l_c^n / \text{nm}$	$l_t^n / \text{nm}$
$[\text{DiC}_6]_2\text{MoO}_4$	3.55	1.77	0.80	0.9
$[\text{DiC}_6]_2\text{WO}_4$	3.54	1.77	0.80	0.9
$[\text{DiC}_8]\text{Cl}$	3.03	2.07	0.93	1.16
$[\text{DiC}_8]_2\text{MoO}_4$	2.90	2.17	0.97	1.16
$[\text{DiC}_8]_2\text{WO}_4$	2.88	2.18	0.98	1.16
$[\text{DiC}_{10}]\text{Cl}$	2.52	2.49	1.12	1.41
$[\text{DiC}_{10}]_2\text{MoO}_4$	2.40	2.62	1.18	1.41
$[\text{DiC}_{10}]_2\text{WO}_4$	2.45	2.56	1.15	1.41

The comparison of the values  $l_c^n$  with their corresponding  $l_t^n$  values shows an increased deviation from **[DiC<sub>6</sub>]** to **[DiC<sub>8</sub>]** and to **[DiC<sub>10</sub>]**, which can be related to the disorder degree of the fluid alkyl chain in the lamellar phase: the longer the alkyl chain, the larger disorder of the chain and lower the measured length  $l_c^n$  compared with  $l_t^n$ .<sup>235</sup> Indeed, the deviation is more pronounced for surfactant with longer alkyl chain: for **[DiC<sub>n</sub>]<sub>2</sub>[WO<sub>4</sub>]**,  $l_c^{10} = 1.15$  nm vs  $l_t^{10} = 1.41$  nm and  $l_c^6 = 0.80$  nm vs  $l_t^6 = 0.91$  nm. In addition, a slight increase in  $l_c^n$  is observed from monovalent (**[Cl]**:  $l_c^{10} = 1.12$  nm) to divalent (**[MoO<sub>4</sub>]**:  $l_c^{10} = 1.18$  nm). Divalent ion leads to lower repulsive interactions between the polar heads and reduces the available space for the alkyl chain and the chain disorder. This effect results in the increase in the lamella thickness. It is noteworthy that cubic phases are only observed for **[DiC<sub>8</sub>]<sub>2</sub>[MoO<sub>4</sub>]** and **[DiC<sub>8</sub>]<sub>2</sub>[WO<sub>4</sub>]**, whereas the analogous **[DiC<sub>8</sub>][Cl]** shows only a lamellar phase. The replacement of a mono valent counter ion by a divalent counter ion in a given system results in significant changes due to the variation of counter ion hydration. The similar results were also reported previously, *e. g.* the hexadecyltrimethyl ammonium bromide does not give cubic phases at room temperature, whereas the substitution of bromide by sulfate allows the occurrence of a cubic phase at a concentration around 45%.<sup>236</sup> The ion hydration free energy,  $\Delta G_{\text{hydr}}$ , which provides indirect measures of the ion–water interactions, is relevant parameter of ionic properties. Although  $\Delta G_{\text{hydr}}$  values for many ions were carefully tabulated by Marcus,<sup>237</sup> **[WO<sub>4</sub>]** and **[MoO<sub>4</sub>]** data are missing.  $\Delta G_{\text{hydr}}$  can be predicted for all anions from PM6/SCF-MO calculation with MOPAC 2009. For **[Br]**, **[Cl]**, **[WO<sub>4</sub>]**, **[MoO<sub>4</sub>]**, and **[SO<sub>4</sub>]**, the following  $\Delta G_{\text{hydr}}$  values were obtained: 76.2, 80.2, 224.2, 228.2, and 242.7 kcal·mol<sup>-1</sup> respectively. Where **[Br]**, **[Cl]**, and **[SO<sub>4</sub>]** are in good agreement with the values from Marcus (75.3, 81.3, and 258.2 kcal·mol<sup>-1</sup>, respectively).<sup>237</sup> As  $\Delta G_{\text{hydr}}$  of **[Cl]** is close to **[Br]** and as **[WO<sub>4</sub>]** and **[MoO<sub>4</sub>]** are comparable to **[SO<sub>4</sub>]**, in the sense that they are divalent oxo-anions, we can suppose that the formation of the cubic phase is related to the high hydration of divalent oxo-anions compared with monovalent anions. In other words, the hydration of divalent anion acts as a promoter in the formation of the cubic phase. Indeed, as **[DiC<sub>8</sub>]<sub>2</sub>[MoO<sub>4</sub>]** and **[DiC<sub>8</sub>]<sub>2</sub>[WO<sub>4</sub>]**, **[DiC<sub>8</sub>][SO<sub>4</sub>]** also gave cubic phase region between micellar solution and lamellar phase (**Figure 2.14**). Moreover, the cubic phase is converted to micellar solution as increase of the temperature. As the hydrogen bonds are disrupted by increasing temperature, thereby releasing weakly bound water, the cubic phase is destabilized in favor of the micellar solution. It is noteworthy that **[MoO<sub>4</sub>]** shows a better resistance of the cubic phase by increasing temperature. This observation confirms the influence of the counter ion hydration on the stability of the cubic phase. On the other side, as the packing parameter is clearly modified with the increase of the carbon number of the cationic moiety, spontaneous curvature is then modified, resulting in the disappearance of the cubic phase in favor of the lamellar phase from **[DiC<sub>8</sub>]** to **[DiC<sub>10</sub>]**. On the other hand, for divalent anions, the decrease of the chain length leads to a simplification of the diagrams, *i.e.*, a decrease of the number of phases. It is thus clearly shown that the



surfactant chain length as well as the nature of the counter ion acts as key parameters on the nature of the liquid crystal phases in the dialkyldimethylammonium series.

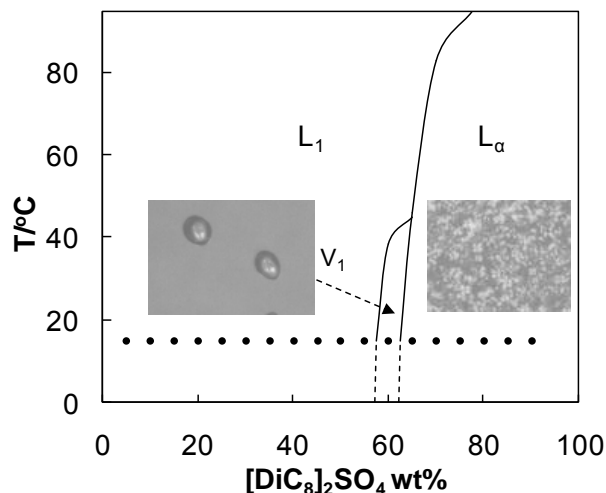


**Figure 2.14**  $[DiC_8]_2[SO_4]/water$  binary diagram as function of temperature.

#### 2.1.4 Microemulsion phase diagrams and amphiphile classification

Microemulsions ( $\mu em$ ) are macroscopically isotropic mixtures of surfactant, hydrophilic (aqueous phase) and hydrophobic (oily phase) components, requiring sometimes addition of a co-surfactant. Different from the ordinary emulsion, the  $\mu em$  is a thermodynamic stable system. It was firstly observed by Schulman<sup>238</sup> and Winsor<sup>239</sup> in 1950s and extensively investigated in the 1980s, when the phase behavior of  $\mu em$ s stabilized by nonionic surfactant,<sup>240</sup> ionic surfactants<sup>241</sup> or both of them<sup>242</sup> were studied in details. Depending on the values of the formulation variables (temperature, salinity, and oil hydrophobicity, *etc.*) and the amount of surfactant, four different types of  $\mu em$  can be obtained: Winsor I (O/W  $\mu em$  in equilibrium with an excess oil phase), Winsor II (W/O  $\mu em$  in equilibrium with an excess water phase), Winsor III (bicontinuous  $\mu em$  in equilibrium with both excess oil and water phase), and Winsor IV (a single phase  $\mu em$  in which oil and water are completely cosolubilized).<sup>29,243,244</sup>

The simplest system to describe the  $\mu em$  phase behavior is the ternary system consisting of water, oil and nonionic *n*-alkyl polyglycol ethers ( $C_iE_j$ ), which ascribes to thermal sensitive of the hydration degree of polyglycol ether head group. Increase of the temperature turns the nonionic surfactant into more hydrophobic one. As depicted in **Figure 2.15a** to **2.15c**, the isothermal Gibbs triangles of Water (A)-Oil (B)-Nonionic surfactant (C) evolve from dominated by Winsor I at low temperature to Winsor II at high temperature *via* an intermediate temperature region where the Winsor III triangle exists inside. Stacking of isothermal Gibbs triangles as a function of the temperature gives the phase prism which indicates the temperature-dependant phase behavior of ternary system (**Figure 2.16a**).<sup>240</sup> The  $T(\gamma)$  section at constant oil/water ratio ( $\alpha = 0.5$ ) from the phase prism give the well-known “Fish diagram” (**Figure 2.16b**), which

provides extremely important information on the surfactant and also on the oils (here  $\gamma$  is defined as a surfactant mass fraction in the system and  $\alpha$  as the oil mass fraction in the mixture of oil and water).

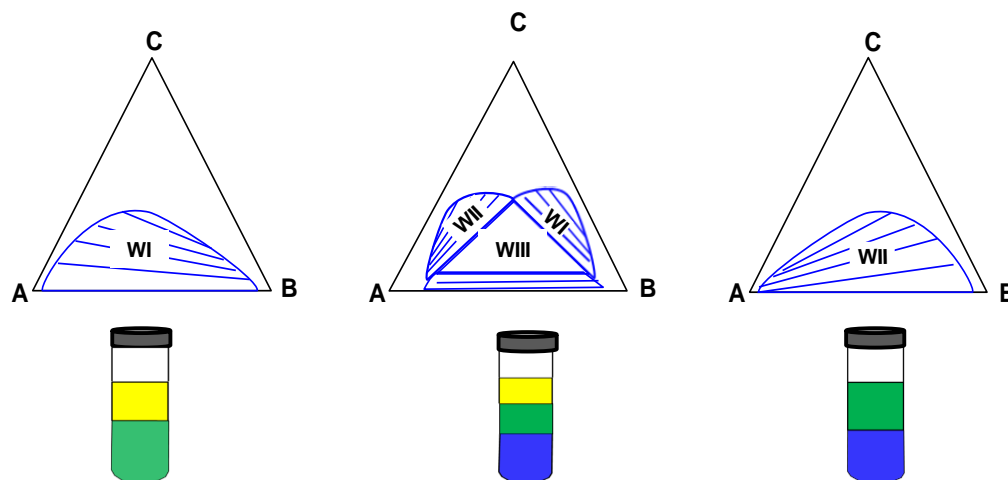


**Figure 2.15** Isothermal Gibbs triangles of water (A)/oil (B)/nonionic surfactant (C) system at different temperatures and the triangle region are dominated by: a) Winsor I at low temperature, b) Winsor III at Intermediate temperature, c) Winsor II at high temperature. The tubes illustrate the phase behavior of different types of  $\mu\text{ems}$ .<sup>16</sup>

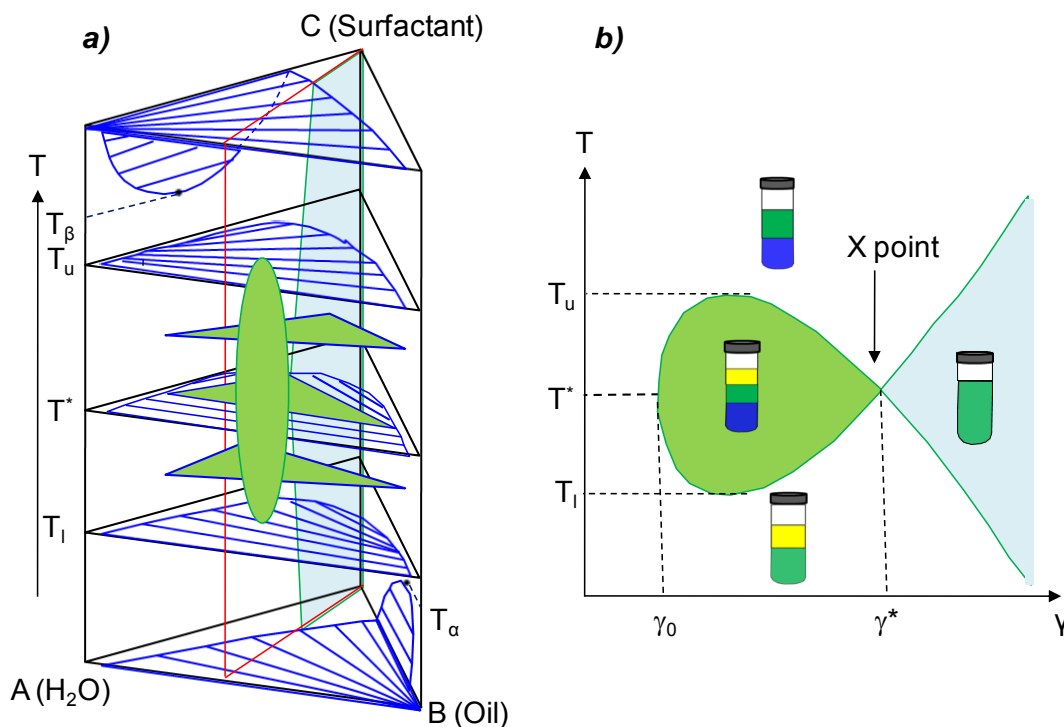


**Figure 2.16** Schematic phase prism of water (A)/oil (B)/nonionic surfactant (C) system as function of temperature (a) and the “Fish diagram” from the  $T(\gamma)$  section at constant oil/water ratio (b).  $T_\omega$ ,  $T_\beta$ , represent the upper critical point of Oil (B)-Surfactant (C) miscibility gap and lower critical point of Water (A)-Surfactant (C) binary diagram, respectively;  $T_b$ ,  $T_u$  represent the lower, upper temperature of

three-phase body;  $\gamma_0$  is the minimal surfactant mass fraction to obtain three-phase  $\mu em$ ;  $T^*$  and  $\gamma^*$  are the phase inversion temperature (PIT) and the minimal mass fraction of surfactant required to solubilize water and oil.<sup>240</sup>

The shape of the “Fish diagram” and the position of the critical X point (**Figure 2.16b**) are dependent on the surfactant type, oil polarity, presence and concentration of salts, addition of co-surfactant *etc.*<sup>240,242</sup> When appropriate surfactant and oil are chosen, the “Fish diagram” can be obtained without additional salts or co-surfactants<sup>29,90,245,246</sup> and with a well characterized surfactant, The polarity of different oils can be evaluated from the evolution of the “Fish diagrams”, especially the evolution of the critical X points, and vice versa.<sup>206,247-249</sup> For example, with  $C_{10}E_4$  or  $C_{12}E_6$  as surfactants at a constant oil/(oil + water) mass fraction of 0.5, the evolution of  $T^*$  value at the X point was found linearly increased with the alkyl carbon number of the linear alkanes from hexane to eicosane, which can be deduced from the equation of the Hydrophilic-Lipophilic Deviation (**Equation 2.1-2.2**).<sup>206,248</sup> HLD, which is a dimensionless number, is described as:

$$HLD = (\alpha - EON) + bS - k(ACN) + aA + t\Delta T \quad (\text{Eq. 2.1})$$

Where  $ACN$  is the carbon number of the  $n$ -alkane,  $\alpha$  and  $k$  are constant for a given nonionic surfactant;  $EON$  is the number of ethylene oxide units in the head group;  $A$  and  $S$  are the concentrations of alcohol and salt, respectively;  $b$  and  $a$  are constants characteristic for the alcohol and salt.  $t$  and  $\Delta T$  are temperature coefficient and temperature deviation from 25 °C. In the absence of alcohols and salts and at the optimal formation ( $HLD = 0$ ), the equation is simplified as:

$$0 = cst - k(ACN) + tT^* \quad (\text{Eq. 2.2})$$

Where  $cst$  is constant value,  $T^*$  is the temperature at the optimal formulation corresponding to the X point in the “Fish diagram”. To evaluate the hydrophobicity of other types of oils rather than linear alkanes, the concept of Equivalent Alkyl Chain Number (EACN) was introduced by Wade *et al.*<sup>250</sup> By using the above linear relation as a calibration curve, the Equivalent Alkyl Chain Number (EACN) of more complex oils than linear alkanes can be obtained from the experimental  $T^*$  values measured by constructing the “Fish diagrams” (**Figure 2.17**). On the basis of this relation and an appropriate surfactant, typically a well-defined polyethoxylated fatty alcohol  $C_iE_j$ , the EACNs of several oil series can be established providing a scale of classification of these oils. For example, by using the well-defined  $C_6E_4$ ,  $C_8E_4$  and  $C_{10}E_4$ , the EACN values of alkylbenzenes and alkylcyclohexanes have been reported by Queste *et al.*,<sup>248</sup> terpene oils were studied by Bouton *et al.*,<sup>206</sup> ester oils by Ontiveros *et al.*,<sup>249</sup> ethers by Wormuth *et al.*<sup>245</sup> and monochloroalkanes by Queste.<sup>251</sup> The EACN values of commonly used oils are presented in **Figure 2.18**. The  $\alpha$ ,  $\omega$ -dichloroalkanes could not be determined precisely because of a loss of linearity in the calibration curve, especially for the very short chain ones which exhibit a high polarity, *i.e.* very low EACN values.

On the other side, when the EACNs of oils were determined, the Hydrophilic-Lipophilic property of a surfactant could be evaluated by constructing the “Fish diagram” and determining the “optimal oil”, which also is called PACN (Preferred Alkane Carbon Number of surfactant).<sup>243,246</sup> From the relation of hydrophilic-lipophilic deviation with the parameters of the mixture (**Equation 2.3**), we can consider the PACN as the intrinsic property of surfactant. When temperature is fixed at 25°C and at the optimal formulation, *i.e.* HLD = 0 at X-point, the EACN of the oil which satisfied this condition was the preferred EACN and can be expressed as **Eq. 2.4**. As  $\sigma$  is parameter dependant on the alkyl chain-length of surfactant and  $k$  is the parameter related with the head group of surfactant reflects the intrinsic hydrophilic-lipophilic property of surfactant. Also, the concentration of surfactant required to obtained WIV  $\mu\text{em}$  at PACN (denoted as  $\gamma^*$ ) reflects the efficiency of surfactant.

$$HLD = \sigma - k \times EACN - a_T(T - 25) \quad (\text{Eq.2.3})$$

Where  $\sigma$  is parameter increases with the alkyl chain-length of surfactant and  $k$  is the parameter related with the headgroup of surfactant.

$$PACN = \frac{\sigma}{k} \quad \text{Eq.2.4}$$

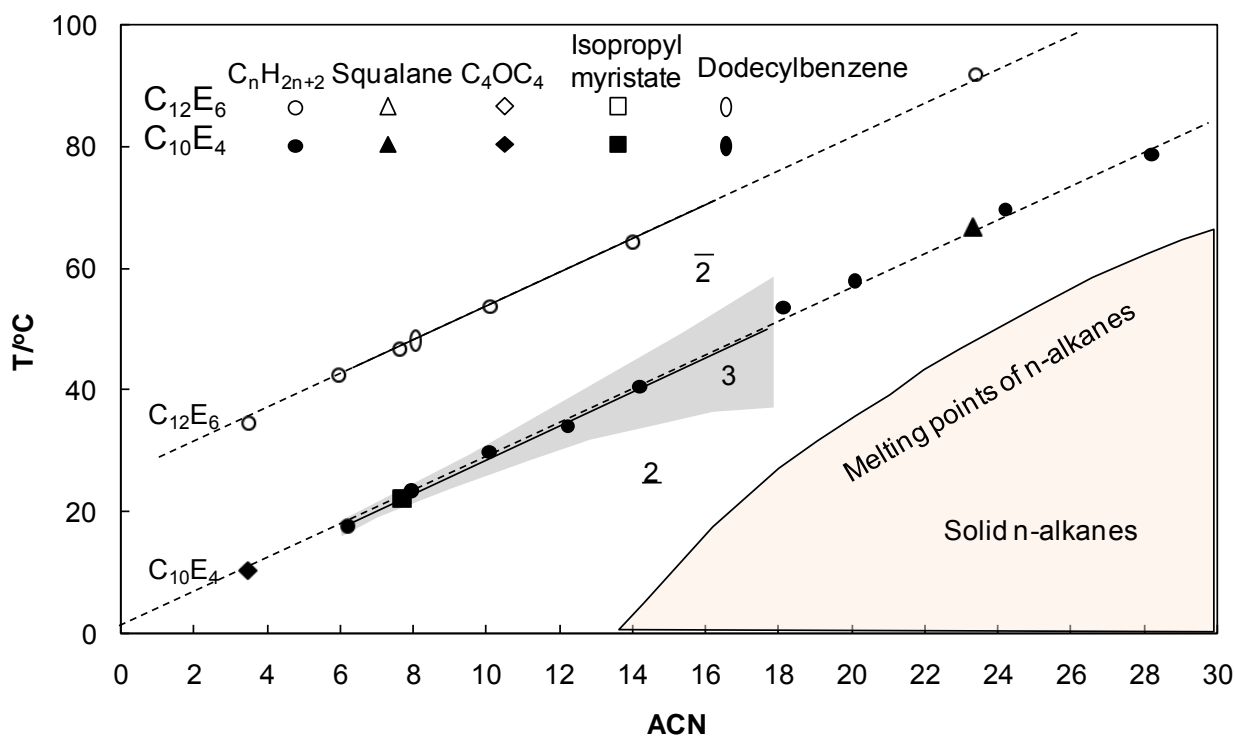


**Figure 2.17**  $T^*$  values for  $C_{10}E_4$  and  $C_{12}E_6$  with  $n$ -alkanes and several selected oils. The widths of the three-phase bodies of  $C_{10}E_4$  are also included (grey area).<sup>248</sup>

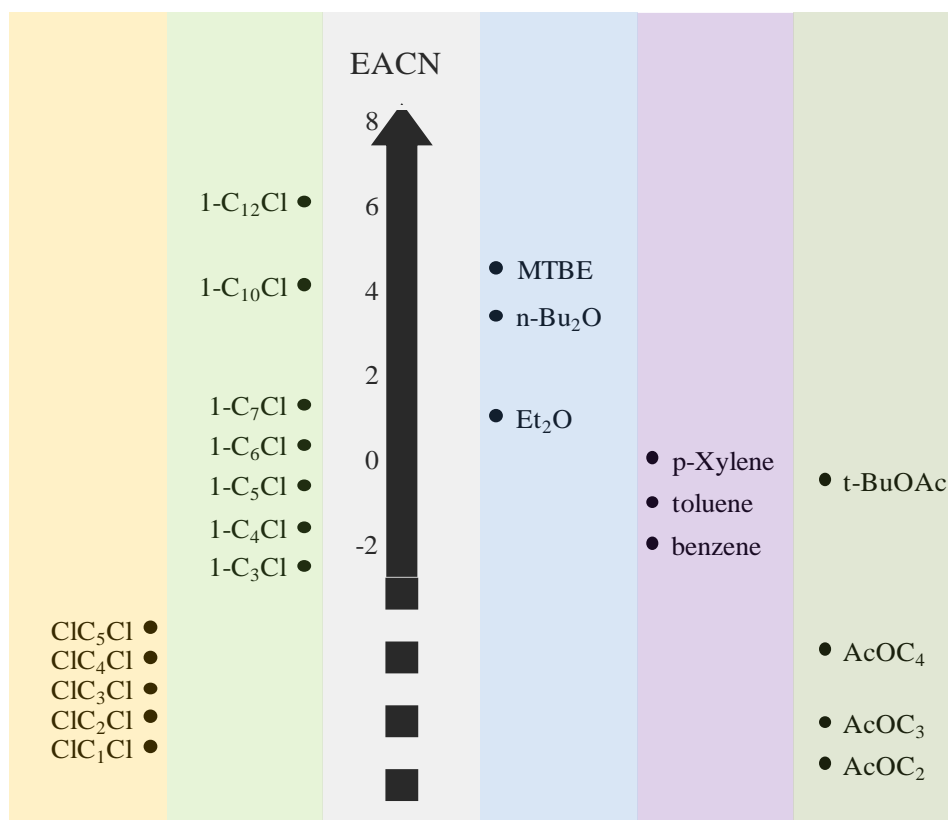


**Figure 2.18** EACN values of common oils: from left to right are  $\alpha, \omega$ -dichloroalkanes (arbitrary values), monochloroalkanes, ethers, alkylbenzene, and esters (arbitrary values except *tert*-BuOAc).<sup>245,248,251</sup>

Different from nonionic surfactants, the temperature has almost no effect on the ternary phase behavior of the ionic surfactants. Ionic surfactants with one single hydrocarbon chain are generally too hydrophilic to build up  $\mu\text{ems}$  alone, and phase inversion can take place only if an electrolyte and/or a cosurfactant is added to the mixture.<sup>16</sup> However, using double-chain ionic surfactants, such as **AOT** and **[DiC<sub>12</sub>]Br (DDAB)**, no co-surfactant is necessary to tune the mean curvature of the interface film from positive to negative.<sup>16</sup> In our case, the salts were forbidden due to the anion exchange between the added electrolyte and the quaternary ammonium salt. On the other side, the oil hydrophobicity, which can modify the relative affinity of the surfactant for the oil and aqueous phase, is a useful scanning variable to tune the phase behavior of the ternary water/surfactant/oil system, even if less effective than temperature or salt additives. Such an absolute oil scale can then further be used to classify surfactants according to the EACN of the oil, providing the optimal formulation at 25°C of true ternary SOW systems without any further additive.<sup>16</sup> When the oil hydrophobicity is the scanning variable, the experiments are usually carried out with *n*-alkanes ranging from 6 to 19 carbon atoms. However, the polarity window afforded by *n*-alkanes is too limited and none of them is enough polar to provide the so-called “optimal formulation” with the cationic surfactants under study. We therefore resorted to two other homologous series of more polar oils, *i.e.* the 1-chloro- and  $\alpha, \omega$ -dichloro-*n*-alkanes, abbreviated respectively as **C<sub>i</sub>Cl** (*i* = 2–16) and **C<sub>i</sub>Cl<sub>2</sub>** (*i* = 1–6). The interest of using homologous series of oils lies in the possibility to vary gradually

their polarity by progressively incrementing the number of carbons of the alkyl chain. Although the  $\omega$ -dichloroalkanes could not be determined due to the high polarity, a partially quantitative scale maybe defined.

Among the different dialkyldimethylammonium surfactants prepared in this work, the [DiC<sub>6</sub>] series is too hydrophilic to be studied with this method, since it always gives Winsor I systems in the range of investigated oils. Ternary surfactant/oil/water systems of [DiC<sub>8</sub>] and [DiC<sub>10</sub>] series were prepared in 2 mL test tubes with the studied compound and chosen oil. Equal amounts (in weight) of water and oil were first introduced, and increasing amounts of amphiphiles were added stepwise. After each addition, the test tubes were gently mixed and placed at 25 °C until the attainment of equilibrium, which generally required ca. 4 h for [DiC<sub>8</sub>]<sub>m</sub>[X] and ca. 6 h for [DiC<sub>10</sub>]<sub>m</sub>[X]. The types of Winsor systems (I–IV) were determined by visual observation. As shown in **Figure 2.19**, the “Fish diagram” of [DiC<sub>8</sub>]Br/oil/water was drawn by screening the oils from 1-chloropropane to 1-chlorododecane. The oils of high polarity, like 1-chloropropane, gave Winsor II  $\mu\text{em}$  at the beginning and gradually addition of surfactant increased the volume of the  $\mu\text{em}$  phase until one phase Winsor IV appeared. In contrast, the oils of high hydrophobicity, like 1-chlorododecane, gave only Winsor I  $\mu\text{em}$  before complete cosolubilization of oil and water. In the region of the three-phase  $\mu\text{em}$  body, the Winsor III  $\mu\text{em}$  was firstly obtained with addition of surfactant, gradually addition of surfactant enlarged the volume of the middle  $\mu\text{em}$  phase until Winsor II or Winsor I  $\mu\text{em}$ , depending on the polarity of the oils, and finally Winsor IV  $\mu\text{em}$  was obtained with further addition of surfactant.

In the “Fish diagram”, the “Fish head” point is characterized by the minimal mass fraction  $\gamma_0$ , which indicates the appearance of the three-phase  $\mu\text{em}$ . When the concentration is further increased, the volume of the middle  $\mu\text{em}$  phase increases, and at the “Fish tail” point (X-point), the three-phase body meets the monophasic region at  $\gamma^*$  corresponding to the minimum amount of surfactant needed to form a one-phase  $\mu\text{em}$ . Hence,  $\gamma^*$  reflects the efficiency of the surfactant.<sup>244,246</sup> At the X-point also defines the “optimal oil” with which the minimal surfactant was required to obtain the one phase  $\mu\text{em}$  and the EACN of this “optimal oil” was defined as PACN of surfactant, which characterizes the amphiphilic property of surfactant. This “optimal” oil is rarely a well-defined one but more often an appropriate mixture of two oils differing only in a single carbon so that it behaves as an ideal mixture.

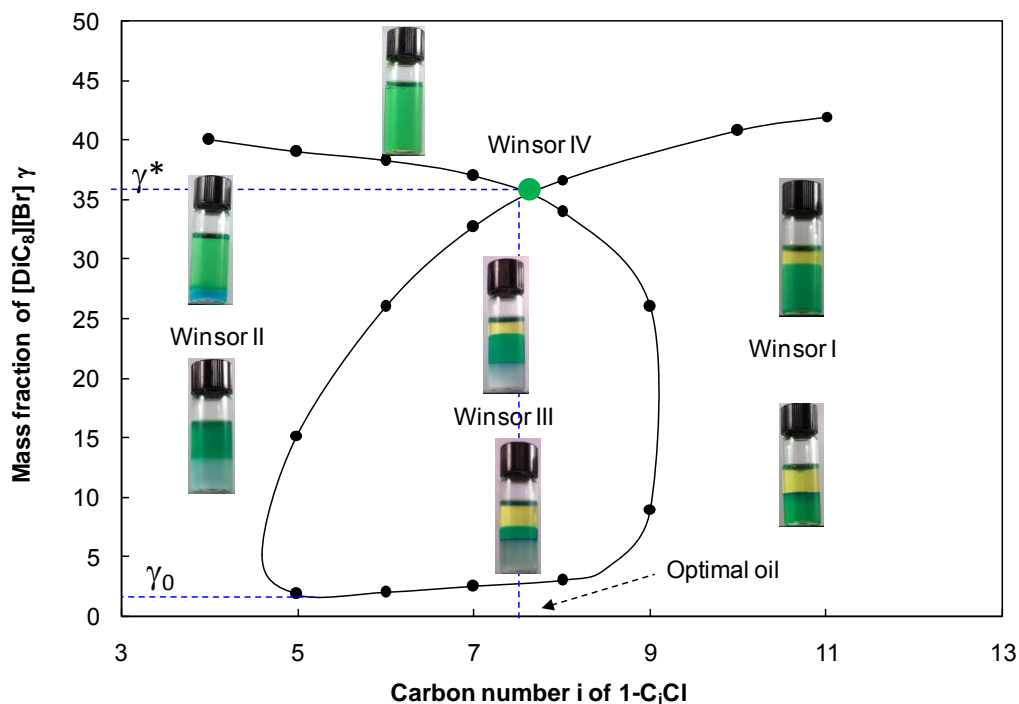


**Figure 2.19** “Fish diagram” of  $[\text{DiC}_8]\text{Br}$  determined with 1-chloroalkanes ( $1\text{-C}_i\text{Cl}$ ) as a scan variable. Tubes represent the different systems (water phase in blue, oil phase in yellow and  $\mu\text{em}$  phase in green in the presence of Jaune au Gras W1201 and Blue soluble W6002).

Besides  $[\text{DiC}_8][\text{Br}]$ , the “Fish diagrams” of the other amphiphiles were also drawn by screening of the monochloroalkanes or  $\alpha,\omega$ -dichloro- $n$ -alkanes. Monochloroalkanes are also suitable for  $[\text{DiC}_{10}]_2\text{WO}_4$  and  $[\text{DiC}_{10}]_2\text{MoO}_4$ , whereas,  $\alpha,\omega$ -dichloro- $n$ -alkanes are more suitable for  $[\text{DiC}_8][\text{Cl}]$ ,  $[\text{DiC}_8]_2\text{WO}_4$  and  $[\text{DiC}_8]_2\text{MoO}_4$ . It is interesting to note that each dialkyldimethylammonium surfactant displays a characteristic “Fish diagram” (**Figure 2.20**). The different  $\gamma_0$ ,  $\gamma^*$  values and optimal oils between these surfactants reflect the effect of the surfactant chain length and counter ions on the hydrophilic-lypophilic balance and efficiency of the surfactant. The values of  $\gamma_0$  and  $\gamma^*$  are reported in **Table 2.4** and the PACN of the surfactants are placed in the EACN axis (**Figure 2.21**).

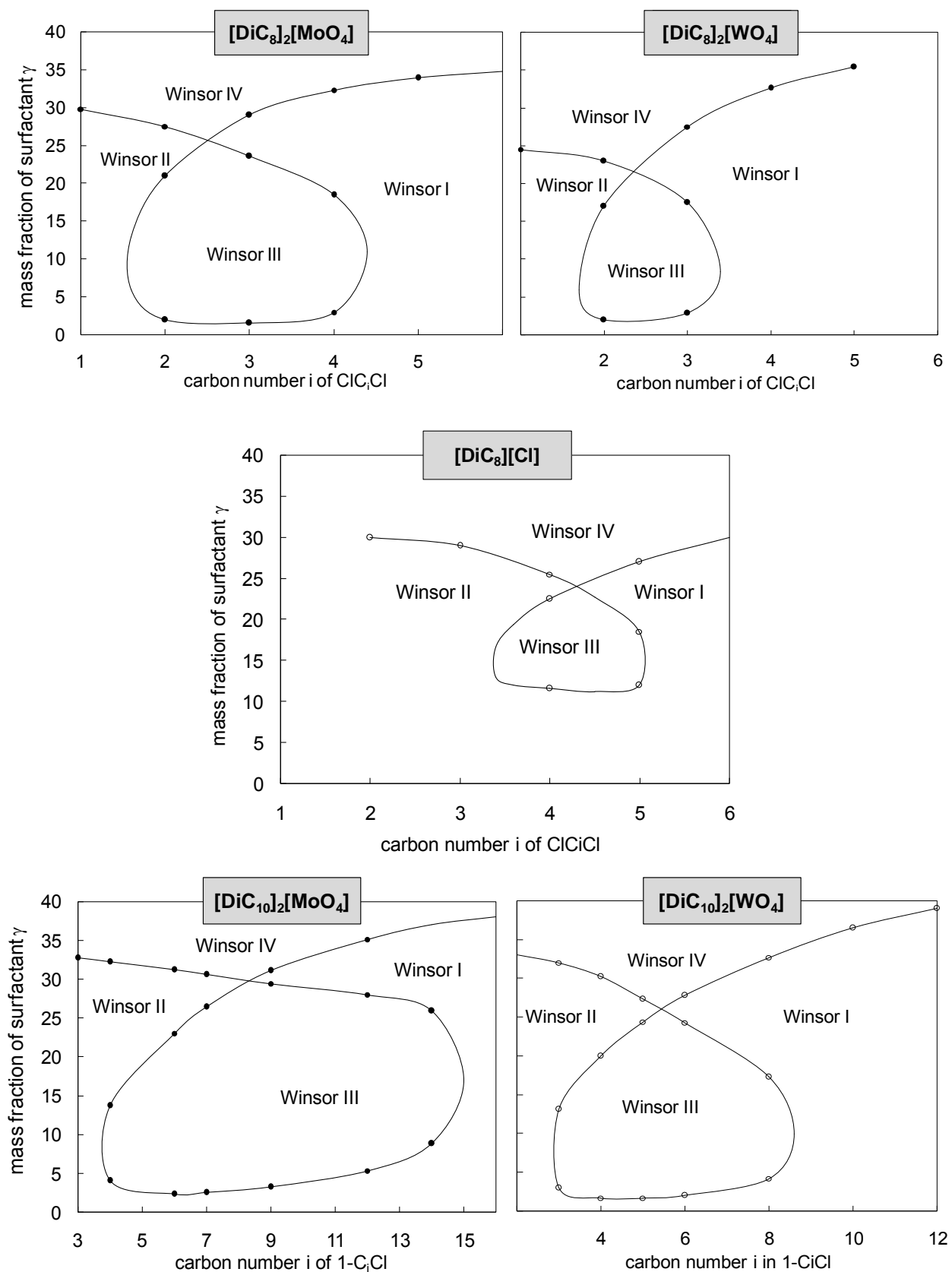


**Figure 2.20** “Fish diagrams” of  $[\text{DiC}_{10}]_2[\text{MoO}_4]$ ,  $[\text{DiC}_{10}]_2[\text{WO}_4]$ ,  $[\text{DiC}_8][\text{Cl}]$ ,  $[\text{DiC}_8]_2[\text{MoO}_4]$ ,  $[\text{DiC}_8]_2[\text{WO}_4]$  determined with 1-chloroalkanes ( $1\text{-C}_i\text{Cl}$ ) or  $\alpha,\omega$ -dichloroalkanes ( $\text{C}_i\text{C}_i\text{Cl}$ ) as scan variables.



The “Fish diagrams” exhibit variable body shapes with a relatively larger body Fish with molybdate salts. Finding an explanation is not trivial at all because the oil is used as a tuning parameter, thus changing the ternary system, and because the hydrophobicity of dichloroalkanes does not follow a linear variation according to the number of carbons. However, Strey and co-workers<sup>252</sup> have reported that for a series of polyethoxylated alcohols  $C_iE_j$  and for the same  $n$ -alkanes, the extension of the three-phase body is small for the shortest ones, passes through a maximum for medium-chain ones and decreases again for long-chain ones. The maximum in the temperature extension of the Fish body indicates the frontier between weakly and strongly structures mixtures, also called the Lifshitz line.<sup>252</sup> In the present case, we are above this maximum that corresponds to  $C_6$  chain length. Hence, when the chain length increases, the Fish body should be narrower but the phenomena are here more intricate since we have to compare mono-, *i.e.* chloride and bromide, with divalent, *i.e.* molybdate and tungstate, anions.

**Table 2.4** Minimal amounts required to obtained a Winsor III  $\mu\text{em}$  ( $\gamma_0$ ), a Winsor IV  $\mu\text{em}$  ( $\gamma^*$ ) and “optimal” oil for  $[\text{DiC}_n][\text{X}]$  with  $X = \text{Br}$  or  $\text{Cl}$  and  $[\text{DiC}_n]_2[\text{X}]$  with  $X = \text{MoO}_4$  or  $\text{WO}_4$  ( $n = 8$  and  $10$ ).

X	[DiC <sub>8</sub> ][X]		[DiC <sub>8</sub> ] <sub>2</sub> [X]		[DiC <sub>10</sub> ] <sub>2</sub> [X]	
	Cl	Br	MoO <sub>4</sub>	WO <sub>4</sub>	MoO <sub>4</sub>	WO <sub>4</sub>
$\gamma_0$ (wt.%)	11	2	2	2	2	2
$\gamma^*$ (wt.%)	24.0	35.1	25.1	22.5	29.1	25.1
“Optimal oil”	C <sub>4,2</sub> Cl <sub>2</sub> <sup>a</sup>	C <sub>7,2</sub> Cl <sup>b</sup>	C <sub>2,5</sub> Cl <sub>2</sub> <sup>c</sup>	C <sub>2,4</sub> Cl <sub>2</sub> <sup>d</sup>	C <sub>8,2</sub> Cl <sup>e</sup>	C <sub>5,4</sub> Cl <sup>f</sup>

<sup>a</sup> 0.8C<sub>4</sub>Cl<sub>2</sub>/0.2C<sub>5</sub>Cl<sub>2</sub>; <sup>b</sup> 0.8C<sub>7</sub>Cl/0.2C<sub>8</sub>Cl; <sup>c</sup> 0.5C<sub>2</sub>Cl<sub>2</sub>/0.5C<sub>3</sub>Cl<sub>2</sub>; <sup>d</sup> 0.6C<sub>2</sub>Cl<sub>2</sub>/0.4C<sub>3</sub>Cl<sub>2</sub>; <sup>e</sup> 0.8C<sub>8</sub>Cl/ 0.2C<sub>9</sub>Cl; <sup>f</sup> 0.6C<sub>5</sub>Cl/0.4C<sub>6</sub>Cl.

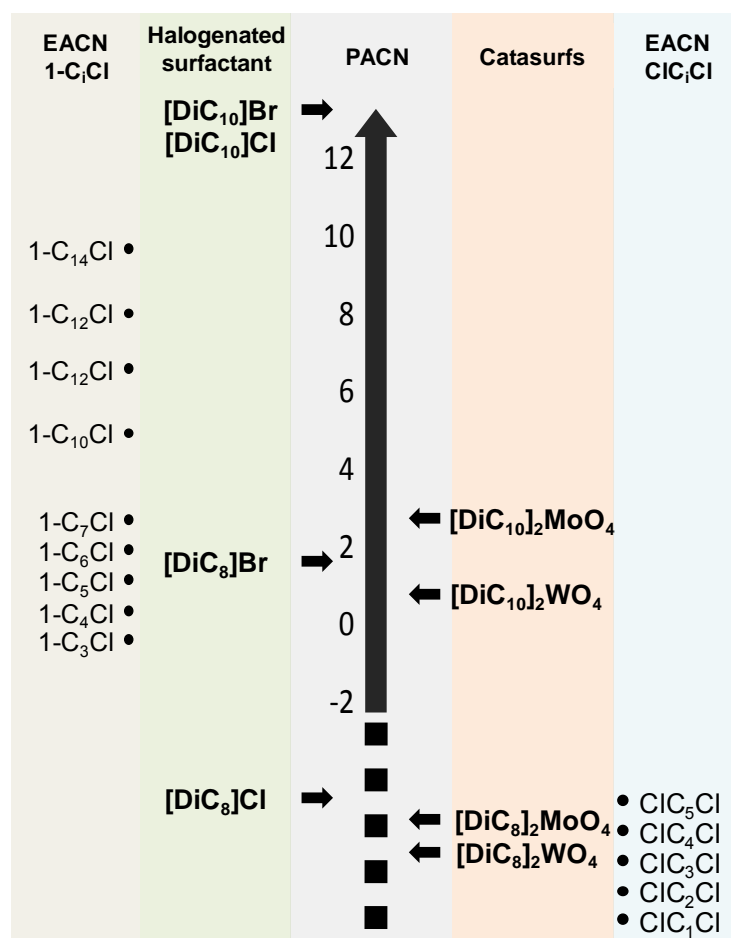


**Figure 2.21** Range of EACN values accessible with two series of homologous oils: 1-chloroalkanes noted  $C_iCl$  with  $i = 3-14$  and  $\alpha, \omega$ -dichloroalkanes noted  $C_iCl_2$  with  $i = 1-6$ ; Classification of the quaternary ammonium amphiphiles according to the PACN scale.

At the optimal formulation, *i.e.* at X-point, the amphiphile has the same affinity for water and oil. Accordingly, if its affinity for water increases, then, the oil should be more polar to compensate for and conversely. The order found, besides the chain length, is mainly governed by the counter anion and rationalized by its hydration degree, in agreement with the Hofmeister anion effect, which classifies the anions by the effects of salts on the protein solubility and stability.<sup>253-255</sup> Though divalent anions are electrostatically associated with two dialkyl hydrophobic chains, molybdate and tungstate salts are highly hydrated (see above  $\Delta G_{hydr}$ ) and thus, require more polar oils. Indeed, the process involved in the formation of bicontinuous  $\mu em$  will be less energetically favorable: it must be dehydrated to make contact with the oil phase. On the other hand, the efficiency of the amphiphiles to form  $\mu ems$  is reflected by the value of  $\gamma^*$ . The difference between different surfactants could be rationalized by the modified Winsor R ratio qualitatively (**Figure 2.22**).<sup>244</sup>  $R = 1$  corresponds the optimal formulation and the efficiency of surfactant is determined by the value of numerator and denominator. When the surfactant chain length increases, the interaction between surfactant chain and oil  $A_{i0}$  increases more rapidly than the interaction

between different surfactant chains  $A_{ll}$ , which results the increase of the numerator value, so more hydrophobic oil is required to keep the numerator value as in this case, the interaction between the oils  $A_{oo}$  increases more rapidly than  $A_{lo}$ . The magnitude of the denominator does not change when the counter ion is kept the same, so the total efficiency is almost unchanged. On the other side, when less hydrated counter ion is chosen as a counter ion, the value of the denominator decreases, which indicates the decrease of the surfactant efficiency and increase of  $\gamma^*$  and at the same time, a more hydrophobic oil is required to keep  $R = 1$ . To illustrate this, we can see that  $[\text{DiC}_8]_2[\text{WO}_4]$  is much more efficient than  $[\text{DiC}_8][\text{Br}]$ . Indeed, the oils providing the “optimal” formulation with the tungstate salt are much more polar than those required for the bromide salt which is also more hydrophobic. This might also explain the good efficiency of  $[\text{DiC}_8][\text{Cl}]$  for which  $\gamma^*$  is equal to 24 wt.% for an optimal oil equivalent to a  $0.8\text{Cl}_4\text{Cl}/0.2\text{Cl}_5\text{Cl}$  mixture.

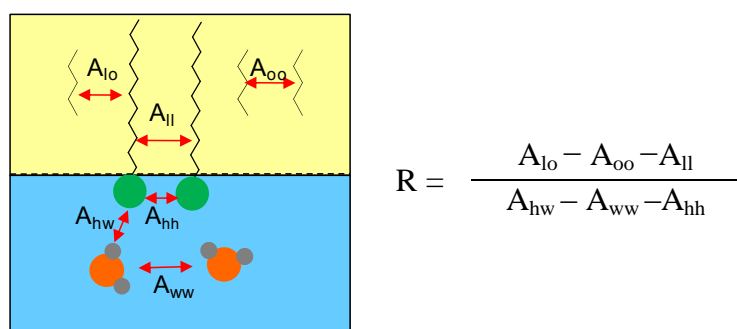


**Figure 2.22** Interaction between the surfactant molecule at the interface and nearby oil and water molecules, respectively. Where  $A_{lo}$ ,  $A_{ll}$  and  $A_{oo}$  are the interaction energies between lipophilic chain (l) with oil (o), lipophilic chain and lipophilic chain, and oil and oil, respectively.  $A_{hw}$ ,  $A_{hh}$  and  $A_{ww}$  represent the interaction energies between hydrophilic head group (h) and water (w), head group and head group, and water and water, respectively.

The  $\gamma_0$  value, *i.e.* the minimum amount of surfactant needed to enter the three-phase region, characterizing the “Fish head” position, is also relevant information. It is of ca. 2 wt.% for all the amphiphiles except for  $[\text{DiC}_8][\text{Cl}]$  for which at least 11 wt.% of amphiphile is required to form a WIII system, which was probably ascribed to the partition of free surfactant molecules between water and the “optimal oil”. On the other side, the previous research indicated that  $[\text{DiC}_8][\text{Cl}]$  dimers was formed between 0.2 - 10 mM at dilution aqueous solution, followed by bilayers at 10- 30 mM and finally, the first true “micelles” appear only above 30 mM (**Figure 2.23**).<sup>31</sup> Therefore, as the formation of micelles in the aqueous phase is a prerequisite for a  $\mu\text{em}$  to form, a high value of the CMC also contributes to the high  $\gamma_0$ .

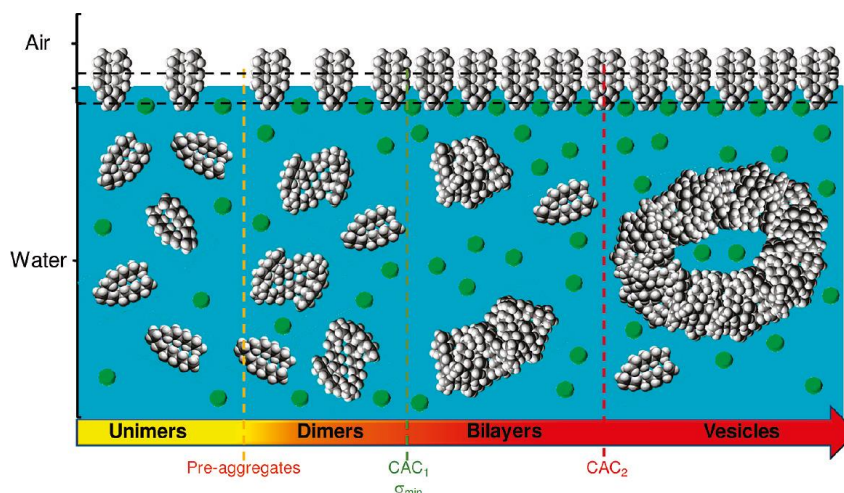


**Figure 2.23** The aggregation process model of  $[\text{DiC}_8]\text{Cl}$ .<sup>139</sup>

All these results demonstrate that several key parameters govern the ternary phase behavior of the dialkyldimethylammonium salts, notably the hydration degree and the valence of the counter anion, the chain length of the hydrophobic tail and the polarity or EACN of the oil. Rationalization is not straightforward as several effects overlap but tendencies can be deduced affording amphiphiles classification and ternary phase behavior prediction.

### 2.1.5 Conclusion

The CACs, the binary diagrams and the  $\mu\text{em}$  phase behavior have been investigated for a series of double-chain quaternary ammonium molybdate and tungstate,  $[\text{DiC}_n]_2[\text{MO}_4]$  with  $M = \text{W}$  or  $\text{Mo}$  and  $n = 6, 8$  and  $10$  in comparison with their chloride and bromide counterparts.  $[\text{DiC}_6]$  salts behave as hydrotropes and do not form well-defined aggregates in water. The evolution of the phase behavior from  $[\text{DiC}_{10}]$  to  $[\text{DiC}_6]$  was reflected by the binary phase diagrams. The boundary of isotropic solution and anisotropic phase moved to higher concentrations when the alkyl chain length decreases. This was ascribed to the hydrophobic effects of the alkyl chain of the surfactant. The  $[\text{DiC}_{10}]_2[\text{MoO}_4]$  and  $[\text{DiC}_{10}]_2[\text{WO}_4]$  gave wide range of biphasic mixture region whereas the  $[\text{DiC}_{10}][\text{Cl}]$  do not, which was consistent with Monte-Carlo simulation and the conclusion that there is a significant attraction between the lamellae derived from the charge fluctuation for divalent counter ions. The micellar, cubic and lamellar phases were clearly distinguished and identified with polarized optical microscopy and SAXS. From the “Fish diagrams” of the  $\text{H}_2\text{O}$ -surfactant-chloroalkanes systems, the hydrophilic-lipophilic balance of these amphiphiles could be assessed, at least qualitatively. The behavior of the  $[\text{DiC}_8]$  series with the four counter anions can be rationalized by the Hofmeister anion sequence. In all the manuscript, the unusual behavior of the  $[\text{DiC}_8][\text{Cl}]$  and  $[\text{DiC}_8]_2[\text{MO}_4]$  ( $M = \text{W}$  or  $\text{Mo}$ ) is emphasized again. The particular behavior observed in diluted aqueous solution (previously reported)<sup>220</sup> is maintained to a great extent in liquid crystal phase and ternary system.

## 2.2 Double-chain sulphonate catalytic surfactants

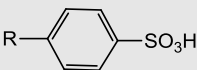
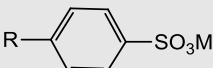
### 2.2.1 Applications of ionic surfactants and synthesis of double-chain sulphonate surfactants

As shown in **Figure 2.1**, anionic surfactants occupied about 41% of the market share of the surfactants in 2010, four times as much as the cationic surfactant. Among them, alkylsulphonates and alkylsulfates are the most widely used surfactants in the fields of detergency, personal care, foams, emulsions and so on.<sup>256</sup> For example, **sodium dodecyl sulfate (SDS)** is an effective ingredient in detergents for laundry with many cleaning applications; it is found in many toothpaste, shampoo, shaving cream and bubble bath formulations. Another example, **dioctyl sodium sulfosuccinate (Aerosol OT or AOT)**, is the most widely used surfactant in the research of reverse micelle encapsulation;<sup>257</sup> it also used as a pesticide, excipient in the production of tablets and in medical treatments of constipation.<sup>258-260</sup> Besides these two common anionic surfactants, a large number of other anionic head groups and counterions are also encountered in the widely used commercial products (**Table 2.5**).

As reviewed in chapter 1, the anionic surfactant-combined Brønsted and water compatible Lewis acids have been successfully applied to various reactions in aqueous phase, especially the carbon-carbon formation reaction.<sup>53-58</sup> While most of the reactions proceed in aqueous micelle systems, some drawbacks such as the limited substrate concentration and the incompatibility of water sensitive products are still present. With the **dodecylbenzene sulfonic acid (DBSA)** esterification as an example, the reaction is limited to hydrophobic substrates due to easy hydrolysis of hydrophilic esters in acidic aqueous phase.<sup>71</sup>

Inspired from the “Catasurf” concept developed by our group and advantages of  $\mu$ ems as reaction media, a series of double-chain sulfonic acids and sulphonates with various water tolerable Lewis acids as counter ions have been designed and synthesized.<sup>29</sup> Sulphonates were preferred over sulfates since these latter are most sensitive towards hydrolysis. To elaborate the  $\mu$ ems, the common used solvents like cyclohexane, methyl *tert*-butyl ether (MTBE), *tert*-butyl acetate, ether *etc.* were preferred not only for their accessibility, good solvent properties but also for their low toxicity. The screening of salt concentration as a function of interfacial tension for several double-chain sulphonate sodium were reported previously (**Figure 2.24**).<sup>261,262</sup> Depending on these results, the EACN values of solvents used and considering that the multiphase  $\mu$ em systems should be elaborated without salts, the chain lengths of the developed sulphonate surfactants were fixed at 6, 7 and 8 carbon atoms. The alkyl anionic part of the surfactants is abbreviated as **DiC<sub>n</sub>CHSO<sub>3</sub>** with n = 6, 7, 8 (**Figure 2.25**).

**Table 2.5** Commonly used sulphonate and sulfate surfactants and their main applications.

Name	R	Application
<b>Alkyl benzene sulfonic acid</b>		
<b>Dodecyl benzene sulfonic acid</b>	C <sub>12</sub> H <sub>25</sub>	<ul style="list-style-type: none"> <li>• Household detergents (industrial uses)</li> <li>• Powder and liquid laundry detergents</li> </ul>
<b>Alkyl benzene sulphonate</b>		
<b>Sodium dodecyl benzene sulphonate</b>	C <sub>12</sub> H <sub>25</sub>	<ul style="list-style-type: none"> <li>• Detergent, emulsifier, dispersant for household and industrial detergents</li> <li>• Detergent for food containers</li> </ul>
<b>Calcium dodecyl benzene sulphonate</b>	C <sub>12</sub> H <sub>25</sub>	<ul style="list-style-type: none"> <li>• Household detergents</li> <li>• Wetting agent</li> <li>• Emulsifier for agricultural herbicides</li> </ul>
<b>Isopropylamine dodecyl benzene sulphonate</b>	C <sub>12</sub> H <sub>25</sub>	<ul style="list-style-type: none"> <li>• Detergent for personal care product</li> <li>• Surface coating</li> <li>• Dry cleaning</li> </ul>
<b>Alpha olefin sulphonate</b>	$\left. \begin{array}{l} RCH_2CH(OH)(CH_2)_mSO_3Na \\ RCH=CH(CH_2)_nSO_3Na \end{array} \right\} \text{Mixture}$	
<b>Sodium C<sub>14-16</sub> olefin Sulphonate</b>	C <sub>10</sub> H <sub>21</sub> -C <sub>13</sub> H <sub>27</sub> n, m = 1 or 2	<ul style="list-style-type: none"> <li>• Emulsifier for emulsion polymerization</li> <li>• Fine and rich foaming agent</li> <li>• Detergents</li> </ul>
<b>Alkyl sulfate</b>	ROSO <sub>3</sub> M	
<b>Sodium lauryl sulfate</b>	C <sub>12</sub> H <sub>25</sub>	<ul style="list-style-type: none"> <li>• Detergents</li> <li>• Refining agent and penetrant</li> </ul>
<b>Sulfosuccinates</b>	$\begin{array}{c} \text{ROCOCH}_2 \\   \\ \text{ROCOCHSO}_3\text{Na} \end{array}$	
<b>Aerosol OT</b>	2-ethylhexyl	<ul style="list-style-type: none"> <li>• Penetrant, Emulsion breaker</li> <li>• Emulsifier for agricultural applications</li> </ul>
<b>Disodium lauryl Sulfosuccinate</b>	C <sub>12</sub> H <sub>25</sub>	<ul style="list-style-type: none"> <li>• High foaming agent</li> </ul>

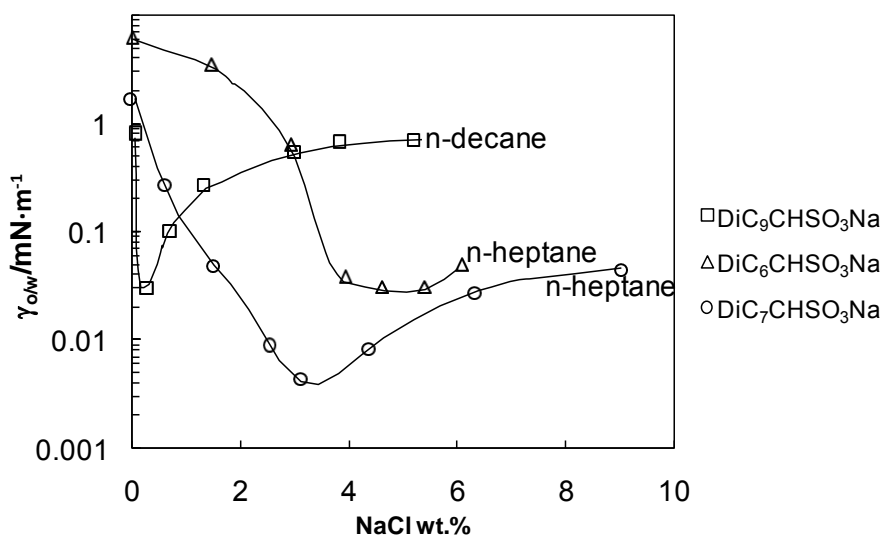


**Figure 2.24** Variation of water/surfactant/n-alkane interfacial tension versus salinity.<sup>80,81</sup>

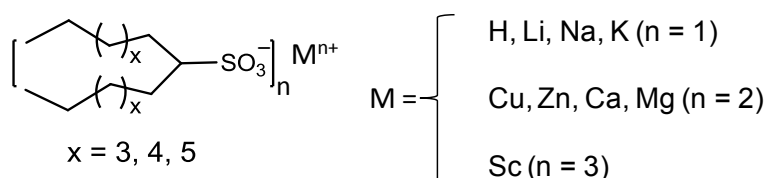
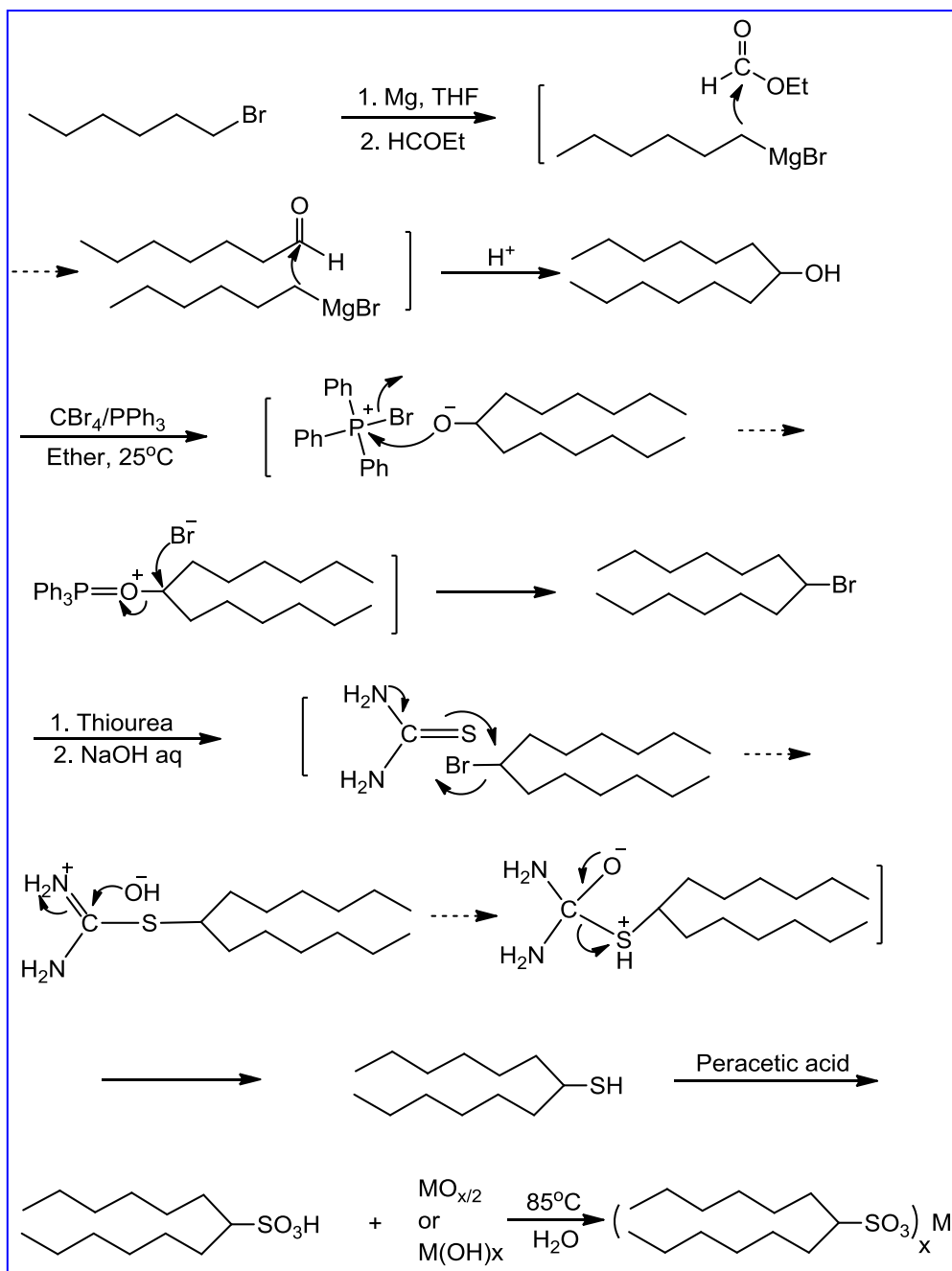


**Figure 2.25** Symmetric dialkyl methanesulfonic acid and sulphonates with different counter ions.

The synthesis of the sulphonate surfactants was carried out with 1-bromoalkane as a starting material, which could be transformed to Grignard reagent quantitatively via the reaction with Mg in dry THF solution and then reacted with 0.5 equivalent ethyl formate afforded the symmetric dialkyl substituted methanol in high yield ( $> 85\%$ ).<sup>263</sup> Then the hydroxyl group was transferred to bromide *via* Appel reaction: the corresponding alcohol was dissolved in dry ether ether with  $\text{PPh}_3$ , and under Ar atmosphere,  $\text{CBr}_4$  was added stepwisely, the byproduct diphenylphosphine oxide precipitated and was eliminated by filtration and the desired alkyl bromide was purified by distillation in vacuum ( $> 82\%$  yield). Refluxed with thiourea in ethanol, the dialkyl substituted bromomethane was readily converted to the corresponding thiol, which separated from the reaction mixture directly as a result of the low solubility in water and ethanol and further purified by distillation in vacuum ( $> 78\%$  yield). Finally, the sulfonic acid could be obtained by oxidation of the thiol with peracetic acid in acetic acid solution quantitatively.<sup>264</sup> The solubility of dihexyl methanethiol was sufficient to allow the oxidation, while the solubility of diheptyl and dioctyl methanethiols in acetic acid was too low to be oxidized. In this case, THF was added as a co-solvent (THF/acetic acid = 1:1) to solve the solubility problem. Removing the solvent afforded the crude product of sulfonic acid with several organic impurities, which could be purified by azeotropic distillation. The metal sulphonates could be prepared directly by the acid-base reaction between the metal

oxide and sulfonic acid. All the reaction steps are summarized in **Scheme 2.2** and the key intermediates during the reactions were also presented in the brackets.



**Scheme 2.2** Synthesis of symmetric dialkyl substituted methanesulfonic acid and corresponding sulphonate salts ( $X = 1, 2, 3$ ).

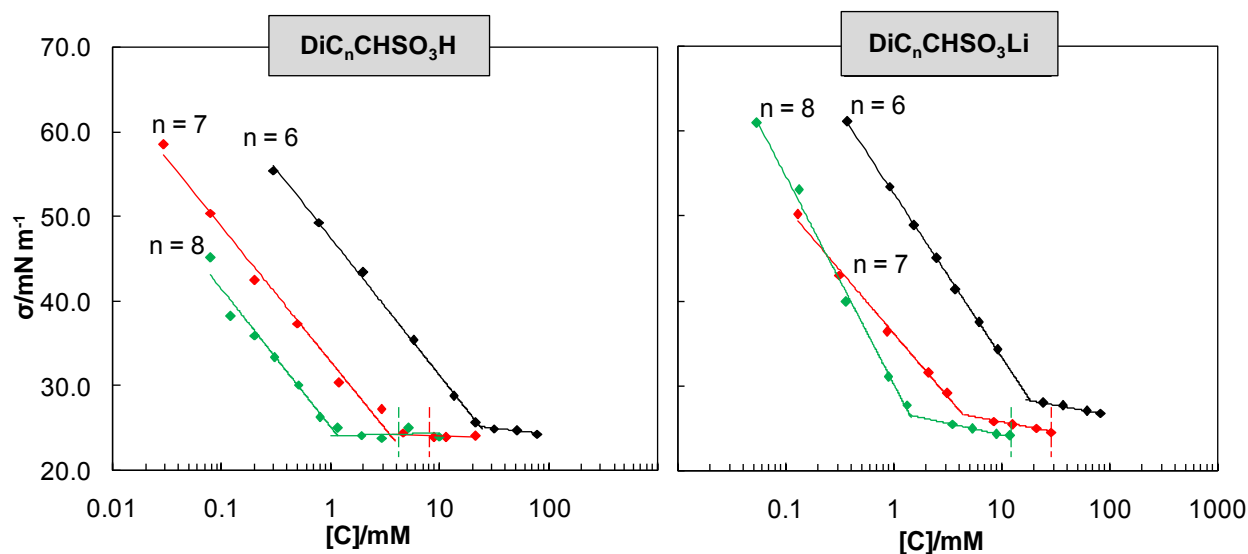
Among the different metallic cations,  $\text{Cu}^{2+}$ ,  $\text{Zn}^{2+}$ ,  $\text{Ni}^{2+}$ ,  $\text{Co}^{2+}$ ,  $\text{Fe}^{2+}$ ,  $\text{Fe}^{3+}$  and  $\text{Sc}^{3+}$  have been widely applied to Lewis acid catalyzed reactions in aqueous phase, while among the metal oxides, the acidity of the prepared acids was not enough strong to afford their reaction with  $\text{NiO}$ ,  $\text{CoO}$  and  $\text{Fe}_2\text{O}_3$ . Instead, the  $\text{NiCl}_2$ ,  $\text{CoCl}_2$ , and  $\text{FeCl}_3$  were chosen rather than the metal oxide. Under acidic aqueous condition, the floccus of the corresponding metal sulphonate dispersed in the solution which was centrifugated and dried

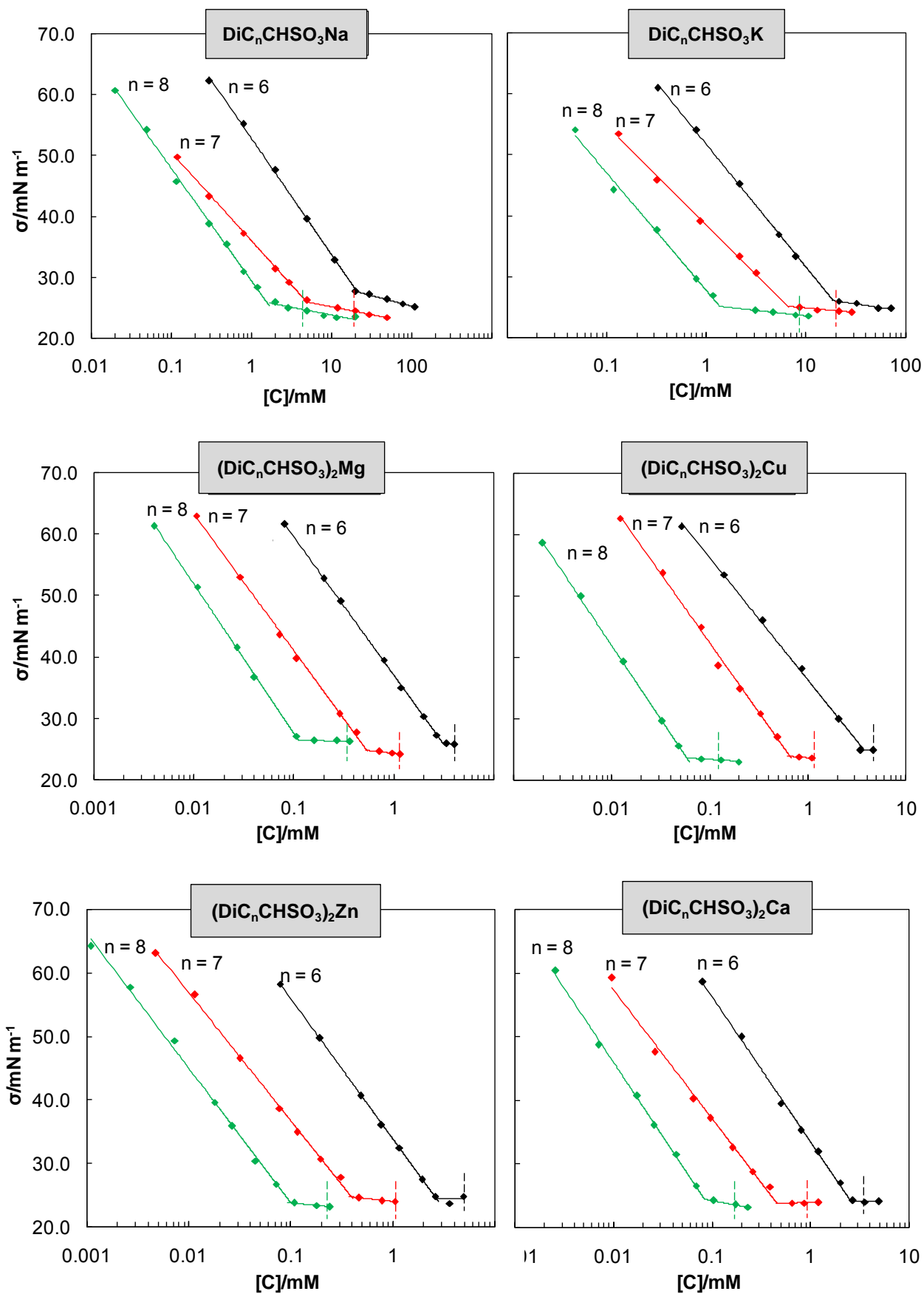


by lyophilisation, instead of the desired sulphonates solid, the sulfonic acid and metal oxide or hydroxide were obtained due to the hydrolysis during the lyophilisation. Besides these useful Lewis acid metallic cations, others common metallic cations, including the alkali and alkaline metallic cations were selected for comparison of phase behavior affected by different counter ions.

### 2.2.2 CMCs of the $\text{DiC}_n\text{CHSO}_3\text{M}$ ( $\text{M}=\text{H}, \text{Li}, \text{Na}, \text{K}$ ), $[\text{DiC}_n\text{CHSO}_3]_2\text{M}$ ( $\text{M} = \text{Cu}, \text{Zn}, \text{Ca}$ ) and $[\text{DiC}_n\text{CHSO}_3]_3\text{Sc}$

Once the different sulfonic acids and sulphonates synthesized, the CMC of the surfactants, which is the most important physicochemical property for a surfactant, was firstly determined by measuring the surface tensions with the tensiometer K11 (Krüss) using the Wilhelmy plate method as described previously for the double-chain ammonium salts. The stock solutions were prepared with ultrapure water (Millipore water,  $\sigma = 72.0 \text{ mN}\cdot\text{m}^{-1}$  at  $25 \text{ }^\circ\text{C}$ ) and a series of various surfactant concentrations were prepared by dilution. Surface tension was recorded after equilibration for each mixture. All equilibrium surface tension values were mean quantities of at least three measurements. The temperature was stabilized at the desired temperature with a thermo-regulated bath Lauda RC6. The standard deviation was estimated at  $\pm 10\%$  for the CAC value. The results are shown in **Figure 2.26** and **Table 2.6**. The effects of the alkyl chain length and counter-ions on the CMC values are obvious. Different from  $[\text{DiC}_6]$  series salts (considered as a hydrotrope),  $[\text{DiC}_6\text{CHSO}_3]_x[\text{M}]$  present clear breaking points in the diagram of concentration vs surface tension and act as a true surfactant instead of a hydrotrope. In the diagrams, it was found that after the breaking point, the surface tension still decreased with smaller slope rather a constant value, especially for the surfactant with longer alkyl tails, which could be rationalized by the situation of surfactant molecules on the surface at the CMC. The adsorption of surfactant with long alkyl tails at the water/air interface was less saturated than shorter ones and the molecules prefer lying on the surface rather than vertical at the CMC. Then the surfactant film became more condensed as the surfactant concentration increases after CMC, which results in the slow decrease of the surface tension.





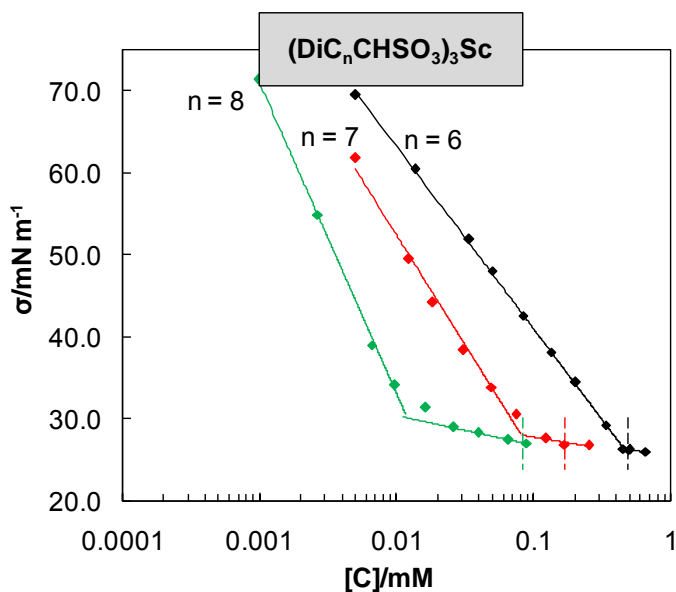


**Figure 2.26** Surface tension ( $\sigma$ ) plotted against surfactant concentration for  $[\text{DiC}_n\text{CHSO}_3]_x[\text{M}]$  ( $x = 1$ ,  $M = \text{H, Li, Na, K}$ ;  $x = 2$ ,  $M = \text{Cu, Zn, Ca, Mg}$ ;  $x = 3$ ,  $M = \text{Sc}$ ). The dashed line indicated the limit of solubility of corresponding sulfonic acid or sulphonate.

The effect of alkyl chain length is ascribed to the so called “hydrophobic effect”, which has been used to explicate the CACs of dialkyldimethylammonium salts.<sup>213,214</sup> From the quantitative view, the relation of CMC with alkyl chain length of ionic surfactant was also investigated several decades ago, which was described in **Eq. 2.5**.<sup>219,265</sup>

$$\ln \text{CMC} = \frac{\phi_m' n}{(1+K_g)kT} + K'' \quad (\text{Eq. 2.5})$$

Where  $\phi_m'$  is the free energy to transfer each  $\text{CH}_2$  group from water to hydrocarbon environment, the value from solution to solution-air interface is about  $-1.08kT$ ,  $n$  is the carbon number in the alkyl chain of surfactant,  $K_g$  is degree of counter ions association,  $K''$  is experimental constant,  $k$  is Boltzmann constant, and  $T$  is the absolute temperature. As shown in **Table 2.6**, for surfactants with the same cation, one more carbon on each alkyl chain caused about 4 times decrease of the corresponding CMC, which agreed well with the **Eq. 2.5**.  $K_g$  could also be calculated here from the  $\ln \text{CMC}-n$  curve as shown in **Table 2.7**, while only inaccurate results were obtained as only three points were used; besides, for the same cation, the chain length and the ion strength play also crucial roles for the  $K_g$  values. The values calculated here followed the order monovalent cations > divalent cations > trivalent cations, which was ascribed to the decrease of ion strength of the solution as CMCs of trivalent cations were much lower than monovalent cations.

**Table 2.6** Solubilities in water, Critical Aggregation Concentration (CAC) values and surface tensions at CAC ( $\sigma_{CAC}$ ) for  $[DiC_nCHSO_3]_x[X]$  ( $x = 1, M = H, Li, Na, K; x = 2, M = Cu, Zn, Ca, Mg; x = 3, M = Sc$ ) as a function of the alkyl chain carbon number ( $n = 6, 7, 8$ ).

Cation	Solubility (mM)	CAC (mM)	$\sigma_{CAC}$ (mN.m <sup>-1</sup> )
<b>[DiC<sub>6</sub>CHSO<sub>3</sub>]<sub>m</sub> (m = 1, 2, 3)</b>			
<b>H<sup>+</sup></b>	>100	23	25.5
<b>Li<sup>+</sup></b>	>100	18	28.3
<b>Na<sup>+</sup></b>	>100	21	27.6
<b>K<sup>+</sup></b>	>100	18	26.2
<b>Mg<sup>2+</sup></b>	4.1	3.1	25.9
<b>Ca<sup>2+</sup></b>	3.6	2.7	24.2
<b>Cu<sup>2+</sup></b>	4.6	3.8	24.7
<b>Zn<sup>2+</sup></b>	3.7	2.7	24.4
<b>Sc<sup>3+</sup></b>	0.45	0.46	26.3
<b>[DiC<sub>7</sub>CHSO<sub>3</sub>]<sub>m</sub> (m = 1, 2, 3)</b>			
<b>H<sup>+</sup></b>	8.9	3.0	24.4
<b>Li<sup>+</sup></b>	28.9	4.4	26.5
<b>Na<sup>+</sup></b>	20.0	5.2	25.7
<b>K<sup>+</sup></b>	21.8	6.8	25.0
<b>Mg<sup>2+</sup></b>	1.2	0.54	24.8
<b>Ca<sup>2+</sup></b>	0.88	0.44	23.9
<b>Cu<sup>2+</sup></b>	1.1	0.68	23.9
<b>Zn<sup>2+</sup></b>	1.0	0.41	24.6
<b>Sc<sup>3+</sup></b>	0.16	0.081	27.9
<b>[DiC<sub>8</sub>CHSO<sub>3</sub>]<sub>m</sub> (m = 1, 2, 3)</b>			
<b>H<sup>+</sup></b>	5.2	1.2	24.1
<b>Li<sup>+</sup></b>	12.1	1.4	26.5
<b>Na<sup>+</sup></b>	5.0	1.6	25.7
<b>K<sup>+</sup></b>	7.9	1.5	25.0
<b>Mg<sup>2+</sup></b>	0.36	0.11	26.4
<b>Ca<sup>2+</sup></b>	0.17	0.081	24.6
<b>Cu<sup>2+</sup></b>	0.44	0.089	23.3
<b>Zn<sup>2+</sup></b>	0.24	0.10	23.7
<b>Sc<sup>3+</sup></b>	0.09	0.012	30.1

The effect of the counter ions on the CMCs is also crucial, which was obviously presented in **Figure 2.26**. With the same sulphonate alkyl chain, the CMC increased dramatically following the order trivalent cations < divalent cations < monovalent cations, which results in the higher screening of charge on the sulphonate head group and less electrostatic repulsion between the micelles and decrease of the CMC. Indeed, from the values of **Table 2.6**, with the same hydrophobic part, the CMCs of the surfactants with monovalent cations were about ten times higher than the CMCs of the divalent cations and for surfactants with trivalent cations, it was about five times smaller than for divalent cations.

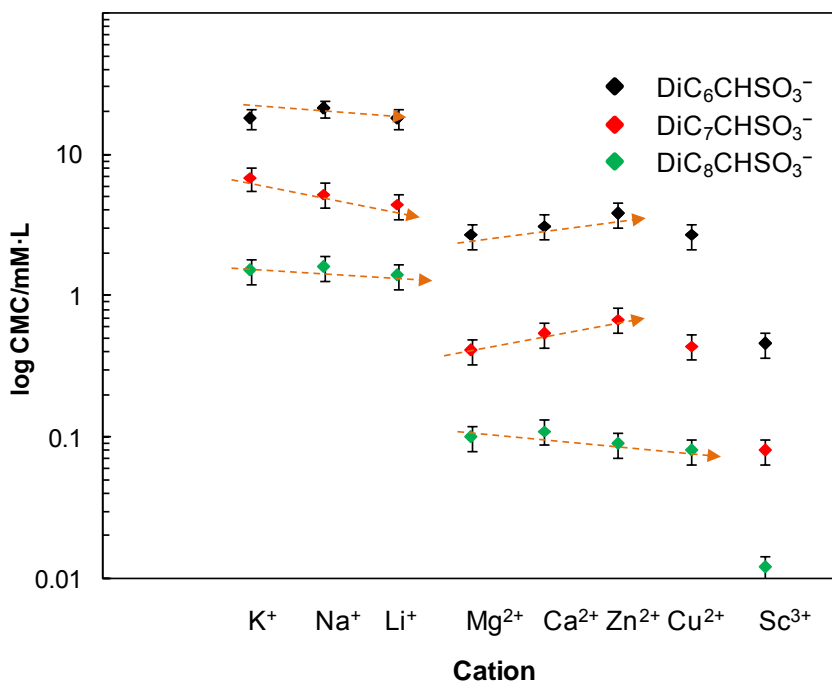


**Figure 2.27** The CMCs of dialkylmethane sulphonates of different counterions.

On the other side, for the same hydrophobic part and the cations of the same charge, the CMCs varied depending on the hydration of the cations, which could be rationalized by so-called “Hofmeister series”,<sup>255</sup> *i.e.* an order of ions in terms of their ability to affect the solubility of proteins. “Hofmeister series” was also widely used to explain the aqueous phase behavior of surfactant. The small and strongly hydrated cations caused the dehydration of the surfactant head group and resulted in the decrease of CMC and increase of CMCs were caused by large and less hydrated cations. The hydration radii of the cations used here were given in **Table 2.7**.<sup>266</sup> As shown **Figure 2.27**, the CMCs were listed according the valence and hydrated radius of the cations. Indeed, for [DiC<sub>8</sub>CHSO<sub>3</sub><sup>-</sup>] series, the CMCs of sulphonates followed the order  $K^+ > Na^+ > Li^+$  for monovalent cations, and  $Mg^{2+} < Ca^{2+} < Zn^{2+} < Cu^{2+}$ , which agreed well with the “Hofmeister series”. While for [DiC<sub>7</sub>CHSO<sub>3</sub><sup>-</sup>] and [DiC<sub>6</sub>CHSO<sub>3</sub><sup>-</sup>] series, the divalent cations presented the converse order *i.e.*  $Zn^{2+} < Ca^{2+} < Mg^{2+}$ , which may be ascribed to the enhanced interaction between the micelles caused by the higher CMCs.

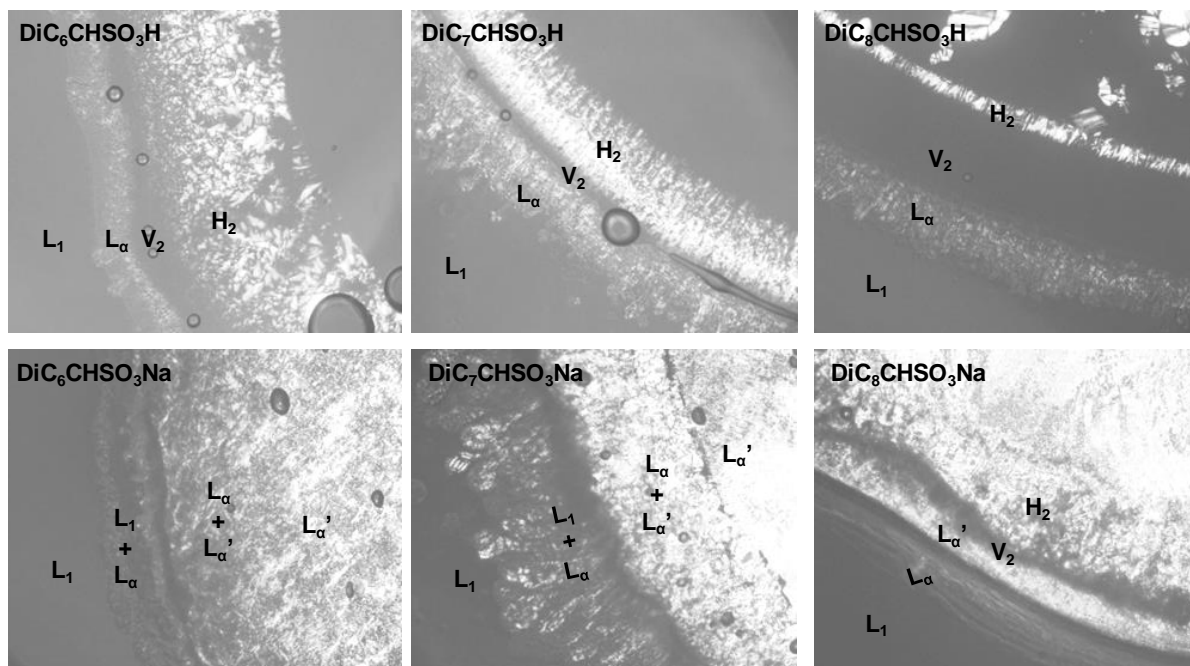
**Table 2.7** The crystal radii  $r$ , hydration radii  $r_h$ , and hydration enthalpies of the cations.<sup>266-268</sup>

Cations	$r_h/\text{Å}$	$K_g$ (Eq. 2.5)
<b>Li<sup>+</sup></b>	1.58	0.68
<b>Na<sup>+</sup></b>	1.78	0.65
<b>K<sup>+</sup></b>	2.01	0.71
<b>Mg<sup>2+</sup></b>	3.00	0.29
<b>Ca<sup>2+</sup></b>	2.53	0.23
<b>Cu<sup>2+</sup></b>	2.28	0.15
<b>Zn<sup>2+</sup></b>	2.80	0.30
<b>Sc<sup>3+</sup></b>	2.33	0.18

### 2.2.3 Water/surfactant binary diagrams

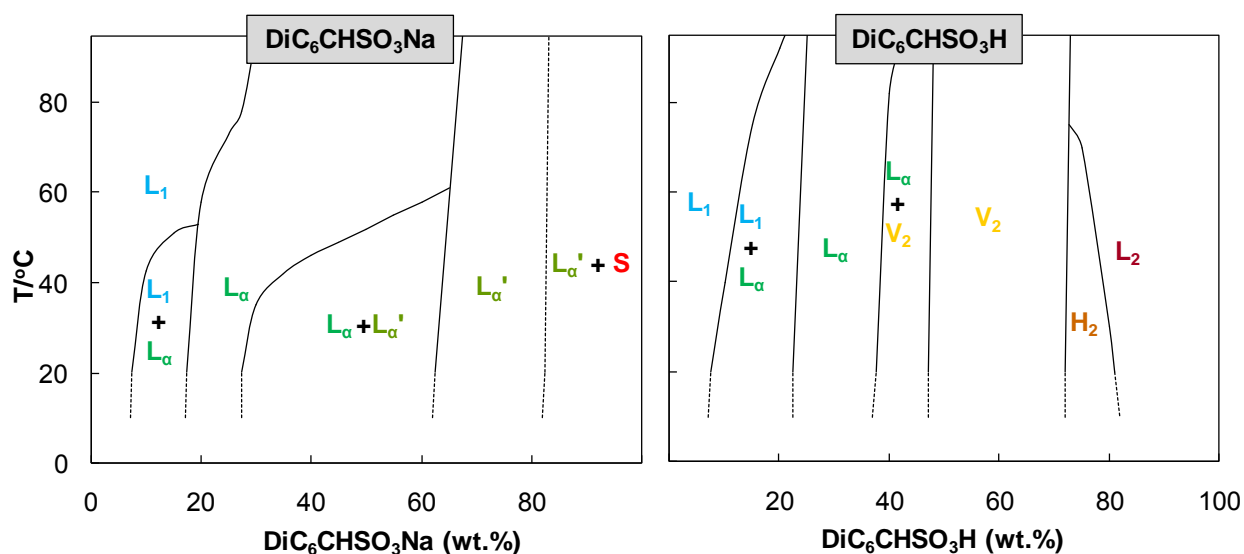
The phase behavior of surfactants in aqueous solution in high concentration regions is also a fundamental property of surfactant. As already been discussed above, the evolution of the lyotropic crystal liquid phases as a function of concentration reflects the molecule structure information, *i.e.* packing parameter of the surfactants.<sup>217</sup> Besides, the water/surfactant diagram also anticipates the water/surfactant/oil ternary behavior in some extent as it is one side of the phase prism.<sup>269</sup>

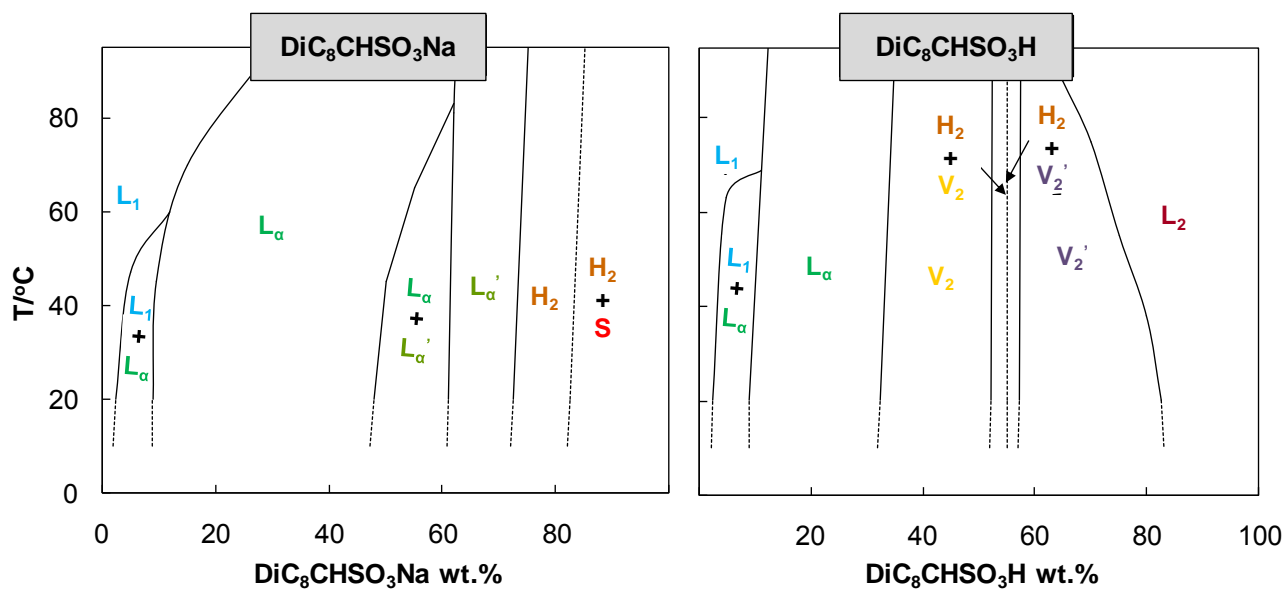
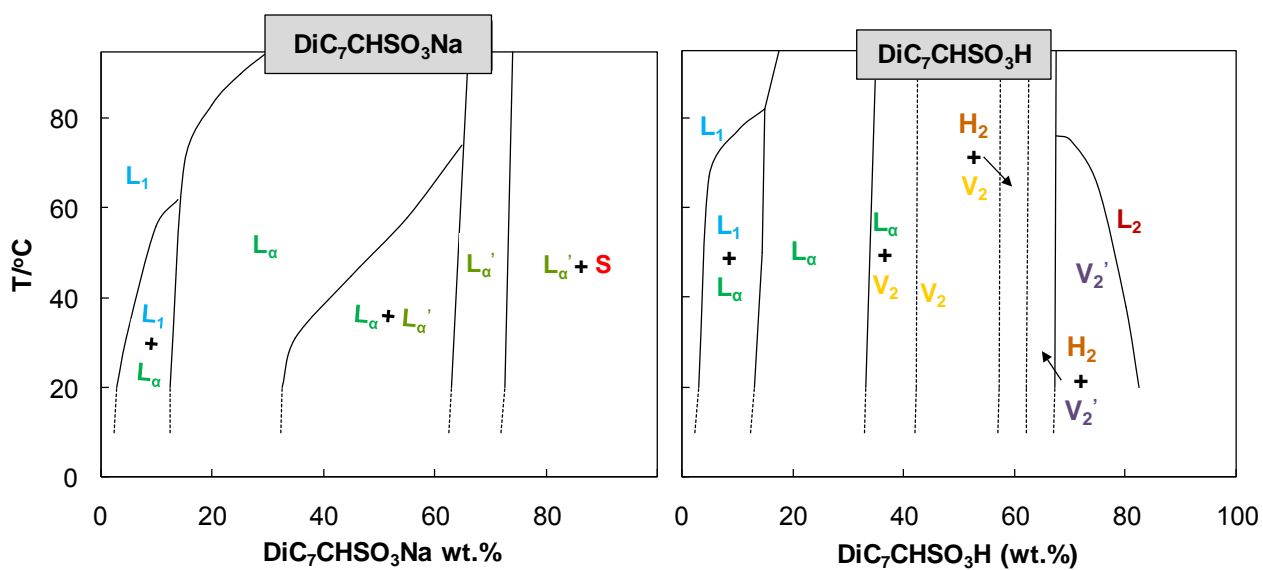
Since the solubility of divalent and trivalent metallic cation salts in water is too low, we focused on the surfactant/water binary diagrams of **DiC<sub>n</sub>CHSO<sub>3</sub>H** and **DiC<sub>n</sub>CHSO<sub>3</sub>Na** (with  $n = 6, 7,$  and  $8$ ). Firstly, samples of different concentrations (from 5wt % to 90wt % with interval of 5wt %) were prepared for each surfactant and then, the lyotropic liquid crystals were studied by polarized optical microscopy (POM), which can discriminate different crystal liquids by different textures. The thermal stability of different phases was determined by controlling the temperature with a LTS120Analyza Peltier temperature stage capable of controlling the temperature at  $\pm 0.1$  °C. Before investigation of the lyotropic crystals in detail, the penetration test was carried out for each surfactant to determine the different types of liquid crystals existing at 20 °C (**Figure 2.28**).



**Figure 2.28** Penetration test for the  $\text{DiC}_n\text{CHSO}_3\text{H}$  and  $\text{DiC}_n\text{CHSO}_3\text{Na}$  ( $n = 6, 7, 8$ ) at 20 °C.

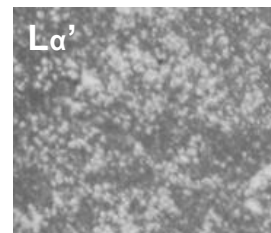
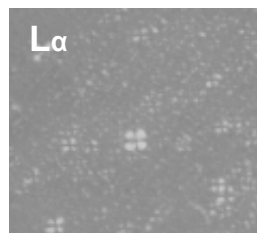
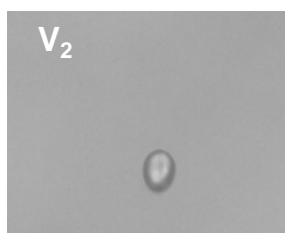
From the penetration test, several different types of liquid crystals could be observed. For example, lamellar, cubic, and hexagonal phases were found for the  $\text{DiC}_n\text{CHSO}_3\text{H}$  series at room temperature. For  $\text{DiC}_n\text{CHSO}_3\text{Na}$  series, the cubic phase was not obvious and the hexagonal phase was not easily observed, instead, another type of lamellar phase existed in the high concentration region. More detailed information on the binary phase diagrams could be obtained by investigating the different concentrations as a function of temperature. Then, the complete binary diagrams were constructed by determining the boundary of the different types of liquid crystal phases, as shown in **Figure 2.29**.





*DiC<sub>6</sub>CHSO<sub>3</sub>H*

*DiC<sub>6</sub>CHSO<sub>3</sub>Na*





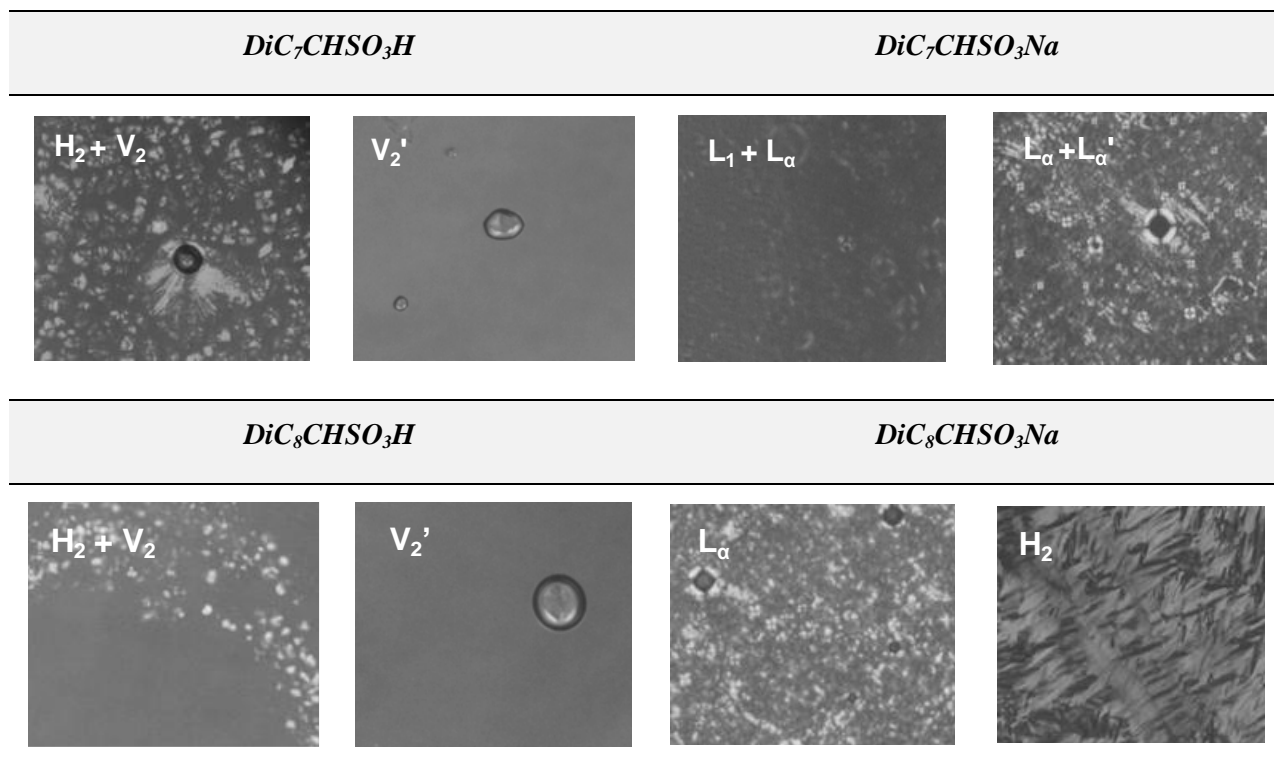


**Figure 2.29** Binary phase diagrams of  $DiC_nCHSO_3H$  and  $DiC_nCHSO_3Na$  determined by polarized light optical microscopy and typical texture pictures of the surfactants ( $n = 6, 7,$  or  $8$ ).  $L_1$  = isotropic solution,  $L_\alpha$  = lamellar phase, and  $L_\alpha'$  = reverse lamellar phase,  $V_2$  = reverse cubic phase,  $H_2$  = reverse hexagonal phase,  $S$  = solid surfactant,  $L$  = liquid surfactant. The solid line indicated the clear boundary and the dash line meant the arbitrary boundary.

For all the surfactants studied here, the progression from micelle solution  $L_1$  to lamellar mixture phase  $L_1+L_\alpha$  was observed at low concentration without any transition to hexagonal or cubic phases, which indicated that the surfactants have a high packing parameter and the bilayered structure was preferred rather than the sphere or cylinder. The  $L_1+L_\alpha$  mixture phase was also observed in the binary diagrams of  $[DiC_{10}]_2WO_4$  and  $[DiC_{10}]_2MoO_4$ . As shown in **Figure 2.28**, the chain length did not change the progression sequence of the binary diagram when the counter cation was the same. For the  $DiC_nCHSO_3Na$  series, the sequence  $L_1 \rightarrow L_1+L_\alpha \rightarrow L_\alpha \rightarrow L_\alpha' \rightarrow L_\alpha+L_\alpha' \rightarrow L_\alpha'$  was observed for all three surfactants with different chain lengths and a reverse hexagonal phase  $H_2$  emerged for  $DiC_8CHSO_3Na$  due to the increase of its packing parameter. As the chain length increases, the  $L_\alpha$  region moved towards low concentrations and occupied larger concentration range. At the same time, the  $L_\alpha+L_\alpha'$  region was reduced and presented a higher thermal stability. Different from the sodium as a counter cation, the phase diagrams of  $DiC_nCHSO_3H$  series were more complex. Different types of reverse liquid crystals were found at high concentration region, which was ascribed to the stronger association with sulphonate for proton than sodium and smaller head group area. Bicontinuous reverse cubic phase  $V_2$  and reverse hexagonal phase  $H_2$  were found next to the lamellar phase successively, while for  $DiC_7CHSO_3H$  and

**DiC<sub>8</sub>CHSO<sub>3</sub>H**, the region of H<sub>2</sub> was too narrow to determine the boundary and reverse micelle cubic phase emerged and occupied the high concentration. Similar binary diagram were also found for sodium 7-dodecyl benzene sulphonate and AOT.<sup>270,271</sup> For example, the lyotropic phase diagram reported by Ma *et al.* was dominated by L<sub>1</sub> + L<sub>α</sub> and L<sub>α</sub> phases, the L<sub>1</sub> phase occupied only the concentration lower than 10 wt% and several inverse crystal liquids, such as L<sub>α</sub>' , V<sub>2</sub>, H<sub>2</sub> appear above the concentration higher than 70 wt%.<sup>270</sup>

#### 2.2.4 Conclusion

The new symmetric dialkylmethane sulfonic acids **DiC<sub>n</sub>CHSO<sub>3</sub>H** and sulphonates [**DiC<sub>n</sub>CHSO<sub>3</sub>**]<sub>x</sub>**M** with n = 6, 7, 8 and **M** = metallic cations (x = 1, M = H, Li, Na, K; x = 2, M = Cu, Zn, Ca, Mg; x = 3, M = Sc) were successfully prepared and characterized. The CMCs were determined by the tensiometer and the effect of the chain length and the nature of the counter cations were obvious. Due to the hydrophobic effect, the increase of the surfactant chain length caused the decrease of the CMC values and could be semi-quantitatively calculated resorted to **Eq. 2.5**. On the other hand, the higher valence state counter cations displayed higher screening of electrostatic interaction between the micelles and thus caused a dramatically decrease of the CMC. For the surfactants with same sulphonate part and equivalent valence of metallic cations, the CMCs were dependent on the hydration of the cations, which agreed with “Hofmeister series”, while the order could be inverse for the surfactants with higher CMCs because of enhanced interaction between the micelles.

Then the water/surfactant diagrams were constructed for the **DiC<sub>n</sub>CHSO<sub>3</sub>H** and **DiC<sub>n</sub>CHSO<sub>3</sub>Na** series. For divalent or trivalent metallic sulphonate, their low solubilities make it impossible to construct their binary phase diagrams. The surfactants of different chain length but the same counter ion showed similar lyotropic liquid crystals evolution patterns in the phase diagrams but the same phase appeared at higher concentration for longer chain. Compared to the sodium alkylsulphonate, the alkylsulfonic acid displayed higher packing parameter and showed various reverse liquid crystals at high concentration range, such as reverse cubic, reverse hexagonal phases, *etc.* Although the novel amphiphilic Brönsted and Lewis acids were successfully prepared and characterized, their catalytic performance in  $\mu$ em reaction media still have to be demonstrated. The possible reactions performed in this  $\mu$ em reaction media based on the novel amphiphilic Brönsted and Lewis acids include the Carbon-Carbon formation reactions, such as aldol reaction, Mannich reaction, Diels-Alder reaction, *etc.*, various oxidation reactions with H<sub>2</sub>O<sub>2</sub> or alkyl perhydroxide as oxidants and dehydration reactions, such as esterification, etherification, *etc.*

**2.3 Experimental section**

---



### 2.3.1 Experimental section for Double-chain alkylammonium catalytic surfactants

**Materials:** All the surfactants were prepared according to the method previously reported and the counter ions exchange was carried out by using the exchange resin Amberlite IRA-400(Cl).<sup>219,220,272</sup> The high purity (> 99.8%) was confirmed by <sup>1</sup>H and <sup>13</sup>C NMR. All the other reagents were purchased from Sigma-Aldrich or TCI chemicals and used as received. Chloropropane (1-ClC<sub>3</sub>) (98%), chloropentane (1-ClC<sub>5</sub>) (99%), chlorohexane (1-ClC<sub>6</sub>) (99%), chloroheptane (1-ClC<sub>7</sub>) (99%), chlorooctane (1-ClC<sub>8</sub>) (99%), chlorononane (1-ClC<sub>9</sub>) (98%), chlorodecane (1-ClC<sub>10</sub>) (98%), chlorotetradecane (1-ClC<sub>14</sub>) (98%) and dichlorobutane (C<sub>4</sub>Cl<sub>2</sub>) (99%) were from Aldrich. Chlorobutane (1-ClC<sub>4</sub>) (99.5%) was from Alfa Aesar. Chlorododecane (1-ClC<sub>12</sub>) (95%) was purchased from TCI. Dichloromethane (C<sub>1</sub>Cl<sub>2</sub>) (99%) and dichloroethane (C<sub>2</sub>Cl<sub>2</sub>) (98%) were from Prolabo. Dichloropropane (C<sub>3</sub>Cl<sub>2</sub>) (98%) was purchased from Fluka and dichloropentane (C<sub>5</sub>Cl<sub>2</sub>) (99%) from Acros Organics. The water used in all the experiments was purified by Millipore (18.2 MΩ/cm; Simplicity 185). <sup>1</sup>H and <sup>13</sup>C NMR spectra were recorded with Bruker Avance AV 300 instrument.

#### Typical procedure of the preparation of [DiC<sub>n</sub>][Br] (n = 6, 8, 10)

**Di-*n*-octyl-dimethylammonium bromide [DiC<sub>6</sub>][Br]:** 1-Bromooctane (28.97 g, 0.15 mol), N,N-dimethyloctylamine (23.60 g, 0.15 mol) were weighed and added in 500 mL reaction flask with 300 mL CH<sub>3</sub>CN. The mixture was reflux overnight and then cooled to room temperature. The solvent was removed by rotary evaporation and 150 mL H<sub>2</sub>O was used to dissolve the crude product. The product was extracted with dichloromethane (50 mL × 3). Combined the organic phase and removed the solvent, 50 mL H<sub>2</sub>O was added and then evaporated in vacuum to remove the organic solvent sufficiently and dried the product by lyophilisation. Finally 51.51g white waxy solid was obtained. <sup>1</sup>H NMR (300 MHz, CDCl<sub>3</sub>, 20 °C, TMS): δ (ppm) = 0.85-0.89 (m, 6H; CH<sub>3</sub>), 1.20-1.50 (m, 20H; CH<sub>2</sub>), 1.67 (m, 4H; N-CH<sub>2</sub>-CH<sub>2</sub>), 3.41 (s, 6H; NCH<sub>3</sub>), 3.50-3.56 (m, 4H; NCH<sub>2</sub>). <sup>13</sup>C NMR (75 MHz, CDCl<sub>3</sub>, 20 °C): δ (ppm) = 14.2, 22.7, 22.7, 26.2, 29.1, 29.3, 31.9, 51.3, 63.7. m.p. = 65 °C. (Yield: 98%).

**Di-*n*-hexyl-dimethylammonium bromide [DiC<sub>6</sub>][Br]:** <sup>1</sup>H NMR (300 MHz, CDCl<sub>3</sub>, 25 °C, TMS): δ (ppm) = 0.88 (t, 6H; CH<sub>3</sub>, <sup>3</sup>J = 6.9 Hz), 1.29-1.41 (m, 12H; CH<sub>2</sub>), 1.64-1.74 (m, 4H; N-CH<sub>2</sub>-CH<sub>2</sub>), 3.37 (s, 6H; NCH<sub>3</sub>), 3.45-3.51 (m, 4H; NCH<sub>2</sub>). <sup>13</sup>C NMR (75 MHz, CDCl<sub>3</sub>, 25 °C): δ (ppm) = 13.8, 22.4, 22.7, 25.9, 31.2, 51.4, 63.9. Colorless gel, m.p. < 20 °C. (Yield: 95.4%).

**Di-*n*-decyl-dimethylammonium bromide [DiC<sub>10</sub>][Br]:** <sup>1</sup>H NMR (300 MHz, CDCl<sub>3</sub>, 25 °C, TMS): δ (ppm) = 0.89 (t, 6H; CH<sub>3</sub>, <sup>3</sup>J = 6.9 Hz), 1.26-1.36 (m, 28H; CH<sub>2</sub>), 1.64-1.77 (m, 4H; N-CH<sub>2</sub>-CH<sub>2</sub>), 3.43 (s, 6H; NCH<sub>3</sub>), 3.48-3.55 (m, 4H; NCH<sub>2</sub>). <sup>13</sup>C NMR (75 MHz, CDCl<sub>3</sub>, 25 °C): δ (ppm) = 14.2, 22.7, 22.8, 26.3, 29.3, 29.4, 29.5, 31.9, 51.5, 63.6. m.p. = 151 °C. (Yield: 95%).

#### Typical procedure of preparation of [DiC<sub>n</sub>][X] (X = Cl) and [DiC<sub>n</sub>]<sub>2</sub>[X] (X = WO<sub>4</sub> or MoO<sub>4</sub>)

**Dimethyl-di-*n*-octylammonium chloride [DiC<sub>8</sub>][Cl]:** The resin Amberlite IRA-400 (100 g) in column (diameter = 2.5 cm) was washed with pure water, NaOH aq. (500 mL, 10wt %) and water again until pH

= 7 consecutively to exchange the resin with OH group. Then **[DiC<sub>8</sub>][Br]** (5.0g, 14.3 mmol) in 50 mL H<sub>2</sub>O was subjected to the column. The solution passed the column slowly by addition of pure water until the elution was neutral. The elution was collected under protection of Ar and titrated with HCl standard solution (53.5 mM, 265 mL). Then HCl (34 wt%, 10.9 M, 1.252 mL, 13.64 mmol) was added in the solution and stirred for 2h, then H<sub>2</sub>O was evaporated in vacuum and the product was dried by lyophilisation (white waxy solid, 4.17 g). <sup>1</sup>H NMR (300 MHz, CDCl<sub>3</sub>, 20 °C, TMS): δ (ppm) = 0.86–0.90 (m, 6H; CH<sub>3</sub>), 1.27–1.36 (m, 20H; CH<sub>2</sub>), 1.69 (m, 4H; N-CH<sub>2</sub>-CH<sub>2</sub>), 3.43 (s, 6H; NCH<sub>3</sub>), 3.50 (m, 4H; NCH<sub>2</sub>). <sup>13</sup>C NMR (75 MHz, CDCl<sub>3</sub>, 20 °C): δ (ppm) = 14.0, 22.5, 22.7, 26.2, 29.0, 29.1, 31.6, 51.3, 63.6. m.p. = 75 °C, (95.4%).

**Di-*n*-hexyl-dimethylammonium chloride [DiC<sub>6</sub>][Cl]**: <sup>1</sup>H NMR (300 MHz, CDCl<sub>3</sub>, 25 °C, TMS): δ (ppm) = 0.91 (t, 6H; CH<sub>3</sub>, <sup>3</sup>J = 6.9 Hz), 1.29–1.45 (m, 12H; CH<sub>2</sub>), 1.71 (m, 4H; N-CH<sub>2</sub>-CH<sub>2</sub>), 3.40 (s, 6H; NCH<sub>3</sub>), 3.47 (m, 4H; NCH<sub>2</sub>). <sup>13</sup>C NMR (75 MHz, CDCl<sub>3</sub>, 25 °C): δ (ppm) = 14.0, 22.4, 22.8, 26.0, 31.3, 51.6, 63.6. Colorless gel, m.p. < 20 °C. (Yield: 93%).

**Di-*n*-decyl-dimethylammonium chloride [DiC<sub>10</sub>][Cl]**: <sup>1</sup>H NMR (300 MHz, CDCl<sub>3</sub>, 25 °C, TMS): δ (ppm) = 0.85 (t, 6H; CH<sub>3</sub>, <sup>3</sup>J = 6.9 Hz), 1.23–1.32 (m, 28H; CH<sub>2</sub>), 1.66 (m, 4H; N-CH<sub>2</sub>-CH<sub>2</sub>), 3.38 (s, 6H; NCH<sub>3</sub>), 3.45 (m, 4H; NCH<sub>2</sub>). <sup>13</sup>C NMR (75 MHz, CDCl<sub>3</sub>, 25 °C): δ (ppm) = 14.1, 22.6, 22.7, 26.2, 29.2, 29.3, 29.4, 31.8, 51.3, 63.5. m.p. = 88 °C. (Yield: 96%).

**Dimethyl-di-*n*-octylammoniummolybdate [DiC<sub>8</sub>]<sub>2</sub>[MoO<sub>4</sub>]**: <sup>1</sup>H NMR (300 MHz, CDCl<sub>3</sub>, 20 °C, TMS): δ (ppm) = 0.85–0.90 (t, 12H; CH<sub>3</sub>, <sup>3</sup>J = 6.9 Hz), 1.22–1.35 (m, 20H; CH<sub>2</sub>), 1.64 (m, 8H; N-CH<sub>2</sub>-CH<sub>2</sub>), 3.37–3.43 (m, 20H; CH<sub>3</sub>NCH<sub>2</sub>). <sup>13</sup>C NMR (75 MHz, CDCl<sub>3</sub>, 20 °C): δ (ppm) = 14.2, 22.6, 22.3, 26.1, 28.7, 29.1, 31.2, 51.5, 63.1. m.p. = 189 °C. (Yield: 93%).

**Di-*n*-hexyldimethylammoniummolybdate [DiC<sub>6</sub>]<sub>2</sub>[MoO<sub>4</sub>]**: <sup>1</sup>H NMR (300 MHz, CDCl<sub>3</sub>, 25 °C, TMS): δ (ppm) = 0.85 (t, 12H; CH<sub>3</sub>, <sup>3</sup>J = 6.9 Hz), 1.26–1.34 (m, 24H; CH<sub>2</sub>), 1.58–1.63 (m, 8H; N-CH<sub>2</sub>-CH<sub>2</sub>), 3.36–3.42 (m, 20H; CH<sub>3</sub>NCH<sub>2</sub>). <sup>13</sup>C NMR (75 MHz, CDCl<sub>3</sub>, 25 °C): δ (ppm) = 13.9, 22.4, 22.7, 26.0, 31.3, 51.3, 63.1. m.p. = 172 °C. (Yield: 98.5%).

**Bis(di-*n*-decyldimethylammonium) molybdate [DiC<sub>10</sub>]<sub>2</sub>[MoO<sub>4</sub>]**: <sup>1</sup>H NMR (300 MHz, CDCl<sub>3</sub>, 25 °C, TMS): δ (ppm) = 0.89 (m, 12H, CH<sub>3</sub>, <sup>3</sup>J = 6.9 Hz), 1.26–1.34 (m, 56H, CH<sub>2</sub>), 1.67 (m, 8H, N-CH<sub>2</sub>-CH<sub>2</sub>), 3.37–3.45 (s, 20H, CH<sub>3</sub>NCH<sub>2</sub>-). <sup>13</sup>C-NMR (CDCl<sub>3</sub>, 75 MHz, 20 °C, ppm): 14.1, 22.7, 22.8, 26.3, 29.3, 29.4, 29.5, 31.9, 52.0, 62.8. m.p. = 165 °C. (Yield: 96%).

**Dimethyl-di-*n*-octylammonium tungstate [DiC<sub>8</sub>]<sub>2</sub>[WO<sub>4</sub>]**: <sup>1</sup>H NMR (300 MHz, CDCl<sub>3</sub>, 20 °C, TMS): δ (ppm) = 0.89 (t, 12H; CH<sub>3</sub>, <sup>3</sup>J = 6.9 Hz), 1.22–1.35 (m, 40H; CH<sub>2</sub>), 1.64 (m, 8H; N-CH<sub>2</sub>-CH<sub>2</sub>), 3.35–3.44 (m, 20H; CH<sub>3</sub>NCH<sub>2</sub>). <sup>13</sup>C NMR (75 MHz, CDCl<sub>3</sub>, 20 °C): δ (ppm) = 14.0, 22.5, 22.9, 26.2, 29.0, 29.1, 31.6, 51.8, 63.6. m.p. = 81 °C. (Yield: 93%).

**Di-*n*-hexyldimethylammoniumtungstate [DiC<sub>6</sub>]<sub>2</sub>[WO<sub>4</sub>]:** <sup>1</sup>H NMR (300 MHz, CDCl<sub>3</sub>, 25 °C, TMS): δ (ppm) = 0.83 (t, 12H; CH<sub>3</sub>, <sup>3</sup>J = 6.9 Hz), 1.24–1.32 (m, 24H; CH<sub>2</sub>), 1.56–1.61 (m, 8H; N-CH<sub>2</sub>-CH<sub>2</sub>), 3.34–3.40 (m, 20H; CH<sub>3</sub>NCH<sub>2</sub>). <sup>13</sup>C NMR (75 MHz, CDCl<sub>3</sub>, 25 °C): δ (ppm) = 13.8, 22.4, 22.7, 25.9, 31.3, 51.7, 63.0. m.p. = 185 °C. (Yield: 97%).

**Bis(di-*n*-decyldimethylammonium) tungstate [DiC<sub>10</sub>]<sub>2</sub>[WO<sub>4</sub>]:** <sup>1</sup>H-NMR (CDCl<sub>3</sub>, 300 MHz, 20 °C, TMS, ppm): 0.88 (m, 12H, CH<sub>3</sub>, <sup>3</sup>J = 6.9 Hz), 1.26–1.33 (m, 56H, CH<sub>2</sub>), 1.66 (m, 8H, N-CH<sub>2</sub>-CH<sub>2</sub>), 3.38–3.45 (m, 20H, CH<sub>3</sub>NCH<sub>2</sub>). <sup>13</sup>C-NMR (CDCl<sub>3</sub>, 75 MHz, 20 °C, ppm): 14.1, 22.6, 22.8, 26.3, 29.2, 29.3, 29.5, 31.9, 52.0, 62.8. m.p. = 179 °C. (Yield: 93%).

### 2.3.2 Double-chain sulphonate catalytic surfactants

#### Typical procedure of preparation of DiC<sub>n</sub>CHOH<sup>263</sup>

**7-tridecanol:** Mg (8.10 g, 333 mmol) was weighed into a 1000 mL three-neck reaction flask and under protection of Ar, 1-bromohexane (50.0 g, 303 mmol) in 200 mL dry THF was added dropwise inside the flask. The addition rate was controlled to kept the reaction solution under slightly reflux. After 1.5h, all the 1-bromohexane solution was added and the mixture was kept stirring for another 30min. Then the reaction solution was cooled to room temperature and incubated with cool water. Ethyl formate (11.22 g, 0.1515 mmol) in 150 mL THF was dropped into the prepared Grignard reagent and the addition rate was also controlled to keep the solution under slightly reflex. After addition of ethyl formate, the reaction mixture was kept stirring for further 30min and then cooled with ice-water. 100 mL H<sub>2</sub>O and 150 mL H<sub>2</sub>SO<sub>4</sub> (2.7 M, 405 mmol) were dropped inside the flask consecutively. Then organic phase was separated and the aqueous phase was extracted by ether (150 mL × 2). Combined the organic phase and dried with MgSO<sub>4</sub>. Removed the solvent by rotary evaporation afforded the crude product and further recrystallization from CH<sub>2</sub>Cl<sub>2</sub> gave the pure product (white solid, 25.6g, 84.4%). <sup>1</sup>H NMR (300 MHz, CDCl<sub>3</sub>, 20 °C, TMS): δ (ppm) = 0.90 (t, 6H; CH<sub>3</sub>, J= 6.9Hz), 1.22–1.52 (m, 20H; CH<sub>2</sub>), 3.55–3.65 (m, 1H; CH). <sup>13</sup>C NMR (75 MHz, CDCl<sub>3</sub>, 20 °C): δ (ppm) = 14.1, 22.6, 25.6, 29.4, 31.8, 37.5, 72.0. m.p. = 40.8 °C.

**8-pentadecanol:** <sup>1</sup>H NMR (300 MHz, CDCl<sub>3</sub>, 20 °C, TMS): δ (ppm) = 0.90 (t, 6H; CH<sub>3</sub>, J= 6.9Hz), 1.19–1.54 (m, 24H; CH<sub>2</sub>), 3.55–3.65 (m, 1H; CH). <sup>13</sup>C NMR (75 MHz, CDCl<sub>3</sub>, 20 °C): δ (ppm) = 14.1, 22.7, 25.7, 29.3, 29.7, 31.8, 37.4, 72.1. m.p. = 53.8 °C. (82.5%)

**9-heptadecanol:** <sup>1</sup>H NMR (300 MHz, CDCl<sub>3</sub>, 20 °C, TMS): δ (ppm) = 0.89 (t, 6H; CH<sub>3</sub>, J= 6.9Hz), 1.18–1.65 (m, 28H; CH<sub>2</sub>), 3.55–3.65 (m, 1H; CH). <sup>13</sup>C NMR (75 MHz, CDCl<sub>3</sub>, 20 °C): δ (ppm) = 14.1, 22.7, 25.6, 29.3, 29.6, 29.7, 31.9, 37.5, 72.0. m.p. = 62.1 °C. (86.9%)

#### Typical procedure of preparation of DiC<sub>n</sub>CHBr<sup>273</sup>

**7-Bromotridecane:** Under argon atmosphere, 7-tridecanol (20.0 g, 99.8 mmol) was dissolved with 500 mL dry ether in 1000 mL reaction flask. Then  $\text{CBr}_4$  (66.2 g, 199.6 mmol, 2 equiv.) was added in the solution at room temperature under stirring.  $\text{PPh}_3$  (53.8 g, 199.6 mmol, 2 equiv.) was added in several portions in 30min and the reaction mixture was kept stirring for another 1h. The white precipitate was removed by filtration and washed with ether (50 mL  $\times$  1). The ether in the filtrate was removed by evaporation and the residue was dissolved with hexane. The precipitate in hexane solution was removed by filtration and the evaporation of hexane afforded the crude product. The pure product was obtained by distillation in vacuum (Colorless oil, 21.0g, 79.9%).  $^1\text{H}$  NMR (300 MHz,  $\text{CDCl}_3$ , 20 °C, TMS):  $\delta$  (ppm) = 0.86–0.95 (m, 6H;  $\text{CH}_3$ ), 1.23–1.63 (m, 16H;  $\text{CH}_2$ ), 1.75–1.90 (m, 4H;  $\text{CH}_2$ ), 4.05 (quintet, 1H, CH,  $J$  = 6.27Hz).  $^{13}\text{C}$  NMR (75 MHz,  $\text{CDCl}_3$ , 20 °C):  $\delta$  (ppm) = 14.0, 22.6, 27.5, 28.7, 31.7, 39.2, 59.0. b.p. = 97–99 °C (0.31 Torr).

**8-bromopentadecane:**  $^1\text{H}$  NMR (300 MHz,  $\text{CDCl}_3$ , 20 °C, TMS):  $\delta$  (ppm) = 0.86–0.95 (m, 6H;  $\text{CH}_3$ ), 1.19–1.63 (m, 20H;  $\text{CH}_2$ ), 1.77–1.88 (m, 4H;  $\text{CH}_2$ ), 4.05 (quintet, 1H, CH,  $J$  = 6.27Hz).  $^{13}\text{C}$  NMR (75 MHz,  $\text{CDCl}_3$ , 20 °C):  $\delta$  (ppm) = 14.10, 22.6, 27.6, 29.0, 29.2, 31.8, 39.2, 59.1. b.p. = 122–125°C (0.36 Torr). (78.1%)

**9-bromoheptadecane:**  $^1\text{H}$  NMR (300 MHz,  $\text{CDCl}_3$ , 20 °C, TMS):  $\delta$  (ppm) = 0.86–0.95 (m, 6H;  $\text{CH}_3$ ), 1.18–1.66 (m, 24H;  $\text{CH}_2$ ), 1.74–1.93 (m, 4H;  $\text{CH}_2$ ), 4.05 (quintet, 1H, CH,  $J$  = 6.27Hz).  $^{13}\text{C}$  NMR (75 MHz,  $\text{CDCl}_3$ , 20 °C):  $\delta$  (ppm) = 14.1, 22.7, 27.6, 29.1, 29.2, 29.4, 31.8, 39.2, 59.0. b.p. = 135–137°C (0.72 Torr). (75.6%)

#### Typical procedure of preparation of $\text{DiC}_n\text{CHSH}^{264}$

**7-tridecanethiol:** 7-bromotridecane (10.0g, 38.0 mmol) was dissolved with 40 mL ethanol in a 250 mL single-neck reaction flask equipped with condensing tube. Then thiourea (4.34 g, 56.9 mmol, 1.5 equiv.) was added in the solution. The mixture was heated reflux under argon atmosphere overnight and then NaOH aq. (3.4 M, 20 mL, 68 mmol) was added and the solution was kept reflux for 2h. The mixture was kept still and cooled to room temperature. The crude product could be obtained by separation of the upper phase directly and dried by  $\text{MgSO}_4$ . The pure product was obtained by distillation en vacuum (colorless oil, 4.56g, 55.1%).  $^1\text{H}$  NMR (300 MHz,  $\text{CDCl}_3$ , 20 °C, TMS):  $\delta$  (ppm) = 0.82–0.97 (m, 6H;  $\text{CH}_3$ ), 1.21–1.74 (m, 20H;  $\text{CH}_2$ ), 2.72–2.86 (m, 1H, CH).  $^{13}\text{C}$  NMR (75 MHz,  $\text{CDCl}_3$ , 20 °C):  $\delta$  (ppm) = 14.1, 22.6, 27.1, 29.1, 31.8, 39.0, 41.2. b.p. = 55–58°C (0.23 Torr).

**8-pentadecanethiol:**  $^1\text{H}$  NMR (300 MHz,  $\text{CDCl}_3$ , 20 °C, TMS):  $\delta$  (ppm) = 0.84–0.96 (m, 6H;  $\text{CH}_3$ ), 1.20–1.73 (m, 24H;  $\text{CH}_2$ ), 2.73–2.86 (m, 1H, CH).  $^{13}\text{C}$  NMR (75 MHz,  $\text{CDCl}_3$ , 20 °C):  $\delta$  (ppm) = 14.1, 22.7, 27.1, 29.2, 29.4, 31.8, 39.0, 41.2. b.p. = 127–129°C (0.32 Torr). (60.4%)



**9-heptadecanethiol:**  $^1\text{H}$  NMR (300 MHz,  $\text{CDCl}_3$ , 20 °C, TMS):  $\delta$  (ppm) = 0.84–0.96 (m, 6H;  $\text{CH}_3$ ), 1.20–1.72 (m, 28H;  $\text{CH}_2$ ), 2.73–2.86 (m, 1H, CH).  $^{13}\text{C}$  NMR (75 MHz,  $\text{CDCl}_3$ , 20 °C):  $\delta$  (ppm) = 14.1, 22.7, 27.1, 29.3, 29.4, 29.5, 31.9, 39.0, 41.2. b.p. = 155–158°C (0.33 Torr). (60.4%)

**Typical procedure of preparation of  $\text{DiC}_n\text{CHSO}_3\text{H}$ <sup>264</sup>**

**7-tridecanesulfonic acid:** 7-tridecanethiol (6.58g, 30.4 mmol) in acetic acid/THF mixed solvent (1:1) was added dropwise into a 100 mL reaction flask containing peracetic acid (35 wt%, 19.8 g, 91.1 mmol, 3 equiv.) under the ice-water bath. After 1h, all the 7-tridecanethiol was added and the mixture was kept stirring at room temperature for another 1h and then the solvent was removed by evaporation in vacuum at 40°C. The residual acetic acid was removed by high vacuum pump for 12h afforded the pure product (yellow gel, 7.50g, 93.4%).  $^1\text{H}$  NMR (300 MHz,  $\text{CDCl}_3$ , 20 °C, TMS):  $\delta$  (ppm) = 0.84–0.98 (m, 6H;  $\text{CH}_3$ ), 1.23–1.52 (m, 16H;  $\text{CH}_2$ ), 1.55–1.70 (m, 2H,  $\text{CH}_2$ ), 1.79–1.96 (m, 2H,  $\text{CH}_2$ ), 2.77–2.89 (m, 1H, CH).  $^{13}\text{C}$  NMR (75 MHz,  $\text{CDCl}_3$ , 20 °C):  $\delta$  (ppm) = 14.1, 22.6, 26.8, 29.2, 29.3, 31.6, 60.9.

**8-pentadecanesulfonic acid:**  $^1\text{H}$  NMR (300 MHz,  $\text{CDCl}_3$ , 20 °C, TMS):  $\delta$  (ppm) = 0.84–0.98 (m, 6H;  $\text{CH}_3$ ), 1.19–1.55 (m, 20H;  $\text{CH}_2$ ), 1.57–1.72 (m, 2H,  $\text{CH}_2$ ), 1.82–1.99 (m, 2H,  $\text{CH}_2$ ), 2.82–2.93 (m, 1H, CH).  $^{13}\text{C}$  NMR (75 MHz,  $\text{CDCl}_3$ , 20 °C):  $\delta$  (ppm) = 14.0, 22.6, 26.7, 29.0, 29.2, 29.5, 31.8, 61.3. (95.8%)

**9-heptadecanesulfonic acid:**  $^1\text{H}$  NMR (300 MHz,  $\text{CDCl}_3$ , 20 °C, TMS):  $\delta$  (ppm) = 0.84–0.96 (m, 6H;  $\text{CH}_3$ ), 1.19–1.55 (m, 24H;  $\text{CH}_2$ ), 1.57–1.74 (m, 2H,  $\text{CH}_2$ ), 1.83–1.98 (m, 2H,  $\text{CH}_2$ ), 2.83–2.95 (m, 1H, CH).  $^{13}\text{C}$  NMR (75 MHz,  $\text{CDCl}_3$ , 20 °C):  $\delta$  (ppm) = 14.1, 22.7, 26.7, 29.1, 29.3, 29.4, 29.6, 31.9, 61.2. (96.8%)

**Typical procedure of preparation of  $[\text{DiC}_n\text{CHSO}_3]_x[\text{X}]$  (x = 1, Li, Na, K; x = 2, X = Mg, Cu, Zn, Ca; x = 3, X = Sc)**

**$[\text{DiC}_6\text{CHSO}_3]_2\text{Zn}$ :** ZnO (153.9 mg, 1.9 mmol) was weighed in a 10 mL reaction flask containing  **$\text{DiC}_6\text{CHSO}_3\text{H}$**  (1.0 g, 3.8 mmol) and 5 mL  $\text{H}_2\text{O}$ . The mixture was kept at 85°C and stirring overnight. Then the mixture was cooled to room temperature and the water was removed by lyophilisation and pure product was obtained quantitatively.  $^1\text{H}$  NMR (300 MHz,  $\text{CDCl}_3$ , 20 °C, TMS):  $\delta$  (ppm) = 0.83–0.98 (m, 12H;  $\text{CH}_3$ ), 1.19–1.55 (m, 32H;  $\text{CH}_2$ ), 1.57–1.73 (m, 4H,  $\text{CH}_2$ ), 1.86–2.04 (m, 4H,  $\text{CH}_2$ ), 2.86–2.97 (m, 2H, CH).  $^{13}\text{C}$  NMR (75 MHz,  $\text{CDCl}_3$ , 20 °C):  $\delta$  (ppm) = 14.1, 22.7, 26.8, 29.0, 29.5, 31.8, 61.2.

**$[\text{DiC}_6\text{CHSO}_3]_2\text{Ca}$ :**  $^1\text{H}$  NMR (300 MHz,  $\text{CDCl}_3$ , 20 °C, TMS):  $\delta$  (ppm) = 0.83–0.98 (m, 12H;  $\text{CH}_3$ ), 1.19–1.55 (m, 32H;  $\text{CH}_2$ ), 1.54–1.69 (m, 4H,  $\text{CH}_2$ ), 1.83–2.00 (m, 4H,  $\text{CH}_2$ ), 2.69–2.84 (m, 2H, CH).  $^{13}\text{C}$  NMR (75 MHz,  $\text{CDCl}_3$ , 20 °C):  $\delta$  (ppm) = 14.1, 22.7, 27.0, 29.1, 29.5, 31.9, 60.3.

**$[\text{DiC}_6\text{CHSO}_3]_2\text{Mg}$ :**  $^1\text{H}$  NMR (300 MHz,  $\text{CDCl}_3$ , 20 °C, TMS):  $\delta$  (ppm) = 0.83–0.98 (m, 12H;  $\text{CH}_3$ ), 1.19–1.55 (m, 32H;  $\text{CH}_2$ ), 1.54–1.72 (m, 4H,  $\text{CH}_2$ ), 1.85–2.01 (m, 4H,  $\text{CH}_2$ ), 2.76–2.88 (m, 2H, CH).  $^{13}\text{C}$  NMR (75 MHz,  $\text{CDCl}_3$ , 20 °C):  $\delta$  (ppm) = 14.1, 22.7, 26.8, 28.9, 29.4, 31.8, 60.9.

**DiC<sub>6</sub>CHSO<sub>3</sub>Na:** <sup>1</sup>H NMR (300 MHz, CDCl<sub>3</sub>, 20 °C, TMS): δ (ppm) = 0.84–0.98 (m, 6H; CH<sub>3</sub>), 1.19–1.62 (m, 18H; CH<sub>2</sub>), 1.75–1.94 (m, 2H, CH<sub>2</sub>), 2.61–2.74 (m, 1H, CH). <sup>13</sup>C NMR (75 MHz, CDCl<sub>3</sub>, 20 °C): δ (ppm) = 14.1, 22.7, 27.2, 29.6, 29.7, 31.9, 59.7.

**DiC<sub>6</sub>CHSO<sub>3</sub>K:** <sup>1</sup>H NMR (300 MHz, CDCl<sub>3</sub>, 20 °C, TMS): δ (ppm) = 0.84–0.98 (m, 6H; CH<sub>3</sub>), 1.19–1.62 (m, 18H; CH<sub>2</sub>), 1.76–1.93 (m, 2H, CH<sub>2</sub>), 2.59–2.72 (m, 1H, CH). <sup>13</sup>C NMR (75 MHz, CDCl<sub>3</sub>, 20 °C): δ (ppm) = 14.1, 22.7, 27.3, 29.6, 29.8, 31.9, 59.8.

**DiC<sub>6</sub>CHSO<sub>3</sub>Li:** <sup>1</sup>H NMR (300 MHz, CDCl<sub>3</sub>, 20 °C, TMS): δ (ppm) = 0.84–0.98 (m, 6H; CH<sub>3</sub>), 1.19–1.62 (m, 18H; CH<sub>2</sub>), 1.81–1.98 (m, 2H, CH<sub>2</sub>), 2.64–2.77 (m, 1H, CH). <sup>13</sup>C NMR (75 MHz, CDCl<sub>3</sub>, 20 °C): δ (ppm) = 14.1, 22.8, 27.2, 29.4, 29.6, 31.9, 59.6.

### 2.2.3 The physicochemical investigation of surfactants

#### Surface Tension Measurements

Surface tensions were measured with the tensiometer K11 (Krüss) using the Wilhelmy plate method. Ultrapure water (Millipore water,  $\sigma = 72.0 \text{ mN}\cdot\text{m}^{-1}$  at 25 °C) was used to prepare all concentrations. Surface tension was recorded after equilibration for each mixture. All equilibrium surface tension values were mean quantities of at least three measurements. The standard deviation of the mean never deviated  $\pm 1.5\%$  of the mean. The precision of the force transducer of the surface tension apparatus was  $0.1 \text{ mN}\cdot\text{m}^{-1}$ , and before each experiment, the platinum plate was cleaned in red/orange color flame. The temperature was stabilized at  $25 \pm 0.05 \text{ }^\circ\text{C}$  with a thermo-regulated bath Lauda RC6. The standard deviation was estimated at  $\pm 10\%$  for the CAC value.

#### Polarized light optical microscopy

The phase penetration technique was first used for a rough estimate of the sequence of mesophases occurring. A few milligrams of the surfactant powder (usually around 20 mg) were placed between a glass slide and a cover slip. When the powder could not be made sufficiently compact to obtain a well-defined interface, the sample might be heated until softening for homogenization and then cooled back to room temperature, in order to obtain a well-defined interface. The sample was then contacted with a distilled water drop and diffusion of water by capillarity into the surfactant sample took place so that a concentration gradient from extremely dilute aqueous solution to pure surfactant was more or less quickly established. Identification of the different phases was based on visual observation through an optical polarizing microscope Olympus BX60 (100 × magnification) equipped with a LTS120 Analyza Peltier temperature stage capable of controlling to  $\pm 0.1 \text{ }^\circ\text{C}$  the temperature. After having established roughly the succession of liquid crystalline phases from the penetration scan, the transition compositions

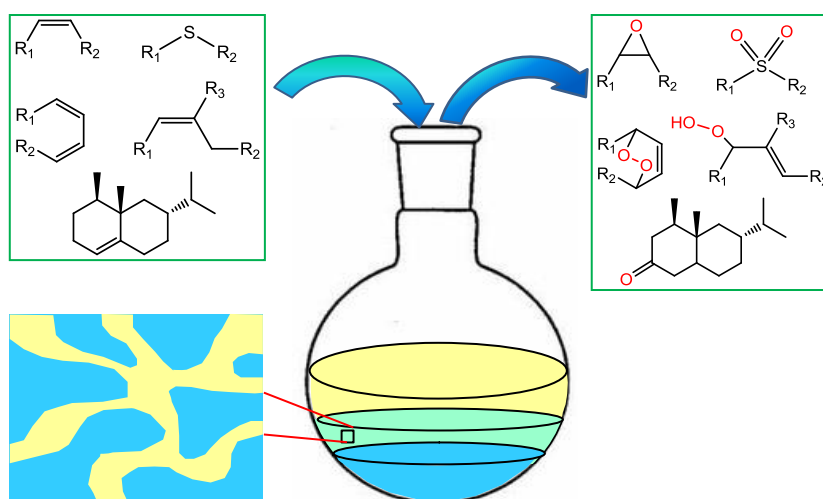
were determined by preparing samples of given concentrations (from 5–95 wt% with 5 wt.% intervals, so that the accuracy of the resulting diagrams was of about  $\pm 2.5\%$ ). Samples of 100 mg or more were prepared in glass tubes which were then sealed with a gas burner placed in water bath at 80 °C for 2h and were then centrifuged at 2500 rpm for one hour at room temperature for homogenization. The rate used during the heating sequence was typically 5 °C.min<sup>-1</sup>. The type of the phase was investigated by the birefringence of the mixture and the texture was given by the liquid crystal type.

#### **Small Angle X-Ray Scattering (SAXS) experiments**

SAXS measurements using Mo-radiation ( $\lambda = 0.71 \text{ \AA}$ ) were performed on a bench built by XENOCSS. The scattered beam was recorded using a large online scanner detector (diameter: 345 mm, from MAR Research). A large Q range ( $2.10\text{-}2.5 \text{ \AA}^{-1}$ ) was covered with an off centre detection. Pre-analysis of data was performed using FIT2D software. The scattered intensities are expressed versus the magnitude of scattering vector  $Q = [(4\pi)/\lambda] \sin(\theta/2)$ , where  $\lambda$  is the wavelength of incident radiation and  $\theta$  the scattering angle. 2mm quartz capillaries were used as sample containers for dilute and fluid solutions, i.e. isotropic micellar solutions. Usual corrections for background (empty cell and detector noise) subtractions and intensity normalization using Lupolen<sup>TM</sup> as standard were applied. For the study of highly viscous lyotropic phases a special home designed cell was used.



### CHAPTER 3: Reactions in Multiphase Microemulsions Elaborated with Catalytic Surfactants





### 3.1 Introduction

Microemulsions as reaction media have been successfully applied to the bioorganic, organic and inorganic synthesis due to their various advantages including solubilization of both hydrophilic and hydrophobic substrates, reaction rate and selectivity enhancement, the easily separation of product and the specific structure of the micro-reactor *etc.*<sup>18,274,275</sup> With lipase catalyzed esterification as an example, which is the most widely reported reaction among the bioorganic reactions catalyzed by enzymes, the reaction proceeds readily in  $\mu\text{em}$  and the stability of enzyme is also improved, which allowed the reaction to occur in a wide temperature range.<sup>276-278</sup> The nanostructure of  $\mu\text{ems}$  can be controlled by the composition and the formulation variables, which is a preferable model to prepare nanoparticles with desired size distribution, geometry, morphology, and surface area *etc.* A number of metal sulfide semiconductor nanoparticles have been thus synthesized in W/O  $\mu\text{ems}$  with AOT as a surfactant and metal dodecylsulfate or metal AOT as a functional surfactant. The average diameter of the particles was depending on the relative amount of metallic cation  $\text{M}^{2+}$  and  $\text{S}^{2-}$ .<sup>279,280</sup> In addition to the inorganic nanoparticles, hydrophobic polymer particles can also be prepared in  $\mu\text{em}$  systems affording high molar mass of polymers in high reaction rate. One-step formation of hollow polystyrene sphere was achieved in O/W  $\mu\text{em}$  with nonionic triblock copolymers of poly(oxyethylene)-poly(oxypropylene)-poly(oxyethylene)-[(EO) $x$ (PO) $y$ (EO) $x$ ] as surfactants. The size of the nanoparticles could be varied by changing the surfactant concentration and [surfactant]/[monomer] ratio.<sup>281</sup>

Besides, the  $\mu\text{em}$  system is also a good reaction medium for various organic reactions, which are commonly carried out in homogenous organic solvents.<sup>18</sup> With etherification in cyclohexane/DBSA/water  $\mu\text{em}$  system as an example, even the short chain carboxylic acid could be transformed to ester in high yield under mild conditions.<sup>179</sup> Another example is the enone epoxidation by the alkaline hydrogen peroxide in nonionic  $\mu\text{em}$ , compared with the biphasic reaction with PTC, the epoxidation of vitamin  $\text{K}_3$  was about 35 times faster.<sup>19</sup> Although the surfactant combined catalysts were widely used in catalytic reactions in aqueous phase as indicated in Chapter 1, their application in  $\mu\text{em}$  were not sufficiently investigated. Recently, our group reported the catalytic oxidation in  $\mu\text{ems}$  with surfactant combined molybdate and tungstate.<sup>27-30,282</sup> In the basic environment, the molybdate or tungstate catalytic dismutation of  $\text{H}_2\text{O}_2$  generates singlet oxygen  $^1\text{O}_2$ , which easily converts to triplet oxygen  $^3\text{O}_2$ , while in the microreactor of  $\mu\text{em}$ , the *in situ* generated  $^1\text{O}_2$  can contact with hydrophobic substrates before being deactivated. Especially in the elegant three-phase  $\mu\text{em}$  with double chain ammonium molybdate as catalyst and surfactant, the efficiency of  $\text{H}_2\text{O}_2$  reached 50%, about 100 times more than with tetrabutyl ammonium bromide as PTC.<sup>29</sup>

Considering the importance of the oxidation reactions in organic synthesis, besides the molybdate catalyzed  $^1\text{O}_2$  oxygenation in three-phase  $\mu\text{em}$ , an acidic three-phase  $\mu\text{em}$  was also elaborated with “Catasurfs” derived from tungstate in the present work and applied to the epoxidation of olefins and

oxidation of refractory sulfides. On the other side, taking advantage of the synergism between ionic surfactant  $[\text{DiC}_8]_2[\text{MoO}_4]$  and nonionic surfactant  $\text{C}_8\text{E}_4$ , a temperature-switch catalytic  $\mu\text{em}$  was sufficiently investigated and applied to the oxygenation of various organic substrates. As  $\mu\text{em}$  facilitates the separation of product and the catalyst recycling at the end of the reaction, here  $[\text{DiC}_8]_2[\text{MoO}_4]$  catalyzed one pot three-step oxidation of valencene to nootkatone was studied at first time. Besides the oxidation reaction, the catalytic  $\mu\text{em}$  medium can also be used for other reactions. For example, an  $\mu\text{em}$  system based on the “Fish diagram” of  $[\text{DiC}_8]\text{Br}$  in the presence of sulphonated phosphine ligands (TPPTS or DPPBS) was prepared for hydroformylation of hydrophobic olefins with  $\text{Rh}(\text{CO})_2(\text{acac})$  as catalyst precursor (Figure 3.1).

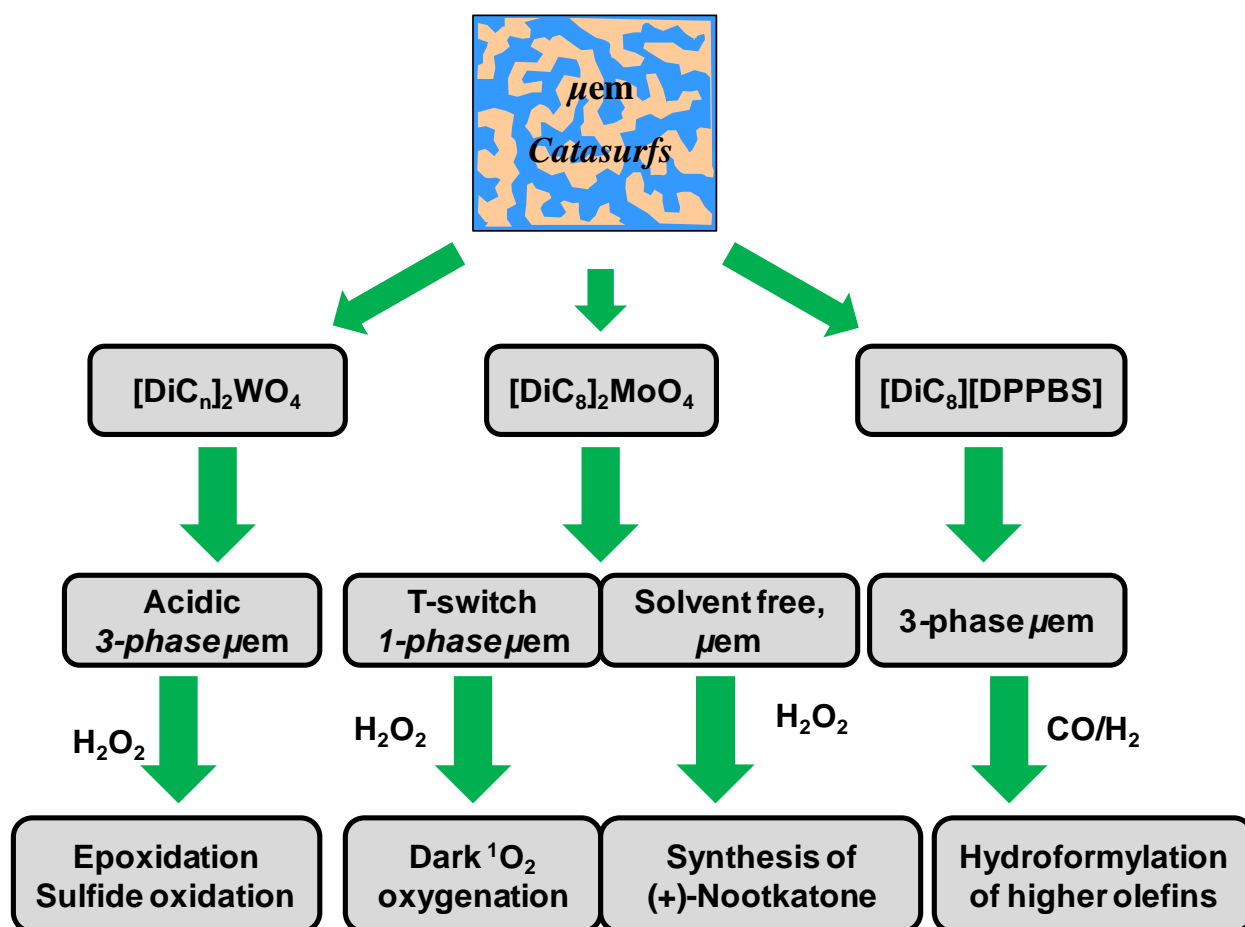


**Figure 3.1** Catalytic reactions in  $\mu\text{em}$  media with surfactant combined catalyst as both catalyst and surfactant

### 3.2 Catalytic oxidation reactions in acidic three-phase microemulsion

#### 3.2.1 The design of acidic microemulsion systems

The physicochemical properties of  $[\text{DiC}_n]_2[\text{MoO}_4]$  and  $[\text{DiC}_n]_2[\text{WO}_4]$  ( $n = 6, 8, 10$ ) have been investigated in Chapter 2, especially the Fish diagrams were established by screening the polarity of the solvents. Among the surfactants, the  $[\text{DiC}_6]$  salts were always too hydrophilic to give a Winsor III  $\mu\text{em}$ , while  $[\text{DiC}_8]$  and  $[\text{DiC}_{10}]$  salts gave “Fish diagrams” when  $\alpha,\omega$ -dichloroalkanes and 1-chloroalkanes were



used as solvents and the optimal oils for  $[\text{DiC}_8]_2[\text{WO}_4]$ ,  $[\text{DiC}_8]_2[\text{MoO}_4]$ ,  $[\text{DiC}_{10}] [\text{WO}_4]$  and  $[\text{DiC}_{10}] [\text{MoO}_4]$  were  $\text{C}_{2,4}\text{Cl}_2$ ,  $\text{C}_{2,5}\text{Cl}_2$ ,  $\text{C}_{5,4}\text{Cl}$  and  $\text{C}_{8,2}\text{Cl}$ , respectively. These values also revealed the  $[\text{DiC}_n]_2[\text{WO}_4]$  are more hydrophilic than their homologues  $[\text{DiC}_n]_2[\text{MoO}_4]$  and depending on the EACN scale in **Figure 2.18**,  $[\text{DiC}_n]_2[\text{WO}_4]$  provides preferentially Winsor I  $\mu\text{em}$ s with most of the common solvents, even in the presence of  $\text{H}_2\text{O}_2$ . Actually addition of excess  $\text{H}_2\text{O}_2$  leads to the peroxidation of  $\text{WO}_4^{2-}$  into the bigger and more polarizable tetraperoxotungstate  $\text{W}(\text{O}_2)_4^{2-}$ , which makes the surfactant more hydrophobic. Previously, the  $[\text{DiC}_n]_2[\text{MoO}_4]$  has been successfully developed in the dark singlet oxygenation in three-phase  $\mu\text{em}$  and its efficiency has been demonstrated on various substrates.<sup>29</sup> Different from  $\text{MoO}_4^{2-}$ , the activity of  $\text{WO}_4^{2-}$  for dismutation of  $\text{H}_2\text{O}_2$  into  $^1\text{O}_2$  is about 3.5 times slower than  $\text{MoO}_4^{2-}$  at neutral or basic condition, while under acidic conditions;  $\text{WO}_4^{2-}$  presents a higher activity in catalytic oxidation reactions involving  $\text{H}_2\text{O}_2$  such as epoxidation, alcohol oxidation, sulfide oxidation and olefin cleavage.<sup>10,127,283-285</sup>

The active species of peroxotungstates in the catalytic oxidation reactions have been widely investigated by Venturello,<sup>100</sup> Griffith,<sup>283</sup> and Bregeault<sup>102,286</sup> *et al.* The possible active species are presented in **Figure 1.14** and the Venturello species  $[\text{PO}_4\{\text{WO}(\text{O}_2)_2\}_4]^{3-}$  was considered as the most active catalyst in the oxidation reaction. The structure of the active species in the presence of  $\text{H}_2\text{O}_2$  was closely dependent on the *pH* and the acid types in the solution and also could convert to each other. Actually, according to the *pH* and the anion assembling, several oxoperoxo complexes formed in the reaction medium were shown in **Figure 3.2**. In order to adjust the acidic condition for the formation of Venturello species during the oxidation reaction, the inorganic acids, such as  $\text{HCl}$ ,  $\text{H}_2\text{SO}_4$  *etc.*, were not of choice due to the anion exchange with  $\text{WO}_4^{2-}$ , which not only changed the amphiphilicity of surfactant, but also decreased the availability of  $\text{WO}_4^{2-}$ . Alternatively, to prevent the ion exchange,  $[\text{DiC}_8][\text{HSO}_4]$  and  $[\text{DiC}_8][\text{H}_2\text{PO}_4]$  containing amphiphilic quaternary ammonium were chosen to adjust the *pH* and as the assemble anion, respectively, in the present work. Before elaborating the catalytic  $\mu\text{em}$ ,  $[\text{DiC}_8]$  and  $[\text{DiC}_{10}]$  salts involved in the catalytic oxidation were classified according their hydrophilic-lipophilic scale by visual observation of phase behavior of water/surfactant/solvent  $\mu\text{em}$  with different solvents. For example, with 1,3-dichloropropane as solvent,  $[\text{DiC}_8]_2[\text{WO}_4]$  gave Winsor III  $\mu\text{em}$ , while in the presence of excess  $\text{H}_2\text{O}_2$ , Winsor III converted to Winsor II, which indicated the  $[\text{DiC}_8]_2[\text{WO}_8]$  was more hydrophobic than the former. When 1-chlorohexane was used as solvent,  $[\text{DiC}_{10}]_2[\text{MoO}_4]$  gave Winsor III, while  $[\text{DiC}_8]_2[\text{WO}_4]$  gave Winsor, which meant  $[\text{DiC}_{10}]_2[\text{MoO}_4]$  was more hydrophobic. The hydrophilic-lipophilic order was given in **Figure 3.3**.

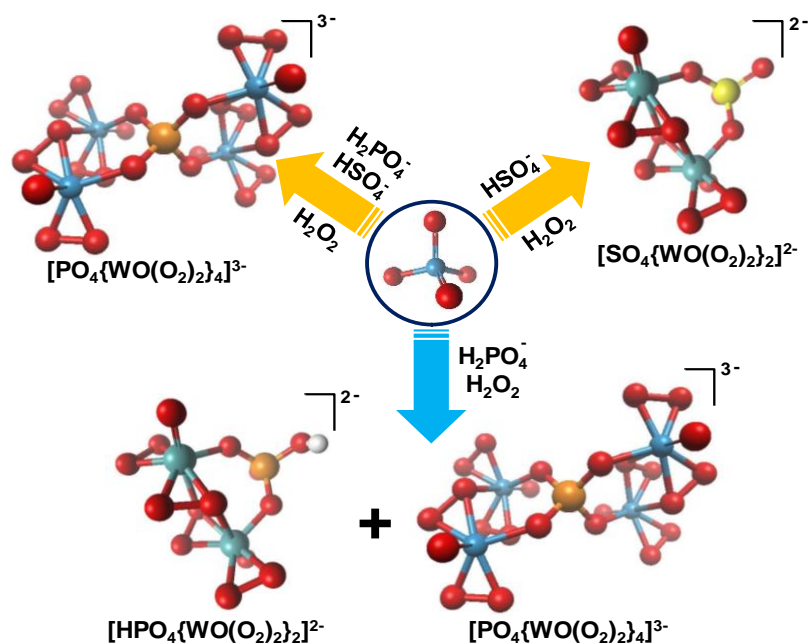


**Figure 3.2** Molecular view of various active tungsten (VI) oxodiperoxo complexes obtained from the  $[WO_4]^{2-}$  catalytic precursor in the presence of  $H_2O_2$  and various anions ( $[HSO_4^-]$  and/or  $[H_2PO_4^-]$ ) (W: blue, O: red, P: orange, S: yellow, H: white, blue arrow: pH 6, orange arrow: pH 2-3).<sup>100,102</sup>

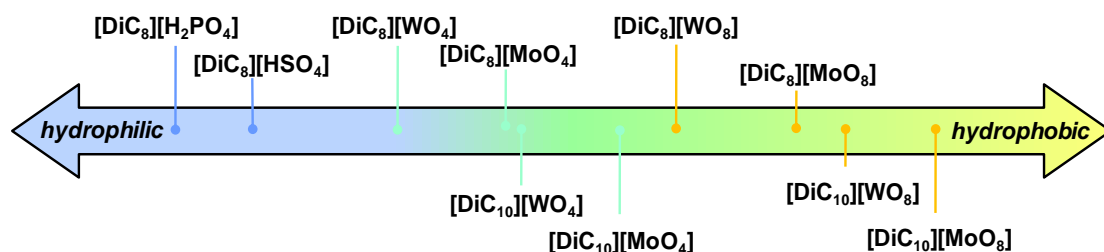


**Figure 3.3** Hydrophilic-lipophilic scale and behavior in ternary systems of catalytic surfactants and amphiphilic acids.

It was found that the  $[DiC_8]_2[WO_4]$  was too hydrophilic to give Winsor III  $\mu em$  with most of the common used solvents in the lab, even in the presence of  $H_2O_2$ . To increase slightly the hydrophobicity of this “Catasurf”, the  $[DiC_{10}]_2[WO_4]$  was preferred rather than  $[DiC_8]_2[WO_4]$ . It was noteworthy that, the tungstate,  $H_2O_2$  and acid should follow a sequence to prepare the desired peroxotungstate. Firstly, the tungstate and  $H_2O_2$  were mixed together under ice-water bath, which was succeeded by the addition of  $[DiC_8][HSO_4]$  to control the pH, then  $[DiC_8][H_2PO_4]$  was added to form the complex. If  $[DiC_{10}]_2[WO_4]$  was mixed  $[DiC_8][HSO_4]$  before  $H_2O_2$ , the polyoxometalate was formed and precipitated.<sup>287</sup> Fortunately, the introduction of  $[DiC_{10}]_2[WO_4]$  provides the desired Winsor III after preparing the desired peroxotungstate with butyl, pentyl, *tert*-butyl acetates as solvents as well as aromatic solvents like toluene (Figure 3.4).

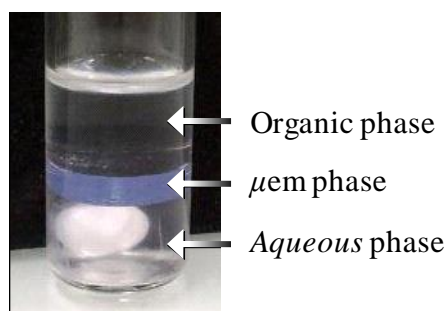


**Figure 3.4** Acidic oxidizing three-liquid-phase  $\mu em$  system spontaneously formed at 25 °C with  $[DiC_{10}]_2[WO_4]$  (30 mM),  $[DiC_8][H_2PO_4]$  (15 mM),  $[DiC_8][HSO_4]$  (115 mM), aqueous  $H_2O_2$  (150 mM), water (1 mL), *p*-xylene (1 mL), pH = 2.

### 3.2.2 Optimization of conditions and epoxidation of various olefins in Winsor III system

Due to its easy and selective conversion into corresponding epoxide, cyclooctene was chosen as a model substrate to optimize the reaction condition. The toluene was chosen as solvent when the other conditions such as the temperature, the ratio of the  $WO_4^{2-}$ ,  $HSO_4^-$  and  $H_2PO_4^-$  etc. were investigated. Besides, replacement of toluene with more green solvents such as *tert*-BuOAc and *tert*-BuOMe was also investigated (Table 3.1). To adjust the pH = 2–3, the concentration of  $[DiC_8][HSO_4]$  115 mM was required in the  $\mu em$ . According to the previously reported method to prepare the Venturello species, the  $[DiC_{10}]_2[WO_4]/[DiC_8][H_2PO_4]$  mol ratio was fixed to 2:1.

**Table 3.1** Epoxidation of cyclooctene in an acidic three-phase  $\mu em$  based on  $[DiC_{10}]_2WO_4$  as a balanced catalytic surfactant.<sup>a</sup>

Entry	Solvent	T/°C	$\Delta t/h$	Winsor (Initial→End)	Conversion (%) <sup>b</sup>
1	Toluene	50	1	III→ III	>99.9
2 <sup>c</sup>	Toluene	50	4	III→ III	0
3 <sup>d</sup>	Toluene	50	2	III→ III	15
4	Toluene	25	4	III→ III	>99.9
5	<i>tert</i> -BuOAc	50	1	III→ III	>99.9
6	<i>tert</i> -BuOMe	50	1	I→ I	97.8

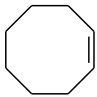
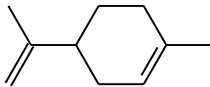
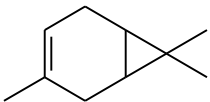
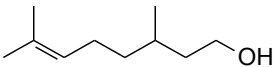
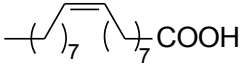
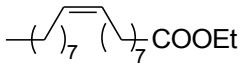
<sup>a</sup> Conditions:  $[DiC_{10}]_2[WO_4] = 30mM$ ;  $[DiC_8][HSO_4] = 115mM$ ,  $[DiC_8][H_2PO_4] = 15 mmol$ ,  $H_2O = toluene = 1mL$ , cyclooctene = 100 mM,  $[H_2O_2] = 150mM$ , pH = 2–3, <sup>b</sup> Determined by GC and <sup>1</sup>H NMR, <sup>c</sup> Without  $[DiC_8][H_2PO_4]$ , <sup>d</sup>  $[DiC_8]HSO_4] = 42.3 mg, 57 mM$ ; pH = 5.

As shown in **Table 3.1**, with toluene as solvent, the three-phase  $\mu\text{em}$  was maintained throughout the reaction with  $[\text{DiC}_{10}]_2[\text{WO}_4]$  as “Catasurf”, which interacted with  $\text{H}_2\text{O}_2$  and assembled with  $[\text{DiC}_8][\text{H}_2\text{PO}_4]$  affording active peroxotungstates, and  $[\text{DiC}_8][\text{HSO}_4]$  as pH regulator. For epoxidation of cyclooctene, high catalytic activity and selectivity were observed. Indeed, after 20 min at  $50^\circ\text{C}$ , 72.2% conversion was obtained and the quantitative conversion was achieved in 1h leading exclusively to the epoxide (**Entry 1, Table 3.1**). Even at room temperature, the epoxidation also proceeded smoothly except that 4h was required to complete the conversion. Control experiments revealed that the  $[\text{DiC}_8][\text{HSO}_4]$  and  $[\text{DiC}_8][\text{H}_2\text{PO}_4]$  were indispensable for the reaction. For example, less  $[\text{DiC}_8][\text{HSO}_4]$  was used (pH = 5–6), the conversion only reached 15% after 2 h (**Entry 3, Table 1**) due to the formation of less efficient oxidiperoxo complex formation like  $[\text{HPO}_4\{\text{WO}(\text{O}_2)_2\}_2]$  (See **Figure 3.2**). While no conversion was observed in the absence of  $[\text{DiC}_8][\text{H}_2\text{PO}_4]$  after 4h (**Entry 2, Table 3.1**), which probably ascribed to the formation of  $[\text{SO}_4\{\text{WO}(\text{O}_2)_2\}_2]^{2-}$ , which does not exhibit catalytic activity towards epoxidation. Finally, *tert*-BuOAc and *tert*-BuOMe were also introduced as solvents and *tert*-BuOAc was preferred as the Winsor III  $\mu\text{em}$  was still obtained at the end of the reaction without loss of activity. As described above, the optimal condition was  $[\text{DiC}_{10}]_2[\text{WO}_4] = 30 \text{ mM}$ ;  $[\text{DiC}_8][\text{HSO}_4] = 115 \text{ mM}$ ;  $[\text{DiC}_8][\text{H}_2\text{PO}_4] = 15 \text{ mmol}$ ,  $T = 50^\circ\text{C}$  and toluene or *tert*-BuOAc as solvent. Under such conditions, various alkenes were readily epoxidized in good yield and selectivity.

In order to extend the scope of this catalytic system, the epoxidation of limonene,  $\Delta^3$ -carene, ethyl oleate, oleic acid and  $\beta$ -citronellol was also carried out under the standard optimized condition (**Table 3.2**). The epoxidation of these substrates proceeded smoothly since all the substrates were completely converted within 2–5h. While the selectivity and final  $\mu\text{em}$  types were closely related with the substrates themselves. Cyclooctene,  $\Delta^3$ -carene, ethyl oleate and limonene did not change the Winsor type after the reaction, because these substrates as well as their corresponding epoxides were poorly amphiphilic and their polarity did not change the properties of the oil phase in great extent. Even in the case of limonene, 35% of diol was formed; the three-phase  $\mu\text{em}$  was still maintained. In contrast, oleic acid and  $\beta$ -citronellol were much stronger amphiphilic and the insertion into the surfactant film between water and oil interface changed the effective packing parameters  $P_{\text{eff}}$  (**Eq. 3.1**), which determined the Winsor types. Before epoxidation, oleic acid and  $\beta$ -citronellol increased the  $v_{\text{eff}}$  effectively, although the  $a_{\text{eff}}$  was also slightly increased, the final  $P_{\text{eff}}$  increased and converted the  $\mu\text{em}$  from Winsor III to Winsor II. At the end of the reaction, the epoxide of oleic acid was more hydrophilic than oleic acid, but was not enough to convert the Winsor types; while in the case of  $\beta$ -citronellol, the diol was the preferred product and Winsor I was obtained due to the increase of  $a_{\text{eff}}$  by the diol and decrease of  $P_{\text{eff}}$ .

$$P_{\text{eff}} = \frac{v_{\text{eff}}}{a_{\text{eff}} \times l_c} \quad (\text{Eq. 3.1})$$

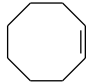
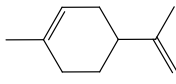
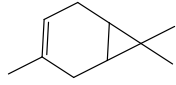
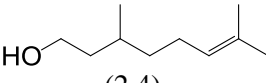
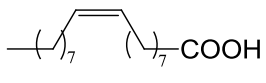
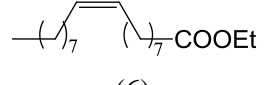
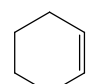
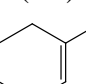
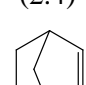
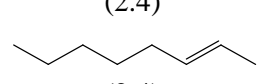
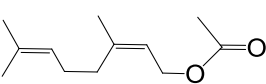
**Table 3.2** Epoxidation of various olefins in the aqueous  $H_2O_2$ /toluene/ $[DiC_{10}]_2[WO_4]$ / $[DiC_8][H_2PO_4]$ / $[DiC_8][HSO_4]$  three-liquid-phase microemulsion systems. <sup>a,b</sup>

Entry	Olefin	$\Delta t$ (h)	Final Winsor	Epoxy. (%)	Diol (%)
1		2	III	> 99	0
2		2	III	65	35
3		4	III	91	9
4		2	I <sup>[c]</sup>	0	> 99
5		3	II <sup>[c]</sup>	> 99	0
6		5	III	> 99	0

<sup>a</sup> Conditions:  $[DiC_{10}]_2[WO_4] = 30$  mM,  $[DiC_8][H_2PO_4] = 15$  mM,  $[DiC_8][HSO_4] = 115$  mM, water = 1 mL, toluene = 1 mL, [olefin] = 100 mM,  $[H_2O_2] = 150$  mM,  $T = 50$  °C; <sup>b</sup> Conversions were > 99% and determined by GC and <sup>1</sup>H NMR. <sup>c</sup> Initial Winsor systems are WII.

The above described catalytic reactions involved only small amount of substrates, which was not practical in the further industrial application, thus the preparative scale epoxidation was also investigated and performed in three-phase  $\mu$ em. The epoxides could be divided into two types: acid stable epoxides and acid sensitive ones. To improve the conversion and selectivity for acid sensitive epoxides, several improvements of the catalytic system were carried out. For example, water was just used for recovering the Winsor III  $\mu$ em at the end of the reaction to facilitate the separation of product and catalyst rather than at the beginning of reaction. Besides, as reported by Grigoropoulou *et al.* the presence of organic solvent was beneficial for selectivity of the acid sensitive olefin epoxide.<sup>288</sup> The amount of the starting substrates was adjusted in such a way that at the end of the reaction, Winsor III  $\mu$ em could be recovered. The reaction conditions for different type of substrates are given in **Table 3.3** and only 1.2 equivalents  $H_2O_2$  was enough for the complete conversion of substrates within reasonable reaction times.

**Table 3.3** Preparative epoxidations of various olefins in the presence of the balanced catalytic  $[DiC_{10}]_2[WO_4]/[DiC_8][H_2PO_4]/[DiC_8][HSO_4]$  system.<sup>a,b</sup>

Entry	Olefin (mmol)	H <sub>2</sub> O/ <i>t</i> -BuOAc (mL/mL)	H <sub>2</sub> O <sub>2</sub> mmol	Δ <i>t</i> (h)	Final Winsor	Epox. (%)	Diol (%)
1	 (6)	0.47/0	7.2	2	III <sup>c</sup>	> 99	0
2	 (2.4)	0/6	3.0	2	III <sup>d</sup>	95 <sup>f</sup>	5
3	 (2.4)	0/6	3.0	4.5	III <sup>d</sup>	94	6
4	 (2.4)	0/6	3.0	2.5	I <sup>d</sup>	28	72
5	 (6)	0.47/0	7.2	4	II <sup>e</sup>	> 99	0
6	 (6)	0.47/0	9.0	6	III <sup>e</sup>	> 99	0
7	 (2.4)	0/6	3.0	4	III <sup>d</sup>	97	3
8	 (2.4)	0/6	3.0	3	III <sup>d</sup>	93	7
9	 (2.4)	0/6	3.0	4	III <sup>d</sup>	94	6
10	 (2.4)	0/6	3.0	4	III <sup>d</sup>	95	5
11	 2.4	0/6	3.0	3.5	I <sup>d</sup>	94 <sup>g</sup>	6

<sup>a</sup> Conditions: Conditions:  $[DiC_{10}]_2[WO_4] = 0.06\text{mmol}$ ,  $[DiC_8][H_2PO_4] = 0.03\text{mmol}$ ,  $[DiC_8][HSO_4] = 0.23\text{mmol}$ ,  $T = 50\text{ }^\circ\text{C}$ . <sup>b</sup> Conversion was determined by GC and <sup>1</sup>H NMR at the end of reaction. <sup>c</sup> 1mL toluene was added after reaction. <sup>d</sup> 1mL H<sub>2</sub>O was added after reaction. <sup>e</sup> 3 mL *tert*-BuOAc was added after reaction. <sup>f</sup> 8.1% diepoxide, <sup>g</sup> 2,3-epoxide: 6,7-epoxide:diepoxide = 20:67:13.

For cyclooctene, ethyl oleate, and oleic acid, the epoxides are stable, thus the reaction could be carried out without addition of organic solvent and epoxide was the unique product. At end of the reaction, the addition of 1 mL toluene or *tert*-BuOAc was enough to recover Winsor III  $\mu\text{em}$  in the cases of cyclooctene and ethyl oleate as substrates (**Entry 1 and 6, Table 3.3**). For ethyl oleate (75% purity), the Winsor III  $\mu\text{em}$  was unexpectedly obtained without additional solvent at the end of the reaction (**Figure 3.5**). Although the epoxidation of oleic acid was similar with ethyl oleate, the final Winsor II  $\mu\text{em}$  was always formed even after addition of solvent due to the effect of product on the effective packing parameter discussed above (**Entry 5, Table 3.3**). While for the rest of olefins, 6 mL of *tert*-BuOAc were required at the beginning of reaction since in the absence of solvent, the diol was the major product. The amount of substrates was adjusted to 2.4 mmol to ensure Winsor III as the final  $\mu\text{em}$  after addition of 1 mL water at the end of reaction. It was noteworthy that although the selectivity of epoxide was improved for  $\beta$ -citronellol oxidation under this conditions, but the diol still dominated the product (72% diol), which led to the Winsor I as the final  $\mu\text{em}$  (**Entry 4, Table 3.3**). Similar phase behavior was also obtained with neryl acetate as substrate (**Entry 11, Table 3.3**).

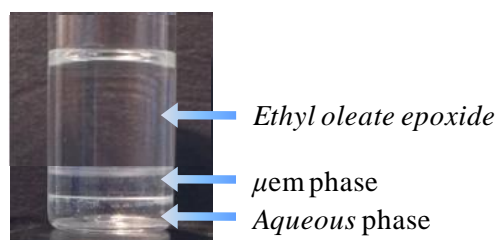


**Figure 3.5** The spontaneous formed three-phase  $\mu\text{em}$  after epoxidation of ethyl oleate without additional solvent.

The epoxidation of terpenes is of particular interest as terpene epoxides are widely used in fragrances, flavors, drugs and agrochemicals,<sup>289</sup> while their sensitivity to the acids makes epoxidation of terpenes still challenging. Numerous different catalytic systems have been developed to improve the epoxide selectivity. For example, the tungstate heterogeneous catalyst developed by De Villa *et al.*,<sup>290</sup> with the peroxotungstate amberlite as a solid catalyst, high epoxide selectivity could be obtained in  $\text{CH}_3\text{CN}$  but this heterogeneous catalyst showed low reactivity (generally 24h was required). The epoxidation in  $\text{NaH}_2\text{PO}_3/\text{H}_3\text{PO}_4$  buffer was reported by Grigoropoulou *et al.*<sup>288</sup> The authors mentioned that the use of  $[\text{triC}_8]\text{H}_2\text{PO}_3$  alone resulted in a significant decrease of the conversion due to the high pH ( $\text{pH} \approx 4$ ). On the other side, to avoid the acidic condition, Sato *et al* reported the epoxidation of terpenes under neutral condition with  $\text{PhP(O)(OH)}_2$  as assembling core of peroxotungstate, which improved the epoxide selectivities of the limonene and  $\Delta^3$ -carene up to 82% and 93%, respectively.<sup>120,291</sup> By comparison, higher reactivity and selectivity could be obtained in our catalytic  $\mu\text{em}$  medium without addition of water (**Entry 2, 3, Table 3.3**). At the end of reaction, the addition of 1mL water afforded the three-phase  $\mu\text{em}$  and the product is readily isolated by phase separation. In addition, several other substrates were also successfully

epoxidized under such condition, including cyclohexene, 1-methylcyclohexene, 2-norbornene and 2-octene (**Entry 7-10**) and providing good selectivities (> 93% epoxide). Finally the reactivity of recycled catalyst was evaluated with ethyl oleate (75% purity) as substrates under solvent-free conditions (**Table 3.4**). Each run caused a partial loss of the activity, and after fourth run, the Winsor II  $\mu$ em was obtained instead of Winsor III.

**Table 3.4** The recycling of the catalyst in the epoxidation of ethyl oleate. <sup>a</sup>

Run <sup>b</sup>	H <sub>2</sub> O (mL)	H <sub>2</sub> O <sub>2</sub> (mmol)	$\Delta t$ (h)	Final Winsor	Epox. (%)	Diol (%)
1	0.47	9.0	6	III	> 99	0
2	0	9.0	8	III	98.6	0
3	0	9.0	12	III	97.9	0
4	0	9.0	14	II	97.2	0

<sup>a</sup> Conditions:  $[DiC_{10}]_2[WO_4] = 0.06$  mmol,  $[DiC_8][H_2PO_4] = 0.03$  mmol,  $[DiC_8][HSO_4] = 0.23$  mmol, ethyl oleate: 6mmol,  $T = 50$  °C. <sup>b</sup> At the end of reaction, the mixture was kept still for 3h and the product was removed by separation, then the fresh ethyl oleate was added and the next run started.

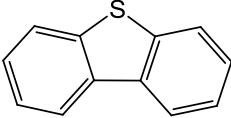
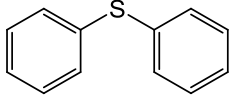
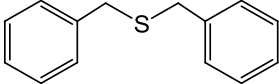
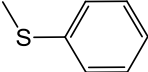
### 3.2.3 Oxidation of sulfides and thiophenes

As the organosulfur compounds play important roles in biochemical processes, the fossil fuels, coal, petroleum and natural gas, which are derived from fossil organisms, contain different kinds of organosulfurs, These organosulfurs in gasoline and diesel are the major source of acid rain,<sup>292</sup> thus the sulfur removing plays an important role in the petroleum refineries. The conventional desulfurization method hydrodesulfurization (HDS) is highly efficient to remove the thiol, aliphatic sulfide, and disulfide, while the refractory benzothiophene (DBT) and its derivatives show low activity and require high pressure and temperature.<sup>293,294</sup> Alternatively, the oxidative desulfurization (ODS) with H<sub>2</sub>O<sub>2</sub> as an oxidant is a safe, economic and eco-friendly method to oxidize the inert DBT and its derivatives to sulfones and remove them from diesel by extraction or simple phase separation.<sup>110,292</sup> As reviewed in Chapter 1, peroxotungstate and polyoxometalates are commonly used as catalysts in ODS process, for example, the oxidation in the metastable emulsion with  $[(C_{18}H_{37})_2N(CH_3)_2]_3[PW_{12}O_{40}]$  as catalyst by Can Li *et al.*,<sup>105</sup> or in the emulsion based on ionic liquid with lacunary  $[C_{18}]_7PW_{11}O_{39}$  as catalyst by Ge *et al.*<sup>109</sup>. Our acidic three-phase catalytic  $\mu$ em was also capable of oxidizing different types of sulfides and thiophenes efficiently (**Table 3.5**). The DBT was readily converted to sulfoxide and sulfone in 15 min with only 1.5 equivalents H<sub>2</sub>O<sub>2</sub> (**Entry 1, Table 3.5**). Besides DBT, the oxidation diphenylsulfide, dibenzylsulfide and phenylmethylsulfide also gave high yield (>93%). Among them, the sulfoxide was



main product for oxidation of dibenzyl sulfide (83%, **Entry 3, Table 3.5**), which indicated the sulfide was easily oxidized than sulfoxide. On the other side, complete conversion could be obtained by addition of 2 equivalents  $H_2O_2$ . Different from the epoxidation of olefins, the sulfide, sulfoxide and sulfone showed weak effect on the phase behavior, indeed, the three-phase was maintained during the reaction. For diphenylsulfide and dibenzyl sulfide, almost 95% of sulfoxide and sulfone precipitated during the reaction and could be isolated straight forward.

**Table 3.5** Oxidation of organosulfides in the three-liquid-phase  $\mu\text{em}$ .<sup>a</sup>

Entry	Substrates (S)	Conv. (%)	Selectivity	
			SO (%)	SO <sub>2</sub> (%)
1		> 99	54	46
2		93 <sup>b</sup>	53	47
3		95 <sup>b</sup>	83	17
4		95	54	46

<sup>a</sup>  $[DiC_{10}]_2[WO_4] = 30 \text{ mM}$ ,  $[DiC_8][H_2PO_4] = 15 \text{ mM}$ ,  $[DiC_8][HSO_4] = 115 \text{ mM}$ ,  $H_2O_2 = 300 \text{ mM}$ , organosulphur =  $200 \text{ mM}$ , water =  $1 \text{ mL}$ , AcOtBu =  $1 \text{ mL}$ ,  $25 \text{ }^\circ\text{C}$ ,  $t = 15 \text{ min}$ . <sup>b</sup> Precipitation of oxidation products (> 95%).

### 3.2.4 Conclusion

Depending on the hydrophilic-lipophilic properties of “Catasurf”  $[DiC_n]_2[WO_4]$ , the pH regulator  $[DiC_8][HSO_4]$ , and the amphiphilic Venturello species formed from the interaction with  $H_2O_2$  and assembling with  $DiC_8[H_2PO_4]$ , the acidic three-phase  $\mu\text{ems}$  were successfully elaborated with toluene or *tert*-BuOAc as solvent, which are particularly suitable for the epoxidation of olefins and the oxidation of refractory sulfides. For acid stable epoxides, the reactions could be carried out even without of additional solvent during the reaction and for acid sensitive epoxides, only a small adjustment like elimination of additional water at the beginning was necessary to improve the selectivity. The three-phase  $\mu\text{em}$  was disturbed when high amphiphilic substrates or products were present, but the Winsor I  $\mu\text{em}$  was also acceptable since the product and catalyst could also be separated. The oxidation of sulfides proceeded also very well in these  $\mu\text{em}$  systems and the products showed little effect on the phase behavior. Such three-phase  $\mu\text{ems}$  not only exhibit high activity system but also facilitate the separation of products, thus constituting interesting alternatives to the phase transfer catalysts and the heterogeneous catalysts.

### 3.3 Temperature–switch $\mu$ ems for dark singlet oxygenation

#### 3.3.1 Description of the synergism between ionic and nonionic surfactants

The mixtures of ionic and nonionic surfactants always lead to interesting synergic effects, which are widely applied to improve properties of surfactants in the detergent,<sup>295,296</sup> foaming,<sup>297-299</sup> emulsification,<sup>300</sup> solubilization<sup>301-303</sup> or biocide.<sup>11,12</sup> In the past decades, several different theories were proposed to explain and quantify this kind of interaction, such as the phase-separation model proposed by Holland,<sup>304</sup> the electrostatic model by Scamehorn<sup>305</sup> and the molecular-thermodynamic model of Blankschtein,<sup>306</sup> *etc.* Among them, regular solution theory is widely used for the explanation and quantification of the interaction of surfactants in the mixture,<sup>304,307-309</sup> although the enthalpy of mixing is supposed to be ideal and the experimental results are not always in agreement with the theoretical prediction. To qualify the interaction extent, the so-called  $\beta$  parameter is introduced to describe the interaction between nonionic and ionic surfactant. The  $\beta$  parameter could be calculated by measuring the CMCs of the surfactant mixture and the deduction of  $\beta$  parameter is given from **Eq.3.2-Eq. 3.10**.<sup>304</sup>

From the phase separation model, the chemical potential of surfactant  $i$  monomer in bulk solution can be written as:

$$\mu_i = \mu_i^0 + RT \ln C_i^m \quad (\text{Eq. 3.2})$$

Where  $C_i^m$  is the monomer concentration in bulk solution and activity coefficient is considered as 1. In the mixed micelle, the chemical potential of surfactant  $i$  is described as:

$$\mu_i' = \mu_i'^0 + RT \ln f_i x_i \quad (\text{Eq. 3.3})$$

Where  $f_i$ ,  $x_i$  are the activity coefficient and mole fraction in the micelle, respectively. When the micellation reach equilibrium, for the pure surfactant  $i$ , the chemical potential of monomer in solution equals to the molecule in micellar phase:

$$\mu_i^0 = \mu_i'^0 + RT \ln C_i \quad (\text{Eq. 3.4})$$

Where  $C_i$  is the CMC of surfactant  $i$ . In the surfactants mixture system, at the equilibrium, from the **Eq. 3.3** and **Eq. 3.4**, the following relationship can be obtained:

$$C_i^m = x_i f_i C_i \quad (\text{Eq. 3.5})$$

On the other hand, at the point of CMC of surfactant mixture  $C^*$ , the monomer concentration  $C_i^m$  can also be calculated from the mole fraction of surfactant  $i$  denoted as  $\alpha_i$ :

$$C_i^m = \alpha_i C^* \quad (\text{Eq. 3.6})$$

Combined **Eq. 3.5** and **Eq. 3.6**, the relation between the CMC of pure surfactant  $i$   $C_i$  and the CMC of the surfactant mixture  $C^*$  is obtained:

$$\frac{1}{C^*} = \sum_{i=1}^n \left( \frac{\alpha_i}{f_i C_i} \right) \quad (\text{Eq.3.7})$$

From the regular solution theory, which regards the mixture entropy as ideal, the chemical potential of surfactant **1** in the mixture of two different kind of surfactant can be written as:

$$\mu_1' = \mu_1^0 + RT \ln x_1 + \beta RT x_2^2 \quad (\text{Eq. 3.8})$$

Where  $\beta$  is the interaction parameter and from **Eq. 3.3**, **Eq.3.8**, the activity coefficient is expressed as:

$$\ln f_1 = \beta \times (1-x_1)^2 \quad (\text{Eq. 3.9})$$

and **Eq. 3.7**, the  $\beta$  can be calculated from the following expression by measuring the CMC of the surfactant mixture:

$$\frac{1}{(1-x_1)^2} \ln \left[ \frac{\alpha_1 C^*}{x_1 C_1} \right] = \frac{1}{x_1^2} \ln \left[ \frac{\alpha_2 C^*}{(1-x_1) C_2} \right] = \beta \quad (\text{Eq. 3.10})$$

The mole fraction of the ionic surfactant in the aggregated pseudo-phase,  $x_1$ , can be solved iteratively from each  $\alpha_1$  and its corresponding  $C^*$ .<sup>210,310</sup> Then the  $\beta$  for each  $\alpha_1$  can be obtained. A negative value of  $\beta$  indicates a synergistic interaction between the different surfactants while a positive value means an antagonism effect and the ideal mixture gives  $\beta = 0$ .

Such synergies are also observed in ternary systems and sometimes, dramatic efficiency enhancement of nonionic surfactant can be obtained by addition of very small amounts of an ionic surfactant.<sup>311,312</sup> From phenomenologic interpretation, Kahlweit *et al.* explained this efficiency increase by the boundaries changes of the water-surfactant and oil-surfactant binary diagrams in the phase prism,<sup>269,311</sup> while the hydrophilic-lipophilic balance (HLB) has also been used to rationalize the particular application.<sup>313</sup> On the other side, the additional affinity between surfactant molecules in the mixed micelles also existed in the interface, which resulted in the electronic and structural properties changes of the surfactant membrane in the  $\mu\text{em}$ .<sup>314,315</sup>

Molybdate ions are efficient catalysts to disproportionate hydrogen peroxide into singlet oxygen,  $^1\text{O}_2$ . As discussed previously, the  $\text{H}_2\text{O}_2/\text{MoO}_4^{2-}$  system has been efficiently applied to the dark singlet oxygenation of various organic substrates.<sup>21,25,27,316,317</sup> Especially, the three-phase  $\mu\text{em}$  based on  $[\text{DiC}_8]_2[\text{MoO}_4]$ .<sup>29</sup> Here, **tetraethylene glycol monoethyl ether**, abbreviated as  $\text{C}_8\text{E}_4$ , was used to elaborate a thermo-sensitive catalytic  $\mu\text{em}$ . The synergistic effect between  $[\text{DiC}_8]_2[\text{MoO}_4]$  and  $\text{C}_8\text{E}_4$  is discussed in terms of cloud point, surface tension measurement, mixed micelle size and pseudo-ternary  $\mu\text{em}$  where the microstructure was investigated by SAXS experiment. The effect of  $[\text{DiC}_8]_2[\text{MoO}_4]$  on the  $\text{H}_2\text{O}/\text{C}_8\text{E}_4/\text{cyclohexane}$   $\mu\text{em}$  is highlighted providing a temperature-switch catalytic  $\mu\text{em}$  which is successfully applied to the dark singlet oxygenation. After the reaction, the monophasic reaction media could be turned to WI  $\mu\text{em}$  for recycling the catalyst and separation of product.

### 3.3.2 The synergism between nonionic $\text{C}_8\text{E}_4$ and cationic $[\text{DiC}_8]_2[\text{MoO}_4]$

The critical micelle concentration (CMC) of  $\text{C}_8\text{E}_4$  (7.2 mM at 25 °C) and  $[\text{DiC}_8]_2[\text{MoO}_4]$  (6.8 mM) were determined by surface tension measurements and were in good agreement with the values previously reported (7.2 mM and 8.0 mM for  $\text{C}_8\text{E}_4$  and  $[\text{DiC}_8]_2[\text{MoO}_4]$ , respectively).<sup>31,318</sup> Then, the CMCs of surfactant mixtures were determined for different  $[\text{DiC}_8]_2[\text{MoO}_4]$  mole fractions  $\alpha_1$ . The surface tension

vs concentration curves were given in **Figure 3.6** and the CMCs,  $x_1$  solved iteratively from each  $\alpha_1$  and the  $\beta$  for each  $\alpha_1$  were given in **Table 3.6**. On the other side,  $\beta$  can be calculated from the **Eq. 3.11** (deduced from the combination of **Eq.3.7** and **Eq. 3.9**):

$$C^* = \frac{C_1 C_2 e^{\beta(-1+x_1)^2 + \beta x_1^2}}{\alpha_1 (C_2 e^{\beta x_1^2} - C_1 e^{\beta(-1+x_1)^2}) + C_1 e^{\beta(-1+x_1)^2}} \quad (\text{Eq. 3.11})$$

For each  $\alpha_1$ , the theoretical  $C^*_{cal}$  can be calculated from **Eq. 3.10** and **Eq. 3.11** in order to determine  $x_{1cal}$  and to fit the adjustable parameters ( $\beta_{fit}$ ) with an algorithm.<sup>210</sup> The best fit is obtained by choosing the  $\beta$  value that would minimize the deviations of the experimental critical aggregate concentration of the mixture ( $C^*$ ) from the theoretical curve ( $C^*_{cal}$ ). The experimental and calculated values of the CMC of the surfactant mixtures as well as the **[DiC<sub>8</sub>]<sub>2</sub>[MoO<sub>4</sub>]** mole fraction in the micelles ( $x_1$ ) as a function of **[DiC<sub>8</sub>]<sub>2</sub>[MoO<sub>4</sub>]** mole fraction ( $\alpha_1$ ) are presented in **Figure 3.7**. According to the negative  $\beta$  value, a strong synergistic interaction of **[DiC<sub>8</sub>]<sub>2</sub>[MoO<sub>4</sub>]** with **C<sub>8</sub>E<sub>4</sub>** takes place in the mixed micelles. The similar CMC of **[DiC<sub>8</sub>]<sub>2</sub>[MoO<sub>4</sub>]** and **C<sub>8</sub>E<sub>4</sub>** indicates that the contribution of the hydrophobic effect to the synergy is not the key factor contrary to the interaction between the headgroups which is the main driving force.<sup>210,319</sup> The electrostatic repulsion, which is weakened by insertion of the nonionic surfactant, and the ion-dipole interaction between the ionic and the nonionic surfactant headgroups have been previously reported to cause the synergism in mixed micelles.<sup>210</sup> Besides, the quaternary ammonium-polyoxyethylene complex which is similar to a crown ether-cation complex or podands tends to form and further increases the attractive interaction.<sup>320-322</sup>

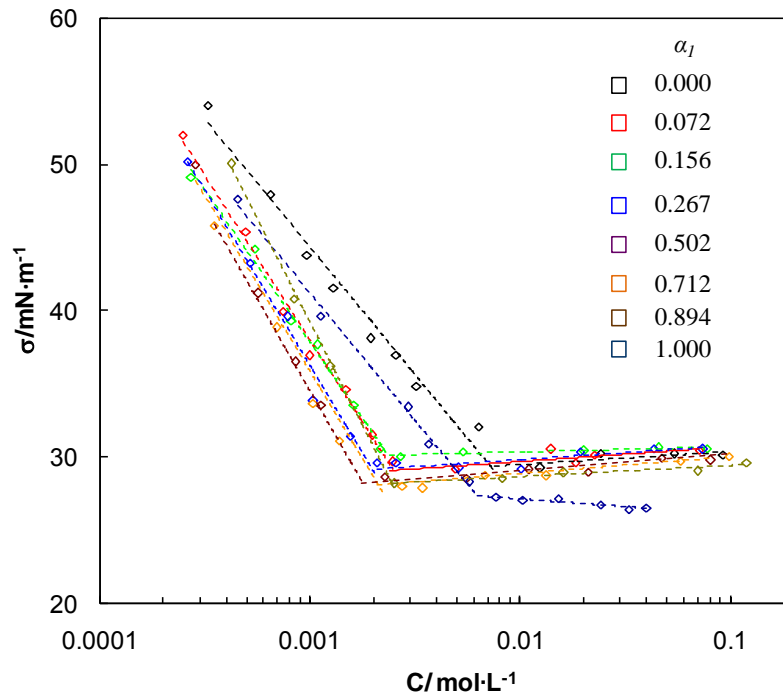


**Figure 3.6** Surface tension ( $\sigma$ ) plotted against surfactant concentration for the mixture of **C<sub>8</sub>E<sub>4</sub>** and **[DiC<sub>8</sub>]<sub>2</sub>MoO<sub>4</sub>** at different mole fraction of **[DiC<sub>8</sub>]<sub>2</sub>MoO<sub>4</sub>** ( $\alpha_1$ ) at 25.0 °C.

**Table 3.6** Critical micelle concentrations ( $C^*$ ) for various  $C_8E_4/[DiC_8]_2MoO_4$  mixtures and related calculated parameters.

$\alpha_1$	$C^*$ (mM)	$x_1$	$\beta$	$x_{1cal}^a$	$C^*_{cal}$ (mM) <sup>b</sup>	$C^*_{Clint}$ (mM) <sup>c</sup>
0.000	7.20	0.00	-	0.00	7.20	7.20
0.072	2.34	0.35	-6.25	0.32	3.05	7.16
0.156	2.36	0.388	-5.25	0.39	2.49	7.12
0.267	2.11	0.434	-5.13	0.43	2.17	7.06
0.502	2.08	0.505	-4.84	0.5	1.98	6.94
0.712	2.37	0.573	-4.57	0.57	2.11	6.84
0.894	3.03	0.665	-4.54	0.66	2.70	6.75
1.000	6.77	1.00	-	1.00	6.77	6.77

<sup>a</sup> Calculated from Eq. 3.8 with  $\beta_{fit} = -5.01$ . <sup>b</sup> Calculated from Eq. 3.9 with corresponding  $x_{1cal}$ . <sup>c</sup> CMCs of the ideal surfactant mixtures.

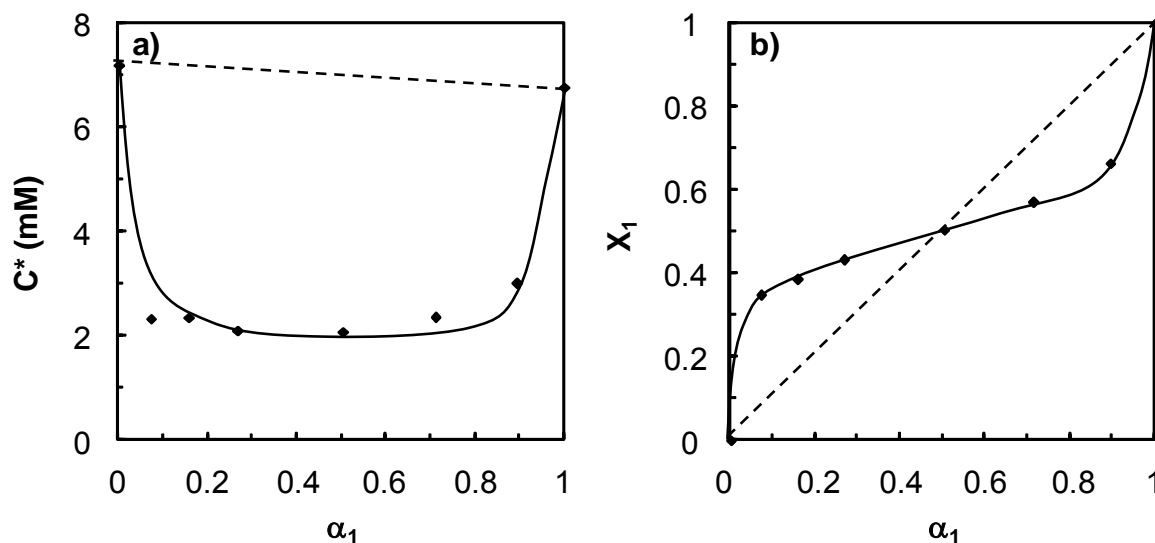


**Figure 3.7** Variation of: a) the critical micelle concentration ( $C^*$ ) and b)  $[DiC_8]_2[MoO_4]$  mole fraction in the micellar phase ( $x_1$ ) as a function of  $[DiC_8]_2[MoO_4]$  mole fraction ( $\alpha_1$ ) in  $[DiC_8]_2[MoO_4]/C_8E_4$  surfactant mixtures at 25 °C. Diamonds correspond to experimental values. Dashed lines represent ideal mixed aggregates ( $\beta = 0$ ) whereas continuous lines are calculated from the regular solution theory (eqs. 3 and 4,  $\beta = -5.01$ ).

The  $C_8E_4/[DiC_8]_2[MoO_4]$  mixed micelles were investigated by dynamic light scattering. DLS was performed at 25 °C for different surfactant ratios at a fixed total surfactant concentration of 30 mM ( $\approx 4$  times the CMC of  $[DiC_8]_2[MoO_4]$  or  $C_8E_4$ , **Figure 3.8**).

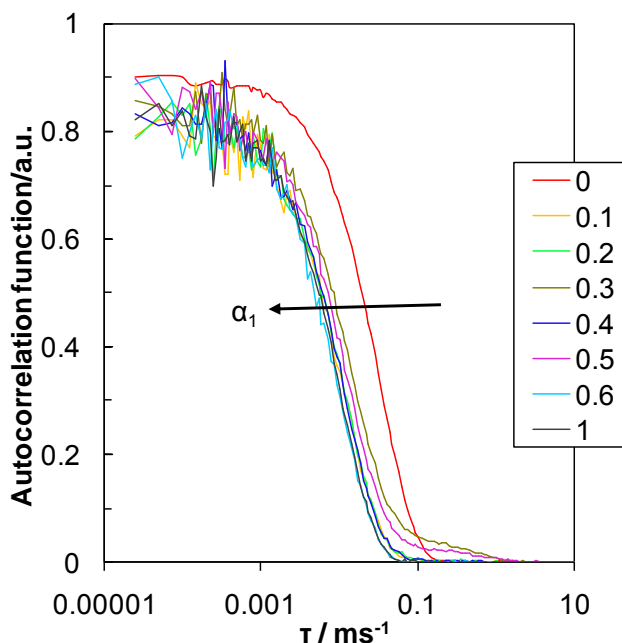


**Figure 3.8** DLS auto-correlation functions of  $[DiC_8]_2[MoO_4]/C_8E_4$  mixtures recorded at different  $[DiC_8]_2[MoO_4]$  mole fractions ( $\alpha_1$ ) (total surfactant concentration = 30 mM,  $T = 25$  °C and detection angle =  $90^\circ$ )

The auto-correlation functions presented in **Figure 3.8** can be described with a single exponential decay for all  $[DiC_8]_2[MoO_4]$  mole fractions ( $\alpha_1$ ) reflecting the presence of mono-sized mixed  $[DiC_8]_2[MoO_4]/C_8E_4$  micelles. The auto-correlation function decays more rapidly, *i.e.* at smaller  $\tau$  values, by increasing  $\alpha_1$  and doesn't change for  $\alpha_1 > 0.1$ . This indicates that the micelle size decreases when  $\alpha_1$  increases from 0 to 0.1 while for  $\alpha_1 > 0.1$ , the micelle size remains constant. The self-diffusion coefficient of mixed  $[DiC_8]_2[MoO_4]/C_8E_4$  micelles ( $D_{obs}$ ) can be calculated by fitting the auto-correlation functions using the cumulant analysis. The hydrodynamic radius ( $R_h$ ) of the mixed micelles can be calculated from  $D_{obs}$  by using the Stokes-Einstein equation.  $D_{obs}$  and  $R_h$  obtained by fitting the auto-correlograms are reported in **Table 3.7** for various  $[DiC_8]_2[MoO_4]$  mole fractions ( $\alpha_1$ ).

From **Table 3.7**, it can be seen that the presence of  $[DiC_8]_2[MoO_4]$  has a dramatic effect on the size of the mixed micelles for the very low mole fractions  $\alpha_1$ . Then, for  $\alpha_1 > 0.1$ , its effect is almost imperceptible up to the pure  $[DiC_8]_2[MoO_4]$  micelles. As the alkyl chain length is similar between  $C_8E_4$  and  $[DiC_8]_2[MoO_4]$ , the hydrophobic contribution to the micelle formation is similar. Consequently, we suppose that the dramatic diminution of the micelle size, for  $\alpha_1 < 0.1$ , is caused by the strong interaction between the headgroups of the two surfactants as observed with the evolution of the CMC values. As described in the literature, the micelle size of  $C_iE_j$  surfactants are determined by the balance between the

hydrophobic effect of alkyl chain and the hydration and the steric repulsion of hydrophilic polyethylene oxide groups.<sup>323</sup> Besides the temperature, the salt effect also causes dramatic change of the head group hydration extent.<sup>324-326</sup> Indeed, the water-structure-breaking ions increase the hydration of the polyethylene oxide part (salting-in effect), whereas, the water-structure-making ions result in its dehydration (salting-out effect).<sup>327</sup> Therefore, the addition of ionic surfactants, for  $\alpha_l < 0.1$ , which can be considered as strong water-structure-breaking ions, increases the hydration of the head group. Therefore, the increase in the effective head group area can be related to a decrease of micelle size from  $R_h = 5.8$  to 2.2 nm. Above  $\alpha_l = 0.1$ , the electrostatic repulsion between the headgroups plays the most important role on the size of micelles, so further addition of the cationic surfactant has no significant impact on the micelle size.

**Table 3.7** Hydrodynamic radius ( $R_h$ ) and self-diffusion coefficient of mixed  $[\text{DiC}_8]_2[\text{MoO}_4]/\text{C}_8\text{E}_4$  micelles ( $D_{obs}$ ) as a function of  $[\text{DiC}_8]_2[\text{MoO}_4]$  mole fractions ( $\alpha_l$ ).

$\alpha_l$	$D_{obs} (\times 10^{-11} \text{ m}^2 \cdot \text{s}^{-1})$	$R_h$ (nm)
<b>0.00</b>	4.20	5.8
<b>0.01</b>	7.10	3.4
<b>0.1</b>	11.2	2.2
<b>0.2</b>	10.8	2.2
<b>0.4</b>	11.3	2.1
<b>0.5</b>	10.5	2.3
<b>0.7</b>	10.4	2.3
<b>1.00</b>	12.7	1.9

The cloud point of  $\text{C}_8\text{E}_4$  is 40.9 °C at 7 wt.%, which is in good agreement with the values previously reported.<sup>328,329</sup> The amount of ionic surfactant was defined as the mass fraction in the total surfactants (Eq. 3.12) and addition of small amounts of  $[\text{DiC}_8]_2[\text{MoO}_4]$  induces a profound modification of the phase behavior of the water- $\text{C}_8\text{E}_4$  system as shown in Figure 3.9. The temperature boundary of phase separation was increased by 10 °C in the presence of only 1 wt.% of  $[\text{DiC}_8]_2[\text{MoO}_4]$  in total amount of surfactants, whereas  $\delta = 5\%$  resulted in a phase separation above 70 °C. These changes could be explicated Hofmeister effect.<sup>269,330,331</sup> The lyotropic (salting-out) salts such as NaCl,  $\text{Na}_2\text{SO}_4$  and NaBr facilitate the phase separation of nonionic surfactants in water solution, while the hydrotropic salts (salting-in) such as NaI and NaSCN increase their solubility and cloud points.<sup>332,333</sup> The ionic surfactants,

including anionic and cationic ones which were proved to have similar effects, are considered as very hydrotropic salts and enlarge dramatically the miscibility gap of nonionic/water binary mixtures.<sup>312,334,335</sup> On the other hand, the insertion of ionic surfactant molecules in the nonionic micelles also causes electrostatic repulsions besides the hydration repulsion of the nonionic surfactant.

$$\delta = \frac{m_{[DiC_8]_2MoO_4}}{m_{C_8E_4} + m_{[DiC_8]_2MoO_4}} \quad (\text{Eq.3.12})$$

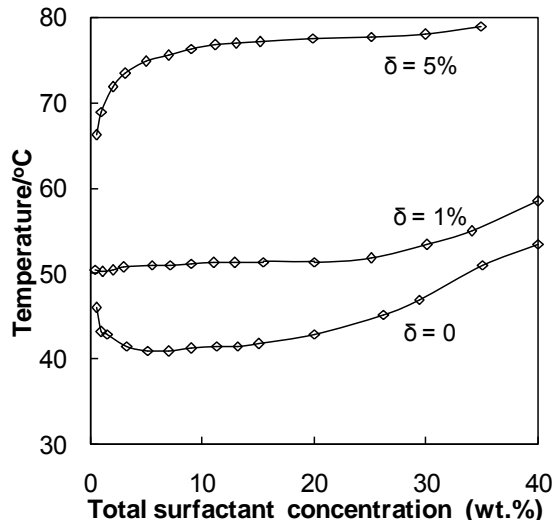


**Figure 3.9** Miscibility gap of  $C_8E_4$ - $[DiC_8]_2[MoO_4]/H_2O$  as a function of total surfactant concentration (wt.%) with various  $[DiC_8]_2[MoO_4]$  mass fraction ( $\delta$ ).

The “Fish diagram”, representing the phase behavior of a SOW system as a function of surfactant concentration and a scan variable, *e.g.* temperature as in the present case, of the ternary  $C_8E_4$ /cyclohexane/ $H_2O$  and pseudo-ternary  $C_8E_4$ - $[DiC_8]_2[MoO_4]$ /cyclohexane/ $H_2O$  systems as a function of total surfactant concentration (wt.%) for different  $[DiC_8]_2[MoO_4]$  mass fractions ( $\delta$ ) have been constructed (**Figure 3.10**). The “Fish diagram” for pure  $C_8E_4$  shows a large symmetric region of three-phase  $\mu em$  (Winsor III) and at least 14 wt.% surfactant is required to completely solubilize equal amounts of water and oil (Winsor IV). While the addition of only 1 wt.% of  $[DiC_8]_2[MoO_4]$  ( $\delta = 0.01$ ) induces a dramatic increase of the  $C_8E_4$  efficiency as well as the disappearance of the three-phase  $\mu em$  body. Thus, Winsor IV  $\mu em$  can be obtained with only 6 wt.% in total of amphiphiles. 0.5 wt.% is not enough to suppress completely the three-phase region but improves its efficiency. Further addition of  $[DiC_8]_2[MoO_4]$  ( $\delta \geq 0.01$ ) does not change the efficiency of the nonionic surfactant while it enhances the temperature stability of monophasic  $\mu em$ .



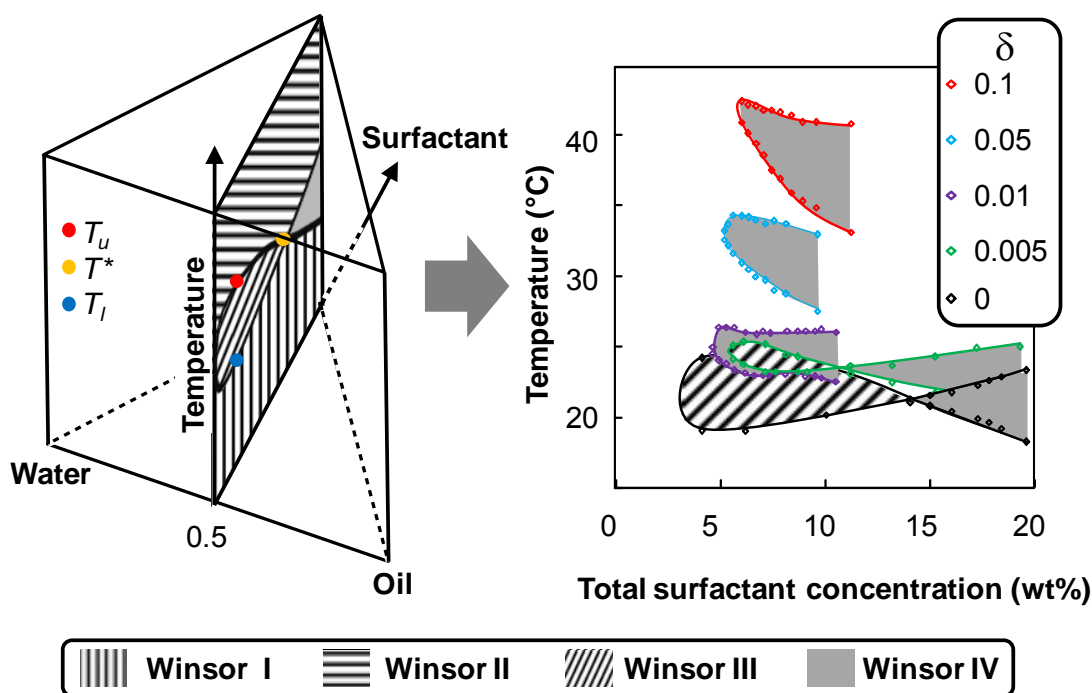


**Figure 3.10** Vertical section through the phase prism at a fixed water/oil mass ratio of 1, yielding a “Fish diagrams” of the  $H_2O/C_8E_4-[DiC_8]_2[MoO_4]/\text{cyclohexane}$  system for different  $[DiC_8]_2[MoO_4]$  mass fractions ( $\delta$ ) in the temperature-surfactant content space (only WIII and WIV are indicated for sake of clarity).

To understand the disappearance of the Winsor III and the enhance of the thermo stability of the WIV  $\mu\text{ems}$  through addition of  $[DiC_8]_2[MoO_4]$ , it is important to keep in mind that the “Fish diagram” represents only a vertical section through the phase prism at a fixed water/oil mass ratio of 1.<sup>269</sup> Therefore, to connect the binary diagram with the sectional ternary “Fish diagram”, all compositions and temperatures must be known. The upper temperature,  $T_u$  of the WIII (*i.e.* the temperature at which the WIII  $\rightarrow$  WII transition occurs for a given total surfactant concentration) is closely related to the upper critical temperature in the oil-surfactant binary diagram, while the lower temperature,  $T_l$ , (*i.e.* the temperature of the WI  $\rightarrow$  WIII transition) is associated with the low critical temperature of the water-surfactant binary diagram. Generally, the addition of ionic surfactant to the ethoxylated alcohols increased their hydrophilicity. As shown in **Figure 3.9**, addition of 1 wt%  $[DiC_8]_2[MoO_4]$  ( $\delta = 0.01$ ) enhances the critical temperature of  $C_8E_4/H_2O$  binary diagram for about 10 °C. On the other hand, the effect of ionic surfactant on the upper critical temperature of the immiscible gap of  $C_8E_4/\text{water}$  pseudo-binary diagram was not observed because it is lower than the melting point of the solvent. Efficiency of the mixed  $C_8E_4$  and  $[DiC_8]_2[MoO_4]$  could be related to the lower value of CMC compare to pure  $C_8E_4$ .

The effect of  $[DiC_8]_2[MoO_4]$  addition on the  $\mu\text{em}$  microstructure was examined by the SAXS measurement. As shown in **Figure 3.10**, the “Fish diagrams” of  $C_8E_4$  with different amount of

**[DiC<sub>8</sub>]<sub>2</sub>[MoO<sub>4</sub>]** share the single phase region at  $\gamma = 25$  wt.% and at 20°C, which allows the comparison of difference of microstructure as  $\delta$  changes while kept other variables constant. The  $\mu\text{em}$  topology were investigated in the realm of existence of WIV  $\mu\text{em}$  at a constant surfactant concentration of 25 wt.% by varying the volume fraction of water ( $\Phi_w$ ). It is noteworthy that viscous lamellar phases are formed at  $\Phi_w > 0.55$  and thus, SAXS spectra are shown here only for  $\Phi_w < 0.5$  where intensity  $I(q)$  is plotted as a function of the scattering vector  $q$  defined as  $q = 4\pi/\lambda \sin(\theta/2)$  and  $\theta$  the scattering angle (**Figure 3.11**). A typical broad scattering peak is observed in all cases for the  $\mu\text{em}$  systems. It is known for a long time that different types of  $\mu\text{ems}$  like isolated droplets, flexible random films or connected cylinders have similar scattered bell shaped patterns which can be fitted by the Teubner Strey model:<sup>336,337</sup>

$$I(q) = \frac{I}{a + bq^2 + cq^4} + I_{incoh} \quad (\text{Eq. 3.13})$$

where  $I_{incoh}$  is the incoherent scattering of the solvent and in our case  $a, b, c$  are fitting parameters related to the persistence length  $\xi$  and the water/oil domains size  $D^*$ :

$$\xi = \left[ \frac{1}{2} \times \sqrt{\frac{a}{c}} + \frac{1}{4} \times \frac{b}{c} \right]^{\frac{1}{2}} \quad (\text{Eq. 3.14})$$

$$D^* = 2\pi \left[ \frac{1}{2} \times \sqrt{\frac{a}{c}} - \frac{1}{4} \times \frac{b}{c} \right]^{\frac{1}{2}} \quad (\text{Eq. 3.15})$$

The fitting parameters by Teubner Strey model were given in **Table 3.9**. In addition, an amphiphilicity factor,  $f$ , can be defined in terms of the coefficient  $a, b, c$  as:

$$f = \frac{b}{(4ac)^{1/2}} \quad (\text{Eq. 3.16})$$

The value of  $f$  ranges from 1 for a completely disordered solution to -1 for completely ordered lamellar phase. On the other side,  $|c|$  and  $\xi/D^*$  increase with the surfactant concentration, which could explain the ubiquitous appearance of lamellar phase following the  $\mu\text{em}$ . The addition of alcohol to lamellar phase of the nonionic surfactant may stabilize or destabilize the lamellar phase depending on the chain length, while the addition of ionic surfactant generally stabilizes the lamellar phase,<sup>315</sup> which indeed could be reflected from **Table 3.8**. At the same water volume fraction, the addition of **[DiC<sub>8</sub>]<sub>2</sub>[MoO<sub>4</sub>]** caused the decrease of amphiphilicity factor ( $f$ ) values, besides, the  $|c|$  and  $\xi/D^*$  were also give higher value than pure C<sub>8</sub>E<sub>4</sub>. This indicated that the addition of **[DiC<sub>8</sub>]<sub>2</sub>[MoO<sub>4</sub>]** showed the similar effect of increase of the surfactant concentration.

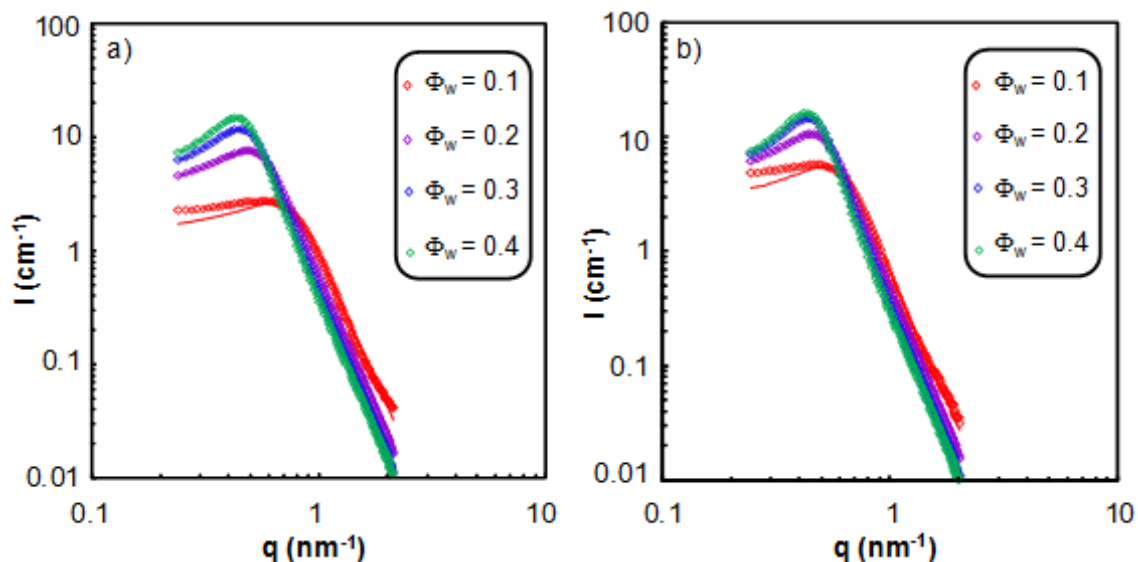


**Figure 3.11** SAXS spectra of a)  $\mu\text{ems } \text{C}_8\text{E}_4/\text{Cyclohexane}/\text{H}_2\text{O}$  and b)  $\text{C}_8\text{E}_4\text{-}[\text{DiC}_8]_2[\text{MoO}_4]/\text{Cyclohexane}/\text{H}_2\text{O}$  at  $\Phi_w = 0\text{-}0.4$  fitted by Teubner Strey model (lines).<sup>336</sup>

**Table 3.8** The fitting parameters by Teubner Strey model for water/ $\text{C}_8\text{E}_4$ /cyclohexane and water/ $\text{C}_8\text{E}_4\text{-}[\text{DiC}_8]_2\text{MoO}_4$ /cyclohexane  $\mu\text{em}$  systems.

	$\Phi_w$	$a$	$b$	$c$	$\xi/\text{nm}$	$D^*/\text{nm}$	$\xi/D^*$	$f$
<b><math>\text{C}_8\text{E}_4</math> (25 wt.%)</b>	0.1	0.48	-0.93	1.49	2.80	9.47	0.30	-0.54
	0.2	0.22	-0.92	2.16	4.34	12.18	0.36	-0.66
	0.3	0.20	-1.21	3.05	5.89	13.18	0.45	-0.77
	0.4	0.22	-1.58	4.15	7.08	13.70	0.52	-0.82
<b><math>\text{C}_8\text{E}_4\text{-}[\text{DiC}_8]_2\text{MoO}_4</math> (25 wt.%, <math>\delta = 1.1\%</math>)</b>	0.1	0.25	-0.81	1.92	3.65	11.75	0.31	-0.58
	0.2	0.20	-1.10	2.87	5.26	13.16	0.40	-0.72
	0.3	0.21	-1.56	4.16	7.33	13.84	0.53	-0.83
	0.4	0.22	-1.81	4.99	8.36	14.20	0.59	-0.86

### 3.3.3 Dark singlet oxygenation in temperature-switch $C_8E_4$ - $[DiC_8]_2[MoO_4]$ /cyclohexane/ $H_2O$ $\mu$ ems

Molybdate salts have been widely used for catalytic singlet oxygen ( $^1O_2$ ) generation from hydrogen peroxide disproportionation.<sup>25,282,316,317</sup> From the “Fish diagrams” depicted in **Figure 3.10**, the WIV  $\mu$ em could be obtained with 10 wt.% in total amphiphiles for pseudo-ternary  $C_8E_4$ - $[DiC_8]_2[MoO_4]$ /cyclohexane/ $H_2O$  system and different types of  $\mu$ ems could be controlled by only temperature. By considering the temperature range of WIV  $\mu$ em, the composition with 10wt.% total surfactant and  $\delta = 5\%$  was chosen. The different catalytic effects in different  $\mu$ ems were carried out with  $\alpha$ -terpinene as a model substrate. The reactions were conducted for comparison in the different  $\mu$ em systems at different temperature, *i.e.* 15, 28 and 40 °C which give WI, WIV and WII respectively under these conditions (**Figure 3.12**). At first, control experiments were performed with  $[DiC_8]_2[MoO_4]$  and  $[Na]_2[MoO_4]$  as catalysts in the absence of  $C_8E_4$  in order to determine precisely the influence of the cationic catalytic surfactant (Entries 1 and 2, **Table 3.9**). Both experiments take place in biphasic conditions due to the absence or the very weak amount of surfactant. As expected, no catalytic activity was obtained with  $[Na]_2[MoO_4]$  in the absence of  $C_8E_4$  (Entry 1), while the conversion of  $\alpha$ -terpinene into ascaridole was observed for  $[DiC_8]_2[MoO_4]$  but still low due to the deactivation of singlet oxygen ( $^1O_2$  lifetime in  $H_2O \approx 3 \mu s$ ) before reaching the substrate in the organic phase (Entry 2).<sup>338</sup> This better activity clearly results from the placement of the catalyst in the cyclohexane/water interfacial layer. These finding clearly shows the importance of resorting to a  $\mu$ em system with nano domains for an efficient dark singlet oxygenation process of hydrophobic substrates. Thus, in order to know the influence of WI, WIV and WII  $\mu$ em on the conversion of  $\alpha$ -terpinene and efficiency of  $H_2O_2$ , three experiments have been performed in which the total mass fraction of  $C_8E_4$  and  $[DiC_8]_2[MoO_4]$  was fixed at 10% and the  $[DiC_8]_2[MoO_4]$  mass fractions ( $\delta$ ) were fixed at 0.05.

**Table 3.9** Oxidation of  $\alpha$ -terpinene catalyzed by the  $[DiC_8]_2[MoO_4]/H_2O_2$  in thermo-sensitive  $\mu$ ems.<sup>a</sup>

Entry	$\gamma$ (%)	$\delta$	$T_r$ (°C)	Phase behavior	$\Delta t$ (min) <sup>b</sup>	Conversion (%) <sup>c</sup>	$H_2O_2$ Efficiency (%)
1 <sup>d,e</sup>	0	0	28	2 phases	15	0	0
2 <sup>e</sup>	0.5	1	28	2 phases	15	33	24.1
3	10	0.05	15	WI	40	36	27.7
4	10	0.05	28	WIV	15	100	73.3
5	10	0.05	40	WII	5	90	66.1

<sup>a</sup>  $[DiC_8]_2[MoO_4] = 0.016$  mmol,  $C_8E_4 = 0.69$  mmol,  $H_2O/cyclohexane = 1$ ,  $\alpha$ -terpinene **1** = 0.367 mmol,  $H_2O_2 = 0.102$  mmol. <sup>b</sup> Time interval between each batch of  $H_2O_2$ . <sup>c</sup> Determined by  $^1H$  NMR. <sup>d</sup>  $[Na]_2[MoO_4] = 0.016$  mmol was used as a catalyst. <sup>e</sup> Without  $C_8E_4$ .

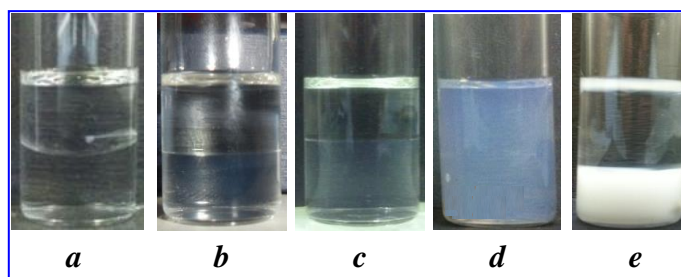


**Figure 3.12** The photos of different reaction systems: (a)-(e) correspond to the Entries 1-5, Table 3.9, respectively.

Under such conditions, temperature becomes the key parameter to obtain WI, WIV and WII  $\mu\text{em}$ . In the presence of  $\text{C}_8\text{E}_4$  at 15 °C, a WI  $\mu\text{em}$  was formed. In this case, the interface area is increased by the formation of nano-droplets of oil-in-water  $\mu\text{em}$  and, despite the low reaction temperature, the conversion is slightly improved (conversion  $\approx$  36% after 4h) compared to the biphasic system without  $\text{C}_8\text{E}_4$  (**Entry 3** vs. **Entry 2, Table 3.9**). This can be ascribed to the Winsor I type which spreads the headgroups containing catalyst outside of the droplets. In consequence, the singlet oxygen generated is easily quenched by the water molecules. The best results were obtained when the temperature was increased in the range of the WIV region of the phase diagram due to the formation of a largest W/O interface. Addition of the same amount of  $\text{H}_2\text{O}_2$  converted the substrate completely in 1.5h and the  $\text{H}_2\text{O}_2$  efficiency could reach up to 73% (**Entry 4, Table 3.9**). Interestingly, the WII type  $\mu\text{em}$ , which was formed by further increase of the temperature up to 40 °C, also gave good conversion (90% in 30 min, **Entry 5, Table 3.9**). This can be rationalized by W/O nano droplet formation in the  $\mu\text{em}$  phase which assembles the headgroups inside the micelles where  $^1\text{O}_2$  is produced; then, the excited species freely diffuse in the continuous organic phase of the  $\mu\text{em}$  where it is chemically trapped by the substrate. However, the  $\text{H}_2\text{O}_2$  efficiency is lower than in the case of a WIV  $\mu\text{em}$  (compare **Entries 4 and 5, Table 3.9**).

Finally, as a proof of concept, the scope of substrates in the temperature-switch catalytic WIV type  $\mu\text{em}$  system was extended. The temperature range giving WIV denoted as  $T_{\text{WIV}}$  was measured before the reaction and the reaction temperature,  $T_r$ , was determined to maintain the WIV  $\mu\text{em}$  during the reaction. Aqueous  $\text{H}_2\text{O}_2$  was added by batch each 20 min to optimize the kinetics of  $^1\text{O}_2$  generation by favoring the formation of the precursor of the excited species, *i.e.* the triperoxomolybdate  $\text{MoO}(\text{O}_2)_3^{2-}$ ,<sup>207</sup> until complete conversion of the substrates. All the results are summarized in **Table 3.10**. Throughout the reactions, no phase transition occurred and the WIV  $\mu\text{ems}$  were kept. At the end of the reaction, the catalytic  $\mu\text{em}$  reaction media were cooled down to 5 °C for 3h to induce a WIV $\rightarrow$ WI phase transition. Indeed, the biphasic WI  $\mu\text{em}$  has an excess oil phase which makes easier the product recovery while the  $[\text{DiC}_8]_2[\text{MoO}_4]$  and most of  $\text{C}_8\text{E}_4$  remains in the  $\mu\text{em}$  phase. For  $\alpha$ -terpinene and thioanisole, the crude products were efficiently extracted in the excess cyclohexane phase but small amounts of  $\text{C}_8\text{E}_4$  were also present (*e.g.* 6 wt% in the case of **Entry 1, Table 3.10**). However, in such cases, the crude products are easily purified using a short column chromatography on silica gel.

**Table 3.10** Peroxidation of substrates by the  $[\text{DiC}_8]_2[\text{MoO}_4]/\text{H}_2\text{O}_2$  system in a temperature-switch one-phase (WIV)  $\mu\text{em}$  based on  $\text{C}_8\text{E}_4$ .<sup>a</sup>

Entry	Substrate	$T_{\text{WIV}}$ ( $^{\circ}\text{C}$ ) <sup>b</sup>	$T_{\text{r}}$ ( $^{\circ}\text{C}$ ) <sup>c</sup>	$\text{H}_2\text{O}_2$ (mM) <sup>d</sup>	t (h) <sup>e</sup>	Product	Sel. (%)	Yield (%) <sup>f</sup>
1		25-32	28	0.5	1.5		100	91 <sup>g</sup>
2		24-28	25	1.2	2.5		100	86 <sup>g</sup>
3		25-30	28	1.7	3.3		100	89 <sup>h</sup>
4		25-30	26	8.5	17		100	84 <sup>h</sup>
5		24-30	26	12.0	23.5		100	82 <sup>h</sup>
6		25-30	26	0.70	1.5		16	67 <sup>h</sup>
							84	
7		11-21	19	2.72	9.3		55	7 <sup>g</sup>
							45	
8		23-29	25	2.72	6.6		65	66 <sup>g</sup>
							35	
9		24-30	25	2.72	6.6		65	76 <sup>g</sup>
							35	

<sup>a</sup> Conversion > 99.9%,  $[\text{DiC}_8]_2[\text{MoO}_4] = 16 \mu\text{mol}$ ,  $\text{C}_8\text{E}_4 = 0.69 \text{ mmol}$ ,  $\text{H}_2\text{O}/\text{cyclohexane} = 1$  (w/w), substrate = 0.2 mM. <sup>b</sup> Temperature range of the WIV in the presence of the substrate. <sup>c</sup> Reaction temperature. <sup>d</sup> Total amount of  $\text{H}_2\text{O}_2$ . <sup>e</sup> Reaction time. <sup>f</sup> Isolated yield. <sup>g</sup> Purified by cyclohexane extractions and by column chromatography. <sup>h</sup> Isolated yield by filtration.

In the cases of **methylphenylsulfide** (**Entry 3, Table 3.10**) to **dibenzylsulfide** (**Entry 6, Table 3.10**), the products precipitated at the end of the reaction and could thus be simply recovered by filtration or centrifugation. It is noteworthy that the oxidation of sulfides presents gave exclusively the sulfone (**Entry 3-5, Table 3.10**) except that 16% sulfoxide was obtained for dibenzyl sulfide. The catalytic  $\mu\text{em}$  system was also applied to the ene reaction, which was widely used in organic synthesis.<sup>339</sup> In contrast to the [4+2] cycloaddition which produces endoperoxides, the ene reaction gives allylic hydroperoxides which can present some amphiphilicity likely to disturb the  $\mu\text{em}$  system because of its interfacial activity. We have thus investigated terpenoids **citronellyl acetate** and **citronellyl stearate** based on  $\beta$ -citronellol but with a different hydrophobicity. In the case of  $\beta$ -citronellol (**Entry 7, Table 3.10**), the two isomer hydroperoxides are indeed prevalent in the  $\mu\text{em}$  phase (> 98%).

**Table 3.11** Octanol-water partition coefficient (log P) and polar surface area (PSA) of substrates and products and experimental ratio of products in the  $\mu\text{em}$  phase after reaction.

Entry	Substrates	log P <sup>a</sup>	%PSA <sup>a</sup>	Products (% in $\mu\text{em}$ ) <sup>b</sup>	log P <sup>a</sup>	%PSA <sup>a</sup>
1		2.23	13.6		1.71	26.3
				(98)		1.53
2		2.86	9.4		2.24	20.3
				(79)		2.06
3		10.12	4.53		9.50	11.0
				(42)		9.43
				(45)		

<sup>a</sup> Calculated with Vega ZZ after PM7/RHF optimization with MOPAC2012<sup>TM</sup>; <sup>b</sup> Determined by <sup>1</sup>H NMR analysis with naphthalene as a standard.

To get a better understanding of this effect, the octanol-water partition coefficient,  $\log P$ , and the percentage of molecular polar surface area, %PSA, were calculated for these three substrates from molecular simulation (Table 3.11). There is a clear modification of the hydrophobicity between  $\beta$ -citronellol and its products. Indeed, the hydroperoxides have lower  $\log P$  than  $\beta$ -citronellol itself. On the other hand, the percentage of molecular polar surface area, *i.e.* %PSA, confirms that  $\beta$ -citronellol has a higher hydrophobic surface than its hydroperoxides. Under such conditions, the extraction of the products from the  $\mu\text{em}$  phase is possible but tedious as several successive extractions with cyclohexane are required. The combination of alkyl part by esterification modified the hydrophilic-lipophilic balance of the products effectively. Thus,  $\log P$  for the hydroperoxides of citronellyl acetate was about 2.1 and  $\log P \approx 9.5$  for the hydroperoxides of citronellyl stearate, which led more products into the oil phase and facilitated the separation.

### 3.3.4 Conclusion

The interaction of the cationic catalytic  $[\text{DiC}_8]_2[\text{MoO}_4]$  and the nonionic  $\text{C}_8\text{E}_4$  amphiphiles was evaluated by measuring the CMCs of the pure surfactants and of their mixtures. Although the theory is based on some approximations, the interaction parameter  $\beta$  provides a credible evaluation of the strength of the interaction. The effect of small amounts of  $[\text{DiC}_8]_2[\text{MoO}_4]$  to the binary  $\text{C}_8\text{E}_4/\text{water}$  and ternary  $\text{water}/\text{C}_8\text{E}_4/\text{cyclohexane}$  is obviously due to the synergism between ionic and nonionic surfactants. Addition of only 1 wt% of  $[\text{DiC}_8]_2[\text{MoO}_4]$  in  $\text{C}_8\text{E}_4$  caused the increment of the cloud point by almost 10 °C and the disappearance of the WIII region in the ternary  $\text{water}/\text{C}_8\text{E}_4/\text{cyclohexane}$  “Fish diagram”. This strong synergism was also reflected by the results of the DLS analysis of mixed micelles with different ratio of the cationic surfactants. The insertion of small amounts of the  $[\text{DiC}_8]_2[\text{MoO}_4]$  dramatically changes the hydration of the  $\text{C}_8\text{E}_4$  head group and results in the diminution of the micelle radius. For the pseudo-ternary  $\text{C}_8\text{E}_4\text{-}[\text{DiC}_8]_2[\text{MoO}_4]/\text{cyclohexane}/\text{water}$  system, the increase of  $[\text{DiC}_8]_2[\text{MoO}_4]$  not only enhances the stability of the one-phase  $\mu\text{em}$  but also enlarges the range of the WIV region. This can be interpreted by the interaction of both surfactants that form the interfacial film of the  $\mu\text{em}$ . Finally, the WIV  $\mu\text{em}$  system based on  $\text{C}_8\text{E}_4$  and  $[\text{DiC}_8]_2[\text{MoO}_4]$  was applied in the singlet oxygenation of several substrates with  $[\text{DiC}_8]_2[\text{MoO}_4]$  as a catalyst. The presence of the thermo-sensitive  $\text{C}_8\text{E}_4$  amphiphile allows transitions between the Winsor type systems by temperature change. The reaction takes place in the very efficient WIV system which presents the largest interfacial area of the Winsor systems but which does not allow an easy separation of products and catalyst. However, at the end of the reaction, a simple cooling down of the reaction medium allows the formation of two distinct phases (*i.e.* Winsor I  $\mu\text{em}$  with an excess oil phase). Due to the current interest in new catalytic processes, further developments of such temperature-switch catalytic  $\mu\text{ems}$  taking advantage of the synergy between thermo-sensitive nonionic and catalytic amphiphiles are expected for other catalytic processes in which the incompatibility between hydrophilic and hydrophobic reactants has to be overcome.



### 3.4 Photochemical and chemical singlet oxygenation of valencene: (+)-Nootkatone

(+)-Nootkatone (Figure 3.13a), a sesquiterpene firstly isolated from the heartwood of Alaskan yellow cedar and also present in citrus species,<sup>340,341</sup> is a sought after molecule widely used in flavor and cosmetic fields thanks to its unique grapefruit odor and low perception threshold.<sup>342</sup> Besides, recent research also revealed the impressive repellent and toxic activity making it an interesting additive in insecticides against various insects, like termites, ticks *etc.*<sup>343,344</sup> The trace amount of (+)-Nootkatone in plant sources results in the high price of this flavor which is extracted from natural plants and in an industrial demand which cannot be met.

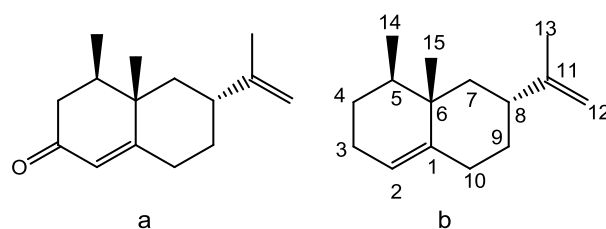


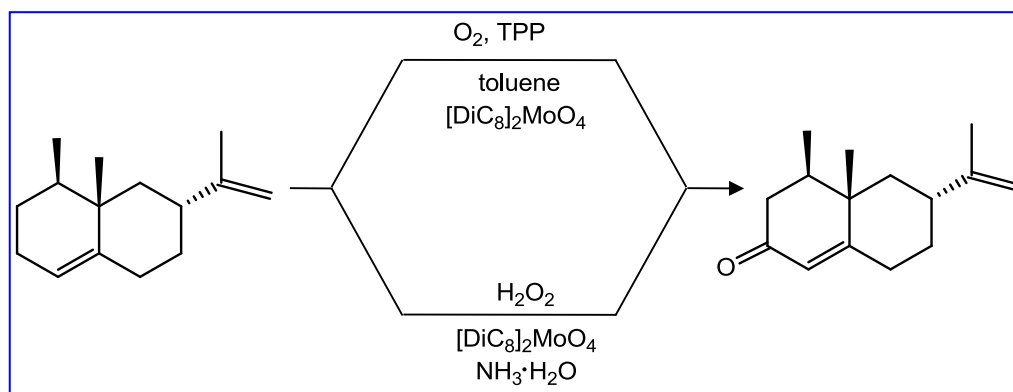
**Figure 3.13** Chemical structures of (a) (+)-Nootkatone, (b) (+)-Valencene.

Accordingly, several chemical synthetic approaches have been developed since the exact structure is known. However, the early synthetic strategies *via* the Robinson annulation with cyclohexanone derivatives,<sup>345-349</sup> Diels-Alder reaction between the cyclohexa-1,4-diene derivatives and appropriate dienophiles,<sup>350,351</sup> cyclopentenone annulation & ring enlargement,<sup>352</sup> intermolecular Sakurai reaction<sup>353</sup> and more recently the Diels-Alder/Aldol tandem reaction<sup>354</sup> suffer from a poor control of the configuration of the methyl groups at the C<sub>5</sub> and C<sub>6</sub> positions as well as the isopropyl group at C<sub>8</sub> position, which generally provide the racemic (±)-Nootkatone. Different from (+)-Nootkatone, (–)-Nootkatone shows a spicy and woody flavor making it less useful.<sup>342</sup> The synthesis of enantiopure (+)-Nootkatone was firstly reported by Yoshikoshi's group from (–)-β-Pinene in 11~14% overall yield *via* the acid catalyzed cyclobutane cleavage-Aldol cyclization tandem reaction as a key step<sup>355,356</sup> and was improved by Laine *et al.* *via* the stereoselective Grignard/anionic oxy-Cope reaction giving an overall yield up to 33%.<sup>357,358</sup> However, the lengthy reaction procedure, the toxic solvent used, the strict reaction conditions, the tedious work-up and the low overall yield make the total synthesis of (+)-Nootkatone not the best choice from an economic and ecological point of view.

Alternatively, (+)-Nootkatone can also be prepared by the allylic oxidation of the parent hydrocarbon, (+)-Valencene (Figure 3.13b), which is easily obtained from Valencia orange and successfully fermented with biotechnology by Allylix and Isobionics.<sup>359</sup> The oxidation of (+)-Valencene with the carcinogenic *tert*-butyl chromate or sodium dichromate was reported by Hunter *et al.*<sup>360</sup> and Shaffer *et al.*<sup>361</sup> *tert*-Butyl peracetate was also used for allylic oxidation of Valencene but the chromic acid was required for the oxidation of intermediate nootkatol.<sup>362</sup> One pot catalytic conversion of (+)-Valencene to (+)-Nootkatone

was realized with *tert*-butyl hydroperoxide in combination with silica-supported  $\text{Co}(\text{OAc})_2$ ,  $\text{Cu}(\text{OAc})_2$  or  $\text{V}(\text{OAc})_2$  catalyst.<sup>363</sup> Nevertheless, the explosive, corrosive and toxic properties of the catalysts above mentioned leads to the urgent requirement of more green and effective methods for preparing (+)-**Nootkatone** from (+)-**Valencene**. On the other side, various biocatalysts, such as *G. pentaphyllum* cultures,<sup>364</sup> green algae *Chlorella species* and fungi *Bothryosphaeria dothidea*,<sup>365</sup> the lyophilisate of edible mushroom *Pleurotus sapidus*,<sup>366-368</sup> and several bacterial cytochrome P450 enzymes<sup>369-371</sup> were also studied for this conversion.<sup>372</sup> However, the costly culture conditions, the low conversion rate and yield, the inhibition of enzymes by products, the presence of various byproducts *etc.* still hamper the industrial preparation of (+)-**Nootkatone** *via* biocatalysts.

Hence, we report herein two novel green routes to synthesize (+)-**Nootkatone** from (+)-**Valencene**. Both methods involve singlet oxygen ( $^1\text{O}_2$ ,  $^1\Delta_g$ ) as the oxidizing agent and molybdate ions as catalysts but one is based on photooxidation and the other one is the dark singlet oxygenation (**Scheme 3.1**).

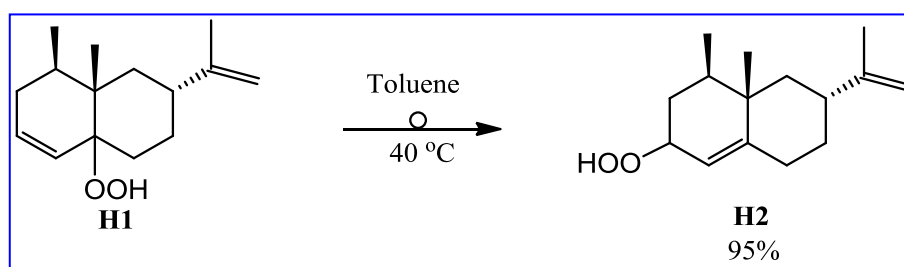


**Scheme 3.1** The photochemical and chemical processes of oxidation conversion from (+)-Valencene to (+)-Nootkatone (TPP: 5, 10, 15, 20-tetraphenyl-21H, 23H-porphine).

Although the oxidation of (+)-**Valencene** by  $^1\text{O}_2$  has already been reported,<sup>361,373</sup> the molybdate catalyzed (+)-**Nootkatone** formation *via* one pot tandem reactions, *i.e.*  $^1\text{O}_2$  generation, ene reaction, Schenck rearrangement, and catalytic conversion of hydrogen peroxide into ketone has never been described before. For the photochemical process, the solvent was crucial for the Schenck rearrangement due to the different stability of the intermediates in different solvents and the ready formed hydroperoxide species converted to the desired (+)-**Nootkatone** catalyzed by molybdate ions. To adjust the solubility of the ionic catalyst in the investigated solvent, the catalytic surfactant  $[\text{DiC}_8]_2[\text{MoO}_4]$  was used instead of the common sodium molybdate. As far as the chemical process is concerned,  $[\text{DiC}_8]_2[\text{MoO}_4]$  was also used for two main reasons: 1) it catalyzes efficiently the disproportionation of hydrogen peroxide, a green and safe oxidant, into  $^1\text{O}_2$ <sup>20,28,29,282</sup> and 2) it has been shown to behave as a "balanced catalytic surfactant" providing three-liquid-phase  $\mu\text{em}$  systems in the presence of water and solvent at room temperature. Indeed, in this case, the reaction proceeded in the absence of organic solvent and the double chain of ammonium counter ion overcame the immiscibility between the substrates and aqueous  $\text{H}_2\text{O}_2$ . At the end



solvent, hydroperoxide **H1** was stable and almost no rearrangement product was obtained after one month, while, in toluene, the rearrangement could reach up to 95% to **H2** in two days at room temperature and only 5h was required under 40 °C (**Scheme 3.3**). Several other solvents were also investigated at room temperature, such as chloroform, acetonitrile, and acetone. The conversions of **H2** in the different solvents after 48h are given in **Table 3.12**. The Schenck rearrangement is reversible and the equilibrium between **H1** and **H2** depends on the energy difference of these two hydroperoxides. However, the kinetics of the reaction is greatly affected by the solvent.<sup>376,380</sup> As shown in **Table 3.12**, toluene gave the highest rearrangement rate, while as viscosity of the solvent decreases, the conversion in hydroperoxide **H2** also slowed down, which could be ascribed to the “solvent cage around intermediate radical” by the high viscous solvent molecule. And this solvent cage prevents the inter-molecule interaction, *e.g.* hydrogen bond, and facilitates the intra-molecule rearrangement. As previously reported, the hydroperoxide dimer combined by hydrogen bond showed much lower activity than free hydroperoxide.<sup>381,382</sup> The high stability of hydroperoxide **H1** in methanol can also be explained by the hydrogen bond formation between the solvent and hydroperoxide molecule.



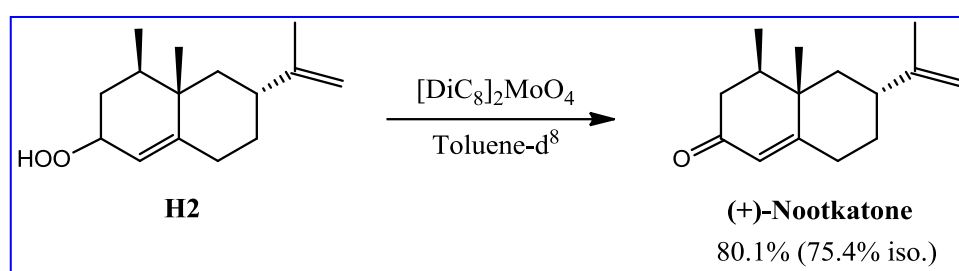
**Scheme 3.3** The rearrangement of hydroperoxide **H1** to **H2** in toluene.

**Table 3.12** The hydroperoxides **H1** and **H2** ratio after of **H1** in various solvents for 48h at room temperature<sup>a</sup>

Solvents	Viscosity $\eta$ /cP	<b>H1</b> : <b>H2</b>
<b>MeOH</b>	0.59	> 99:1
<b>Acetone</b>	0.32	45:55
<b>Acetonitrile</b>	0.37	23:77
<b>CDCl<sub>3</sub></b>	0.56	6:94
<b>Toluene</b>	0.59	5:95

<sup>a</sup> Conditions: the hydroperoxide **H1** was prepared by photooxidation of (+)-Valencene in MeOH with about 17% hydroperoxide **H1** inside. MeOH was then evaporated and other types of solvents were added to dissolve the residue directly and the ratio of hydroperoxides **H1**:**H2** was detected by <sup>1</sup>H NMR.

The dehydration of allylic hydroperoxide to corresponding enone catalysed by the Lewis acids, such as  $\text{Cu}^{2+}$ ,  $\text{Co}^{2+}$ ,  $\text{Mn}^{2+}$ ,  $\text{Zr}^{4+}$  etc. was previously reported and the coordination of the metal with the peroxide was considered to weaken the O-O bond and facilitates the dehydration.<sup>383-385</sup> During our studies on molybdate catalytic reactions, the catalytic dehydration of hydroperoxide was found also catalyzed by  $[\text{DiC}_8]_2\text{MoO}_4$ , which was firstly reported (Scheme 3.4). The reaction was carried out in toluene- $\text{d}^8$  solution, in which the hydroperoxide **H1** was transformed to hydroperoxide **H2** and the following dehydration to (+)-Nootkatone in the presence of  $[\text{DiC}_8]_2\text{MoO}_4$  was detected directly by  $^1\text{H}$  NMR. As shown in Figure 3.15, the reaction rate with 0.2 equiv. molybdate was much slower than with stoichiometric molybdate at room temperature, which the reaction rate could be dramatically increased at 50 °C.



**Scheme 3.4** The  $[\text{DiC}_8]_2\text{MoO}_4$  catalyzed dehydration of hydroperoxide **H2** into (+)-Nootkatone.

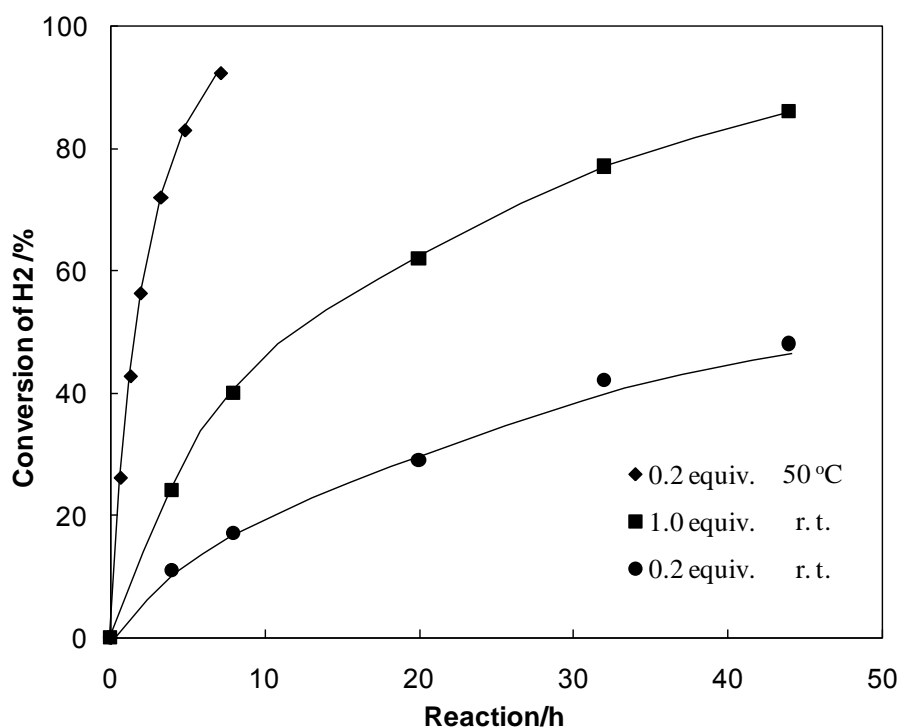


**Figure 3.15** The dehydration of hydroperoxide **H2** catalyzed by different amount of  $[\text{DiC}_8]_2\text{MoO}_4$ .

The possible catalytic cycle was also proposed in Figure 3.16. The coordination of hydroperoxide to the molybdate anion and the proton transfer generates the active species **B**. The  $\alpha$ -hydrogen of alkylperoxy ligand is subtracted *via* a six-membered transition state by the oxygen anion of molybdate, which affords

the acetone product and the molybdate is regenerated by dehydration of intermediate species **C**. Similar six-membered ring transition state was also proposed in the tungstate catalyzed alcohol oxidation by  $\text{H}_2\text{O}_2$ .<sup>386</sup> The  $\alpha$ -hydrogen elimination of alkylperoxy ligand was considered as the rate-determined step, which was also supported by the experiment. The yellow solution obtained after the addition of  $[\text{DiC}_8]_2\text{MoO}_4$  in the hydroperoxide **H2** toluene- $d^8$  solution indicated the complex formation. On the other side, the complex formation could also be referred from the  $^1\text{H}$  NMR analysis, where  $\alpha$  and adjacent alkene protons of alkyl hydroperoxide group moved to the low field after addition of  $[\text{DiC}_8]_2\text{MoO}_4$ . Although the complex was readily formed, depending on the analysis of NMR, (+)-**Nootkatone** was not rapidly generated.

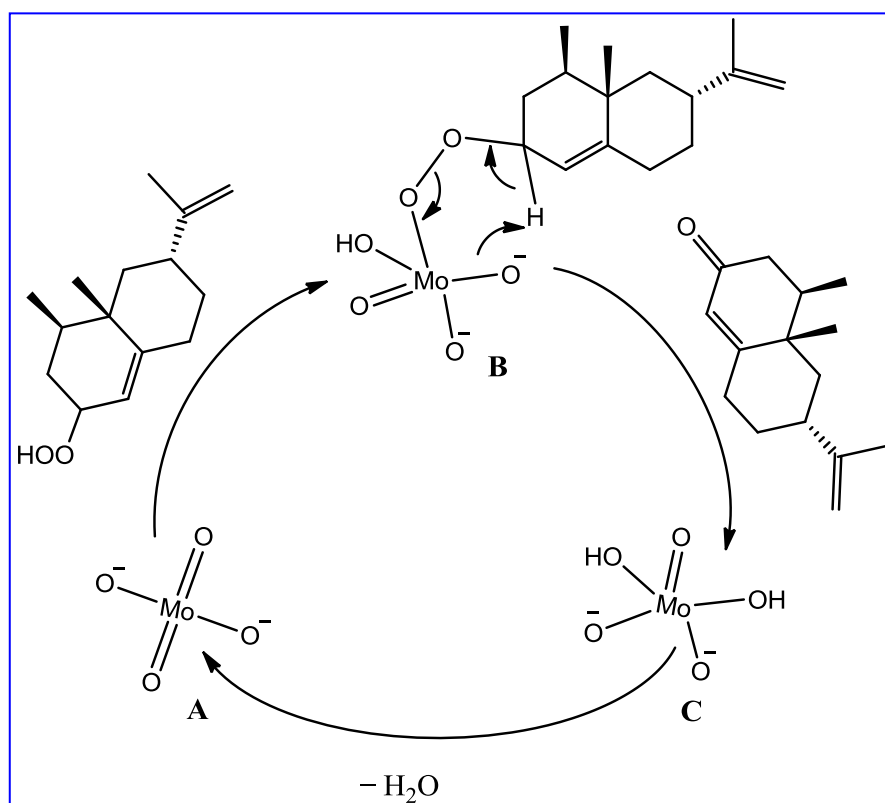


**Figure 3.16** The possible catalytic cycle of  $[\text{DiC}_8]_2\text{MoO}_4$  catalyzed dehydration of hydroperoxide **H2**.

Based on the studies of the above mentioned reactions, the one-pot, and three-step conversion of (+)-**Valencene** to (+)-**Nootkatone** was carried out in toluene- $d^8$  solution in the presence of 0.2 equiv.  $[\text{DiC}_8]_2\text{MoO}_4$ . Considering the low solubility of Rose Bengal in toluene, another photosensitizer 5, 10, 15, 20-tetraphenyl-21H, 23H-porphine (**TPP**) was used. The ene reaction between  $^1\text{O}_2$  and (+)-**Valencene** proceeded at room temperature and the conversion was complete in 18 h, and then kept the solution under  $50\text{ }^\circ\text{C}$  for 4 h to complete the rearrangement and the dehydration steps. The solvent was removed and the pure product could be isolated by chromatograph on silica gel afforded 35% isolated yield.

### 3.4.2 Dark singlet oxygenation of (+)-Valencene with a catalytic surfactant based on molybdate

Besides the photochemical process to generate  $^1\text{O}_2$  with various photosensitizer, the dark  $^1\text{O}_2$  generation from the catalytic dismutation of  $\text{H}_2\text{O}_2$  by various mineral compounds, especially the molybdate, was also widely used in the organic synthesis.<sup>20,21,28,29,207,282</sup> On the other side, the “green chemistry”, which is research focus these years, required the eco-friendly process, the easy work up process and high efficiency of atomic economy.<sup>1</sup> Various green reaction mediums were developed to increase the reaction efficiency, selectivity and facilitate the separation and recycling, such as ionic liquid, supercritical  $\text{CO}_2$ , *etc.*<sup>3</sup> However, compared with water, the high price or complicated preparing processes make them not of the choice. In the last two decades, the reaction in aqueous solution received great attention and several different kinds of reactions could be carried out in water with amphiphilic catalysts.<sup>38,387</sup> Recently, the oxidation reactions in  $\mu\text{em}$ s based on the amphiphilic molybdate or tungstate were reported by our group.<sup>29,388</sup> The advantages of the catalytic  $\mu\text{em}$  medium are obvious, including: 1) the overcoming of the immiscibility of organic substrate and water, 2) the high efficiency with large interface area, 3) selectivity improvement, *etc.* Here the (+)-**Valencene** oxygenation to (+)-**Nootkatone** was also tested without additional organic solvent with  $\text{H}_2\text{O}_2$  as a  $^1\text{O}_2$  source and  $[\text{DiC}_8]_2\text{MoO}_4$  as a catalyst. Thus a “green” one pot, and three-step process of oxidation of (+)-**Valencene** to (+)-**Nootkatone** was proposed.

The reaction was carried out in a normal reaction tube without special equipment compared with the photochemical process. (+)-**Valencene** and  $[\text{DiC}_8]_2\text{MoO}_4$  were mixed and the  $\text{H}_2\text{O}_2$  was added stepwise and to keep the reaction mixture weak basic, several drops of  $\text{NH}_3\cdot\text{H}_2\text{O}$  was added, as the most active peroxomolybdate affording  $^1\text{O}_2$  was  $[\text{MoO}(\text{O}_2)_3]^{2-}$  at weak basic condition.<sup>209</sup> The addition of  $\text{H}_2\text{O}_2$  could be controlled by the color of the reaction mixture as the red color was presented by the peroxomolybdate at the beginning and faded to pale yellow when the  $\text{H}_2\text{O}_2$  was consumed (**Figure 3.17a**). When the conversion of (+)-**Valencene** was complete, the mixture was incubated at 50 °C for 5 h to confirmed the complete formation of nootkatone. For the final separation of product and catalyst, the three-phase  $\mu\text{em}$  extraction was an alternative than conventional methods. According the “Fish diagram” of  $[\text{DiC}_8]_2\text{MoO}_4$  by screening of solvent polarity<sup>374</sup> and the EACN (Equivalent alkane carbon number) of widely used green solvent, such as ether, ester, *etc.*,<sup>248</sup> toluene, diethyl ether, *tert*-BuOAc, dibutyl ether were tested to elaborate the three-phase  $\mu\text{em}$  with the reaction mixture. Among them, only diethyl ether gave three-phase  $\mu\text{em}$  (**Figure 3.17b**), as toluene, *tert*-BuOAc gave W/O (Winsor II)  $\mu\text{em}$ , while dibutyl ether afforded O/W (Winsor I)  $\mu\text{em}$ . The final pure product could be obtained by removing the solvent and purified by chromatograph on silica gel afforded 38.9% isolated yield. The rest  $\mu\text{em}$  part could be separated and the  $[\text{DiC}_8]_2\text{MoO}_4$  could be recycled just by removing the solvent and applied in the next run reaction without lost of activity.

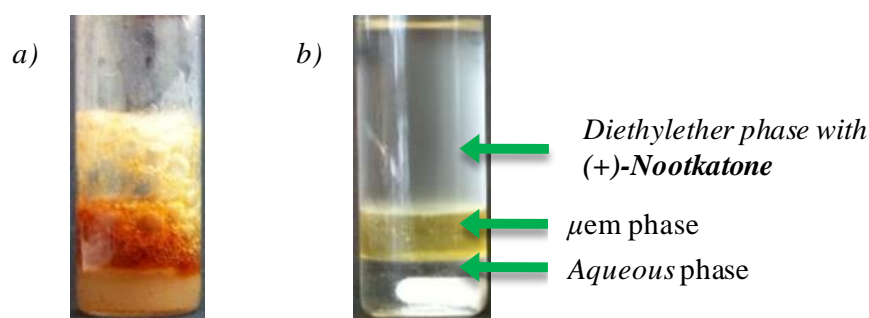


**Figure 3.17** The dark  $^1\text{O}_2$  oxygenation of (+)-Valencene: a) during the reaction after addition of  $\text{H}_2\text{O}_2$ ; b) After the addition of diethyl ether at the end of the reaction.

The surfactant part of amphiphilic molybdate catalyst played an indispensable role during the reaction. At the ene reaction step,  $[\text{DiC}_8]_2\text{MoO}_4$  overcame the immiscibility of hydrophobic substrate and water; furthermore, the  $\text{H}_2\text{O}_2$  efficiency was increased as the  $^1\text{O}_2$  generated in the nanoscale droplets could reach the substrate before deactivation by water.<sup>25</sup> The oxygenation products was expected in the micelle hydrophobic cores when all the  $\text{H}_2\text{O}_2$  was added to complete the (+)-Valencene conversion, which was crucial for the Schenck rearrangement from hydroperoxide **H1** to hydroperoxide **H2**; as discussed in the photochemical process, the high viscosity of solvent results in the equilibrium towards hydroperoxides **H2** and the protic solvents almost inhibit the reaction due to the hydrogen bond formation. Finally, the  $[\text{DiC}_8]_2\text{MoO}_4$  catalyzed dehydration of hydroperoxide **H2** afforded the (+)-Nootkatone.

### 3.4.3 Conclusion

Two different processes of (+)-Valencene oxygenation to (+)-Nootkatone were developed and the  $[\text{DiC}_8]_2\text{MoO}_4$  catalyzed dehydration of hydroperoxide to ketone was firstly reported. During the process of photooxygenation, although the ene reaction was independent on the solvents, the Schenck rearrangement of **H1** to **H2** was closely related with the viscosity of solvent, which was probably ascribed to the “solvent cage around intermediate radical” by the high viscous solvent molecule. On the other side, the protic solvents like MeOH could stabilize the hydroperoxide by hydrogen bond, which inhibits the rearrangement absolutely. Compared with the photooxygenation process, the dark singlet oxygenation of valencene avoided the use of organic solvent during the reaction. Both of the double octyl chains and molybdate were indispensable. Molybdate was required to catalyze the disproportionation of  $\text{H}_2\text{O}_2$  to generate  $^1\text{O}_2$  for the ene reaction and the dehydration of hydroperoxide to ketone; while, the hydrophobic droplets stabilized by the octyl chain was crucial for the rearrangement of **H1** to **H2**, not only overcame the immiscible problem between hydrophobic substrates and water, but also increased the efficiency of  $^1\text{O}_2$  as the molybdate ions were located on the surface.



### 3.5 Hydroformylation of hydrophobic terminal alkenes in three-phase microemulsion

The hydroformylation, discovered in 1938<sup>389</sup> and widely applied since 1984 (Ruhchemie/Rhône-Poulenc (RCH/RP) process),<sup>390</sup> is one of the most important industrial catalytic homogenous reactions. In this process, the catalytic rhodium complex is immobilized by the water-soluble sodium triphenylphosphine-3, 3', 3''-trisulphonate (TPPTS) (Figure 3.18) ligand in aqueous phase. As the olefin substrate and the aldehyde products form the oil phase, the catalyst could be easily recovered just by phase separation. The RCH/RP process was considered as “green” reaction as the unique solvent involved is water. Moreover, the easy separation and the catalyst recycling are also attractive in the context of “green chemistry”. However, only propene and 1-butene are sufficiently soluble in the aqueous phase (*i.e.* catalytic phase). Indeed, for the higher olefins, the mass-transfer is the rate-determining step of the hydroformylation process. In such condition, this kind of process is acceptable from an economic point of view.

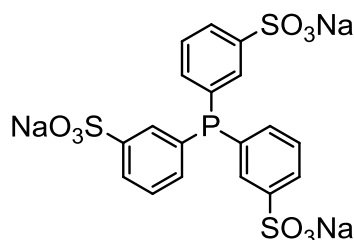


**Figure 3.18** The chemical structure of TPPTS.

Several approaches have been developed to improve the solubility of hydrophobic substrate in the aqueous phase, such as the addition of co-solvents or the use of inverse phase transfer catalysis.<sup>391</sup> The co-solvents, *e.g.* methanol, ethanol, acetonitrile, or polyethylene glycol increase significantly the concentration of hydrophobic olefin in aqueous phase and accelerate the reaction rate. However, the linear aldehyde selectivity decreases and the catalyst leaching in the organic phase could not be avoided.<sup>392,393</sup> Native cyclodextrins (CDs) (Figure 3.19a) and its derivatives, have been used to improve the hydroformylation of hydrophobic olefins via inverse phase transfer catalysis.<sup>394,395</sup> Indeed, CDs are able to form inclusion complexes with various organic substrates due to their hydrophobic cavity. The presence of  $\beta$ -CDs improved the reaction rate only in 2 times but accompanied with the decrease of linear aldehyde selectivity in the 1-decene hydroformylation with TPPTS as ligand.<sup>396</sup> This behavior is due to the formation of inclusion complex the phenyl rings and the CD cavity. In contrast, the sulphonated xantphos (Figure 3.19b) ligands in the presence of the hydrophobic group modified  $\alpha$ - or  $\beta$ -CDs improved the reaction rate and selectivity due to the steric hinderance of the ligands while the CDs increase the mass transfer.<sup>397</sup>

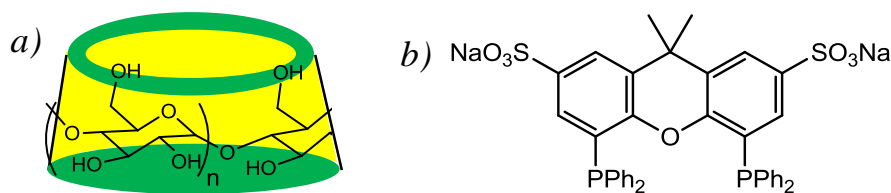


**Figure 3.19** a) Structures of cyclodextrins ( $n = 6, 7, 8$  for  $\alpha, \beta, \gamma$ -cyclodextrin, respectively); b) sulphonated xantphos.

The preparation of amphiphilic phosphine ligands also received great attention.<sup>391,398-401</sup> The formation of nano-droplets and the large interface area overcome the immiscibility between the hydrophobic olefins and the aqueous catalytic phase. Accordingly the reaction rate is greatly accelerated. As high linear aldehyde selectivity was obtained with sulphonated Xantphos for the hydroformylation of propene,<sup>402</sup> the amphiphilic homologues (**Figure 3.20a**) was prepared by Goedheijt *et al.* and applied to the hydroformylation of 1-octene, 1-decene *etc.* The authors reported excellent selectivity but the catalytic activity was very low (TOF = 12 mol aldehyde/(mol Rh·h)).<sup>400</sup> In 2012, Monflier *et al.* reported the synthesis of a amphiphilic ligand, sodium 4'-(diphenylphosphino)-[1,1'-biphenyl]-4-sulphonate (**DPPBS**) (**Figure 3.20b**). The combination of this ligand with modified  $\beta$ -CDs resulted in a competitive process and afforded good activities and selectivities.<sup>401</sup> However, the numerous steps involved in the preparation of amphiphilic ligand limit the generalization of this process. As an alternative, the simple addition of surfactant in the reaction medium is a good choice. The nano-droplets containing olefins in aqueous phase could be formed with different types of surfactants, including anionic, neutral and cationic surfactants, which can increase the mass transfer of substrates in aqueous phase. However, only cationic surfactant gives dramatic reaction rate enhancement due to the electrostatic interaction between the micellar surface and ligand molecules.<sup>403</sup> Indeed, in the hydroformylation of higher olefins in a three-phase microemulsion based on the nonionic surfactant with sulphonated xantphos as ligand reported by Schomäcker, *et al.*, low reaction rate was obtained due to the weak interaction between ligand and surfactant, furthermore, the loss of surfactant in oil phase was also significant, which resulted in the dramatic decrease of reactivity and selectivity of the recycled reaction.<sup>404</sup> In contrast, the reaction rate could be obviously accelerated by various cationic surfactants in the hydroformylation of hydrophobic olefins (**Figure 3.21**). As example, with didodecyldimethyl ammonium bromide, the TOF under stirring could reach up to 7 472 h<sup>-1</sup>. The recycled experiments also showed gradually decrease of hydroformylation activity and byproducts increased dramatically, which was possible ascribed to the surfactant loss in product and the oxidation of Rh.<sup>405</sup> Beside, the effect of cationic surfactants on the selectivity was negligible.<sup>405-408</sup>

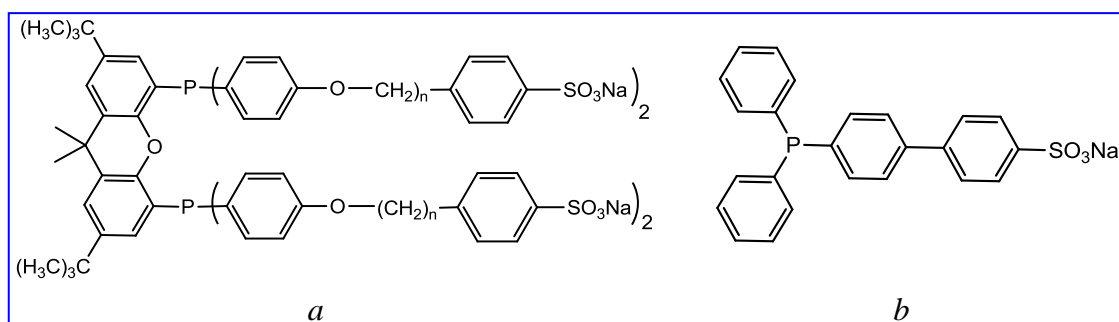


**Figure 3.20** Typical amphiphilic phosphine used as ligands in hydroformylation reaction<sup>400, 401</sup>

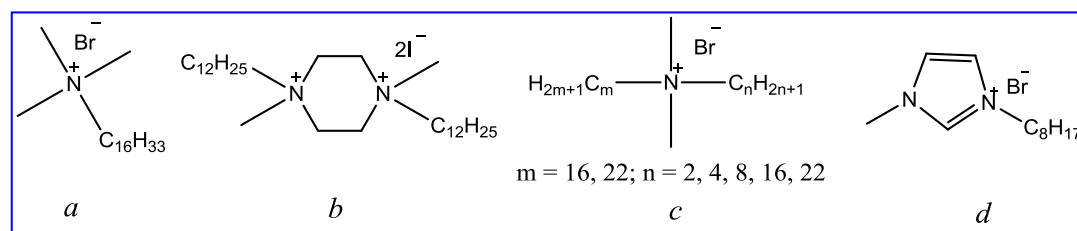


**Figure 3.21** Selected cationic surfactants applied in the hydroformylation of high olefins<sup>405-408</sup>

In the present work, an elegant three-phase  $\mu\text{em}$  (Winsor III) for the hydroformylation of hydrophobic olefins was prepared according to the “Fish diagrams” of short chain dialkyldimethylammonium salts presented in Chapter 2. The hydroformylation of hydrophobic olefins in Winsor III  $\mu\text{em}$  has been investigated with the readily available phosphine ligands in the laboratory **TPPTS** and **DPPBS** as ligand. Although Winsor III  $\mu\text{em}$  system for hydroformylation has been reported by Schomäcker *et al.* with nonionic surfactants, the most of the hydrophilic catalytic complexes stay in the aqueous phase due to the of specific interaction between the nonionic surfactant and sulphonated residues. As results, the catalytic activity is much lower than homogeneous media. On the other hand, the partition of nonionic surfactant between organic and aqueous phase leads to a loss of the reactivity after each recycling run.<sup>391,404</sup> According to the Winsor III  $\mu\text{em}$  bodies and PACNs (Preferred Alkane Chain Number) of **[DiC<sub>n</sub>]Br** and **[DiC<sub>n</sub>]Cl** ( $n = 6, 8, 10$ ) surfactants, the **[DiC<sub>8</sub>]Br** was preferred to elaborate the  $\mu\text{ems}$  as its three-phase body covered the EACN of various common used nontoxic solvents, including diethyl ether, dibutylether, and cyclohexane, *etc.* Before the catalytic reaction, the effect of **TPPTS** and **DPPBS** on “Fish diagrams” of **[DiC<sub>8</sub>]Br** was evaluated and the results were shown in **Figure 3.22**. The method to construct the “Fish diagram” has been described previously in chapter 2. As depicted in **Figure 3.22**, in the presence of **TPPTS** or **DPPBS** (5 mg), the shape of the Winsor III  $\mu\text{em}$  in the “Fish diagram” is enlarged in great extent towards the more hydrophobic oils. We can assume that the ion metathesis between the bromides and the hydrophobic sulphonates occurs and due to this combination, the Winsor III body is enlarged.<sup>409</sup> As the mass of phosphine ligand in  $\mu\text{em}$  was constant, the fraction decreased after the gradual addition of **[DiC<sub>8</sub>]Br** and  $\mu\text{em}$  phase behavior approached to pure **[DiC<sub>8</sub>]Br**. Indeed, the boundary of Winsor IV  $\mu\text{em}$  region in the presence of phosphine ligand almost overlapped with the boundary of pure **[DiC<sub>8</sub>]Br**.

Compared with the  $\mu\text{em}$  elaborated by nonionic surfactant, the cationic surfactant was almost insensitive to the temperature and the solubility in organic phase was much lower than nonionic surfactant.

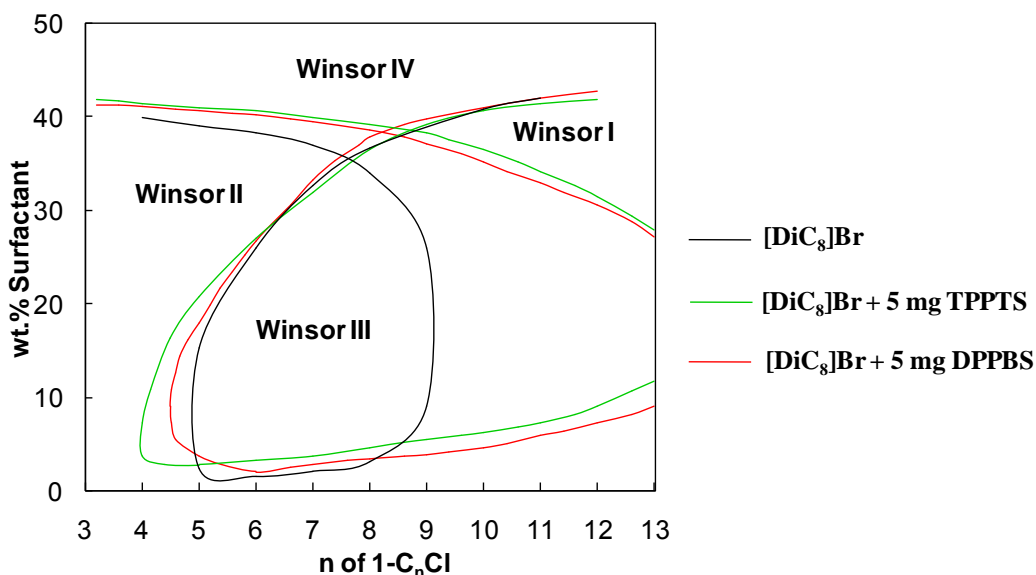


**Figure 3.22** The Fish diagrams of  $[\text{DiC}_8]\text{Br}$  in the absence and presence of TPPTS or DPPBS.

As the EACNs of cyclohexane and *n*-butyl ether were close to the optimal oils of  $[\text{DiC}_8]\text{Br}$  in the presence of phosphine ligands (**Figure 3.22**), the partition of  $[\text{DiC}_8]\text{Br}$  and DPPBS in the Winsor III  $\mu\text{ems}$  with cyclohexane or *n*-butyl ether was determined by  $^1\text{H}$  NMR analyses. The Winsor III systems were prepared under the condition in **Table 3.13**. The organic phase was separated and the amount of  $[\text{DiC}_8]\text{Br}$  and DPPBS were determined with MeOD as solvent and DMSO as standard after removing the solvent. The components in aqueous phase could be analyzed directly as the  $\text{D}_2\text{O}$  was used instead of  $\text{H}_2\text{O}$ . The fractions of  $[\text{DiC}_8]\text{Br}$  and DPPBS in organic phase and aqueous phase before the addition of Rh catalyst precursor were given in **Table 3.13**. It was found that  $> 99$  mol% of DPPBS stayed in the middle  $\mu\text{em}$  phase after combined with dioctyldimethyl ammonium cation and 0.67 mol% was dissolved in oil phase, which was higher than 0.1 mol% for  $[\text{DiC}_8]\text{Br}$  due to its higher hydrophobicity.

**Table 3.13** The more fraction of  $[\text{DiC}_8]\text{Br}$  and DPPBS in oil and aqueous phases of Winsor III  $\mu\text{em}$  with cyclohexane or *n*-butyl ether as solvent.<sup>a</sup>

Ligand	Solvent	$[\text{DiC}_8]\text{Br}$		DPPBS	
		Oil phase (%)	$\text{D}_2\text{O}$ phase (%)	Oil phase (%)	$\text{D}_2\text{O}$ phase (%)
1	Cyclohexane	0.1	1.1	0.67	0
DPPBS					
2	<i>n</i> -Butyl ether	0.2	0.87	1.62	0

<sup>a</sup> The component of three-phase  $\mu\text{em}$ :  $[\text{DiC}_8]\text{Br} = 100.0$  mg,  $\text{D}_2\text{O} = 500.0$  mg, Organic solvent = 500.0 mg, DPPBS = 10.0 mg.

Then this three-phase  $\mu\text{em}$  system was applied in catalytic hydroformylation of hydrophobic olefins with  $\text{Rh}(\text{CO})_2(\text{acac})$  as catalyst precursor. 1-decene was chosen as model substrate for optimizing the reaction condition. The catalytic three-phase  $\mu\text{em}$  system was prepared in a Schlenk flask under the  $\text{N}_2$  atmosphere. (**Figure 3.23a**). Then the mixture was transferred into the autoclave (**Figure 3.23b**) and filled with syngas ( $\text{CO}/\text{H}_2$ ) of 50 bar at  $80\text{ }^\circ\text{C}$ . The reaction solution was stirring for 2h under this pressure of syngas and 4 bar of pressure was consumed by the hydroformylation at the end of reaction. Finally the autoclave was cooled to r. t., depressurized and organic phase was separated for the GC analysis after the three-phase  $\mu\text{em}$  was recovered (**Figure 3.23c**). Finally, 97.7% conversion was obtained with aldehyde selectivity up to 99.3% ( $1/b = 3.0$ ) (**Table 3.14, Entry 1**). The effect of  $\mu\text{em}$  types played an important role during the reaction, for example, when  $[\text{DiC}_6]\text{Br}$  was used instead of  $[\text{DiC}_8]\text{Br}$ , Winsor I  $\mu\text{em}$  was obtained and under the same condition, only 7.6% conversion was obtained after 2h although the selectivity was improved (**Table 3.14, Entry 2**). On the other side, the Winsor II  $\mu\text{em}$  with  $[\text{DiC}_{10}]\text{Br}$  as surfactant also gave high conversion (97.6%), while the mixture of catalyst in the product caused the work-up problem (**Table 3.14, Entry 3**). Besides, different types of  $\mu\text{ems}$  could be also obtained with solvents of different hydrophobicity, such as toluene, dodecane and n-butyl ether gave Winsor II, I and III  $\mu\text{em}$ , respectively. As shown in **Table 3.14 (Entry 4-6)**, the Winsor III  $\mu\text{em}$  was preferred as Winsor I  $\mu\text{em}$  gave lower reaction rate and Winsor II caused the difficulty of the separation of product. Finally, **TPPTS** as ligand instead of **DPPBS** was also investigated as the addition of **TPPTS** presented similar effect on the “Fish diagram” of  $[\text{DiC}_8]\text{Br}$ . High conversion and selectivity of aldehyde were also obtained except the slight decrease of linear aldehyde selectivity ( $1/b = 2.4$ ) (**Table 3.14, Entry 7**). As with  $[\text{DiC}_8]\text{Br}$  as surfactant, **DPPBS** as ligand and cyclohexane as solvent gave the best result, this catalytic system was also applied in hydroformylation of other hydrophobic olefins. Besides 1-decene, 1-octene and 1-dodecene were also converted to corresponding aldehyde in high yield and selectivity (**Table 3.14, Entry 8 and 9**).

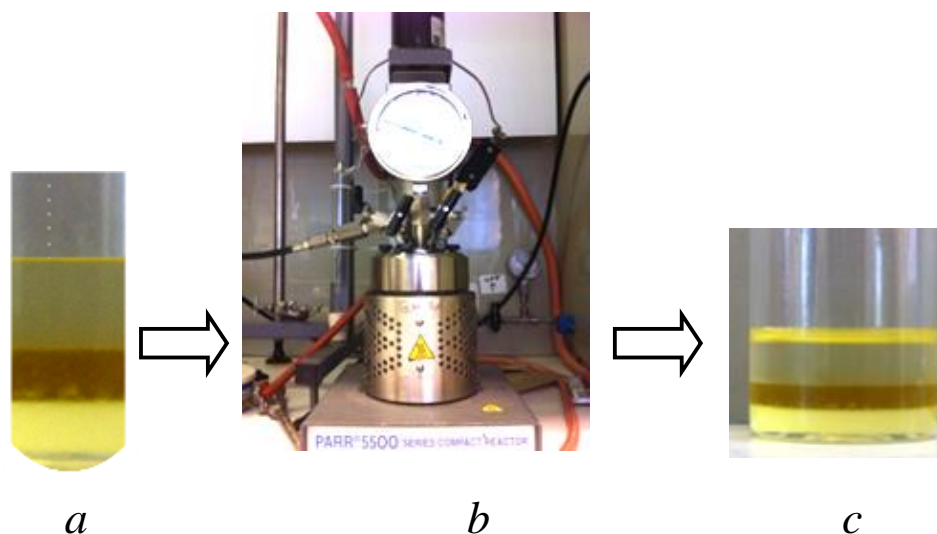


**Figure 3.23** a) The prepared catalytic system before reaction; b) autoclave; and c) recovered Winsor III  $\mu\text{em}$  after reaction.

**Table 3.14** The hydroformylation of 1-decene in  $\mu\text{em}$  system<sup>a</sup>

	Solvent	Surfactant	Conversion	Winsor	Aldehyde selec.(%)	l/b
1	Cyclohexane	[DiC <sub>8</sub> ]Br	97.7	III	99.3	2.97
2	Cyclohexane	[DiC <sub>6</sub> ]Br	7.6	I	97.37	4.49
3	Cyclohexane	[DiC <sub>10</sub> ]Br	98.6	II	97.64	2.82
4	Toluene	[DiC <sub>8</sub> ]Br	98.5	II	96.7	2.79
5	Dodecane	[DiC <sub>8</sub> ]Br	57.3	I	98.04	3.21
6	n-Bu <sub>2</sub> O	[DiC <sub>8</sub> ]Br	98.6	III	95.95	2.53
7	Cyclohexane <sup>b</sup>	[DiC <sub>8</sub> ]Br	98.3	III	97.66	2.39
8	Cyclohexane <sup>c</sup>	[DiC <sub>8</sub> ]Br	98.1	III	99.3	2.33
9	Cyclohexane <sup>d</sup>	[DiC <sub>8</sub> ]Br	98.41	III	95.4	2.80

<sup>a</sup> Reaction condition:  $\text{Rh}(\text{CO})_2(\text{acac}) = 0.01 \text{ mM}$ ,  $\text{DPPBS} = 0.05 \text{ mM}$ ,  $\text{H}_2\text{O} = 2 \text{ mL}$ ,  $\text{Solvent} = 2 \text{ mL}$ ,  $[\text{DiC}_n]\text{Br} = 400 \text{ mg}$ ,  $1\text{-decene} = 5 \text{ mM}$ ,  $\text{CO}/\text{H}_2 = 50 \text{ Bar}$ ,  $T = 80^\circ\text{C}$ ,  $t = 2\text{h}$ . <sup>b</sup> TPPTS (28.4 mg, 0.05mM) was used as ligand. <sup>c</sup> 1-octene as substrate. <sup>d</sup> 1-dodecene as substrate.

In conclusion, a elegant three-phase  $\mu\text{em}$  with [DiC<sub>8</sub>]Br as surfactant was elaborated for the hydroformylation of hydrophobic olefins with  $\text{Rh}(\text{CO})_2(\text{acac})$  as catalyst precursor and DPPBS as ligand. The three-phase  $\mu\text{em}$  based on [DiC<sub>8</sub>]Br is insensitive to the temperature and overcome the immiscibility between hydrophobic substrate and aqueous phase. The large interface area ensured the high reaction activity. Several hydrophobic terminal olefins were easily converted to aldehydes in this Winsor III  $\mu\text{em}$  in high reaction rate and the easy separation at the end of reaction facilitated the purification of product and recycling of catalyst.

**3.6 Experimental section**

---





### 3.6.1 Catalytic oxidation reactions in acidic three-phase $\mu\text{em}$

**[C<sub>8</sub>C<sub>8</sub>N(CH<sub>3</sub>)<sub>2</sub>][H<sub>2</sub>PO<sub>4</sub>]:** The product was prepared according the method described in chapter 2. <sup>1</sup>H NMR (300 MHz, CD<sub>3</sub>OD, rt):  $\delta$  3.27–3.33 (m, 4H), 3.09 (s, 6H), 1.73–1.76 (m, 4H), 1.34–1.41 (20H), 0.90–0.95 (6H); <sup>13</sup>C NMR (75 MHz, CDCl<sub>3</sub>, rt):  $\delta$  63.8, 50.0, 31.5, 28.8, 28.7, 26.0, 22.2, 22.1, 13.1 (95% yield).

**[C<sub>8</sub>C<sub>8</sub>N(CH<sub>3</sub>)<sub>2</sub>][HSO<sub>4</sub>]:** <sup>1</sup>H NMR (300 MHz, CD<sub>3</sub>OD, rt):  $\delta$  3.27–3.34 (m, 4H), 3.08 (s, 6H), 1.73–1.78 (m, 4H), 1.34–1.41 (m, 20H), 0.90–0.95 (m, 6H); <sup>13</sup>C NMR (75 MHz, CDCl<sub>3</sub>, rt):  $\delta$  63.9, 49.8, 31.5, 28.8, 28.7, 26.0, 22.3, 22.1, 13.0 (93% yield).

**Typical procedure for epoxidation of olefins giving acid stable epoxides:** [DiC<sub>10</sub>]<sub>2</sub>WO<sub>4</sub> (54mg, 0.06 mM) was dissolved in 0.43 mL H<sub>2</sub>O<sub>2</sub> (50wt%, 7.2 mM) under ice-water bath and the pre-prepared [DiC<sub>8</sub>][HSO<sub>4</sub>] (88mg, 0.23 mM, in 0.25 mL H<sub>2</sub>O) and [DiC<sub>8</sub>][H<sub>2</sub>PO<sub>4</sub>] (11mg, 0.03 mM, in 0.25 mL H<sub>2</sub>O) were added consecutively and the mixture was stirred for 5min. Then cyclooctene (0.779 mL, 6 mM) was added and the mixture was stirred for 2h at 50°C. Finally the Winsor III  $\mu\text{em}$  was recovered by addition of 1 mL toluene or *tert*-BuOAc. The product was obtained by separation of the oil phase and and extracted for two more times from  $\mu\text{em}$  phase and removed the solvent by rotary evaporation.

**Cyclooctene oxide:** <sup>1</sup>H NMR (300 MHz, CDCl<sub>3</sub>, rt, TMS):  $\delta$  (ppm) = 1.2–1.7 (m, 10H), 2.16 (m, 2H), 2.89 (m, 2H). <sup>13</sup>C NMR (75 MHz, CDCl<sub>3</sub>, 20 °C):  $\delta$  (ppm) = 25.6, 26.3, 26.6, 55.6.

**Ethyl trans-9,10-epoxyoctadecanoate:** <sup>1</sup>H NMR (300 MHz, CDCl<sub>3</sub>, rt):  $\delta$  4.13 (dd, *J* = 14.4, 7.2Hz, 2H), 2.89–2.98 (m, 2H), 2.29 (t, *J* = 7.2Hz, 2H), 1.23–1.64 (m, 29H), 0.86–0.91 (m, 3H); <sup>13</sup>C NMR (75 MHz, CDCl<sub>3</sub>, rt):  $\delta$  173.9, 60.2, 57.2, 57.1, 34.4, 34.3, 31.8, 29.6, 29.5, 29.4, 29.3, 29.2, 29.0, 27.8, 27.7, 26.6, 26.5, 24.9, 22.6, 14.2, 14.1.

**9, 10-epoxystearic acid:** <sup>1</sup>H NMR (300 MHz, CDCl<sub>3</sub>, rt):  $\delta$  2.91–2.96 (m, 2H), 2.36 (t, *J* = 7.5Hz, 2H), 1.27–1.68 (m, 26H), 0.87–0.92 (m, 3H); <sup>13</sup>C NMR (75 MHz, CDCl<sub>3</sub>, rt):  $\delta$  179.4, 57.4, 57.3, 34.1, 31.9, 29.6, 29.5, 29.3, 29.2, 29.1, 29.0, 27.8, 27.7, 26.6, 26.5, 24.7, 22.7, 14.1.

**Typical procedure for epoxidation of olefins giving acid sensitive epoxides:** [DiC<sub>10</sub>]<sub>2</sub>WO<sub>4</sub> (54mg, 0.06 mmol) was added in 2 mL *tert*-BuOAc and 0.18 mL H<sub>2</sub>O<sub>2</sub> (50wt%, 3mmol) was added under ice-water bath and the pre-prepared [DiC<sub>8</sub>][HSO<sub>4</sub>] (88mg, 0.23mmol, in 2 mL *tert*-BuOAc) and [DiC<sub>8</sub>][H<sub>2</sub>PO<sub>4</sub>] (11mg, 0.03mmol, in 2 mL *tert*-BuOAc) were added consecutively and the mixture was stirred for 5min. Then limonene (0.388 mL, 2.4mmol) was added and the mixture was stirred for 2h at 50°C. Finally the Winsor III  $\mu\text{em}$  was recovered by addition of 1 mL H<sub>2</sub>O. The product was obtained by separation of the oil phase and removed the solvent by rotary evaporation.

**Limonene 2,3-epoxide:** <sup>1</sup>H NMR (300 MHz, CDCl<sub>3</sub>, rt, TMS):  $\delta$  (ppm) = 1.13–2.27 (m, 7H), 1.29 (s, 3H), 1.71 (s, 3H), 3.02 (t, 1H, *J* = 5.5 Hz), 4.75 (s, 2H). <sup>13</sup>C NMR (75 MHz, CDCl<sub>3</sub>, rt, TMS):  $\delta$  (ppm) = 20.2, 22.1, 25.8, 28.5, 30.7, 40.7, 57.3, 59.2, 109.0, 148.8.

**3,4-Epoxy-carane:**  $^1\text{H}$  NMR (300 MHz,  $\text{CDCl}_3$ , rt, TMS):  $\delta$  (ppm) = 0.44 (td,  $J = 9.1, 2.3$  Hz, 1H), 0.52 (td,  $J = 9.1, 2.3$  Hz, 1H), 0.72 (s, 3H), 1.00 (s, 3H), 1.25 (s, 3H), 1.48 (dd,  $J = 16.5, 2.3$  Hz, 1H), 1.63 (dt,  $J = 16.5, 2.3$  Hz, 1H), 2.13 (dd,  $J = 16.5, 9.2$  Hz, 1H), 2.29 (ddd,  $J = 16.5, 9.2, 1.8$  Hz, 1H), 2.82 (s, 1H).  $^{13}\text{C}$  NMR (75 MHz,  $\text{CDCl}_3$ , rt, TMS): = 13.8, 14.6, 16.0, 19.2, 23.1, 23.3, 27.7, 55.9, 58.2.

**Cyclohexene epoxide:**  $^1\text{H}$  NMR (300 MHz,  $\text{CDCl}_3$ , rt, TMS):  $\delta$  (ppm) = 1.16–1.48 (m, 4H), 1.76–1.99 (m, 4H), 3.12 (dd,  $J = 2.1, 1.0$  Hz, 2H).  $^{13}\text{C}$  NMR (75 MHz,  $\text{CDCl}_3$ , rt, TMS):  $\delta$  (ppm) = 19.4, 24.4, 52.2.

**1-methylcyclohexene epoxide:**  $^1\text{H}$  NMR (300 MHz,  $\text{CDCl}_3$ , rt, TMS):  $\delta$  (ppm) = 1.18–1.32 (m, 5H), 1.36–1.48 (m, 2H), 1.62–1.71 (m, 1H), 1.80–1.94 (m, 3H), 2.96 (d,  $J = 3.3$  Hz, 1H),  $^{13}\text{C}$  NMR (75 MHz,  $\text{CDCl}_3$ , rt, TMS):  $\delta$  (ppm) = 19.6, 20.1, 23.8, 24.8, 29.9, 57.7, 59.7.

**2-octene epoxide (cis + trans):** (cis):  $^1\text{H}$  NMR (300 MHz,  $\text{CDCl}_3$ , rt, TMS):  $\delta$  (ppm) = 0.92 (t, 3H,  $J = 6.9$  Hz), 1.26–1.52 (m, 11H), 2.87–2.93 (m, 1H), 3.01–3.08 (m, 1H).  $^{13}\text{C}$  NMR (75 MHz,  $\text{CDCl}_3$ , rt, TMS):  $\delta$  (ppm) = 13.2, 13.9, 22.6, 26.1, 27.4, 31.6, 52.6, 57.1. (trans):  $^1\text{H}$  NMR (300 MHz,  $\text{CDCl}_3$ , rt, TMS):  $\delta$  (ppm) = 0.90 (t, 3H,  $J = 6.8$  Hz), 1.26–1.52 (m, 11H), 2.60–2.64 (m, 1H), 2.73–2.75 (m, 1H).  $^{13}\text{C}$  NMR (75 MHz,  $\text{CDCl}_3$ , rt, TMS):  $\delta$  (ppm) = 14.0, 17.7, 22.6, 25.7, 31.7, 32.0, 54.6, 59.9.

**Norbornene epoxide:**  $^1\text{H}$  NMR (300 MHz,  $\text{CDCl}_3$ , rt, TMS):  $\delta$  (ppm) = 0.70 (m, 1H), 1.19–1.35 (m, 2H), 1.46–1.59 (m, 3H), 2.46 (s, 2H), 3.08 (s, 2H).  $^{13}\text{C}$  NMR (75 MHz,  $\text{CDCl}_3$ , rt, TMS):  $\delta$  (ppm) = 25.1, 26.2, 36.7, 51.8.

**6,7-Epoxy-3,7-dimethyloctanol:**  $^1\text{H}$  NMR (300 MHz,  $\text{CDCl}_3$ , rt, TMS):  $\delta$  (ppm) = 0.92 (d, 3H,  $J = 6.6$  Hz), 1.26 (s, 3H), 1.30 (s, 3H), 1.35–1.68 (m, 8H), 2.70 (t, 1H,  $J = 6.1$  Hz), 3.69 (m, 2H).  $^{13}\text{C}$  NMR (75 MHz,  $\text{CDCl}_3$ , rt, TMS):  $\delta$  (ppm) = 18.6, 18.7, 19.4, 19.6, 24.8, 26.2, 26.4, 29.2, 29.4, 33.6, 33.7, 39.5, 39.8, 60.9, 64.6.

**Typical procedure for epoxidation of sulfides:** (54mg, 0.06mmol) was dissolved in 0.5 mL  $\text{H}_2\text{O}_2$  aq. (0.6mmol  $\text{H}_2\text{O}_2$ ) under ice-water bath and the pre-prepared  $[\text{DiC}_8][\text{HSO}_4]$  (88mg, 0.23mmol, in 0.25 mL  $\text{H}_2\text{O}$ ) and  $[\text{DiC}_8][\text{H}_2\text{PO}_4]$  (11mg, 0.03mmol, in 0.25 mL  $\text{H}_2\text{O}$ ) were added consecutively and the mixture was stirred for 5min. Then DBT (73.7mg, 0.4mmol) in 1 mL *tert*-BuOAc was added and the mixture was kept stirring at room temperature for 15 min. Then the product precipitate was obtained by filtration and the oil phase of three-phase  $\mu\text{em}$  was separated and the solvent was removed afforded the final sulfoxide and sulfone.

**Dibenzothiophen-5-oxide:**  $^1\text{H}$  NMR (300 MHz,  $\text{CDCl}_3$ , rt, TMS):  $\delta$  (ppm) = 7.48–7.52 (m, 2H), 7.58–7.62 (m, 2H), 7.81 (d,  $J = 7.8$  Hz, 2H), 7.99 (d,  $J = 7.8$  Hz, 2H).  $^{13}\text{C}$  NMR (75 MHz,  $\text{CDCl}_3$ , rt, TMS):  $\delta$  (ppm) = 121.8, 127.5, 129.5, 132.5, 137.1, 145.1.

**Dibenzothiophene-5,5-dioxide:**  $^1\text{H}$  NMR (300 MHz,  $\text{CDCl}_3$ , rt, TMS):  $\delta$  (ppm) = 7.50–7.54 (m, 2H), 7.61–7.65 (m, 2H), 7.78–7.80 (m, 2H), 7.81–7.83 (m, 2H).  $^{13}\text{C}$  NMR (75 MHz,  $\text{CDCl}_3$ , rt, TMS):  $\delta$  (ppm) = 121.6, 122.1, 130.3, 131.6, 133.8, 137.7

**Diphenyl sulfoxide:**  $^1\text{H}$  NMR (300 MHz,  $\text{CDCl}_3$ , rt, TMS):  $\delta$  (ppm) = 7.41–7.43 (m, 6H), 7.63–7.65 (m, 4H).  $^{13}\text{C}$  NMR (75 MHz,  $\text{CDCl}_3$ , rt, TMS):  $\delta$  (ppm) = 124.7, 129.3, 131.0, 145.5.

**Diphenyl sulfone:**  $^1\text{H}$  NMR (300 MHz,  $\text{CDCl}_3$ , rt, TMS):  $\delta$  (ppm) = 7.45–7.55 (m, 6H), 7.93–7.95 (m, 4H).  $^{13}\text{C}$  NMR (75 MHz,  $\text{CDCl}_3$ , rt, TMS):  $\delta$  (ppm) = 127.7, 129.3, 133.2, 141.5.

**Dibenzyl sulfoxide:**  $^1\text{H}$  NMR (300 MHz,  $\text{CDCl}_3$ , rt, TMS):  $\delta$  (ppm) = 3.85 (d,  $J = 12.8$  Hz, 2H), 3.91 (d,  $J = 12.8$  Hz, 2H), 7.25–7.38 (m, 10H).  $^{13}\text{C}$  NMR (75 MHz,  $\text{CDCl}_3$ , rt, TMS):  $\delta$  (ppm) = 57.2, 128.3, 128.9, 130.1, 130.4.

**Dibenzyl sulfone:**  $^1\text{H}$  NMR (300 MHz,  $\text{CDCl}_3$ , rt, TMS):  $\delta$  (ppm) = 4.11 (s, 4H), 7.37–7.39 (m, 10H).  $^{13}\text{C}$  NMR (75 MHz,  $\text{CDCl}_3$ , rt, TMS):  $\delta$  (ppm) = 58.0, 127.5, 128.3, 128.9, 130.1, 130.9.

**Methyl phenyl sulfoxide:**  $^1\text{H}$  NMR (300 MHz,  $\text{CDCl}_3$ , rt, TMS):  $\delta$  (ppm) = 2.72 (s, 3H), 7.48–7.55 (m, 3H), 7.64–7.66 (m, 2H).  $^{13}\text{C}$  NMR (75 MHz,  $\text{CDCl}_3$ , rt, TMS):  $\delta$  (ppm) = 43.7, 123.3, 129.2, 130.8, 145.4.

**Methyl phenyl sulfone:**  $^1\text{H}$  NMR (300 MHz,  $\text{CDCl}_3$ , rt, TMS):  $\delta$  (ppm) = 3.06 (s, 3H), 7.55–7.59 (m, 2H), 7.64–7.67 (m, 1H), 7.93–7.95 (m, 2H).  $^{13}\text{C}$  NMR (75 MHz,  $\text{CDCl}_3$ , rt, TMS):  $\delta$  (ppm) = 44.9, 121.6, 122.1, 130.3, 131.5, 133.9, 137.9.

### 3.6.2 Dark singlet oxygen oxygenation in temperature-switch $\mu\text{ems}$

#### DLS measurements

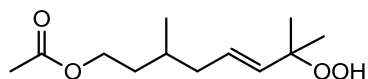
DLS measurements were performed on a ALV/CGS-3 Super Compact Goniometer System at 25 °C (thermo regulated bath  $\pm 0.1$  °C). Pseudo Cross correlation mode is used with two APD to improve the detection of small size micelle ( $< 5$  nm). Each sample were centrifuged directly in the glass cell to avoid dust signal (30min, 4500 rpm) during the DLS analysis. 13 angles from 30-150° were record to determine the diffusion coefficient ( $R_h \pm 0.1$ nm). Cumulant method was apply as data treatment of the correlogram for each angle and polydispersity index was in all case lower than 0.2 that indicate that only monodisperse micelles was observed.

#### Binary diagrams

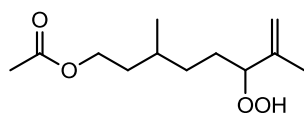
The water/surfactant mixture pseudo-binary diagram as function of temperature was determined by visual inspection. At each constant  $\delta$ , the solutions of different concentrations were prepared and kept in the thermostatic bath. The temperature was increased slowly (1.0 °C/min) from 15 to 80 °C and then decreased to 15 °C, the temperature resulted in the turbid and phase separation for each sample was recorded and this process was repeated for three times to affirm the deviation under 0.1 °C.

**Oxidation of  $\alpha$ -terpinene:**  $[\text{DiC}_8\text{I}_2][\text{MoO}_4]$  (11.1 mg, 15.8  $\mu\text{mol}$ ),  $\text{C}_8\text{E}_4$  (211.1 mg, 0.689 mmol),  $\text{H}_2\text{O}$  (1.0 g), cyclohexane (1.0 g) were added consecutively to prepare the  $\mu\text{em}$  in a reaction tube. Then  $\alpha$ -terpinene (50 mg, 0.367 mmol) was added into the mixture and kept at 30 °C (Winsor IV), the  $\text{H}_2\text{O}_2$  (50 wt.%, 17 M) was added stepwise and each batch of  $\text{H}_2\text{O}_2$  was 10  $\mu\text{L}$ . The conversion was complete after the addition of  $6 \times 10 \mu\text{L}$  (1.02 mmol). Then the reaction tube was kept still at 5 °C for 4h, the oil phase was separated and the  $\mu\text{em}$  phase was washed with cyclohexane (1 mL) at 5 °C, the organic phases were combined and cyclohexane was removed by evaporation, the crude product was purified by a small chromatography on silica gel (cyclohexane/AcOEt = 5 : 1) and pure colorless oil was obtained (56.6 mg, 92 %).  $^1\text{H}$  NMR (300 MHz,  $\text{CDCl}_3$ , 20 °C, TMS):  $\delta$  (ppm) = 1.01 (d,  $J$  = 2.25, 3H;  $\text{CH}_3$ ), 1.03 (d,  $J$  = 2.25, 3H;  $\text{CH}_3$ ), 1.39 (s, 3H;  $\text{CH}_3$ ), 1.19–1.57 (m, 2H,  $-\text{CH}_2-\text{CH}_2-$ ), 1.87–2.03 (m, 1H; isopropyl), 2.03–2.14 (m, 2H;  $-\text{CH}_2-\text{CH}_2-$ ), 6.47 (dd,  $J$  = 25.77, 8.55Hz;  $\text{CH} = \text{CH}$ ).  $^{13}\text{C}$  NMR (75 MHz,  $\text{CDCl}_3$ , 20 °C):  $\delta$  (ppm) = 17.2, 17.3, 21.4, 25.6, 29.5, 32.1, 133.0, 136.4.

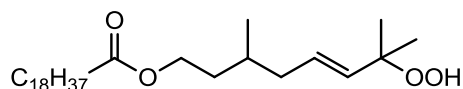
#### Oxidation of citronellyl acetate



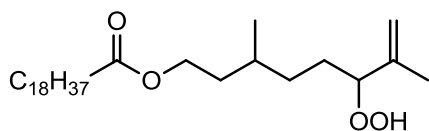
$^1\text{H}$ -NMR ( $\text{CDCl}_3$ , 300 MHz, 20 °C, TMS, ppm):  $\delta$  = 5.49–5.72 (m, 2H;  $\text{CH}=\text{CH}$ ), 4.10 (t,  $J$  = 6.72 Hz, 2H;  $\text{CH}_2-\text{OCO}$ ), 1.90–2.14 (m, 5H;  $\text{CH}_3-\text{COO}$ ,  $\text{CH}_2-\text{CH}=\text{}$ ), 1.36–1.79 (m, 3H;  $\text{CH}_2-\text{CH}-$ ), 1.33 (s, 3H;  $\text{CH}_3-\text{C}-\text{OOH}$ ), 1.32(s, 3H;  $\text{CH}_3-\text{C}-\text{OOH}$ ), 0.91 (d,  $J$  = 6.56Hz, 3H;  $\text{CH}_3-\text{CH}(\text{CH}_2)_2$ );  $^{13}\text{C}$ -NMR ( $\text{CDCl}_3$ , 75 MHz, 20 °C, ppm):  $\delta$  = 171.5, 135.3, 129.4, 82.0, 62.9, 39.6, 34.8, 29.9, 24.3, 24.2, 21.0, 19.5.



$^1\text{H}$ -NMR ( $\text{CDCl}_3$ , 300 MHz, 20 °C, TMS, ppm):  $\delta$  = 4.95–5.04 (m, 2H;  $\text{CH}_2=\text{C}$ ), 4.27 (t,  $J$  = 6.60Hz, 1H;  $\text{CH}-\text{OOH}$ ), 4.10 (t,  $J$  = 6.63 Hz, 2H;  $\text{CH}_2-\text{OCO}$ ), 2.04 (s, 3H;  $\text{CH}_3-\text{COO}$ ), 1.68–1.78 (m, 3H;  $\text{CH}_3-\text{C}=\text{}$ ), 1.37–1.70 (m, 5H,  $\text{CH}_2-\text{CH}$ ;  $\text{CH}_2-\text{CHOOH}$ ), 1.21–1.32 (m, 2H;  $\text{CH}_2-\text{CH}$ ), 0.90 (d,  $J$  = 6.56Hz, 3H;  $\text{CH}_3-\text{CH}(\text{CH}_2)_2$ );  $^{13}\text{C}$ -NMR ( $\text{CDCl}_3$ , 75 MHz, 20 °C, ppm):  $\delta$  = 171.4, 143.8, 114.4, 89.8, 62.8, 35.4, 32.6, 29.7, 28.1, 19.4, 19.2, 17.1.



$^1\text{H}$ -NMR ( $\text{CDCl}_3$ , 300 MHz, 20 °C, TMS, ppm):  $\delta$  = 5.53–5.77 (m, 2H;  $\text{CH}=\text{CH}$ ), 4.12 (t,  $J$  = 6.63 Hz, 2H;  $-\text{CH}_2-\text{OCO}$ ), 2.30 (t,  $J$  = 7.48Hz, 2H;  $\text{CH}_2-\text{COO}$ ), 1.94–2.13 (m, 2H,  $\text{CH}_2-\text{CH}=\text{}$ ), 1.54–1.83 (m, 3H,  $\text{CH}$ ,  $\text{CH}_2-\text{CH}_2-\text{COO}$ ), 1.39–1.53 (m, 2H,  $\text{CH}_2-\text{CH}-$ ), 1.22–1.38 (m, 34H;  $-\text{CH}_2-$ ,  $\text{CH}_3-\text{C}-\text{OOH}$ ), 0.87–0.96 (m, 6H;  $\text{CH}_3-\text{CH}(\text{CH}_2)_2$ ,  $\text{CH}_3-\text{CH}_2$ );  $^{13}\text{C}$ -NMR ( $\text{CDCl}_3$ , 75 MHz, 20 °C, ppm):  $\delta$  174.2, 135.2, 129.7, 82.1, 62.6, 39.6, 34.9, 34.4, 31.9, 29.9, 29.7, 29.6, 29.5, 29.3, 29.2, 29.1, 25.0, 24.3, 24.2, 22.7, 19.5, 14.1.



$^1\text{H-NMR}$  ( $\text{CDCl}_3$ , 300 MHz, 20 °C, TMS, ppm):  $\delta$  4.99–5.08 (m, 2H;  $\text{CH}_2=\text{C}$ ), 4.30 (t,  $J = 6.60\text{Hz}$ , 1H;  $\text{CH-OOH}$ ), 4.12 (t,  $J = 6.63\text{ Hz}$ , 2H;  $-\text{CH}_2\text{-OCO}$ ), 2.30 (t,  $J = 7.48\text{Hz}$ , 2H;  $\text{CH}_2\text{-COO}$ ), 1.39–1.82 (m, 10H,  $\text{CH}_3\text{-CH=}$ ,  $\text{CH}_2\text{-CH}_2\text{-COO}$ ,  $\text{CH}_2\text{-CH}$ ,  $\text{CH}_2\text{-CHOOH}$ ) 1.22–1.38 (m, 30H;  $-\text{CH}_2-$ ), 0.87–0.96 (m, 6H;  $\text{CH}_3\text{-CH}(\text{CH}_2)_2$ ,  $\text{CH}_3\text{-CH}_2$ );  $^{13}\text{C-NMR}$  ( $\text{CDCl}_3$ , 75 MHz, 20 °C, ppm):  $\delta$  174.1, 143.7, 114.5, 89.9, 62.5, 35.4, 34.4, 32.6, 31.9, 29.9, 29.7, 29.6, 29.5, 29.3, 29.2, 29.1, 28.1, 25.0, 19.4, 17.1, 14.1.

### 3.6.3 Photochemical and chemical singlet oxygenation of (+)-Valencene

**The photochemical oxygenation of (+)-Valencene in  $\text{CH}_3\text{OH}$  with Rose Bengal as photosensitive dye (H1):** 10.0 mL  $\text{CD}_3\text{OH}$  solution with 0.125 mg Rose Bengal was prepared in a 25 mL special flat flask for photooxidation. Valencene (204.4mg, 1.0 mmol) was dissolved in the solution and then the reaction was triggered by the bubbling of the oxygen under the light of sodium lamp of Comodore Tiger 250W E40 floodlight at 20°C. The reaction was detected each 2h by NMR analyst of the reaction mixture directly until the conversion was complete (another 0.125mg Rose Bengal was added at 16h). At the end of the reaction, the solvent was evaporated in vacuum and the crude product was purified with chromatograph on silica gel (Petroleum ether/ ethyl ether = 4:1), afforded the pure desired product **H1** 96.9 mg (41%).  $^1\text{H NMR}$  (300 MHz,  $\text{CD}_3\text{OD}$ )  $\delta = 5.83$  (dt,  $J = 3.1\text{ Hz}$ , 9.9 Hz, 1H), 5.61 (d,  $J = 9.9\text{ Hz}$ , 1H), 4.71–4.77 (m, 1H), 4.66–4.70 (m, 1H), 2.09–2.34 (m, 4H), 1.74–1.82 (m, 5H), 1.38–1.64 (m, 4H), 0.89 (s, 3H), 0.80 (d,  $J = 6.7\text{ Hz}$ , 3H);  $^{13}\text{C NMR}$  (75Hz,  $\text{CD}_3\text{OD}$ )  $\delta = 131.0$ , 130.5, 107.6, 39.7, 35.4, 32.9, 30.7, 26.9, 25.2, 19.4, 13.9, 13.3. HRMS (ESI): calcd for  $\text{C}_{15}\text{H}_{24}\text{O}_2$  ( $\text{M}+\text{H}$ ) $^+$  237.3578, found 237.1849.

**The conversion of hydroperoxide H1 to H2 via Schenck rearrangement (H2) and further catalytic conversion to (+)-Nootkatone: H1** (42 mg, 0.18mmol) was dissolved in 1 mL toluene- $d_8$  and incubated at 40°C for 4.5h and the **H1** was converted to **H2** quantitatively.  $^1\text{H NMR}$  (300 MHz, Toluene- $d_8$ )  $\delta = 5.40$ –5.43 (m, 1H), 4.74–4.77 (m, 2H), 4.20–4.24 (m, 1H), 1.78–2.18 (m, 5H), 1.60–1.68 (m, 4H), 1.30–1.41 (m, 2H), 0.94–1.19 (m, 2H), 0.82 (d,  $J = 6.9\text{ Hz}$ , 3H), 0.78 (s, 3H);  $^{13}\text{C NMR}$  (75Hz, Toluene- $d_8$ )  $\delta = 137.1$ , 116.8, 108.7, 77.6, 44.4, 40.6, 35.0, 32.6, 32.5, 30.9, 20.4, 16.6, 14.8. HRMS (ESI): calcd for  $\text{C}_{15}\text{H}_{24}\text{O}_2$  ( $\text{M}+\text{H}$ ) $^+$  237.3578, found 237.1849.

Then  $[\text{DiC}_8]_2\text{MoO}_4$  (24.9mg, 0.036 mmol) was dissolved in the reaction mixture as catalyst to convert **H2** to nootkatone. The mixture was incubated at 50°C for 7.5h and the conversion was complete depending on the detection of NMR. Then the solvent was evaporated in vacuum and the reaction residue was subject to the chromatography on silica gel (PE/ethyl ether = 3:1) afforded 29.0 mg (+)-Nootkatone as colorless oil with the flavor of grapefruit (74.8%).  $^1\text{H NMR}$  (300 MHz, Toluene- $d_8$ )  $\delta = 5.74$  (s, 1H), 4.75–4.79 (m, 1H), 4.70–4.73 (m, 1H), 1.87–2.14 (m, 5H), 1.67–1.73 (m, 1H), 1.54–1.61 (m, 5H), 0.97–1.12 (m, 1H), 0.79–0.87 (m, 1H), 0.70 (s, 3H), 0.59 (d,  $J = 6.9\text{ Hz}$ , 3H);  $^{13}\text{C NMR}$  (75Hz, Toluene-

$d_8$ )  $\delta = 137.1, 125.0, 109.3, 43.8, 41.9, 40.2, 40.1, 32.4, 31.5, 20.4, 16.1, 14.4$ . HRMS (ESI): calcd for  $C_{15}H_{22}O$  (M+H)<sup>+</sup> 219.1749, found 219.1748.

**Photochemical oxygenation of (+)-Valencene to (+)-Nootkatone in toluene- $d_8$  in the presence of  $[DiC_8]_2MoO_4$ :** (+)-Valencene (202.4 mg, 1.0 mmol) and  $[DiC_8]_2MoO_4$  (140.2 mg, 0.2 mmol) were dissolved into 5.0 mL Tol- $d_8$  containing 0.5 mg TPP. The solution was bubbled with oxygen and irradiated with a sodium lamp. The conversion of (+)-Valencene was complete after 18h at r.t. tracked by  $^1H$  NMR. Then the solution was kept at 50 °C for 4h to complete the (+)-Nootkatone formation. The product was isolated by chromatography on silica gel (PE/ethyl ether = 3:1) and 75.6 mg pure Nootkatone was isolated (35.0%). The spectra were agreed with previously described.

**Chemical oxygenation of (+)-Valencene to (+)-Nootkatone (Product Nootkatone):**  $[DiC_8]_2MoO_4$  (175 mg, 0.25 mmol), Valencene (102.2 mg, 0.5 mmol),  $H_2O_2$  (58  $\mu$ l 50 wt% solution, 1.0mmol) and 30  $\mu$ l  $NH_3$  saturated solution were subject to the reaction tube. The reaction mixture was stirred and kept at 30°C. Another batch of  $H_2O_2$  (58  $\mu$ l 50 wt% solution, 1.0mmol) was added when the red color faded and the addition of  $H_2O_2$  was repeated and finally 15 batches, 0.87 mL  $H_2O_2$ , 15 mmol in total were used to complete the conversion of (+)-Valencene. Then the reaction mixture was incubated at 50°C overnight for the complete formation of nootkatone. The solution was cooled to room temperature and 2.0 mL ethyl ether was added and sufficiently mixed. The three-phase  $\mu$ em was obtained after standstill for 5 min. The organic phase was separated and the reaction mixture was extracted for another two times (2 mL  $\times$ 2). The organic phase was combined and evaporated. The residue was subject to the chromatography on silica gel (PE/ethyl ether = 3:1) afforded the desired product nootkatone 42.4 mg (38.9%). The spectra were agreed with previously described.

### 3.6.4 Typical procedure of hydroformylation

The  $Rh(CO)_2(Acac)$  (2.6mg, 0.01mmol) and DPPBS (24.1 mg, 0.05 mmol) was weighed inside a Schlenk flask under the protection of  $N_2$ , 2 mL  $H_2O$  deoxygenated by  $N_2$  was introduced and the flask was incubated for 3h at 40°C. Then 2.6 mL cyclohexane (deoxygenated by  $N_2$ ) containing  $[DiC_8]Br$  (400 mg) and 1-decene (710 mg, 5 mmol) was added in the flask and the mixture was stirred for 3min. Then the catalytic system was introduced into the autoclave and kept the temperature at 80°C. The reaction was triggered by filled the autoclave with syngas until 50 Bar. After 2 h, the autoclave was cooled to room temperature and depressurized. The reaction mixture was poured into a flacon and kept still for 5 min to recover the three-phase  $\mu$ em. The oil phase was analyzed by GC directly to determine the product composition. *n*-nonanal:  $^1H$  NMR (300 MHz,  $CDCl_3$ )  $\delta = 9.78$  (t,  $J = 1.8$  Hz, 1H), 2.43 (dt,  $J = 1.8$  Hz, 7.3 Hz, 2H), 1.65 (m, 2H), 1.21–1.34 (m, 14H), 0.90 (t,  $J = 7.0$  Hz, 3H);  $^{13}C$  NMR (75Hz,  $CDCl_3$ )  $\delta = 202.8, 43.9, 31.9, 29.5, 29.4, 29.3, 29.2, 29.1, 22.6, 22.0, 14.0$ . 2-nonal:  $^1H$  NMR (300 MHz,  $CDCl_3$ )  $\delta = 9.63$  (d,  $J = 2.0$  Hz, 1H), 2.36 (quint,  $J = 7.4$  Hz, 1H), 1.66 (m, 2H), 1.23–1.34 (m, 12H), 1.11 (d,  $J = 7.2$  Hz, 3H), 0.90 (t,  $J = 7.0$  Hz, 3H).  $^{13}C$  NMR (75Hz,  $CDCl_3$ )  $\delta = 205.2, 46.2, 31.8, 30.4, 29.5, 29.3, 29.1, 26.8, 22.5, 13.9, 13.1$

**General Conclusion**

---







The concept of “Balanced Catasurfs” (abbreviation for “Balanced Catalytic Surfactants”) was developed in our laboratory in 2008 highlighting numerous advantages of the optimal three-phase microemulsion systems as reaction media for catalytic oxidation reactions involving  $\text{H}_2\text{O}_2$  as the oxidant. In this context, the present work has been focused on the further development of the “Catasurfs” concept, including the synthesis, the physicochemical property investigation and the application to fine chemistry of novel Catasurfs. The physicochemical characterization (*e.g.* CMC determination, elaboration of binary and ternary phase diagrams, etc) helped us in the evaluation of their amphiphilic character and their phase behavior, which facilitates the elaboration of optimal catalytic  $\mu\text{em}$  systems. The successful reactions in elegant  $\mu\text{em}$  media, such as epoxidation, sulfide oxidation, “dark singlet oxygenation”, *etc.* in this thesis also enlarged the application scope of the concept.

In a first part, the water/surfactant binary diagrams of **short chain dialkyldimethylammonium**  $[\text{DiC}_n]_m\text{X}$  ( $n = 6, 8, 10$ ;  $m = 1$ ;  $\text{X} = \text{Cl}^-$ ;  $m = 2$ ;  $\text{X} = \text{SO}_4^{2-}$ ,  $\text{MoO}_4^{2-}$  or  $\text{WO}_4^{2-}$ ) from dilute isotropic solutions to high concentrated liquid crystal phases as a function of temperature were investigated by polarized optical microscopy and SAXS. The effect of chain length and counter ions on the evolution of the phase behavior was well elucidated.  $[\text{DiC}_6]\text{Cl}$  behaves as hydrotropes and no lyotropic crystal phase was found in the binary diagram, while a lamellar phase region emerged in the diagram of  $[\text{DiC}_8]\text{Cl}$  and expanded to lower concentration for  $[\text{DiC}_{10}]\text{Cl}$ . The molybdate, tungstate, and sulfates salts presented similar phase pattern when the hydrophobic part was the same. For example, all the diagrams of  $[\text{DiC}_8]_2\text{WO}_4$ ,  $[\text{DiC}_8]_2\text{MoO}_4$ , and  $[\text{DiC}_8]_2\text{SO}_4$ , showed the cubic phase at similar concentration range and the **Ia3d** structure was identified by the SAXS analysis as the molybdate, tungstate and sulfate have similar  $\Delta G_{\text{hydr}}$ , while for the corresponding  $[\text{DiC}_{10}]$  salts, the mixture of isotropic and lamellar phases appeared due to their larger packing parameters than  $[\text{DiC}_8]$  salts (**Figure C1**).

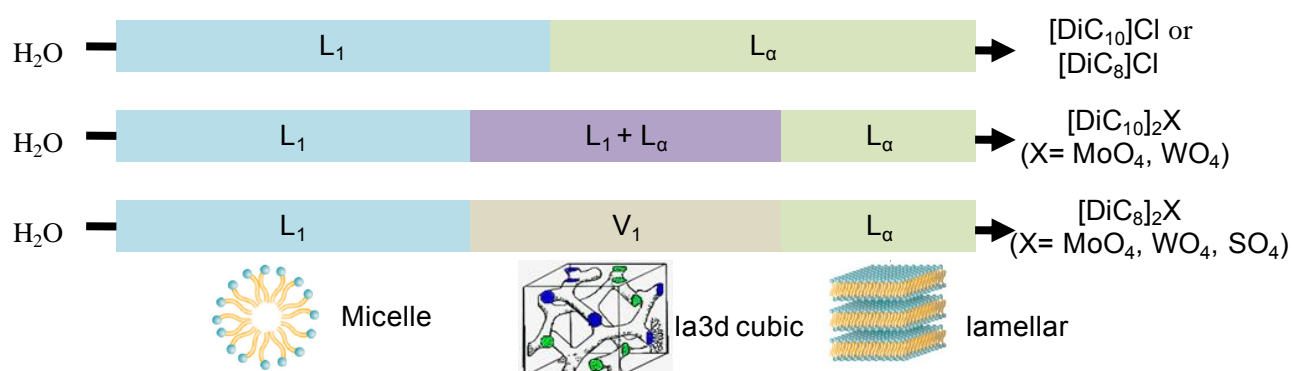


**Figure C1** The binary phase evolution patterns of  $[\text{DiC}_n]_m\text{X}$  ( $n = 6, 8, 10$ ;  $m = 1$ ,  $\text{X} = \text{Cl}^-$ ;  $m = 2$   $\text{X} = \text{SO}_4^{2-}$ ,  $\text{MoO}_4^{2-}$  or  $\text{WO}_4^{2-}$ ).

Besides the binary diagram, the  $[\text{DiC}_n]_m\text{X}$  ( $n = 6, 8, 10$ ;  $m = 1$ ,  $\text{X} = \text{Br}^-$ ,  $\text{Cl}^-$ ;  $m = 2$   $\text{X} = \text{SO}_4^{2-}$ ,  $\text{MoO}_4^{2-}$  or  $\text{WO}_4^{2-}$ ) were also classified according to their relative hydrophilic-lipophilic character by the construction

of the so-called “Fish diagrams” with surfactant, water and terminal monochloroalkanes or dichloroalkanes as oils. From the “Fish diagrams”, the X-point, *i.e.* the connecting point of Winsor III and Winsor IV  $\mu\text{em}$  regions and the amphiphile has the same affinity for water and oil, gave the intrinsic amphiphilic property of the surfactant PACN. The amphiphilicity of the  $[\text{DiC}_8]$  series with the four counter anions were found depending on the degree of counter ion, in agreement with the Hofmeister anion sequence. For example, molybdate and tungstate are greatly more hydrated than bromide and chloride, and thus more polar organic phase was required to compensate for the strong interaction between the hydrophilic part and water (**Figure C2**).

Anion	strongly hydrated	weakly hydrated
$[\text{DiC}_n]_m\text{X}$	$\text{X} = \text{WO}_4^{2-}$ $\text{MoO}_4^{2-}$	$\text{Cl}^-$ $\text{Br}^-$
Surfactant	hydrophilic	hydrophobic

**Figure C2** The correlation between the amphiphilicity of surfactant and the hydration of counter ions.

In a second part, an acidic three-phase  $\mu\text{em}$  medium based on  $[\text{DiC}_n]_2\text{WO}_4$  ( $n = 8, 10$ ) was elaborated and successfully applied to the epoxidation of olefins and oxidation of sulfides. The Venturello peroxotungstate was considered as the catalyst once  $[\text{DiC}_n]_2\text{WO}_4$  had reacted with  $\text{H}_2\text{O}_2$  in the presence of both the acid amphiphiles  $[\text{DiC}_8][\text{HSO}_4]$  and  $[\text{DiC}_8][\text{H}_2\text{PO}_4]$ . This acidic three-phase  $\mu\text{em}$  was successfully applied to the epoxidation of olefins and afforded high reaction reactivity and selectivity. Several water-sensitive monoterpene epoxides could thus be obtained in high yield by oxidation of the corresponding monoterpenes, such as (+)-limonene,  $\Delta$ -carene *etc.* as the hydrophobic part of the  $\mu\text{em}$  phase and the excess oil phase prevent the desired epoxides from hydrolyzation. The purification and recycling of the catalyst were also easily performed by phase separation at the end of reaction. For example, the epoxidation of ethyl oleate could be even carried out without additional solvent and the catalyst could be reused for five times. Besides the epoxidation of olefins, this acidic three-phase  $\mu\text{em}$  could also be used for oxidative desulfurization of refractory sulfides (**Figure C3**).

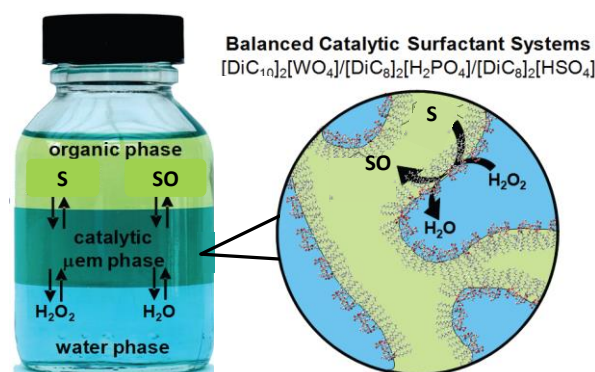


**Figure C3** The model of oxidation in acidic three-phase  $\mu\text{em}$  medium.

By taking advantage of the synergism between the nonionic  $C_8E_4$  and the ionic  $[DiC_8]_2[MoO_4]$  surfactants, a one-phase thermo-sensitive  $\mu em$  was elaborated with only 6% of amphiphiles. The cloud point and the “Fish diagram” of the ternary water/ $C_8E_4$ /cyclohexane system were dramatically affected by the presence of small amounts of  $[DiC_8]_2[MoO_4]$ . This strong synergism in aqueous phase was quantified by the interaction parameter  $\beta$  from the CMCs of the surfactant mixture and investigated also by DLS analysis of mixed micelles. The SAXS analysis of the  $\mu em$ s revealed that the great enhancement of surfactant efficiency was correlated to the topology of the  $\mu em$  in the presence of  $[DiC_8]_2[MoO_4]$  caused by the increase of the hydrophilic character compared with pure  $C_8E_4$ , which also increased the  $\mu em$  thermal stability. This temperature-switch  $\mu em$  medium was applied to  $^1O_2$  oxygenations, in particular [4+2] cycloaddition and ene reaction, and sulfide oxidation, which provided higher  $H_2O_2$  efficiency than previously reported for catalytic  $\mu em$  systems. The interest of such systems lies in the separation of the product at the end of reaction since, thanks to a temperature control, the one-phase  $\mu em$  provided a two-phase Winsor I system, with an excess oil phase containign the product(s) (**Figure C4**).

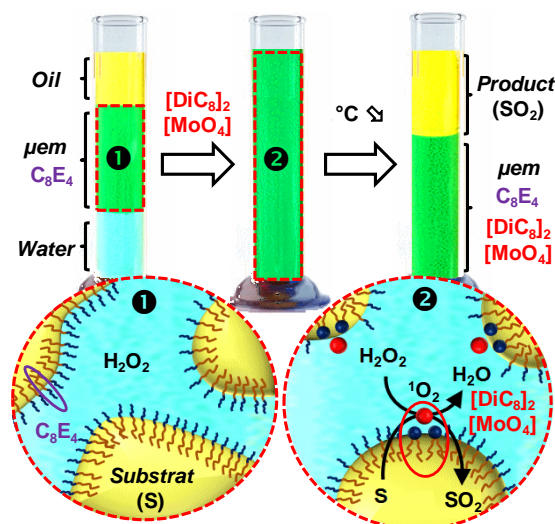


**Figure C4** The phase behavior and reaction process in the temperature-switch  $\mu em$  medium.

On the other side, the catalytic surfactant  $[DiC_8]_2[MoO_4]$  was used for the one pot, three-step (ene oxygenation, Schenck rearrangement, dehydration) conversion of (+)-**Valencene** into (+)-**Nootkatone**, a high value-added molecule widely used in flavors and cosmetics and the dual catalytic roles of molybdate in the reaction was for the first time unveiled. During the photooxygenation process, the viscosity of solvent played a crucial role for the Schenck rearrangement process, which was probably ascribed to the high viscous “solvent cage” facilitating the intramolecular rearrangement. Moreover,  $[DiC_8]_2[MoO_4]$  not only catalyzes the disproportionation of  $H_2O_2$  into  $^1O_2$  but we showed that it also catalyzed the dehydration of hydroperoxide into ketone which has never been reported before. Based on that, the dark singlet oxygenation of (+)-**valencene** was carried out under solvent free condition in the presence of  $[DiC_8]_2[MoO_4]$ . The surfactant chains were indispensable as the hydrophobic core of the micelle formed by the octyl chain was crucial for the Schenck rearrangement. Besides, the micelles not only overcame the

immiscible problem with water, but also increased the efficiency of  $^1\text{O}_2$  as the molybdate was located at the surface. At the end of reaction, the addition of diethyl ether afforded three-phase  $\mu\text{em}$ , which made the separation of product and catalyst easily achieved by phase separation (**Figure C5**).

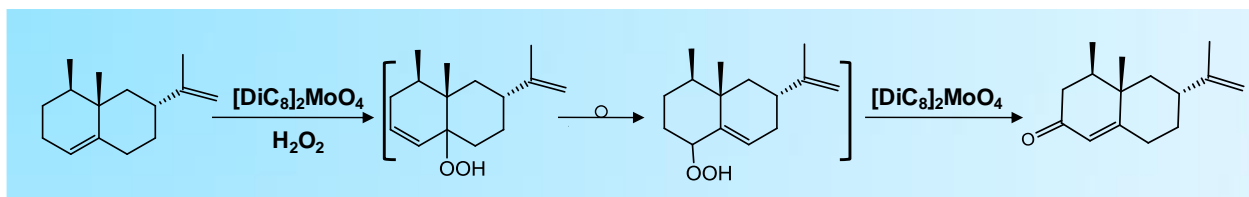


**Figure C5** The process of one pot, three-step conversion of (+)-Valencene to Nootkatone.

In addition of the oxidation reactions with  $\text{H}_2\text{O}_2$  as oxidant, the scope of the three-phase  $\mu\text{ems}$  was also extended to the hydroformylation of olefins. Based on the effect of the **TPPTS** and **DPPBS** ligands on the “Fish diagram” of  $[\text{DiC}_8]\text{Br}$ , the hydroformylation of hydrophobic olefins with  $\text{Rh}(\text{CO})_2(\text{acac})$  as a catalyst precursor was successfully achieved. Compared with the hydroformylation in non-ionic surfactant elaborated  $\mu\text{em}$ , this three-phase  $\mu\text{em}$  was temperature insensitive and the loss of surfactant in oil phase could be avoided as the NMR analysis indicated  $> 99$  mol% of the ligand remained in the middle  $\mu\text{em}$  phase. The large interface area ensured the high reaction activity and the thermal stability of three-phase  $\mu\text{em}$  facilitated the separation of product and recycling of catalyst (**Figure C6**).

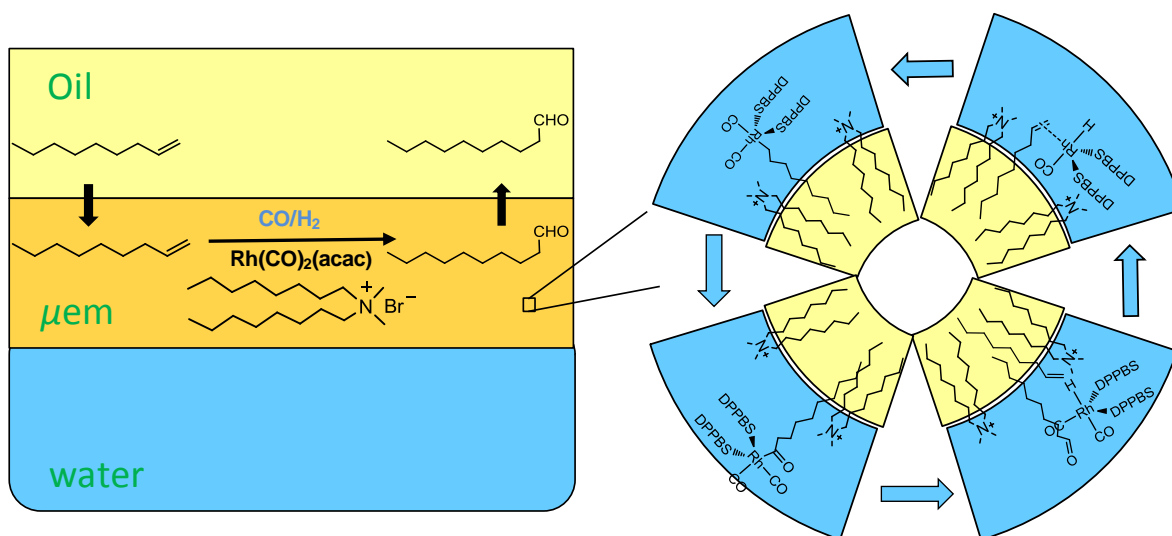


**Figure C6** Hydroformylation of hydrophobic olefins in three-phase  $\mu\text{em}$ .

Finally, as the surfactant-combined Lewis acids were widely used as catalyst in micellar solution, a series of pure Lewis acids combined double tailed methane sulphonates  $[\text{DiC}_n\text{CHSO}_3]_x[\text{M}]$  ( $n = 6, 7, 8$ ;  $x = 1$ ,  $\text{M} = \text{H}, \text{Li}, \text{Na}, \text{K}$ ;  $x = 2$ ,  $\text{M} = \text{Mg}, \text{Ca}, \text{Zn}, \text{Cu}$ ;  $x = 3$ ,  $\text{M} = \text{Sc}$ ) were synthesized. Some important properties such as the solubility in water, the CMC as well as their temperature *versus* concentration binary diagram were investigated.

To summarize, in this work, the phase behavior of several  $[\text{DiC}_n]_m\text{X}$  ( $n = 6, 8, 10$ ;  $m = 1, \text{X} = \text{Cl}^-$ ;  $m = 2, \text{X} = \text{SO}_4^{2-}, \text{MoO}_4^{2-}$  or  $\text{WO}_4^{2-}$ ) in aqueous phase and in water/oil biphasic system has largely been investigated with both physicochemical and synthetic approaches. The advantages of the multiphase  $\mu\text{em}$  systems based on Catasurfs were proved through their activity, selectivity and work-up. Besides oxidation reactions, these systems were shown to be expandable to other reactions like hydroformylation. Furthermore, novel amphiphilic Brønsted and Lewis acid catalysts ( $[\text{DiC}_n\text{CHSO}_3]_x[\text{M}]$ ) were also prepared and characterized, while their catalytic performance in microemulsion reaction media still have to be demonstrated. The possible reactions performed in  $\mu\text{ems}$  elaborated with these amphiphilic Brønsted and Lewis acid catalysts include the Carbon-Carbon formation reactions, such as aldol reaction, Mannich reaction, Diels-Alder reaction, *etc.*, various oxidation reactions with  $\text{H}_2\text{O}_2$  or alkyl perhydroxide as oxidants and dehydration reactions, such as esterification, etherification, *etc.*



---

## References

---

- (1) **Green Chemistry: Theory and Practice** Anastas, P.; Warner, J. *Oxford University Press* **1998**, 30.
- (2) **Recent Advancements in The Production of Hydroxymethylfurfural** Dashtban, M.; Gilbert, A.; Fatehi, P. *RSC Adv.* **2014**, *4*, 2037-2050.
- (3) **Green Reaction Media in Organic Synthesis** Mikami, K.; Wiley Online Library, **2005**.
- (4) **Green oxidation with aqueous hydrogen peroxide** Noyori, R.; Aoki, M.; Sato, K. *Chem. Commun. (Cambridge, U. K.)* **2003**, 1977-1986.
- (5) **Catalytic oxidation of organic substrates by molecular oxygen and hydrogen peroxide by multistep electron transfer. A biomimetic approach** Piera, J.; Backvall, J. E. *Angew. Chem., Int. Ed.* **2008**, *47*, 3506-3523.
- (6) **Organic chemistry in water** Li, C.-J.; Chen, L. *Chem. Soc. Rev.* **2006**, *35*, 68-82.
- (7) **Development of Novel Lewis Acid Catalysts for Selective Organic Reactions in Aqueous Media** Kobayashi, S.; Manabe, K. *Acc. Chem. Res.* **2002**, *35*, 209-217.
- (8) **Organic Synthesis "On Water"** Chanda, A.; Fokin, V. V. *Chem. Rev. (Washington, DC, U. S.)* **2009**, *109*, 725-748.
- (9) **Combinatorial Biosynthesis of Natural Products** Zhang, W.; Tang, Y. *J. Med. Chem.* **2008**, *51*, 2629-2633.
- (10) **Modern oxidation methods** Bäckvall, J.-E.; John Wiley & Sons, **2011**.
- (11) **Pursuing practical elegance in chemical synthesis** Noyori, R. *Chem. Commun.* **2005**, 1807-1811.
- (12) **Transitioning organic synthesis from organic solvents to water. What's your E Factor?** Lipshutz, B. H.; Ghorai, S. *Green Chem.* **2014**, *16*, 3660-3679.
- (13) **Aqueous catalytic polymerization of olefins** Mecking, S.; Held, A.; Bauers, F. M. *Angew. Chem., Int. Ed.* **2002**, *41*, 544-561.
- (14) **Pickering-Emulsion Inversion Strategy for Separating and Recycling Nanoparticle Catalysts** Yu, Y.; Fu, L.; Zhang, F.; Zhou, T.; Yang, H. *ChemPhysChem* **2014**, *15*, 841-848.
- (15) **Pickering Emulsion Stabilized by Catalytic Polyoxometalate Nanoparticles: A New Effective Medium for Oxidation Reactions** Leclercq, L.; Mouret, A.; Proust, A.; Schmitt, V.; Bauduin, P.; Aubry, J.-M.; Nardello-Rataj, V. *Chem. - Eur. J.* **2012**, *18*, 14352-14358.
- (16) **Microemulsions: Background, New Concepts, Applications, Perspectives** Stubenrauch, C.; Editor; John Wiley & Sons Ltd., **2009**.
- (17) **Organic and bioorganic reactions in microemulsions** Holmberg, K. *Adv. Colloid Interface Sci.* **1994**, *51*, 137-174.
- (18) **Organic reactions in microemulsions** Holmberg, K. *Eur. J. Org. Chem.* **2007**, 731-742.
- (19) **Dramatic Enhancement of Enone Epoxidation Rates in Nonionic Microemulsions** Wielpütz, T.; Sottmann, T.; Strey, R.; Schmidt, F.; Berkessel, A. *Chemistry – A European Journal* **2006**, *12*, 7565-7575.
- (20) **Search for singlet oxygen in the decomposition of hydrogen peroxide by mineral compounds in aqueous solutions** Aubry, J. *J. Am. Chem. Soc.* **1985**, *107*, 5844-5849.
- (21) **Chemical sources of singlet oxygen. 2. Quantitative generation of singlet oxygen from hydrogen peroxide disproportionation catalyzed by molybdate ions** Aubry, J. M.; Cazin, B. *Inorg. Chem.* **1988**, *27*, 2013-2014.
- (22) **Chemical sources of singlet oxygen. 3. Peroxidation of water-soluble singlet oxygen carriers with the hydrogen peroxide-molybdate system** Aubry, J. M.; Cazin, B.; Duprat, F. *J. Org. Chem.* **1989**, *54*, 726-728.
- (23) **Advances in singlet oxygen chemistry** Clennan, E. L.; Pace, A. *Tetrahedron* **2005**, *61*, 6665-6691.
- (24) **Chemistry of singlet oxygen. 42. Effect of solvent, solvent isotopic substitution, and temperature on the lifetime of singlet molecular oxygen ( $^1\Delta_g$ )** Ogilby, P. R.; Foote, C. S. *J. Am. Chem. Soc.* **1983**, *105*, 3423-3430.

- (25) **Preparative Oxidation of Organic Compounds in Microemulsions with Singlet Oxygen Generated Chemically by the Sodium Molybdate/Hydrogen Peroxide System** Aubry, J.-M.; Bouttemy, S. *J. Am. Chem. Soc.* **1997**, *119*, 5286-5294.
- (26) **"Dark" singlet oxygenation of hydrophobic substrates in environmentally friendly microemulsions** Nardello, V.; Herve, M.; Alsters, P. L.; Aubry, J.-M. *Adv. Synth. Catal.* **2002**, *344*, 184-191.
- (27) **Reactivity, Chemoselectivity, and Diastereoselectivity of the Oxyfunctionalization of Chiral Allylic Alcohols and Derivatives in Microemulsions: Comparison of the Chemical Oxidation by the Hydrogen Peroxide/Sodium Molybdate System with the Photooxygenation** Nardello, V.; Caron, L.; Aubry, J.-M.; Bouttemy, S.; Wirth, T.; Saha-Möller Chantou, R.; Adam, W. *J. Am. Chem. Soc.* **2004**, *126*, 10692-10700.
- (28) **A gemini amphiphilic phase transfer catalyst for dark singlet oxygenation** Borde, C.; Nardello, V.; Wattebled, L.; Laschewsky, A.; Aubry, J.-M. *J. Phys. Org. Chem.* **2008**, *21*, 652-658.
- (29) **Oxidation in Three-Liquid-Phase Microemulsion Systems Using "Balanced Catalytic Surfactants"** Nardello-Rataj, V.; Caron, L.; Borde, C.; Aubry, J.-M. *J. Am. Chem. Soc.* **2008**, *130*, 14914-14915.
- (30) **Convenient singlet oxygenation in multiphase microemulsion systems** Caron, L.; Nardello, V.; Alsters, P. L.; Aubry, J.-M. *J. Mol. Catal. A: Chem.* **2006**, *251*, 194-199.
- (31) **Counter Anion Effect on the Self-Aggregation of Dimethyl-di-N-octylammonium Cation: A Dual Behavior between Hydrotropes and Surfactants** Collinet-Fressancourt, M.; Leclercq, L.; Bauduin, P.; Aubry, J.-M.; Nardello-Rataj, V. *J. Phys. Chem. B* **2011**, *115*, 11619-11630.
- (32) **Epoxidation of olefins with hydrogen peroxide catalyzed by polyoxometalates** Mizuno, N.; Yamaguchi, K.; Kamata, K. *Coord. Chem. Rev.* **2005**, *249*, 1944-1956.
- (33) **Organic Synthesis in Water** Grieco, P. A.; Editor; Blackie, **1998**.
- (34) **Immobilized Catalysts in Industrial Research and Application** End, N.; Schöning, K.-U.; Kirschning, A., Ed.; Springer Berlin Heidelberg: **2004**; Vol. 242, p 241-271.
- (35) **Immobilised catalysts and their use in the synthesis of fine and intermediate chemicals** Holderich, W. F.; Wagner, H. H.; Valkenberg, M. H.; Sherrington, D. C., Kybett, A. P., Eds.; The Royal Society of Chemistry: **2001**, p 76-93.
- (36) **Ionic liquids: perspectives for organic and catalytic reactions** Olivier-Bourbigou, H.; Magna, L. *J. Mol. Catal. A: Chem.* **2002**, *182-183*, 419-437.
- (37) **Ionic liquids: solvent properties and organic reactivity** Chiappe, C.; Pieraccini, D. *J. Phys. Org. Chem.* **2005**, *18*, 275-297.
- (38) **Development of Novel Lewis Acid Catalysts for Selective Organic Reactions in Aqueous Media** Kobayashi, S.; Manabe, K. *Accounts of Chemical Research* **2002**, *35*, 209-217.
- (39) **Surfactant-type catalysts in organic reactions** Shiri, M.; Zolfigol, M. A. *Tetrahedron* **2009**, *65*, 587-598.
- (40) **Effects of metal cations in Lewis acid-surfactant combined catalyst-mediated aldol reactions in water** Manabe, K.; Kobayashi, S. *Synlett* **1999**, 547-548.
- (41) **Surfactant-type asymmetric organocatalyst: Organocatalytic asymmetric Michael addition to nitrostyrenes in water** Luo, S.; Mi, X.; Liu, S.; Xu, H.; Cheng, J.-P. *Chem. Commun. (Cambridge, U. K.)* **2006**, 3687-3689.
- (42) **Lewis Acids and Selectivity in Organic Synthesis** Pons, J.-M.; Santelli, M.; Editors; CRC, **1995**.
- (43) **NATO ASI Series, Ser. C: Mathematical and Physical Sciences, Vol. 289: Selectivities in Lewis Acid Promoted Reactions** Schinzer, D.; Editor; Kluwer, **1989**.
- (44) Taguchi, T.; Yanai, H.; Al(III) Lewis acids, Wiley-VCH Verlag GmbH & Co. KGaA: 2008; Vol. 1, p 241-345.
- (45) **Tin(II) compounds as synthetic control elements in organic synthesis** Mukaiyama, T. *Pure Appl. Chem.* **1986**, *58*, 505-512.
- (46) **Structural, mechanistic, and theoretical aspects of chelation-controlled carbonyl addition reactions** Reetz, M. T. *Acc. Chem. Res.* **1993**, *26*, 462-468.



- (47) **Rare earth metal trifluoromethanesulfonates as water-tolerant Lewis acid catalysts in organic synthesis** Kobayashi, S. *Synlett* **1994**, 689-701.
- (48) **Lanthanide Triflates as Water-Tolerant Lewis Acids. Activation of Commercial Formaldehyde Solution and Use in the Aldol Reaction of Silyl Enol Ethers with Aldehydes in Aqueous Media** Kobayashi, S.; Hachiya, I. *J. Org. Chem.* **1994**, *59*, 3590-3596.
- (49) **Lewis Acid Catalysts Stable in Water. Correlation between Catalytic Activity in Water and Hydrolysis Constants and Exchange Rate Constants for Substitution of Inner-Sphere Water Ligands** Kobayashi, S.; Nagayama, S.; Busujima, T. *J. Am. Chem. Soc.* **1998**, *120*, 8287-8288.
- (50) *The Hydrolysis of Cations* Baes, C. F., Jr.; Mesmer, R. E.; Wiley-Interscience, **1976**.
- (51) *ACS Monograph, No. 174: Coordination Chemistry, Vol. 2* Martell, A. E.; Editor; ACS, **1978**.
- (52) **Effects of Lewis acid-surfactant-combined catalysts on aldol and Diels-Alder reactions in water** Manabe, K.; Mori, Y.; Kobayashi, S. *Tetrahedron* **1999**, *55*, 11203-11208.
- (53) **Organic Synthesis Inside Particles in Water: Lewis Acid-Surfactant-Combined Catalysts for Organic Reactions in Water Using Colloidal Dispersions as Reaction Media** Manabe, K.; Mori, Y.; Wakabayashi, T.; Nagayama, S.; Kobayashi, S. *J. Am. Chem. Soc.* **2000**, *122*, 7202-7207.
- (54) **Lewis acid catalysis in water with a hydrophilic substrate: scandium-catalyzed hydroxymethylation with aqueous formaldehyde in water** Kokubo, M.; Ogawa, C.; Kobayashi, S. *Angew. Chem., Int. Ed.* **2008**, *47*, 6909-6911.
- (55) **Facile synthesis of  $\alpha$ -amino phosphonates in water using a Lewis acid-surfactant-combined catalyst** Manabe, K.; Kobayashi, S. *Chem. Commun. (Cambridge)* **2000**, 669-670.
- (56) **Michael reactions in water using Lewis acid-surfactant-combined catalysts** Mori, Y.; Kakumoto, K.; Manabe, K.; Kobayashi, S. *Tetrahedron Lett.* **2000**, *41*, 3107-3111.
- (57) **Catalytic asymmetric ring opening of meso-epoxides with aromatic amines in water** Azoulay, S.; Manabe, K.; Kobayashi, S. *Org. Lett.* **2005**, *7*, 4593-4595.
- (58) **Friedel-Crafts-type conjugate addition of indoles using a Lewis acid-surfactant-combined catalyst in water** Manabe, K.; Aoyama, N.; Kobayashi, S. *Adv. Synth. Catal.* **2001**, *343*, 174-176.
- (59) **Catalytic asymmetric hydroxymethylation of silicon enolates using an aqueous solution of formaldehyde with a chiral scandium complex** Ishikawa, S.; Hamada, T.; Manabe, K.; Kobayashi, S. *J. Am. Chem. Soc.* **2004**, *126*, 12236-12237.
- (60) **Asymmetric direct aldol reaction assisted by water and a proline-derived tetrazole catalyst** Torii, H.; Nakadai, M.; Ishihara, K.; Saito, S.; Yamamoto, H. *Angew. Chem., Int. Ed.* **2004**, *43*, 1983-1986.
- (61) **Friedlander synthesis of quinolines using a Lewis acid-surfactant-combined catalyst in water** Zhang, L.; Wu, J. *Adv. Synth. Catal.* **2007**, *349*, 1047-1051.
- (62) **Synthetic applications of a three-component Mannich reaction. Total synthesis of IL-6 inhibitor (+)-madindoline A and B** Hirose, T.; Sunazuka, T.; Yamamoto, D.; Kaji, E.; Omura, S. *Tetrahedron Lett.* **2006**, *47*, 6761-6764.
- (63) **Synthetic reactions using organometallics in water. Aldol and allylation reactions catalyzed by Lewis acid-surfactant-combined catalysts/Bronsted acids systems** Manabe, K.; Mori, Y.; Nagayama, S.; Odashima, K.; Kobayashi, S. *Inorg. Chim. Acta* **1999**, *296*, 158-163.
- (64) **Rare earth(III) perfluorooctanesulfonates catalyzed Friedel-Crafts alkylation in fluoruous biphasic system** Yi, W.-B.; Cai, C. *J. Fluorine Chem.* **2005**, *126*, 831-833.
- (65) **Mannich-type reactions of aromatic aldehydes, anilines, and methyl ketones in fluoruous biphasic systems created by rare earth(III) perfluorooctanesulfonate catalysts in fluoruous media** Yi, W.-B.; Cai, C. *J. Fluorine Chem.* **2006**, *127*, 1515-1521.
- (66) **Catalytic asymmetric aldol reactions in water** Kobayashi, S.; Mori, Y.; Nagayama, S.; Manabe, K. *Green Chem.* **1999**, *1*, 175-177.



- (67) **Chiral zinc(II) and copper(II)-catalyzed asymmetric ring-opening reactions of meso-epoxides with aniline and indole derivatives** Kokubo, M.; Naito, T.; Kobayashi, S. *Tetrahedron* **2010**, *66*, 1111-1118.
- (68) **Catalytic Asymmetric Synthesis of Antimalarial Alkaloids Febrifugine and Isofebrifugine and Their Biological Activity** Kobayashi, S.; Ueno, M.; Suzuki, R.; Ishitani, H.; Kim, H.-S.; Wataya, Y. *J. Org. Chem.* **1999**, *64*, 6833-6841.
- (69) **Zirconium tetrakis(dodecyl sulfate) [Zr(DS)<sub>4</sub>] as an efficient Lewis acid-surfactant combined catalyst for the synthesis of quinoxaline derivatives in aqueous media** Hasaninejad, A.; Zare, A.; Zolfigol, M. A.; Shekouhy, M. *Synth. Commun.* **2009**, *39*, 569-579.
- (70) **Highly selective and green aqueous-ionic liquid biphasic hydroxylation of benzene to phenol with hydrogen peroxide** Peng, J.; Shi, F.; Gu, Y.; Deng, Y. *Green Chem.* **2003**, *5*, 224-226.
- (71) **Dehydration Reactions in Water. Surfactant-Type Bronsted Acid-Catalyzed Direct Esterification of Carboxylic Acids with Alcohols in an Emulsion System** Manabe, K.; Sun, X.-M.; Kobayashi, S. *J. Am. Chem. Soc.* **2001**, *123*, 10101-10102.
- (72) **Mannich-Type Reactions of Aldehydes, Amines, and Ketones in a Colloidal Dispersion System Created by a Bronsted Acid-Surfactant-Combined Catalyst in Water** Manabe, K.; Kobayashi, S. *Org. Lett.* **1999**, *1*, 1965-1967.
- (73) **A highly efficient and green method for the synthesis of 3,4-dihydropyrimidin-2-ones and 1,5-benzodiazepines catalyzed by dodecyl sulfonic acid in water** Das, S. S.; Gogoi, P.; Konwar, D. *Green Chem.* **2007**, *9*, 153-157.
- (74) **DBSA catalyzed, one-pot three-component "on water" green protocol for the synthesis of 2,3-disubstituted 4-thiazolidinones** Prasad, D.; Preetam, A.; Nath, M. *RSC Adv.* **2012**, *2*, 3133-3140.
- (75) **Synthesis of tetrahydroisoquinolines and isochromans via Pictet–Spengler reactions catalyzed by Brønsted acid–surfactant-combined catalyst in aqueous media** Saito, A.; Takayama, M.; Yamazaki, A.; Numaguchi, J.; Hanzawa, Y. *Tetrahedron* **2007**, *63*, 4039-4047.
- (76) **Dehydration Reactions in Water. Bronsted Acid-Surfactant-Combined Catalyst for Ester, Ether, Thioether, and Dithioacetal Formation in Water** Manabe, K.; Iimura, S.; Sun, X.-M.; Kobayashi, S. *J. Am. Chem. Soc.* **2002**, *124*, 11971-11978.
- (77) **Three-component carbon-carbon bond-forming reactions catalyzed by a Bronsted acid-surfactant-combined catalyst in water** Manabe, K.; Mori, Y.; Kobayashi, S. *Tetrahedron* **2001**, *57*, 2537-2544.
- (78) **Synthesis and antimicrobial activity of novel 2-thiazolylimino-5-arylidene-4-thiazolidinones** Vicini, P.; Geronikaki, A.; Anastasia, K.; Incerti, M.; Zani, F. *Bioorg. Med. Chem.* **2006**, *14*, 3859-3864.
- (79) **Synthesis and Antimalarial Activity of Side Chain Modified 4-Aminoquinoline Derivatives** Solomon, V. R.; Haq, W.; Srivastava, K.; Puri, S. K.; Katti, S. B. *J. Med. Chem.* **2007**, *50*, 394-398.
- (80) **Calix[n]arene sulfonic acids bearing pendant aliphatic chains as recyclable surfactant-type Bronsted acid catalysts for allylic alkylation with allyl alcohols in water** Liu, Y.-L.; Liu, L.; Wang, Y.-L.; Han, Y.-C.; Wang, D.; Chen, Y.-J. *Green Chem.* **2008**, *10*, 635-640.
- (81) **Pictet–Spengler reactions catalyzed by Brønsted acid-surfactant-combined catalyst in water or aqueous media** Saito, A.; Numaguchi, J.; Hanzawa, Y. *Tetrahedron Lett.* **2007**, *48*, 835-839.
- (82) **Hydrophobic Polymer-Supported Catalyst for Organic Reactions in Water: Acid-Catalyzed Hydrolysis of Thioesters and Transprotection of Thiols** Iimura, S.; Manabe, K.; Kobayashi, S. *Organic Letters* **2002**, *5*, 101-103.
- (83) **Phase equilibriums of anionic surfactant mixtures in aqueous solution** Moroi, Y.; Oyama, T.; Matuura, R. *J. Colloid Interface Sci.* **1977**, *60*, 103-111.
- (84) **Mixed micelles of some metal dodecyl sulfates and triton X-100 in aqueous media** Gandhi, H.; Modi, S.; Jain, N.; Bahadur, P. *J. Surfactants Deterg.* **2001**, *4*, 359-365.
- (85) **Critical micelle concentration of multicomponent mixtures of metal alkyl sulfates in aqueous solutions. II** Moroi, Y.; Nishikido, N.; Matuura, R. *J. Colloid Interface Sci.* **1975**, *50*, 344-351.

- (86) **General patterns of the phase behavior of mixtures of water, nonpolar solvents, amphiphiles, and electrolytes.** 2 Kahlweit, M.; Strey, R.; Schomaecker, R.; Haase, D. *Langmuir* **1989**, *5*, 305-315.
- (87) **Structures of metal bis(2-ethylhexylsulfosuccinate) aggregates in cyclohexane** Eastoe, J.; Towey, T. F.; Robinson, B. H.; Williams, J.; Heenan, R. K. *J. Phys. Chem.* **1993**, *97*, 1459-1463.
- (88) **Mesostructured Fluids. 2. Microstructure and Supra-aggregation** Lisiecki, I.; Andre, P.; Filankembo, A.; Petit, C.; Tanori, J.; Gulik-Krzywicki, T.; Ninham, B. W.; Pileni, M. P. *J. Phys. Chem. B* **1999**, *103*, 9176-9189.
- (89) **Mesostructured Fluids. 1. Cu(AOT)2-H2O-Isooctane in Oil Rich Regions** Lisiecki, I.; Andre, P.; Filankembo, A.; Petit, C.; Tanori, J.; Gulik-Krzywicki, T.; Ninham, B. W.; Pileni, M. P. *J. Phys. Chem. B* **1999**, *103*, 9168-9175.
- (90) **A survey of the phases and the metastable phases in the ternary systems of divalent metal [bis-2-ethylhexyl]-sulphosuccinate/iso-octane/water** Garza, C.; Delgado, J.; Castillo, R. *J. Phys.: Condens. Matter* **2002**, *14*, 4805-4814.
- (91) **Solution chemistry of surfactants** Mittal, K. L.; Plenum Press New York, **1979**; Vol. 1.
- (92) **Rheology Theory and Applications** Frish, H.; Simha, R.; Academic Press: New York, **1956**; Vol. 1.
- (93) **Phase Diagram of Copper(II) Bis(2-ethylhexyl)sulfosuccinate, Cu(AOT)2-Isooctane-Water** Tanori, J.; Gulik-Krzywicki, T.; Pileni, M. P. *Langmuir* **1997**, *13*, 632-638.
- (94) **Catalysis by Heteropoly Acids and Multicomponent Polyoxometalates in Liquid-Phase Reactions** Kozhevnikov, I. V. *Chem. Rev. (Washington, D. C.)* **1998**, *98*, 171-198.
- (95) **Homogeneous catalysis by transition metal oxygen anion clusters** Hill, C. L.; Prosser-McCartha, C. M. *Coord. Chem. Rev.* **1995**, *143*, 407-455.
- (96) **Green Oxidation Reactions by Polyoxometalate-Based Catalysts: From Molecular to Solid Catalysts** Mizuno, N.; Kamata, K.; Yamaguchi, K. *Top. Catal.* **2010**, *53*, 876-893.
- (97) **Activation of Molecular Oxygen, Polyoxometalates, and Liquid-Phase Catalytic Oxidation** Neumann, R. *Inorg. Chem.* **2010**, *49*, 3594-3601.
- (98) **Catalytic oxidation of hydrocarbons with hydrogen peroxide by vanadium-based polyoxometalates** Mizuno, N.; Kamata, K. *Coord. Chem. Rev.* **2011**, *255*, 2358-2370.
- (99) **Liquid Phase Oxidation Reactions Catalyzed by Polyoxometalates** Neumann, R.; Wiley-VCH Verlag GmbH & Co. KGaA: **2010**, p 315-352.
- (100) **A new peroxotungsten heteropoly anion with special oxidizing properties: synthesis and structure of tetrahexylammonium tetra(diperoxotungsto)phosphate(3-)** Venturello, C.; D'Aloisio, R.; Bart, J. C. J.; Ricci, M. *J. Mol. Catal.* **1985**, *32*, 107-110.
- (101) **Hydrogen peroxide oxidation catalyzed by heteropoly acids combined with cetylpyridinium chloride. Epoxidation of olefins and allylic alcohols, ketonization of alcohols and diols, and oxidative cleavage of 1,2-diols and olefins** Ishii, Y.; Yamawaki, K.; Ura, T.; Yamada, H.; Yoshida, T.; Ogawa, M. *J. Org. Chem.* **1988**, *53*, 3587-3593.
- (102) **31P and 183W NMR Spectroscopic Evidence for Novel Peroxo Species in the "H3[PW12O40]·yH2O/H2O2" System. Synthesis and X-ray Structure of Tetrabutylammonium (μ-Hydrogen phosphato)bis(μ-peroxo)bis(oxoperoxotungstate) (2-): A Catalyst of Olefin Epoxidation in a Biphasic Medium** Salles, L.; Aubry, C.; Thouvenot, R.; Robert, F.; Doremieux-Morin, C.; Chottard, G.; Ledon, H.; Jeannin, Y.; Bregeault, J. M. *Inorg. Chem.* **1994**, *33*, 871-878.
- (103) **Studies on polyoxo- and polyperoxo-metalates. 1. Tetrameric heteropolyperoxotungstates and heteropolyperoxomolybdates** Dengel, A. C.; Griffith, W. P.; Parkin, B. C. *J. Chem. Soc., Dalton Trans.* **1993**, 2683-2688.
- (104) **Bifunctional Activation and Racemization in the Catalytic Asymmetric Aza-Baylis-Hillman Reaction** Buskens, P.; Klankermayer, J.; Leitner, W. *J. Am. Chem. Soc.* **2005**, *127*, 16762-16763.

- (105) **Ultra-deep desulfurization of diesel: Oxidation with a recoverable catalyst assembled in emulsion** Li, C.; Jiang, Z.; Gao, J.; Yang, Y.; Wang, S.; Tian, F.; Sun, F.; Sun, X.; Ying, P.; Han, C. *Chem. - Eur. J.* **2004**, *10*, 2277-2280.
- (106) **Ultra-deep desulfurization of diesel by selective oxidation with [C<sub>18</sub>H<sub>37</sub>N(CH<sub>3</sub>)<sub>3</sub>][H<sub>2</sub>NaPW<sub>10</sub>O<sub>36</sub>] catalyst assembled in emulsion droplets** Lue, H.; Gao, J.; Jiang, Z.; Jing, F.; Yang, Y.; Wang, G.; Li, C. *J. Catal.* **2006**, *239*, 369-375.
- (107) **A direct imaging of amphiphilic catalysts assembled at the interface of emulsion droplets using fluorescence microscopy** Gao, J.; Zhang, Y.; Jia, G.; Jiang, Z.; Wang, S.; Lu, H.; Song, B.; Li, C. *Chem. Commun. (Cambridge, U. K.)* **2008**, 332-334.
- (108) **The oxidation of benzothiophene using the Keggin-type lacunary polytungstophosphate as catalysts in emulsion** Zhang, Y.; Lue, H.; Wang, L.; Zhang, Y.; Liu, P.; Han, H.; Jiang, Z.; Li, C. *J. Mol. Catal. A: Chem.* **2010**, *332*, 59-64.
- (109) **Catalytic Oxidative Desulfurization of Gasoline Using Ionic Liquid Emulsion System** Ge, J.; Zhou, Y.; Yang, Y.; Xue, M. *Ind. Eng. Chem. Res.* **2011**, *50*, 13686-13692.
- (110) **Aerobic oxidative desulfurization of benzothiophene, dibenzothiophene and 4,6-dimethyldibenzothiophene using an Anderson-type catalyst [(C<sub>18</sub>H<sub>37</sub>)<sub>2</sub>N(CH<sub>3</sub>)<sub>2</sub>][IMo<sub>6</sub>O<sub>24</sub>]** Lue, H.; Zhang, Y.; Jiang, Z.; Li, C. *Green Chem.* **2010**, *12*, 1954-1958.
- (111) **Oxidative desulfurization of dibenzothiophene with dioxygen and reverse micellar peroxotitanium under mild conditions** Jiang, C.; Wang, J.; Wang, S.; Guan, H. y.; Wang, X.; Huo, M. *Appl. Catal., B* **2011**, *106*, 343-349.
- (112) **Oxidation of dibenzothiophene catalyzed by [C<sub>8</sub>H<sub>17</sub>N(CH<sub>3</sub>)<sub>3</sub>][H<sub>3</sub>V<sub>10</sub>O<sub>28</sub>] using molecular oxygen as oxidant** Tang, N.; Zhang, Y.; Lin, F.; Lue, H.; Jiang, Z.; Li, C. *Chem. Commun. (Cambridge, U. K.)* **2012**, *48*, 11647-11649.
- (113) **Catalytic wet air oxidation of phenol with air and micellar molybdovanadophosphoric polyoxometalates under room condition** Zhao, S.; Wang, X.; Huo, M. *Appl. Catal., B* **2010**, *97*, 127-134.
- (114) **The oxidation of pyridine and alcohol using the Keggin-type lacunary polytungstophosphate as a temperature-controlled phase transfer catalyst** Ding, Y.; Zhao, W. *J. Mol. Catal. A: Chem.* **2011**, *337*, 45-51.
- (115) **A Ti-substituted polyoxometalate as a heterogeneous catalyst for olefin epoxidation with aqueous hydrogen peroxide** Hua, L.; Qiao, Y.; Yu, Y.; Zhu, W.; Cao, T.; Shi, Y.; Li, H.; Feng, B.; Hou, Z. *New J. Chem.* **2011**, *35*, 1836-1841.
- (116) **A micellar polyoxoperoxometalate [C<sub>16</sub>H<sub>33</sub>N(CH<sub>3</sub>)<sub>3</sub>][PW<sub>10</sub>Ti<sub>2</sub>O<sub>38</sub>(O<sub>2</sub>)<sub>2</sub>]: A highly efficient and stable catalyst for air oxidation of thiocyanate under room conditions** Sun, C.; Zhang, C.; Li, A.; Jiang, C.; Wang, X.; Huo, M. *Catal. Commun.* **2011**, *12*, 384-387.
- (117) **Quaternary ammonium tetrakis(diperootungsto)phosphates(3-) as a new class of catalysts for efficient alkene epoxidation with hydrogen peroxide** Venturello, C.; D'Aloisio, R. *J. Org. Chem.* **1988**, *53*, 1553-1557.
- (118) **Selective oxidation of alcohols and aldehydes with hydrogen peroxide catalyzed by methyltrioctylammonium tetrakis(oxodiperootungsto)phosphate(3-) under two-phase conditions** Venturello, C.; Gambaro, M. *J. Org. Chem.* **1991**, *56*, 5924-5931.
- (119) **Efficient Oxidative Cleavage of Olefins to Carboxylic Acids with Hydrogen Peroxide Catalyzed by Methyltrioctylammonium Tetrakis(oxodiperootungsto)phosphate(3-) under Two-Phase Conditions. Synthetic Aspects and Investigation of the Reaction Course** Antonelli, E.; D'Aloisio, R.; Gambaro, M.; Fiorani, T.; Venturello, C. *J. Org. Chem.* **1998**, *63*, 7190-7206.
- (120) **Selective Oxidation of Monoterpenes with Hydrogen Peroxide Catalyzed by Peroxotungstophosphate (PCWP)** Sakaguchi, S.; Nishiyama, Y.; Ishii, Y. *J. Org. Chem.* **1996**, *61*, 5307-5311.

- (121) **Oxidation of aromatic amines with hydrogen peroxide catalyzed by cetylpyridinium heteropolyoxometalates** Sakaue, S.; Tsubakino, T.; Nishiyama, Y.; Ishii, Y. *J. Org. Chem.* **1993**, *58*, 3633-3638.
- (122) **Epoxidation-alcoholysis of cyclic enol ethers catalyzed by Ti(OiPr)<sub>4</sub> or Venturello's peroxophosphotungstate complex** Levecque, P.; Gammon, D.; Kine, H. H.; Jacobs, P.; De, V. D.; Sels, B. *Org. Biomol. Chem.* **2007**, *5*, 1800-1806.
- (123) **Environmentally friendly and highly efficient alkenes epoxidation system consisting of [π-C<sub>5</sub>H<sub>5</sub>N(CH<sub>2</sub>)<sub>11</sub>CH<sub>3</sub>]<sub>3</sub>PW<sub>4</sub>O<sub>32</sub>/H<sub>2</sub>O<sub>2</sub>/ethyl acetate/olefin** Zhao, W.; Ma, B.; Hua, H.; Zhang, Y.; Ding, Y. *Catal. Commun.* **2008**, *9*, 2455-2459.
- (124) **Deep desulfurization from fuel oil via selective oxidation using an amphiphilic peroxotungsten catalyst assembled in emulsion droplets** Gao, J.; Wang, S.; Jiang, Z.; Lu, H.; Yang, Y.; Jing, F.; Li, C. *J. Mol. Catal. A: Chem.* **2006**, *258*, 261-266.
- (125) **Oxidative desulfurization of dibenzothiophene with hydrogen peroxide catalyzed by selenium(IV)-containing peroxotungstate** Hu, Y.; He, Q.; Zhang, Z.; Ding, N.; Hu, B. *Chem. Commun. (Cambridge, U. K.)* **2011**, *47*, 12194-12196.
- (126) **Oxidative desulfurization of fuel catalyzed by metal-based surfactant-type ionic liquids** Zhu, W.; Zhu, G.; Li, H.; Chao, Y.; Chang, Y.; Chen, G.; Han, C. *J. Mol. Catal. A: Chem.* **2011**, *347*, 8-14.
- (127) **Organic Solvent- and Halide-Free Oxidation of Alcohols with Aqueous Hydrogen Peroxide** Sato, K.; Aoki, M.; Takagi, J.; Noyori, R. *J. Am. Chem. Soc.* **1997**, *119*, 12386-12387.
- (128) **A "green" route to adipic acid: direct oxidation of cyclohexenes with 30 percent hydrogen peroxide** Sato, K.; Aoki, M.; Noyori, R. *Science (Washington, D. C.)* **1998**, *281*, 1646-1647.
- (129) **A Practical Method for Epoxidation of Terminal Olefins with 30 % Hydrogen Peroxide under Halide-Free Conditions** Sato, K.; Aoki, M.; Ogawa, M.; Hashimoto, T.; Noyori, R. *J. Org. Chem.* **1996**, *61*, 8310-8311.
- (130) **A halide-free method for olefin epoxidation with 30% hydrogen peroxide** Sato, K.; Aoki, M.; Ogawa, M.; Hashimoto, T.; Panyella, D.; Noyori, R. *Bull. Chem. Soc. Jpn.* **1997**, *70*, 905-915.
- (131) **Oxidation of sulfides to sulfoxides and sulfones with 30% hydrogen peroxide under organic solvent- and halogen-free conditions** Sato, K.; Hyodo, M.; Aoki, M.; Zheng, X. Q.; Noyori, R. *Tetrahedron* **2001**, *57*, 2469-2476.
- (132) **Environmentally friendly epoxidation of olefins under phase-transfer catalysis conditions with hydrogen peroxide** Mahha, Y.; Salles, L.; Piquemal, J.-Y.; Briot, E.; Atlamsani, A.; Bregeault, J.-M. *J. Catal.* **2007**, *249*, 338-348.
- (133) **Polyfluorinated Quaternary Ammonium Salts of Polyoxometalate Anions: Fluorous Biphasic Oxidation Catalysis with and without Fluorous Solvents** Maayan, G.; Fish, R. H.; Neumann, R. *Org. Lett.* **2003**, *5*, 3547-3550.
- (134) **Polyoxometalate-Organic Hybrid Molecules as Amphiphilic Emulsion Catalysts for Deep Desulfurization** Yin, P.; Wang, J.; Xiao, Z.; Wu, P.; Wei, Y.; Liu, T. *Chem. - Eur. J.* **2012**, *18*, 9174-9178.
- (135) **Bicarbonate Surfoxidants: Micellar Oxidations of Aryl Sulfides with Bicarbonate-Activated Hydrogen Peroxide** Yao, H.; Richardson, D. E. *J. Am. Chem. Soc.* **2003**, *125*, 6211-6221.
- (136) **Oxidative desulfurization of dibenzothiophene with molecular oxygen using emulsion catalysis** Lu, H.; Gao, J.; Jiang, Z.; Yang, Y.; Song, B.; Li, C. *Chem. Commun. (Cambridge, U. K.)* **2007**, 150-152.
- (137) **Physicochemistry of bis-alkyltrimethylammonium dichromate, tungstate and molybdate amphiphiles: Synthesis, characterization, behaviors at the air-water interface and self-aggregation in aqueous medium** Mukherjee, S.; Chakraborty, M.; Panda, A. K.; Bhattacharya, S. C.; Moulik, S. P. *Colloids Surf., A* **2011**, *388*, 1-11.
- (138) **Oxidation in Three-Liquid-Phase Microemulsion Systems Using "Balanced Catalytic Surfactants"** Nardello-Rataj, V. r.; Caron, L.; Borde, C. d.; Aubry, J.-M. *J. Am. Chem. Soc.* **2008**, *130*, 14914-14915.

- (139) **Stepwise Aggregation of Dimethyl-di-n-octylammonium Chloride in Aqueous Solutions: From Dimers to Vesicles** Leclercq, L.; Nardello-Rataj, V.; Turmine, M.; Azaroual, N.; Aubry, J.-M. *Langmuir* **2010**, *26*, 1716-1723.
- (140) **Mukaiyama aldolization reactions of  $\alpha,\beta$ -epoxyaldehydes in aqueous media** Ruland, Y.; Noereuil, P.; Baltas, M. *Tetrahedron* **2005**, *61*, 8895-8903.
- (141) **Scandium trisdodecylsulfate (STDS). A new type of lewis acid that forms stable dispersion systems with organic substrates in water and accelerates aldol reactions much faster in water than in organic solvents** Kobayashi, S.; Wakabayashi, T. *Tetrahedron Lett.* **1998**, *39*, 5389-5392.
- (142) **Chiral scandium-catalyzed enantioselective ring-opening of meso-epoxides with N-heterocycle, alcohol and thiol derivatives in water** Boudou, M.; Ogawa, C.; Kobayashi, S. *Adv. Synth. Catal.* **2006**, *348*, 2585-2589.
- (143) **Scandium-catalyzed ring-opening desymmetrization of meso-epoxides** Ogawa, C.; Wang, N.; Boudou, M.; Azoulay, S.; Manabe, K.; Kobayashi, S. *Heterocycles* **2007**, *72*, 589-598.
- (144) **Chiral scandium-catalyzed enantioselective hydroxymethylation of ketones in water** Kobayashi, S.; Kokubo, M.; Kawasumi, K.; Nagano, T. *Chem. - Asian J.* **2010**, *5*, 490-492.
- (145) **Nazarov-type reactions in water** Kokubo, M.; Kobayashi, S. *Chem. - Asian J.* **2009**, *4*, 526-528.
- (146) **Catalysis in water: Synthesis of  $\beta$ -amino amides by Sc(III) promoted condensation of silylketene pyridylthioacetal and imines** Biaggi, C.; Benaglia, M.; Puglisi, A. *J. Organomet. Chem.* **2007**, *692*, 5795-5798.
- (147) **Polycondensation of Dicarboxylic Acids and Diols in Water Catalyzed by Surfactant-Combined Catalysts and Successive Chain Extension** Takasu, A.; Takemoto, A.; Hirabayashi, T. *Biomacromolecules* **2006**, *7*, 6-9.
- (148) **Metal-controlled reversal of enantioselectivity in catalyzed asymmetric ring-opening reactions of meso-epoxides in water** Kokubo, M.; Naito, T.; Kobayashi, S. *Chem. Lett.* **2009**, *38*, 904-905.
- (149) **Remarkable enhancement of reactivity by Brønsted acids in aldol reactions mediated by Lewis acid-surfactant-combined catalysts in water** Manabe, K.; Kobayashi, S. *Tetrahedron Lett.* **1999**, *40*, 3773-3776.
- (150) **Scandium perfluoroalkanesulfonate-catalyzed Diels-Alder reactions in an organic solvent** Kobayashi, S.; Tsuchiya, T.; Komoto, I.; Matsuo, J. *J. Organomet. Chem.* **2001**, *624*, 392-394.
- (151) **A novel ytterbium/perfluoroalkylated-pyridine catalyst for Baylis-Hillman reactions in a fluororous biphasic system** Yi, W.-B.; Cai, C.; Wang, X. *J. Fluorine Chem.* **2007**, *128*, 919-924.
- (152) **Mannich-type reaction of (1-methoxy-2-methylpropenyloxy)trimethylsilane with arylaldehydes and aromatic amines catalyzed by perfluorinated rare earth metal salts in fluororous phase** Shi, M.; Cui, S.-C.; Liu, Y.-H. *Tetrahedron* **2005**, *61*, 4965-4970.
- (153) **Heterogeneous catalysis of novel polymeric rare earth complexes under solvent-free conditions: Zero-emission synthesis of  $\beta$ -amino alcohols** Ishida, S.; Suzuki, S.; Hayano, T.; Furuno, H.; Inanaga, J. *J. Alloys Compd.* **2006**, *408-412*, 441-443.
- (154) **Aldol condensations of aldehydes and ketones catalyzed by rare earth(III) perfluorooctane sulfonates in fluororous solvents** Yi, W.-B.; Cai, C. *J. Fluorine Chem.* **2005**, *126*, 1553-1558.
- (155) **Friedel-Crafts reaction catalyzed by perfluorinated rare earth metals** Shi, M.; Cui, S.-C. *J. Fluorine Chem.* **2002**, *116*, 143-147.
- (156) **Aza-Diels-Alder reaction catalyzed by perfluorinated metal salts in fluororous phase** Shi, M.; Cui, S.-C. *New J. Chem.* **2004**, *28*, 1286-1288.
- (157) **Scandium(III) perfluorooctanesulfonate [Sc(OPf)<sub>3</sub>]: a novel catalyst for the hetero Diels-Alder reaction of aldehydes with non-activated dienes** Hanamoto, T.; Sugimoto, Y.; Jin, Y. Z.; Inanaga, J. *Bull. Chem. Soc. Jpn.* **1997**, *70*, 1421-1426.
- (158) **Perfluorinated rare earth metals catalyzed nitration of aromatic compounds** Shi, M.; Cui, S.-C. *J. Fluorine Chem.* **2002**, *113*, 207-209.

- (159) Lewis acid catalyzed reactions of methylenecyclopropylcarbinols with acetals for the construction of 3-oxabicyclo[3.1.0]hexane derivatives Shao, L.-X.; Shi, M. *Tetrahedron* **2010**, *66*, 4551-4554.
- (160) Lewis acid-catalyzed Prins-type reactions of methylenecyclopropylcarbinols with aldehydes and aldimines Shao, L.-X.; Qi, M.-H.; Shi, M. *Tetrahedron Lett.* **2008**, *49*, 165-168.
- (161) Controlled Ring-Opening Polymerization of  $\epsilon$ -Caprolactone Catalyzed by Rare-Earth Perfluoroalkanesulfonates and Perfluoroalkanesulfonylimides Oshimura, M.; Takasu, A. *Macromolecules (Washington, DC, U. S.)* **2010**, *43*, 2283-2290.
- (162) Polyester synthesis at moderate temperatures via the direct polycondensation of dicarboxylic acids and diols catalyzed by rare-earth perfluoroalkanesulfonates and bis(perfluoroalkanesulfonyl)imides Takasu, A.; Makino, T.; Yamada, S. *Macromolecules (Washington, DC, U. S.)* **2010**, *43*, 144-149.
- (163) Million-fold acceleration of a Diels-Alder reaction due to combined Lewis acid and micellar catalysis in water Otto, S.; Engberts, J. B. F. N.; Kwak, J. C. T. *J. Am. Chem. Soc.* **1998**, *120*, 9517-9525.
- (164) Chemoselective (trans)thioacetalization of carbonyl compounds with a reusable Lewis acid-surfactant-combined copper bis(dodecyl sulfate) catalyst in water Weng, S.-S.; Chang, S.-C.; Chang, T.-H.; Chyn, J.-P.; Lee, S.-W.; Lin, C.-A.; Chen, F.-k. *Synthesis* **2010**, 1493-1499.
- (165) Lanthanide-surfactant-combined catalysts for the allylation of benzaldehyde with tetraallyltin in aqueous solutions Deleersnyder, K.; Shi, D.; Binnemans, K.; Parac-Vogt, T. N. *J. Alloys Compd.* **2008**, *451*, 418-421.
- (166) An efficient and expeditious synthesis of phytostanyl esters in a solvent-free system Zhou, Y.; Jia, C.; Li, R.; Zhang, X.; He, W.; Li, J.; Feng, B.; Xia, Q. *Eur. J. Lipid Sci. Technol.* **2012**, *114*, 896-904.
- (167) Highly selective oxidation of benzyl alcohol to benzaldehyde with hydrogen peroxide by biphasic catalysis Yu, Y.; Lu, B.; Wang, X.; Zhao, J.; Wang, X.; Cai, Q. *Chem. Eng. J. (Amsterdam, Neth.)* **2010**, *162*, 738-742.
- (168) An Environmentally Benign Catalytic Method for Efficient and Selective Nucleophilic Ring Opening of Oxiranes by Zirconium Tetrakis(dodecyl Sulfate) Jafarpour, M.; Rezaeifard, A.; Aliabadi, M. *Helv. Chim. Acta* **2010**, *93*, 405-413.
- (169) Zirconium tetrakis(dodecylsulfate) as an efficient and recyclable lewis acid-surfactant-combined catalyzed C-C and C-N bond forming under mild and environmentally benign conditions Jafarpour, M.; Rezaeifard, A.; Aliabadi, M. *Lett. Org. Chem.* **2009**, *6*, 94-99.
- (170) A new catalytic method for the preparation of bis-indolyl- and tris-indolylmethanes in aqueous media Zolfigol, M. A.; Salehi, P.; Shiri, M.; Tanbakouchian, Z. *Catal. Commun.* **2006**, *8*, 173-178.
- (171) An eco-friendly procedure for the synthesis of polysubstituted quinolines under aqueous media Zolfigol, M. A.; Salehi, P.; Ghaderi, A.; Shiri, M.; Tanbakouchian, Z. *J. Mol. Catal. A: Chem.* **2006**, *259*, 253-258.
- (172) One-pot production of 5-hydroxymethylfurfural with high yield from cellulose by a Bronsted acid-Lewis acid-surfactant-combined heteropoly acid catalyst Zhao, S.; Cheng, M.; Li, J.; Tian, J.; Wang, X. *Chem. Commun. (Cambridge, U. K.)* **2011**, *47*, 2176-2178.
- (173) Fe(DS)<sub>3</sub>, an efficient Lewis acid-surfactant-combined catalyst (LASC) for the one pot synthesis of chromeno[4,3-b]chromene derivatives by assembling the basic building blocks Pradhan, K.; Paul, S.; Das, A. R. *Tetrahedron Lett.* **2013**, *54*, 3105-3110.
- (174) Indium tris(dodecyl sulfonate) [In(DS)<sub>3</sub>]-catalyzed formation of 3-(9H-xanthen-9-yl)-1H-indole derivatives in water at room temperature Wang, S.-Y.; Ji, S.-J. *Synth. Commun.* **2008**, *38*, 465-472.
- (175) Facile synthesis of bis(indolyl)methanes catalyzed by ferric dodecyl sulfonate [Fe(DS)<sub>3</sub>] in water at room temperature Wang, S.-Y.; Ji, S.-J. *Synth. Commun.* **2008**, *38*, 1291-1298.
- (176) A novel micro-emulsion catalytic system for highly selective hydroxylation of benzene to phenol with hydrogen peroxide Liu, H.; Fu, Z.; Yin, D.; Yin, D.; Liao, H. *Catal. Commun.* **2005**, *6*, 638-643.

- (177) **Rare earth(III) perfluorooctane sulfonates and perfluorooctanesulfonic acid in fluorous solvents. Novel and recyclable catalytic systems for Friedel-Crafts acylation of unactivated benzenes** Yi, W.-B.; Cai, C. *J. Fluorine Chem.* **2005**, *126*, 1191-1195.
- (178) **A Bronsted acid-surfactant-combined catalyst for Mannich-type reactions of aldehydes, amines, and silyl enolates in water** Manabe, K.; Mori, Y.; Kobayashi, S. *Synlett* **1999**, 1401-1402.
- (179) **The esterification in cyclohexane/DBSA/water microemulsion system** Jing, L.; Li, X. J.; Han, Y. C.; Chu, Y. *Colloids Surf., A* **2008**, *326*, 37-41.
- (180) **Chemoselective Thioacetalization in Water: 3-(1,3-Dithian-2-ylidene)pentane- 2,4-dione as an Odorless, Efficient, and Practical Thioacetalization Reagent** Dong, D.; Ouyang, Y.; Yu, H.; Liu, Q.; Liu, J.; Wang, M.; Zhu, J. *J. Org. Chem.* **2005**, *70*, 4535-4537.
- (181) **Solvent-free esterification catalyzed by surfactant-combined catalysts at room temperature** Gang, L.; Xinzong, L.; Eli, W. *New J. Chem.* **2007**, *31*, 348-351.
- (182) **Surfactant-Type Bronsted Acid Catalyzed Dehydrative Nucleophilic Substitutions of Alcohols in Water** Shirakawa, S.; Kobayashi, S. *Org. Lett.* **2007**, *9*, 311-314.
- (183) **Micelle promoted supramolecular carbohydrate scaffold-catalyzed multicomponent synthesis of 1,2-dihydro-1-aryl-3H-naphth[1,2-e][1,3]oxazin-3-one and amidoalkyl naphthols derivatives in aqueous medium** Kumar, A.; Gupta, M. K.; Kumar, M. *RSC Adv.* **2012**, *2*, 7371-7376.
- (184) **Mannich-type reactions in water using a hydrophobic polymer-supported sulfonic acid catalyst** Imura, S.; Nobutou, D.; Manabe, K.; Kobayashi, S. *Chem. Commun.* **2003**, 1644-1645.
- (185) **Deep desulfurization of fuels catalyzed by surfactant-type decatungstates using H<sub>2</sub>O<sub>2</sub> as oxidant** Jiang, X.; Li, H.; Zhu, W.; He, L.; Shu, H.; Lu, J. *Fuel* **2009**, *88*, 431-436.
- (186) **Efficient oxidation of sulfides catalyzed by a temperature-responsive phase transfer catalyst [(C<sub>18</sub>H<sub>37</sub>)<sub>2</sub>(CH<sub>3</sub>)<sub>2</sub>N]<sup>7+</sup> PW11O<sub>39</sub> with hydrogen peroxide** Xue, X.; Zhao, W.; Ma, B.; Ding, Y. *Catal. Commun.* **2012**, *29*, 73-76.
- (187) **The oxidation of pyridines catalyzed by surfactant-encapsulated polyoxometalate [(C<sub>18</sub>H<sub>37</sub>)<sub>2</sub>(CH<sub>3</sub>)<sub>2</sub>N]<sup>8+</sup>[HBW11O<sub>39</sub>] with the temperature-responsive property of solubility** Zhao, W.; Yang, C.; Ding, Y.; Ma, B. *New J. Chem.* **2013**, *37*, 2614-2618.
- (188) **Secondary alcohols oxidation with hydrogen peroxide catalyzed by [n-C<sub>16</sub>H<sub>33</sub>N(CH<sub>3</sub>)<sub>3</sub>]<sup>3+</sup>PW12O<sub>40</sub>: Transform-and-retransform process between catalytic precursor and catalytic activity species** Zhang, S.; Zhao, G.; Gao, S.; Xi, Z.; Xu, J. *J. Mol. Catal. A: Chem.* **2008**, *289*, 22-27.
- (189) **Clean production of glucose from polysaccharides using a micellar heteropolyacid as a heterogeneous catalyst** Cheng, M.; Shi, T.; Guan, H.; Wang, S.; Wang, X.; Jiang, Z. *Appl. Catal., B* **2011**, *107*, 104-109.
- (190) **A direct conversion of vic-diols into 1,2-diketones with aqueous hydrogen peroxide catalyzed by peroxotungstophosphate (PCWP)** Iwahama, T.; Sakaguchi, S.; Nishiyama, Y.; Ishii, Y. *Tetrahedron Lett.* **1995**, *36*, 1523-1526.
- (191) **Recovery of homogeneous polyoxometalate catalysts from aqueous and organic media by a mesoporous ceramic membrane without loss of catalytic activity** Chowdhury, S. R.; Witte, P. T.; Blank, D. H. A.; Alsters, P. L.; ten, E. J. E. *Chem. - Eur. J.* **2006**, *12*, 3061-3066.
- (192) **Novel two-phase catalysis with organometallic compounds for epoxidation of vegetable oils by hydrogen peroxide** Jiang, P.-P.; Chen, M.; Dong, Y.-M.; Lu, Y.; Ye, X.; Zhang, W.-J. *J. Am. Oil Chem. Soc.* **2010**, *87*, 83-91.
- (193) **Highly efficient and selective oxidation of various substrates under mild conditions using a lanthanum-containing polyoxometalate as catalyst** Zhao, S.; Jia, Y.; Song, Y.-F. *Appl. Catal., A* **2013**, *453*, 188-194.
- (194) **Polyoxometalate-based protic alkylimidazolium salts as reaction-induced phase-separation catalysts for olefin epoxidation** Qiao, Y.; Hou, Z.; Li, H.; Hu, Y.; Feng, B.; Wang, X.; Hua, L.; Huang, Q. *Green Chemistry* **2009**, *11*, 1955-1960.

- (195) **Polyoxometalate-Based Amphiphilic Catalysts for Selective Oxidation of Benzyl Alcohol with Hydrogen Peroxide under Organic Solvent-Free Conditions** Jing, L.; Shi, J.; Zhang, F.; Zhong, Y.; Zhu, W. *Ind. Eng. Chem. Res.* **2013**, *52*, 10095-10104.
- (196) **One-step aerobic oxidation of cyclohexane to adipic acid using an Anderson-type catalyst [(C18H37)2N(CH3)2]6Mo7O24** Lu, H.; Ren, W.; Liu, P.; Qi, S.; Wang, W.; Feng, Y.; Sun, F.; Wang, Y. *Appl. Catal., A* **2012**, *441-442*, 136-141.
- (197) **A Bronsted-Lewis-surfactant-combined heteropolyacid as an environmental benign catalyst for esterification reaction** Zhao, J.; Guan, H.; Shi, W.; Cheng, M.; Wang, X.; Li, S. *Catal. Commun.* **2012**, *20*, 103-106.
- (198) *Market Report: World Surfactant Market, Acmite Market Intelligence* **2010**.
- (199) **Cationic Vesicles as Bactericides** Martins, L. M. S.; Mamizuka, E. M.; Carmona-Ribeiro, A. M. *Langmuir* **1997**, *13*, 5583-5587.
- (200) **Interactions between Cationic Vesicles and Candida albicans** Campanha, M. T. N.; Mamizuka, E. M.; Carmona-Ribeiro, A. M. *J. Phys. Chem. B* **2001**, *105*, 8230-8236.
- (201) **Interactions between dialkyldimethylammonium bromides (DXDAB) and sterols-a monolayer study** Hac-Wydro, K.; Wydro, P.; Dynarowicz-Latka, P. *J. Colloid Interface Sci.* **2005**, *286*, 504-510.
- (202) **Property modifications of finished textiles by a cationic surfactant** Beal, C. M.; Olson, L. A.; Wentz, M. *J. Am. Oil Chem. Soc.* **1990**, *67*, 689-697.
- (203) **Effect of chain length on physicochemical properties and cytotoxicity of cationic vesicles composed of phosphatidylcholines and dialkyldimethylammonium bromides** Liang, C.-H.; Chou, T.-H. *Chem. Phys. Lipids* **2009**, *158*, 81-90.
- (204) *Surfactant Science Series, Vol. 34: Cationic Surfactants* Richmond, J. M.; Editor; Dekker, **1990**.
- (205) Israelachvili, J. N. *Intermolecular and Surface Forces, 2nd ed, Academic Press, San Diego* **1992**.
- (206) **Classification of terpene oils using the fish diagrams and the Equivalent Alkane Carbon (EACN) scale** Bouton, F.; Durand, M.; Nardello-Rataj, V.; Serry, M.; Aubry, J.-M. *Colloids Surf., A* **2009**, *338*, 142-147.
- (207) **90Mo NMR and kinetic studies of peroxomolybdic intermediates involved in the catalytic disproportionation of hydrogen peroxide by molybdate ions** Nardello, V.; Marko, J.; Vermeersch, G.; Aubry, J. M. *Inorg. Chem.* **1995**, *34*, 4950-4957.
- (208) **183W NMR Study of Peroxotungstates Involved in the Disproportionation of Hydrogen Peroxide into Singlet Oxygen (1O2, 1Ag) Catalyzed by Sodium Tungstate in Neutral and Alkaline Water** Nardello, V.; Marko, J.; Vermeersch, G.; Aubry, J. M. *Inorg. Chem.* **1998**, *37*, 5418-5423.
- (209) **Olefin oxidation by the system H2O2MoO2-4: competition between epoxidation and peroxidation** Nardello, V.; Bouttemy, S.; Aubry, J.-M. *J. Mol. Catal. A: Chem.* **1997**, *117*, 439-447.
- (210) **Aqueous mixtures of di-n-decyldimethylammonium chloride/polyoxyethylene alkyl ether: Dramatic influence of tail/tail and head/head interactions on co-micellization and biocidal activity** Rauwel, G.; Leclercq, L.; Criquelion, J.; Aubry, J.-M.; Nardello-Rataj, V. *J. Colloid Interface Sci.* **2012**, *374*, 176-186.
- (211) **Mixed vesicles and mixed micelles of the cationic-cationic surfactant system: Didecyldimethylammonium bromide/dodecylethyldimethylammonium bromide/water** del Burgo, P.; Aicart, E.; Junquera, E. *Colloids Surf., A* **2007**, *292*, 165-172.
- (212) **Properties of Dilute Aqueous Solutions of Double-Chain Surfactants, Alkyldodecyldimethylammonium Bromides with a Change in the Length of the Alkyl Chains** Hiramatsu, K.; Kameyama, K.; Ishiguro, R.; Mori, M.; Hayase, H. *Bull. Chem. Soc. Jpn.* **2003**, *76*, 1903-1910.
- (213) **Interfaces and the driving force of hydrophobic assembly** Chandler, D. *Nature* **2005**, *437*, 640-647.
- (214) *The Hydrophobic Effect: Formation of Micelles and Biological Membranes 2d Ed* Tanford, C.; J. Wiley., **1980**.
- (215) *The Aqueous Phase Behaviour of Surfactants* Laughlin, R. G.; Academic Press Inc., **1996**.



- (216) **The microscopy of the liquid crystalline neat and middle phases of soaps and synthetic detergents** Rosevear, F. B. *J. Am. Oil Chem. Soc.* **1954**, *31*, 628-639.
- (217) **A model for the chains in amphiphilic aggregates. 1. Comparison with a molecular dynamics simulation of a bilayer** Gruen, D. W. R. *J. Phys. Chem.* **1985**, *89*, 146-153.
- (218) **Microemulsion formation and phase behavior of dialkyldimethylammonium bromide surfactants** Warr, G. G.; Sen, R.; Evans, D. F.; Trend, J. E. *J. Phys. Chem.* **1988**, *92*, 774-783.
- (219) **Solution behavior of dialkyldimethylammonium chloride in water. Basic properties of antistatic fabric softeners** Kunieda, H.; Shinoda, K. *J. Phys. Chem.* **1978**, *82*, 1710-1714.
- (220) **Some observations on phase diagrams and structure in binary and ternary systems of didodecyldimethylammonium bromide** Fontell, K.; Ceglie, A.; Lindman, B.; Ninham, B. *Acta Chem. Scand.* **1986**, *40*, 247-256.
- (221) **Phase behavior and scattering of double-chain surfactants in diluted aqueous solutions** Dubois, M.; Zemb, T. *Langmuir* **1991**, *7*, 1352-1360.
- (222) **Small Angle X-ray Scattering** Glatter, O.; Kratky, O.; Editors; Academic Press, **1982**.
- (223) **Small-angle X-ray diffraction study of the thermotropic and lyotropic phases of five alkyl cyclic and acyclic disaccharides: influence of the linkage between the hydrophilic and hydrophobic moieties** Auvray, X.; Petipas, C.; Dupuy, C.; Louvet, S.; Anthore, R.; Rico-Lattes, I.; Lattes, A. *Eur. Phys. J. E* **2001**, *4*, 489-504.
- (224) **Long-Living Intermediates during a Lamellar to a Diamond-Cubic Lipid Phase Transition: A Small-Angle X-Ray Scattering Investigation** Angelov, B.; Angelova, A.; Vainio, U.; Garamus, V. M.; Lesieur, S.; Willumeit, R.; Couvreur, P. *Langmuir* **2009**, *25*, 3734-3742.
- (225) **An efficient method to determine isothermal ternary phase diagrams using small-angle x-ray scattering** Ricoul, F.; Dubois, M.; Zemb, T.; Heck, M.-P.; Vandais, A.; Plusquellec, D.; Rico-Lattes, I.; Diat, O. *J. Phys. Chem. B* **1998**, *102*, 2769-2775.
- (226) **Soft matter physics: an introduction** Laverntovich, O. D.; Springer, **2003**.
- (227) **Characterization of the Lamellar Phase Aerosol OT/Water System by NMR Diffusion Measurements** Coppola, L.; Muzzalupo, R.; Ranieri, G. A.; Terenzi, M. *Langmuir* **1995**, *11*, 1116-1121.
- (228) **Frontiers in Colloid Science** Fontell, K.; Steinkopff, **1983**; Vol. 68.
- (229) **Trends in Colloid and Interface Science IV** Seddon, J. M.; Hogan, J. L.; Warrender, N. A.; Pebay-Peyroula, E.; Steinkopff, **1990**; Vol. 81.
- (230) **Ordered 2-D and 3-D nanostructured amphiphile self-assembly materials stable in excess solvent** Kaasgaard, T.; Drummond, C. J. *Phys. Chem. Chem. Phys.* **2006**, *8*, 4957-4975.
- (231) **Minimal surfaces and structures: from inorganic and metal crystals to cell membranes and biopolymers** Andersson, S.; Hyde, S. T.; Larsson, K.; Lidin, S. *Chem. Rev.* **1988**, *88*, 221-242.
- (232) **Periodic minimal surface structures in bicontinuous lipid-water phases and nanoparticles** Larsson, K.; Tiberg, F. *Curr. Opin. Colloid Interface Sci.* **2005**, *9*, 365-369.
- (233) **Geometry of interfaces: topological complexity in biology and materials** Hyde, S. T.; Schröder-Turk, G. E. *Interface Focus* **2012**, *2*, 529-538.
- (234) **Electrical double layer forces. A Monte Carlo study** Guldbbrand, L.; Jönsson, B.; Wennerström, H.; Linse, P. *J. Phys. Chem.* **1984**, *80*, 2221-2228.
- (235) **Handbook of applied surface and colloid chemistry** Holmberg, K.; Shah, D. O.; Schwuger, M. J.; Wiley Chichester, **2002**; Vol. 1.
- (236) **Phase equilibria and structures in ternary systems of a cationic surfactant (C16 TABr or (C16 TA)2SO4), alcohol, and water** Fontell, K.; Khan, A.; Lindström, B.; Maciejewska, D.; Puang-Ngern, S. *Colloid Polym Sci* **1991**, *269*, 727-742.
- (237) **Ion Properties** Marcus, Y.; Dekker, **1997**.

- (238) **Transparent water-in-oil dispersions: the oleopathic hydro-micelle** Hoar, T.; Schulman, J. *Nature* **1943**, *152*, 102-103.
- (239) **Solvent Properties of Amphiphilic Compounds** Winsor, P. A.; Butterworths Sci. Pubs., **1954**.
- (240) **Phase behavior of ternary systems of the type water-oil-nonionic amphiphiles (microemulsions)** Kahlweit, M.; Strey, R. *Angew. Chem.* **1985**, *97*, 655-669.
- (241) **The microemulsion concept in nonpolar surfactant solutions** Eicke, H. F.; Plenum, **1982**.
- (242) **Phase behavior of quinary mixtures of the type water-oil-nonionic amphiphile-ionic amphiphile-salt** Kahlweit, M.; Strey, R. *J. Phys. Chem.* **1988**, *92*, 1557-1563.
- (243) **Partitioning of ethoxylated alkylphenol surfactants in microemulsion-oil-water systems** Marquez, N.; Anton, R.; Graciaa, A.; Lachaise, J.; Salager, J.-L. *Colloids Surf., A* **1995**, *100*, 225-231.
- (244) **Surfactant Science Series Vol. 30** Bourrel, M.; Schechter, R. S.; Marcel Dekker, Inc, **1988**.
- (245) **Microemulsifying polar oils** Wormuth, K. R.; Kaler, E. W. *J. Phys. Chem.* **1989**, *93*, 4855-4861.
- (246) **Partitioning of Ethoxylated Alkylphenol Surfactants in Microemulsion-Oil-Water Systems: Influence of Physicochemical Formulation Variables** Marquez, N.; Graciaa, A.; Lachaise, J.; Salager, J.-L. *Langmuir* **2002**, *18*, 6021-6024.
- (247) **Modeling crude oils for low interfacial tension** Cayias, J.; Schechter, R.; Wade, W. *Soc. Petrol. Eng. J.* **1976**, *16*, 351-357.
- (248) **The EACN scale for oil classification revisited thanks to fish diagrams** Queste, S.; Salager, J. L.; Strey, R.; Aubry, J. M. *J. Colloid Interface Sci.* **2007**, *312*, 98-107.
- (249) **Classification of ester oils according to their Equivalent Alkane Carbon Number (EACN) and asymmetry of fish diagrams of C10E4/ester oil/water systems** Ontiveros, J. F.; Pierlot, C.; Catte, M.; Molinier, V.; Pizzino, A.; Salager, J.-L.; Aubry, J.-M. *J. Colloid Interface Sci.* **2013**, *403*, 67-76.
- (250) **Low interfacial tensions involving mixtures of surfactants** Wade, W. H.; Morgan, J.; Jacobson, J.; Schechter, R. *Soc. Petrol. Eng. J.* **1977**, *17*, 122-128.
- (251) **Classement absolu des huiles et des amphiphiles par la méthode de la formulation optimale** Queste, S.; Thèse de Université Lille 1, **2006**.
- (252) **The Lifshitz line in binary systems: structures in water/C4E1 mixtures** Koehler, R. D.; Schubert, K. V.; Strey, R.; Kaler, E. W. *J. Chem. Phys.* **1994**, *101*, 10843-10849.
- (253) **Specific ion effects** Kunz, W.; World Scientific, **2010**.
- (254) **Hofmeister anion effects on surfactant self-assembly and the formation of mesoporous solids** Leontidis, E. *Curr. Opin. Colloid Interface Sci.* **2002**, *7*, 81-91.
- (255) **The Hofmeister effect and the behavior of water at interfaces** Collins, K. D.; Washabaugh, M. W. *Q. Rev. Biophys.* **1985**, *18*, 323-422.
- (256) **Applied Surfactants: Principles and Applications** Tadros, T. F.; John Wiley & Sons, **2005**.
- (257) **Multidimensional multinuclear solution NMR studies of encapsulated macromolecules** Flynn, P. F. *Prog. Nucl. Magn. Reson. Spect.* **2004**, *45*, 31-51.
- (258) **Controlled-release preparations for biologically active materials** Engstroem, S.; Larsson, K.; Lindman, B. **1984**, *25*.
- (259) **Epithelial transport of drugs in cell culture. VII: effects of pharmaceutical surfactant excipients and bile acids on transepithelial permeability in monolayers of human intestinal epithelial (Caco-2) cells** Anderberg, E. K.; Nystroem, C.; Artursson, P. *J. Pharm. Sci.* **1992**, *81*, 879-887.
- (260) **Pharmaceutical excipient comprising microcrystalline cellulose and anionic surfactant with improved compressibility** Staniforth, J. N.; Sherwood, B. E.; Hunter, E. A. *U.S. 5585115* **1998**, *17*
- (261) **Variation of some micellar and interfacial properties with increasing branching for anionic and cationic surfactants** Dusart, O. *Fluid Phase Equilib.* **1985**, *20*, 265-268.
- (262) **Interfacial tension and surfactant distribution in water-oil-sodium chloride systems containing double-tailed sulfonates** Granet, R.; Khadirian, R. D.; Piekarski, S. *Colloids Surf.* **1990**, *49*, 199-209.

- (263) **Synthesis and characterization of novel low-bandgap triphenylamine-based conjugated polymers with main-chain donors and pendent acceptors for organic photovoltaics** Sahu, D.; Padhy, H.; Patra, D.; Huang, J.-h.; Chu, C.-w.; Lin, H.-C. *J. Polym. Sci., Part A: Polym. Chem.* **2010**, *48*, 5812-5823.
- (264) **Foldamers as Reactive Sieves: Reactivity as a Probe of Conformational Flexibility** Smaldone, R. A.; Moore, J. S. *J. Am. Chem. Soc.* **2007**, *129*, 5444-5450.
- (265) **Free-energy changes on transfer of surface-active agents between various colloidal and interfacial states** Lin, I. J.; Somasundaran, P. *J. Colloid Interface Sci.* **1971**, *37*, 731-743.
- (266) **Dynamic hydration numbers for biologically important ions** Kiriukhin, M. Y.; Collins, K. D. *Biophys. Chem.* **2002**, *99*, 155-168.
- (267) **Revised effective ionic radii and systematic studies of interatomic distances in halides and chalcogenides** Shannon, R. *Acta Cryst. Sect. A* **1976**, *32*, 751-767.
- (268) **Metal Ions in Solution** Burgess, J.; Wiley, **1978**.
- (269) **Phase Behavior of Ternary Systems of the Type H<sub>2</sub>O/Oil/Nonionic Amphiphile (Microemulsions)** Kahlweit, M.; Strey, R. *Angew. Chem. Int. Ed.* **1985**, *24*, 654-668.
- (270) **Positional Isomers of Linear Sodium Dodecyl Benzene Sulfonate: Solubility, Self-Assembly, and Air/Water Interfacial Activity** Ma, J.-G.; Boyd, B. J.; Drummond, C. J. *Langmuir* **2006**, *22*, 8646-8654.
- (271) **Optically positive, isotropic, and negative lamellar liquid crystalline solutions** Rogers, J.; Winsor, P. A. *Nature (London)* **1967**, *216*, 477-479.
- (272) **Structure and dynamics in three-component microemulsions** Blum, F. D.; Pickup, S.; Ninham, B.; Chen, S. J.; Evans, D. F. *J. Phys. Chem.* **1985**, *89*, 711-713.
- (273) **Synthesis and biological evaluation of galactofuranosyl alkyl thioglycosides as inhibitors of mycobacteria** Davis, C. B.; Hartnell, R. D.; Madge, P. D.; Owen, D. J.; Thomson, R. J.; Chong, A. K. J.; Coppel, R. L.; Itzstein, M. v. *Carb. Res.* **2007**, *342*, 1773-1780.
- (274) **Microemulsion method: A novel route to synthesize organic and inorganic nanomaterials: 1st Nano Update** Malik, M. A.; Wani, M. Y.; Hashim, M. A. *Arab. J. Chem.* **2012**, *5*, 397-417.
- (275) **Preparation of catalysts from microemulsions and their applications in heterogeneous catalysis** Eriksson, S.; Nysten, U.; Rojas, S.; Boutonnet, M. *Appl. Catal., A* **2004**, *265*, 207-219.
- (276) **Esterification reactions catalyzed by lipases in microemulsions: the role of enzyme localization in relation to its selectivity** Stamatis, H.; Xenakis, A.; Provelegiou, M.; Kolisis, F. N. *Biotechnol. Bioeng.* **1993**, *42*, 103-110.
- (277) **Enantioselective synthesis of ibuprofen esters in AOT/isooctane microemulsions by Candida cylindracea lipase** Hedstrom, G.; Backlund, M.; Slotte, J. P. *Biotechnol. Bioeng.* **1993**, *42*, 618-624.
- (278) **Lipase-catalyzed reactions at interfaces of two-phase systems and microemulsions** Reis, P.; Miller, R.; Leser, M.; Watzke, H. *Appl. Biochem. Biotechnol.* **2009**, *158*, 706-721.
- (279) **Synthesis of cadmium sulfide in situ in reverse micelles. 2. Influence of the interface on the growth of the particles** Petit, C.; Lixon, P.; Pileni, M. P. *J. Phys. Chem.* **1990**, *94*, 1598-1603.
- (280) **Formation of PbS nanoclusters using reversed micelles of lead and sodium Aerosol-OT** Eastoe, J.; Cox, A. R. *Colloids Surf., A* **1995**, *101*, 63-76.
- (281) **Fabrication of Hollow Polystyrene Nanospheres in Microemulsion Polymerization Using Triblock Copolymers** Jang, J.; Ha, H. *Langmuir* **2002**, *18*, 5613-5618.
- (282) **Dark singlet oxygenation of organic substrates in single-phase and multiphase microemulsion systems** Aubry, J.-M.; Adam, W.; Alsters, P. L.; Borde, C.; Queste, S.; Marko, J.; Nardello, V. *Tetrahedron* **2006**, *62*, 10753-10761.
- (283) **Studies on transition metal peroxo complexes. Part 8. The nature of peroxomolybdates and peroxotungstates in aqueous solution** Campbell, N. J.; Dengel, A. C.; Edwards, C. J.; Griffith, W. P. *J. Chem. Soc., Dalton Trans.* **1989**, 1203-1208.

- (284) **Epoxides of the Secondary Side of Cyclodextrins** Khan, A. R.; Barton, L.; D'Souza, V. T. *J. Org. Chem.* **1996**, *61*, 8301-8303.
- (285) **Optimization of Composition of a Directly Combined Catalyst in Dibenzothiophene Oxidation for Deep Desulfurization** Huang, D.; Zhai, Z.; Lu, Y. C.; Yang, L. M.; Luo, G. S. *Ind. Eng. Chem. Res.* **2007**, *46*, 1447-1451.
- (286) **Reinvestigation of epoxidation using tungsten-based precursors and hydrogen peroxide in a biphasic medium** Aubry, C.; Chottard, G.; Platzer, N.; Bregeault, J. M.; Thouvenot, R.; Chauveau, F.; Huet, C.; Ledon, H. *Inorg. Chem.* **1991**, *30*, 4409-4415.
- (287) **Hydrothermal synthesis of polyoxotungstate clusters, surface-modified with M(II)-organonitrogen subunits** Devi, R. N.; Burkholder, E.; Zubieta, J. *Inorg. Chim. Acta* **2003**, *348*, 150-156.
- (288) **A catalytic, environmentally benign method for the epoxidation of unsaturated terpenes with hydrogen peroxide** Grigoropoulou, G.; Clark, J. H. *Tetrahedron Lett.* **2006**, *47*, 4461-4463.
- (289) **Common fragrance and flavor materials: preparation, properties and uses** Bauer, K.; Garbe, D.; Surburg, H.; John Wiley & Sons, **2008**.
- (290) **A Heterogeneous Tungsten Catalyst for Epoxidation of Terpenes and Tungsten-Catalyzed Synthesis of Acid-Sensitive Terpene Epoxides** Villa, d. P. A. L.; Sels, B. F.; De, V. D. E.; Jacobs, P. A. *J. Org. Chem.* **1999**, *64*, 7267-7270.
- (291) **An effective synthesis of acid-sensitive epoxides via oxidation of terpenes and styrenes using hydrogen peroxide under organic solvent-free conditions** Kon, Y.; Hachiya, H.; Ono, Y.; Matsumoto, T.; Sato, K. *Synthesis* **2011**, 1092-1098.
- (292) **New design approaches to ultra-clean diesel fuels by deep desulfurization and deep dearomatization** Song, C.; Ma, X. *Appl. Catal., B* **2003**, *41*, 207-238.
- (293) **An overview of new approaches to deep desulfurization for ultra-clean gasoline, diesel fuel and jet fuel** Song, C. *Catal. Today* **2003**, *86*, 211-263.
- (294) **Intermediates in the hydrodesulfurization of 4,6-dimethyl-dibenzothiophene over Pd/ $\gamma$ -Al<sub>2</sub>O<sub>3</sub>** Roethlisberger, A.; Prins, R. *J. Catal.* **2005**, *235*, 229-240.
- (295) **Heavy duty liquid laundry detergents containing anionic and nonionic surfactant, builder and proteolytic enzyme** Showell, M. S.; Wertz, W. C. *EP Patent 0342177* **1995**.
- (296) **Laundry detergents** Smulders, E.; von Rybinski, W.; Sung, E.; Rähse, W.; Steber, J.; Wiebel, F.; Wiley Online Library, **2001**.
- (297) **A Disjoining Pressure Study of Foam Films Stabilized by Mixtures of Nonionic and Ionic Surfactants** Buchavzov, N.; Stubenrauch, C. *Langmuir* **2007**, *23*, 5315-5323.
- (298) **A disjoining pressure study of foam films stabilized by mixtures of a nonionic (C12DMPO) and an ionic surfactant (C12TAB)** Carey, E.; Stubenrauch, C. *J. Colloid Interface Sci.* **2010**, *343*, 314-323.
- (299) **A surface rheological study of non-ionic surfactants at the water-air interface and the stability of the corresponding thin foam films** Santini, E.; Ravera, F.; Ferrari, M.; Stubenrauch, C.; Makievski, A.; Kraegel, J. *Colloids Surf., A* **2007**, *298*, 12-21.
- (300) **Stability and Rheology of Heavy Crude Oil-in-water Emulsions Stabilized by An Anionic-Nonionic Surfactant Mixture** Ahmed, N. S.; Nassar, A. M.; Zaki, N. N.; Gharieb, H. K. *Petrol. Sci. Technol.* **1999**, *17*, 553-576.
- (301) **Formation of Microemulsions in Mixed Ionic-Nonionic Surfactant Systems** Kunieda, H.; Ozawa, K.; Aramaki, K.; Nakano, A.; Solans, C. *Langmuir* **1998**, *14*, 260-263.
- (302) **Effect of adding an amphiphilic solubilization improver, sucrose distearate, on the solubilization capacity of nonionic microemulsions** Aramaki, K.; Hayashi, T.; Katsuragi, T.; Ishitobi, M.; Kunieda, H. *J. Colloid Interface Sci.* **2001**, *236*, 14-19.
- (303) **The Effect of Mixing of Surfactants on Solubilization in a Microemulsion System** Kunieda, H.; Nakano, A.; Akimaru, M. *J. Colloid Interface Sci.* **1995**, *170*, 78-84.

- 
- (304) **Nonideal multicomponent mixed micelle model** Holland, P. M.; Rubingh, D. N. *J. Phys. Chem.* **1983**, *87*, 1984-1990.
- (305) **Electrostatic model to describe mixed ionic/nonionic micellar nonidealities** Rathman, J. F.; Scamehorn, J. F. *Langmuir* **1986**, *2*, 354-361.
- (306) **Predicting Micellar Solution Properties of Binary Surfactant Mixtures** Shiloach, A.; Blankschtein, D. *Langmuir* **1998**, *14*, 1618-1636.
- (307) Rubingh, D. N.; Mixed micelle solutions: 1979; Vol. 1, p 337-354.
- (308) **Molecular Interactions of Surfactants in Mixed Monolayers at the Air/Aqueous Solution Interface and in Mixed Micelles in Aqueous Media: The Regular Solution Approach** Zhou, Q.; Rosen, M. J. *Langmuir* **2003**, *19*, 4555-4562.
- (309) **Properties of Mixed Micelles of Binary Surfactant Combinations** Haque, M. E.; Das, A. R.; Rakshit, A. K.; Moulik, S. P. *Langmuir* **1996**, *12*, 4084-4089.
- (310) **A Unified Survey of Applicability of Theories of Mixed Adsorbed Film and Mixed Micellization** Chakraborty, T.; Ghosh, S. *J. Surf. Deterg.* **2008**, *11*, 323-334.
- (311) **Microemulsions with Mixtures of Nonionic and Ionic Amphiphiles** Kahlweit, M.; Faulhaber, B.; Busse, G. *Langmuir* **1994**, *10*, 2528-2532.
- (312) **Effect of didodecyldimethylammonium bromide on the phase behavior of nonionic surfactant-silicone oil microemulsions** Silas, J. A.; Kaler, E. W.; Hill, R. M. *Langmuir* **2001**, *17*, 4534-4539.
- (313) **Effect of temperature on the phase behavior of ionic-nonionic microemulsions** Aramaki, K.; Ozawa, K.; Kunieda, H. *J. Colloid Interface Sci.* **1997**, *196*, 74-78.
- (314) **Membrane curvature elasticity in weakly charged lamellar phases** Harden, J. L.; Marques, C.; Joanny, J. F.; Andelman, D. *Langmuir* **1992**, *8*, 1170-1175.
- (315) **Effect of Ionic Surfactants on Nonionic Bilayers: Bending Elasticity of Weakly Charged Membranes** Schomaecker, R.; Strey, R. *J. Phys. Chem.* **1994**, *98*, 3908-3912.
- (316) **Generation of singlet oxygen from hydrogen peroxide disproportionation catalyzed by molybdate ions** Boehme, K.; Brauer, H. D. *Inorg. Chem.* **1992**, *31*, 3468-3471.
- (317) **"Dark" Singlet Oxygenation of  $\beta$ -Citronellol: A Key Step in the Manufacture of Rose Oxide** Alsters, P. L.; Jary, W.; Nardello-Rataj, V.; Aubry, J.-M. *Org. Process Res. Dev.* **2010**, *14*, 259-262.
- (318) **Adsorption of n-alkylpolyethylene glycol non-ionic surfactants from aqueous solution on to silica** Gellan, A.; Rochester, C. H. *J. Chem. Soc., Faraday. Trans.* **1985**, *81*, 2235-2245.
- (319) **Modeling of Multiple Equilibria in the Self-Aggregation of Di-n-decyldimethylammonium Chloride/Octaethylene Glycol Monododecyl Ether/Cyclodextrin Ternary Systems** Leclercq, L.; Lubart, Q.; Aubry, J.-M.; Nardello-Rataj, V. *Langmuir* **2013**, *29*, 6242-6252.
- (320) **Photochemical Charge Separation in Supramolecular Phthalocyanine-Multifullerene Conjugates Assembled by Crown Ether-Alkyl Ammonium Cation Interactions** D'Souza, F.; Maligaspe, E.; Sandanayaka, A. S. D.; Subbaiyan, N. K.; Karr, P. A.; Hasobe, T.; Ito, O. *J. Phys. Chem. A* **2010**, *114*, 10951-10959.
- (321) **N,N'-Disubstituted Methylenediimidazolium Salts: A Versatile Guest for Various Macrocycles** Noujeim, N.; Leclercq, L.; Schmitzer, A. R. *J. Org. Chem.* **2008**, *73*, 3784-3790.
- (322) *Encyclopedia of supramolecular chemistry* Atwood, J. L.; Steed, J. W.; CRC Press, **2004**; Vol. 1.
- (323) *Surfactant Science Series, Vol. 23: Nonionic Surfactants: Physical Chemistry* Schick, M. J.; Editor; Marcel Dekker, Inc., **1987**.
- (324) **On the phase behaviour of polyethoxylated sorbitan (Tween) surfactants in the presence of potassium inorganic salts** Alvarez, M. S.; Moscoso, F.; Deive, F. J.; Sanroman, M. A.; Rodriguez, A. *J. Chem. Thermodyn.* **2012**, *55*, 151-158.
-

- (325) **The effects of salts and ionic surfactants on the micellar structure of tri-block copolymer PEO-PPO-PEO in aqueous solution** Bharatiya, B.; Ghosh, G.; Bahadur, P.; Mata, J. *J. Dispersion Sci. Technol.* **2008**, *29*, 696-701.
- (326) **Hofmeister anion effect on aqueous phase behavior of heptaethylene glycol dodecyl ether** Inoue, T.; Yokoyama, Y.; Zheng, L.-Q. *J. Colloid Interface Sci.* **2004**, *274*, 349-353.
- (327) **The effect of added inorganic salts on the micelle formation of nonionic surfactants in aqueous solutions** Nishikido, N.; Matuura, R. *Bull. Chem. Soc. Jpn.* **1977**, *50*, 1690-1694.
- (328) **Micelle clusters of octylhydroxyoligo(oxyethylenes)** Zulauf, M.; Rosenbusch, J. P. *J. Phys. Chem.* **1983**, *87*, 856-862.
- (329) **Effects of Urea on the Microstructure and Phase Behavior of Aqueous Solutions of Poly(oxyethylene) Surfactants** Bianco, C. L.; Schneider, C. S.; Santonicola, M.; Lenhoff, A. M.; Kaler, E. W. *Ind. Eng. Chem. Res.* **2010**, *50*, 85-96.
- (330) **Salt effects on intramicellar interactions and micellization of nonionic surfactants in aqueous solutions** Carale, T. R.; Pham, Q. T.; Blankschtein, D. *Langmuir* **1994**, *10*, 109-121.
- (331) **Salt Effects on Nonionic Microemulsions Are Driven by Adsorption/Depletion at the Surfactant Monolayer** Kabalnov, A.; Olsson, U.; Wennerstroem, H. *J. Phys. Chem.* **1995**, *99*, 6220-6230.
- (332) **Salting in of nonionic surfactants by complexation with inorganic salts** Schott, H. *J. Colloid Interface Sci.* **1973**, *43*, 150-155.
- (333) **Salting-Out Effects in Aqueous Ionic Liquid Solutions: Cloud-Point Temperature Shifts** Trindade, J. R.; Visak, Z. P.; Blesic, M.; Marrucho, I. M.; Coutinho, J. A. P.; Lopes, J. N. C.; Rebelo, L. P. N. *J. Phys. Chem. B* **2007**, *111*, 4737-4741.
- (334) **Phase behavior of aqueous mixtures of hexaethylene glycol monododecyl ether and sodium alkylsulfonates** Douglas, C. B.; Kaler, E. W. *Langmuir* **1991**, *7*, 1097-1102.
- (335) **Bilayer phases in aqueous mixtures of dodecylpentaoxyethylene glycol monoether (C12E5) and sodium decyl sulfonate (C10SO3Na)** Douglas, C. B.; Kaler, E. W. *J. Chem. Soc., Faraday Trans.* **1994**, *90*, 471-477.
- (336) **Origin of the scattering peak in microemulsions** Teubner, M.; Strey, R. *J. Chem. Phys.* **1987**, *87*, 3195-3200.
- (337) **A small-angle neutron scattering study of nonionic surfactant molecules at the water-oil interface: Area per molecule, microemulsion domain size, and rigidity** Sottmann, T.; Strey, R.; Chen, S.-H. *J. Chem. Phys.* **1997**, *106*, 6483-6491.
- (338) **Rate constants for the decay and reactions of the lowest electronically excited singlet state of molecular oxygen in solution** Wilkinson, F.; Brummer, J. G. *J. Phys. Chem. Ref. Data* **1981**, *10*, 809-999.
- (339) **The Schenck Ene Reaction: Diastereoselective Oxyfunctionalization with Singlet Oxygen in Synthetic Applications** Prein, M.; Adam, W. *Angew. Chem. Int. Ed.* **1996**, *35*, 477-494.
- (340) **The chemistry of the natural order Cupressales. XLVI. The structure of nootkatone** Erdtman, H.; Hirose, Y. *Acta Chem. Scand.* **1962**, *16*, 1311-1314.
- (341) **Sesquiterpenes. I. Nootkatone, a new grapefruit flavor constituent** MacLeod, W. D., Jr.; Buigues, N. M. *J. Food Sci.* **1964**, *29*, 565-568.
- (342) **Olfactory studies on enantiomeric eremophilane sesquiterpenoids** Haring, H. G.; Rijkens, F.; Boelens, H.; Van der Gen, A. *J. Agr. Food Chem.* **1972**, *20*, 1018-1021.
- (343) **Structure-activity of valencenoid derivatives and their repellence to the Formosan subterranean termite** Zhu, B. C. R.; Henderson, G.; Sauer, A. M.; Yu, Y.; Crowe, W.; Laine, R. A. *J. Chem. Ecol.* **2003**, *29*, 2695-2701.
- (344) **Use of novel compounds for pest control: insecticidal and acaricidal activity of essential oil components from heartwood of Alaska yellow cedar** Panella, N. A.; Dolan, M. C.; Karchesy, J. J.; Xiong, Y.; Peralta-Cruz, J.; Khasawneh, M.; Monteneri, J. A.; Maupin, G. O. *J. Med. Entomol.* **2005**, *42*, 352-358.
- (345) **The total synthesis of racemic nootkatone** Pesaro, M.; Bozzato, G.; Schudel, P. *Chem. Commun.* **1968**, 1152-1154.

- (346) **Total synthesis of (+-)-nootkatone** Odom, H. C.; Pinder, A. R. *Chem. Commun.* **1969**, 26-27.
- (347) **Stereoselective total synthesis of racemic nootkatone** Marshall, J. A.; Ruden, R. A. *J. Org. Chem.* **1971**, *36*, 594-596.
- (348) **Synthesis of sesquiterpenoids related to nootkatone. Structure determination by NMR using tris(dipivalomethanato)europium** Leitereg, T. J. *Tetrahedron Lett.* **1972**, 2617-2620.
- (349) **Further synthetic studies in the nootkatane sesquiterpene group. New total synthesis of (+-)-valencene and (+-)-nootkatone** McGuire, H. M.; Odom, H. C., Jr.; Pinder, A. R. *J. Chem. Soc., Perkin Trans. 1* **1974**, 1879-1883.
- (350) **Stereoselective approach to eremophilane sesquiterpenes. Synthesis of (+-)-nootkatone and (+-)- $\alpha$ -vetivone** Dastur, K. P. *J. Am. Chem. Soc.* **1974**, *96*, 2605-2608.
- (351) **A novel entry to the eremophilane and valencane sesquiterpenes via a stereoselective intramolecular Diels-Alder reaction** Naf, F.; Decorzant, R.; Thommen, W. *Helv. Chim. Acta* **1979**, *62*, 114-118.
- (352) **A new stereoselective synthesis of ( $\pm$ )-nootkatone by means of cyclopentenone annulation** Hiyama, T.; Shinoda, M.; Nozaki, H. *Tetrahedron Lett.* **1979**, 3529-3532.
- (353) **A stereoselective synthesis of ( $\pm$ )-nootkatone and ( $\pm$ )-valencene via an intramolecular Sakurai reaction** Majetich, G.; Behnke, M.; Hull, K. *J. Org. Chem.* **1985**, *50*, 3615-3618.
- (354) **Ready Access to Functionally Embellished cis-Hydrindanes and cis-Decalins: Protecting Group-Free Total Syntheses of ( $\pm$ )-Nootkatone and ( $\pm$ )-Noreremophilane** Handore, K. L.; Seetharamsingh, B.; Reddy, D. S. *J. Org. Chem.* **2013**, *78*, 8149-8154.
- (355) **Stereocontrolled synthesis of (+)-nootkatone from (-)- $\beta$ -pinene** Yanami, T.; Miyashita, M.; Yoshikoshi, A. *J. Chem. Soc., Chem. Commun.* **1979**, 525-527.
- (356) **Synthetic study of (+)-nootkatone from (-)- $\beta$ -pinene** Yanami, T.; Miyashita, M.; Yoshikoshi, A. *J. Org. Chem.* **1980**, *45*, 607-612.
- (357) **Efficient and economic asymmetric synthesis of nootkatone, tetrahydronootkatone, their precursors and derivatives** Sauer, A. M.; Crowe, W. E.; Laine, R. A.; Henderson, G. *Board of Supervisors of Louisiana State University and Agricultural and Mechanical College, USA*. **2006**, US7112700B2, 10.
- (358) **An Efficient and Economic Asymmetric Synthesis of (+)-Nootkatone, Tetrahydronootkatone, and Derivatives** Sauer, A. M.; Crowe, W. E.; Henderson, G.; Laine, R. A. *Org. Lett.* **2009**, *11*, 3530-3533.
- (359) **Plant sesquiterpene synthase cDNA, production with recombinant organisms of the enzyme, and its use for production of sesquiterpenes** Chappell, J.; Greenhagen, B. *US 20060218661A1* **2006**, 45.
- (360) **Conversion of valencene to nootkatone** Hunter, G. L. K.; Brogden, W. B., Jr. *J. Food Sci.* **1965**, *30*, 876-878.
- (361) **Oxidations of valencene** Shaffer, G. W.; Eschinasi, E. H.; Purzycki, K. L.; Doerr, A. B. *J. Org. Chem.* **1975**, *40*, 2181-2185.
- (362) **Synthesis of nootkatone from valencene** Wilson, C. W., III; Shaw, P. E. *J. Agric. Food Chem.* **1978**, *26*, 1430-1432.
- (363) **The allylic oxidation of unsaturated steroids by tert-butyl hydroperoxide using surface functionalised silica supported metal catalysts** Salvador, J. A. R.; Clark, J. H. *Green Chem.* **2002**, *4*, 352-356.
- (364) **Biotransformation of valencene by cultured cells of *Gynostemma pentaphyllum*** Sakamaki, H.; Itoh, K.-I.; Taniai, T.; Kitanaka, S.; Takagi, Y.; Chai, W.; Horiuchi, C. A. *J. Mol. Catal. B: Enzym.* **2005**, *32*, 103-106.
- (365) **Highly efficient production of nootkatone, the grapefruit aroma from valencene, by biotransformation** Furusawa, M.; Hashimoto, T.; Noma, Y.; Asakawa, Y. *Chem. Pharm. Bull.* **2005**, *53*, 1513-1514.
- (366) **A dioxygenase of *Pleurotus sapidus* transforms (+)-valencene regio-specifically to (+)-nootkatone via a stereo-specific allylic hydroperoxidation** Krugener, S.; Krings, U.; Zorn, H.; Berger, R. G. *Bioresour Technol* **2010**, *101*, 457-462.
- (367) **Enzymatic allylic oxidations with a lyophilisate of the edible fungus *Pleurotus sapidus*** Rickert, A.; Krombach, V.; Hamers, O.; Zorn, H.; Maison, W. *Green Chem.* **2012**, *14*, 639-644.

- (368) **Bioconversion of (+)-valencene in submerged cultures of the ascomycete *Chaetomium globosum*** Kaspera, R.; Krings, U.; Nanzad, T.; Berger, R. *Appl. Microbiol. Biotechnol.* **2005**, *67*, 477-483.
- (369) **Biotransformation of the sesquiterpene (+)-valencene by cytochrome P450cam and P450BM-3** Sowden, R. J.; Yasmin, S.; Rees, N. H.; Bell, S. G.; Wong, L.-L. *Org. Biomol. Chem.* **2005**, *3*, 57-64.
- (370) **A chicory cytochrome P450 mono-oxygenase CYP71AV8 for the oxidation of (+)-valencene** Cankar, K.; van Houwelingen, A.; Bosch, D.; Sonke, T.; Bouwmeester, H.; Beekwilder, J. *FEBS Lett.* **2011**, *585*, 178-182.
- (371) **Regioselective biooxidation of (+)-valencene by recombinant *E. coli* expressing CYP109B1 from *Bacillus subtilis* in a two-liquid-phase system** Girhard, M.; Machida, K.; Itoh, M.; Schmid, R. D.; Arisawa, A.; Urlacher, V. B. *Microb. Cell Fact.* **2009**, *8*, No pp. given.
- (372) **Nootkatone-a biotechnological challenge** Fraatz, M. A.; Berger, R. G.; Zorn, H. *Appl. Microbiol. Biotechnol.* **2009**, *83*, 35-41.
- (373) **The rearrangements of allylic hydroperoxides derived from (+)-valencene** Davies, A. G.; Davison, I. G. E. *J. Chem. Soc., Perkin Trans. 2* **1989**, 825-830.
- (374) **Binary and Ternary Phase Behaviors of Short Double-Chain Quaternary Ammonium Amphiphiles: Surface Tension, Polarized Optical Microscopy, and SAXS Investigations** Hong, B.; Lai, J.; Leclercq, L.; Collinet-Fressancourt, M.; Aubry, J.-M.; Bauduin, P.; Nardello-Rataj, V. *J. Phys. Chem. B* **2013**, *117*, 14732-14742.
- (375) *Organic Peroxides* Ando, W.; Editor; Wiley, **1992**.
- (376) **The Schenck rearrangement of allylic hydroperoxides** Davies, A. G. *J. Chem. Res.* **2009**, *2009*, 533-544.
- (377) **Stereoselectivity in the formation and allylic rearrangement of 8 $\alpha$ -methyl- and 8 $\alpha$ -ethyl-1,2,3,4,4a,7,8,8a-octahydronaphthalenyl hydroperoxides** Avila, D. V.; Davies, A. G.; Davison, I. G. E. *J. Chem. Soc., Perkin Trans. 2* **1988**, 1847-1852.
- (378) **Singlet-oxygen ene reaction with 3 $\beta$ -substituted stigmastanes. An alternative pathway for the classical Schenck rearrangement** Ponce, M. A.; Ramirez, J. A.; Galagovsky, L. R.; Gros, E. G.; Erra-Balsells, R. *Perkin 2* **2000**, 2351-2358.
- (379) **Chemistry of singlet oxygen. XIII. Solvent effects on the reactions with olefins** Foote, C. S.; Denny, R. W. *J. Am. Chem. Soc.* **1971**, *93*, 5168-5171.
- (380) **The Mechanism of the [3,2] Allylperoxyl Rearrangement: A Radical-Dioxygen Pair Reaction That Proceeds with Stereochemical Memory** Porter, N. A.; Mills, K. A.; Caldwell, S. E.; Dubay, G. R. *J. Am. Chem. Soc.* **1994**, *116*, 6697-6705.
- (381) **The isolation and rearrangement of pure acyclic allylic hydroperoxides** Brill, W. F. *J. Am. Chem. Soc.* **1965**, *87*, 3286-3287.
- (382) **The mechanisms of the rearrangements of allylic hydroperoxides: 5 $\alpha$ -hydroperoxy-3 $\beta$ -hydroxycholest-6-ene and 7 $\alpha$ -hydroperoxy-3 $\beta$ -hydroxycholest-5-ene** Beckwith, A. L.; Davies, A. G.; Davison, I. G.; Maccoll, A.; Mruzek, M. H. *J. Chem. Soc., Perkin Trans. 2* **1989**, 815-824.
- (383) **The effect of zirconium in metal/bromide catalysts during the autoxidation of p-xylene: Part I. Activation and changes in benzaldehyde intermediate formation** Partenheimer, W. *J. Mol. Catal. A: Chem.* **2003**, *206*, 105-119.
- (384) **Propellanes—LIII : The -ene reaction of olefinic propellanes with singlet oxygen** Landheer, I.; Ginsburg, D. *Tetrahedron* **1981**, *37*, 143-150.
- (385) **Neuartige Allyl-Umlagerung von Steroid-Hydroperoxyden. Zur photosensibilisierten Autoxydation der Steroide, II** Schenck, G. O.; Neumüller, O. A.; Eisfeld, W. *Angew. Chem.* **1958**, *70*, 595.
- (386) **A Practical Method for Alcohol Oxidation with Aqueous Hydrogen Peroxide under Organic Solvent- and Halide-Free Conditions** Sato, K.; Aoki, M.; Takagi, J.; Zimmermann, K.; Noyori, R. *Bull. Chem. Soc. Jpn.* **1999**, *72*, 2287-2306.
- (387) *Organic reactions in water: principles, strategies and applications* Lindstrom, U. M.; John Wiley & Sons, **2008**.



- (388) **Acidic Three-Liquid-Phase Microemulsion Systems Based on Balanced Catalytic Surfactant for Epoxidation and Sulfide Oxidation under Mild Conditions** Fressancourt-Collinet, M.; Hong, B.; Leclercq, L.; Alsters, P. L.; Aubry, J.-M.; Nardello-Rataj, V. *Adv. Synth. Catal.* **2013**, *355*, 409-420.
- (389) **Verfahren zur Herstellung von sauerstoffhaltigen Verbindungen A process for the preparation of oxygen-containing compounds** Roelen, O. D. *Patent DE849548* **1952**.
- (390) **Verfahren zur herstellung von aldehyden A process for the production of aldehydes** Boy, C. D. C. D.; Hibbel, J. D. I.; Konkol, W. D. C. D.; Lieder, B. I. G.; Much, J. D. I.; Schmidt, V. D. I.; Wiebus, E. *Patent DE849548* **1984**.
- (391) **Alternative approaches for the aqueous-organic biphasic hydroformylation of higher alkenes** Obrecht, L.; Kamer, P. C. J.; Laan, W. *Catal. Sci. Technol.* **2013**, *3*, 541-551.
- (392) **Gas-liquid-liquid reaction engineering: hydroformylation of 1-octene using a water soluble rhodium complex catalyst** Purwanto, P.; Delmas, H. *Catal. Today* **1995**, *24*, 135-140.
- (393) **Biphasic hydroformylation of olefins using a novel water soluble rhodium polyethylene glycolate catalyst** Borrmann, T.; Roesky, H. W.; Ritter, U. *J. Mol. Catal. A: Chem.* **2000**, *153*, 31-48.
- (394) **Cyclodextrins as mass transfer additives in aqueous organometallic catalysis** Bricout, H.; Hapiot, F.; Ponchel, A.; Tilloy, S.; Monflier, E. *Curr. Org. Chem.* **2010**, *14*, 1296-1307.
- (395) **Calix[n]arenes in action, useful host-guest catalysis in organic chemistry** Simoes, J. B.; da Silva, D. L.; de Fatima, A.; Fernandes, S. A. *Curr. Org. Chem.* **2012**, *16*, 949-971.
- (396) **Molecular recognition between chemically modified  $\beta$ -cyclodextrin and dec-1-ene: new prospects for biphasic hydroformylation of water-insoluble olefins** Monflier, E.; Fremy, G.; Castanet, Y.; Mortreux, A. *Angew. Chem., Int. Ed. Engl.* **1995**, *34*, 2269-2271.
- (397) **Sulfonated Xantphos Ligand and Methylated Cyclodextrin: A Winning Combination for Rhodium-Catalyzed Hydroformylation of Higher Olefins in Aqueous Medium** Leclercq, L.; Hapiot, F.; Tilloy, S.; Ramkisoensing, K.; Reek, J. N. H.; van Leeuwen, P. W. N. M.; Monflier, E. *Organometallics* **2005**, *24*, 2070-2075.
- (398) **Efficient Catalysts for the Two-Phase Hydroformylation of Long-Chain  $\alpha$ -Olefins** Bischoff, S.; Kant, M. *Ind. Eng. Chem. Res.* **2000**, *39*, 4908-4913.
- (399) **Amphiphilic phosphines for catalysis in the aqueous phase** Hanson, B. E.; Ding, H.; Kohlpaintner, C. W. *Catal. Today* **1998**, *42*, 421-429.
- (400) **Accelerated Biphasic Hydroformylation by Vesicle Formation of Amphiphilic Diphosphines** Goedheijt, M. S.; Hanson, B. E.; Reek, J. N. H.; Kamer, P. C. J.; Van, L. P. W. N. M. *J. Am. Chem. Soc.* **2000**, *122*, 1650-1657.
- (401) **Cyclodextrin/Amphiphilic Phosphane Mixed Systems and their Applications in Aqueous Organometallic Catalysis** Ferreira, M.; Bricout, H.; Azaroual, N.; Landy, D.; Tilloy, S.; Hapiot, F.; Monflier, E. *Adv. Synth. Catal.* **2012**, *354*, 1337-1346.
- (402) **New water soluble chelating phosphines for aqueous phase catalysis** Ding, H.; Kang, J.; Hanson, B. E.; Kohlpaintner, C. W. *J. Mol. Catal. A: Chem.* **1997**, *124*, 21-28.
- (403) **CTAB micelles and the hydroformylation of octene with rhodium/TPPTS catalysts Evidence for the interaction of TPPTS with micelle surfaces** Riisager, A.; Hanson, B. E. *J. Mol. Catal. A: Chem.* **2002**, *189*, 195-202.
- (404) **Comparison of phase transfer agents in the aqueous biphasic hydroformylation of higher alkenes** Nowothnick, H.; Rost, A.; Hamerla, T.; Schomaecker, R.; Mueller, C.; Vogt, D. *Catal. Sci. Technol.* **2013**, *3*, 600-605.
- (405) **Higher olefin hydroformylation in organic/aqueous biphasic system accelerated by double long-chain cationic surfactants** Fu, H.; Li, M.; Chen, H.; Li, X. *J. Mol. Catal. A: Chem.* **2006**, *259*, 156-160.
- (406) **Micellar effect in high olefin hydroformylation catalyzed by water-soluble rhodium complex** Chen, H.; Li, Y.; Chen, J.; Cheng, P.; He, Y. e.; Li, X. *J. Mol. Catal. A: Chem.* **1999**, *149*, 1-6.

- (407) **Aqueous biphasic catalytic hydroformylation of higher olefins: Promotion effect of cationic gemini and trimeric surfactants** Fu, H.; Li, M.; Mao, H.; Lin, Q.; Yuan, M.; Li, X.; Chen, H. *Catal. Commun.* **2008**, *9*, 1539-1544.
- (408) **Aqueous-biphasic hydroformylation of higher alkenes promoted by alkyimidazolium salts** Desset, S. L.; Cole-Hamilton, D. J.; Foster, D. F. *Chem. Commun. (Cambridge, U. K.)* **2007**, 1933-1935.
- (409) *Surfactants and Interfacial Phenomena, 3rd Edition* Rosen, M. J.; John Wiley & Sons, **2004**.

**Appendix:** Binary and Ternary Phase Behaviors of Short double-Chain Quaternary Ammonium Amphiphiles: Surface Tension, Polarized Optical Microscopy, and SAXS Investigation

---

# Binary and Ternary Phase Behaviors of Short Double-Chain Quaternary Ammonium Amphiphiles: Surface Tension, Polarized Optical Microscopy, and SAXS Investigations

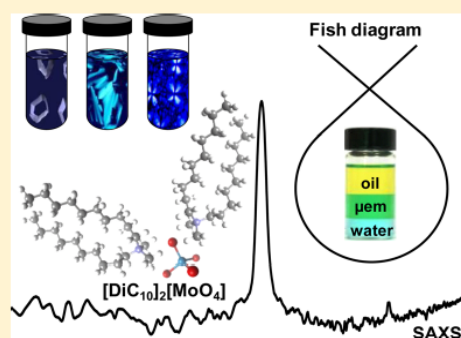
Bing Hong,<sup>†</sup> Jonathan Lai,<sup>‡</sup> Loïc Leclercq,<sup>†</sup> Marion Collinet-Fressancourt,<sup>†</sup> Jean-Marie Aubry,<sup>†</sup> Pierre Bauduin,<sup>\*,‡</sup> and Véronique Nardello-Rataj<sup>\*,†</sup>

<sup>†</sup>Université Lille 1 and ENSCL, EA 4478 Chimie Moléculaire et Formulation, F-59655 Villeneuve d'Ascq Cedex, France

<sup>‡</sup>Institut de Chimie Séparative de Marcoule, UMR 5257 (CEA/CNRS/UM2/ENSCM) BP 17171, 30207 Bagnols sur Cèze Cedex, France

## Supporting Information

**ABSTRACT:** A series of short chain dialkyldimethylammonium amphiphiles ( $[\text{DiC}_n][\text{X}]$  and  $[\text{DiC}_n]_2[\text{X}]$  with  $n = 6, 8, \text{ or } 10$ ) has been investigated as a function of the nature of the counteranion  $[\text{X}]$  ( $\text{Cl}^-$  and  $\text{Br}^-$  as classical references and  $\text{MoO}_4^{2-}$  and  $\text{WO}_4^{2-}$  as catalytic anions). Critical aggregation concentrations (CACs) in water were determined by surface tension measurements, and the binary phase diagrams of the surfactant/water systems were established using polarized optical microscopy (POM) and small angle X-ray scattering (SAXS). The evolution of microstructures and lyotropic phases were discussed in terms of surfactant chain length and counterion effect. A cubic phase region was observed for the divalent counteranions associated with the intermediate chain length, i.e.,  $[\text{DiC}_8]_2[\text{MoO}_4]$  and  $[\text{DiC}_8]_2[\text{WO}_4]$ . Finally, the fish diagrams reflecting the polyphasic microemulsion phase behavior of the water/amphiphile/oil ternary systems were established using the carbon number of mono- and dichlorinated  $n$ -alkanes as a scan variable. The amphiphile efficiency was also discussed according to the chain length and the nature of the counterions. The hydrophilic–lipophilic behavior of the amphiphiles was evaluated on the basis of the fish diagrams allowing their classification according to the Hofmeister anion sequence. The unusual behavior of  $[\text{DiC}_8][\text{Cl}]$  and  $[\text{DiC}_8]_2[\text{MoO}_4]$  ( $M = \text{W or Mo}$ ) is highlighted by all experiments: these compounds are clearly intermediates between hydrotropes,  $[\text{DiC}_6]$  cation, and surfactants,  $[\text{DiC}_{10}]$  cation.



## INTRODUCTION

Double chain quaternary ammonium cationic surfactants are found in many formulations notably because of their adsorption property onto negative surface. Thus, they can be used as fabric softeners,<sup>1</sup> froth floating,<sup>2</sup> antimicrobials<sup>3–6</sup> and as antistatic agents in shampoos.<sup>7</sup> Water–ammonium surfactant systems also have a great potential in size-controlled nanomaterial synthesis.<sup>8</sup> These various applications are based on the electrostatic and geometric properties of double-chain cationic surfactants. The two long alkyl chains make the surfactants very lipophilic with low solubility in water. Due to their cylinder-like shape,<sup>9</sup> long-chain dialkyl surfactants tend to form bilayer structures, like vesicles and lamellar liquid crystal phases in aqueous solution instead of typical spherical micelles.<sup>10</sup> Because of their amphiphilic character, they prefer to reside at the oil–water interface, leading to microemulsion ( $\mu\text{em}$ ) systems at low concentration.<sup>9–12</sup>

In the past few decades, the phase behavior of dialkyldimethylammonium surfactants in water or water/oil mixtures has been extensively investigated by varying the chain length and the nature of the counterion.<sup>11,13–19</sup> Among the

research previously reported, most of the investigated surfactants bear relatively long alkyl chains, generally at least 12 carbons, which can be ascribed to high surfactant efficiency and a multitude of phase behaviors. In contrast, the phase behavior and aggregation properties of two-tailed surfactants with less than 12 carbons has been more rarely reported.<sup>20–23</sup> Recently, the dimethyldialkylammonium molybdate and tungstate, so-called “balanced catalytic surfactants”, abbreviated as  $[\text{DiC}_n]_2[\text{MoO}_4]$  and  $[\text{DiC}_n]_2[\text{WO}_4]$ , respectively, with  $n = 6–12$ , have been developed to perform hydrogen-peroxide-based oxidations in three-liquid-phase microemulsion systems.<sup>24,25</sup> These systems are spontaneously formed at room temperature in the sole presence of water and an appropriate oil without addition of electrolyte nor cosurfactant as generally required. On the other hand, the influence of the counteranions ( $\text{F}^-$ ,  $\text{Cl}^-$ ,  $\text{Br}^-$ ,  $\text{NO}_3^-$ ,  $\text{SO}_4^{2-}$ ,  $\text{MoO}_4^{2-}$ ,  $\text{WO}_4^{2-}$ ) on the aggregation properties of  $[\text{DiC}_8]$  cation has also been recently

Received: June 19, 2013

Revised: October 31, 2013

Published: November 1, 2013

reported.<sup>26,27</sup> It was established that the aggregation process of  $[\text{DiC}_8]$  cation was different with salting-out, salting-in, and intermediate anions. Micelle aggregation occurs at a specific concentration for salting-out counterions ( $\text{F}^-$ ,  $\text{MoO}_4^{2-}$ ,  $\text{WO}_4^{2-}$ ,  $\text{SO}_4^{2-}$ ), whereas, for salting-in counterions ( $\text{Br}^-$ ,  $\text{NO}_3^-$ ), dimers are formed below this specific concentration. Chloride exhibits an intermediate behavior, and two micelle-like structures successively occur after formation of dimers.<sup>27</sup>

In this paper, we focused on the binary and ternary phase behaviors of the molybdate and tungstate “balanced catalytic surfactants” in comparison with the corresponding chlorides and bromides (Figure 1). Indeed, the knowledge of their

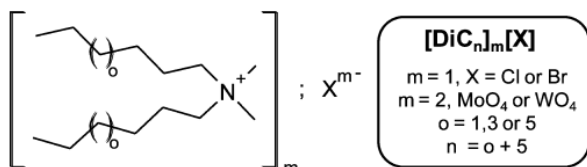


Figure 1. Structure of di-*n*-alkyldimethylammonium salts used in this work.

aggregation properties and amphiphilic character is necessary to predict their ability to form spontaneously three-liquid-phase  $\mu\text{em}$  systems in the presence of a given oil. Such triphasic  $\mu\text{em}$ 's have been proved to be of interest for hydrogen-peroxide-based oxidations especially in terms of recycling and product/catalyst recovery.<sup>24,25</sup> Herein, by means of polarized optical microscopy (POM) and small-angle X-ray scattering (SAXS), we report on the aggregation behavior of short chain dialkyldimethylammonium ( $\text{C}_6$ ,  $\text{C}_8$ , and  $\text{C}_{10}$ ) with  $\text{Br}^-$ ,  $\text{Cl}^-$ ,  $\text{MoO}_4^{2-}$ , or  $\text{WO}_4^{2-}$  as counteranions in water from dilute isotropic solutions to high concentrated liquid crystal phases as a function of temperature. In a second part, the phase behavior of the ternary dialkyldimethylammonium/water/solvent systems is investigated through the construction of “fish” diagrams which afford a classification of the dialkyldimethylammonium amphiphiles according to their relative hydrophilic–lipophilic character, useful information for the prediction of their ternary phase behavior.<sup>28</sup>

## RESULTS AND DISCUSSION

**Aqueous Phase Behavior in Dilute Solution: Critical Aggregation Concentration (CAC) Determination.** Critical aggregation concentration (CAC) is an important characteristic of hydrotropes (chain length  $< 8$  carbons) and true surfactants (chain length  $\geq 8$  carbons). Hydrotropes and surfactants consist of a hydrophilic part and a hydrophobic part; however, the hydrophobic part of hydrotropes is generally too small to cause spontaneous self-aggregation. Indeed, the hydrotropes do not have a critical concentration above which self-aggregation “suddenly” occurs (as found for surfactants at the critical micelle concentration, CMC). Instead, hydrotropes aggregate in a stepwise self-aggregation process, gradually increasing aggregation size at relatively high concentrations, typically above 100 mM. Therefore, hydrotropes do not form well-defined aggregates unlike true surfactants forming micelles. One of the most used methods to determine CACs is the measurement of the surface tension as a function of the concentration of the amphiphile. At very low concentrations of amphiphile, only a slight change in the surface tension is detected. Further addition of surfactant decreases the surface

tension once the surfactant starts to adsorb at the air–water interface. Then, the surface tension reaches a limiting value because the surface becomes fully loaded by the amphiphile. The CAC is determined at the intersection of the two lines defined by the baseline of minimal surface tension ( $\sigma_{\text{CAC}}$ ) at high concentrations and the linear surface tension decrease just before reaching the plateau. It is noteworthy that the surface tension at CAC ( $\sigma_{\text{CAC}}$ ) is a measure of the surface efficiency in lowering the surface tension. CACs of some  $[\text{DiC}_8]$  salts were already investigated in detail previously for interpreting the aggregation mechanism in dilute solution.<sup>27</sup> However, some data are missing especially for  $[\text{DiC}_6]$  cations and catalytic  $[\text{DiC}_{10}]_2[\text{MO}_4]$  with  $\text{M} = \text{MoO}_4$  or  $\text{WO}_4$ . Therefore, the CACs of  $[\text{DiC}_n][\text{X}]$  with  $\text{X} = \text{Cl}$  or  $\text{Br}$  and  $[\text{DiC}_n]_2[\text{MO}_4]$  with  $\text{M} = \text{Mo}$  or  $\text{W}$  and  $n = 6, 8,$  and  $10$  obtained from the surface tension isotherms have been measured (Figure 2) and all CACs are reported in Table 1 as well as the surface tensions at CAC ( $\sigma_{\text{CAC}}$ ).

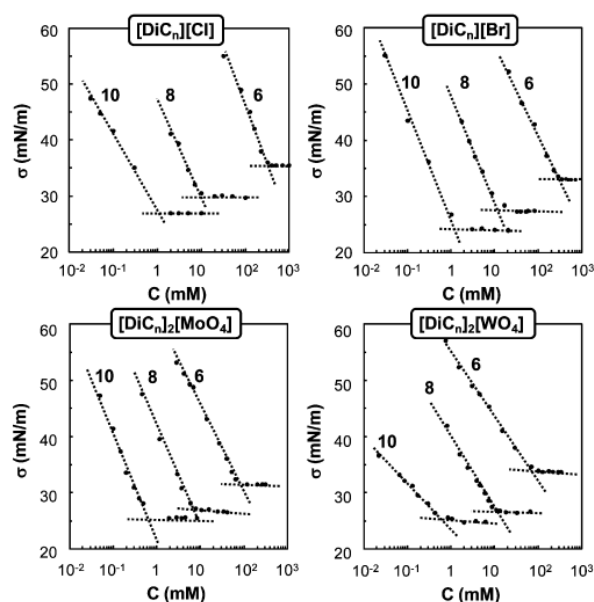


Figure 2. Surface tension ( $\sigma$ ) plotted against surfactant concentration for  $[\text{DiC}_n][\text{X}]$  ( $\text{X} = \text{Cl}$  or  $\text{Br}$ ) and  $[\text{DiC}_n]_2[\text{MO}_4]$  ( $\text{M} = \text{Mo}$  or  $\text{W}$ ) at 25.0 °C ( $n = 6, 8,$  or  $10$ ).

The formation of aggregates in aqueous solution is driven by the so-called “hydrophobic effect”, which originates from the disruption of dynamic H-bonds of the water molecule around the hydrophobic alkyl chain of surfactant and the increase of entropy (water cage around non-polar chain).<sup>30,31</sup> The hydrophobic effect depends on the alkyl chain length. On the other hand, the electrostatics and hydration of the hydrophilic headgroup increase the affinity of the molecule for water, which increases the CAC. These effects were also reflected from our results. Indeed, for the  $[\text{DiC}_n][\text{Cl}]$ , the CAC decreases about 10 times when adding two carbons to each alkyl tail; i.e., there is no clear discontinuity in the aggregation process between  $[\text{DiC}_6]$  and  $[\text{DiC}_{10}]$  amphiphiles. Generally, divalent anions are shown to efficiently screen the electrostatic interaction between the surfactant polar head, resulting in a decrease in the CAC compared to monovalent anions. While in our case the  $[\text{DiC}_6]$  salts behave one way and the octyl  $[\text{DiC}_8]$  and decyl  $[\text{DiC}_{10}]$



**Table 1.** Critical Aggregation Concentration (CAC) Values and Surface Tensions at CAC ( $\sigma_{\text{CAC}}$ ) at 25 °C for  $[\text{DiC}_n][\text{X}]$  ( $\text{X} = \text{Cl}$  or  $\text{Br}$ ) and  $[\text{DiC}_n]_2[\text{MO}_4]$  ( $\text{M} = \text{Mo}$  or  $\text{W}$ ) as a Function of the Alkyl Chain Carbon Number ( $n$ )

amphiphiles	CAC (mM)	$\sigma_{\text{CAC}}$ (mN·m <sup>-1</sup> )
$[\text{DiC}_6][\text{Cl}]$	320 <sup>a</sup>	35.5
$[\text{DiC}_6][\text{Br}]$	280	33.9
$[\text{DiC}_6]_2[\text{WO}_4]$	70	33.3
$[\text{DiC}_6]_2[\text{MoO}_4]$	80	31.2
$[\text{DiC}_8][\text{Cl}]$	10 (10) <sup>a</sup>	29.9
$[\text{DiC}_8][\text{Br}]$	13 (20) <sup>a</sup>	27.9
$[\text{DiC}_8]_2[\text{WO}_4]$	10 (9) <sup>a</sup>	27.5
$[\text{DiC}_8]_2[\text{MoO}_4]$	7 (8) <sup>a</sup>	27.2
$[\text{DiC}_{10}][\text{Cl}]$	1.1 (1.3) <sup>b</sup>	27.2
$[\text{DiC}_{10}][\text{Br}]$	1.3 (1.5) <sup>c</sup>	24.4
$[\text{DiC}_{10}]_2[\text{WO}_4]$	0.6	24.7
$[\text{DiC}_{10}]_2[\text{MoO}_4]$	0.7	25.7

<sup>a</sup>See ref 26. <sup>b</sup>See ref 29. <sup>c</sup>See ref 23.

salts behave the other way, which was ascribed to the nature of the aggregation processes for different surfactants, for example, for  $[\text{DiC}_8][\text{Cl}]$ , dimers were formed at the beginning, followed by ellipsoid aggregates, whereas, for  $[\text{DiC}_8][\text{Br}]$ , discoid aggregation was observed between the dimer and the ellipsoid aggregation. On the other hand, for  $[\text{DiC}_8]_2[\text{WO}_4]$  and  $[\text{DiC}_8]_2[\text{MoO}_4]$ , the ellipsoid aggregation directly occurred when the CAC was reached.<sup>27</sup> The relatively high  $\sigma_{\text{CAC}}$  and CAC values, observed for the  $[\text{DiC}_6]$  series, indicate that it does not behave as a true surfactant and exhibits hydrotropic behavior. The  $[\text{DiC}_6]$  cation does not form well-defined aggregates in water, such as spherical or elongated

micelles.<sup>32–35</sup> Indeed, the presence of well-defined aggregates could not be detected by SAXS (see later) for  $[\text{DiC}_6]_2[\text{WO}_4]$  and  $[\text{DiC}_6]_2[\text{MoO}_4]$  above their CAC values in the dilute regime (concentration <10% w/w, i.e., at concentrations around twice the CAC values,  $\approx 0.2$  M).

**Aqueous Phase Behavior in Concentrated Solution: Lyotropic Liquid Crystal Formation.** A simple way to relate the aggregation type and the geometric shape of a surfactant is the concept called packing parameter ( $P$ ), which is described as follows:<sup>36</sup>

$$P = \frac{\nu}{a_0 \times l_t} \quad (1)$$

where  $\nu$  is the volume of the surfactant chain,  $a_0$  is the area of the polar headgroup, and  $l_t$  is the well-stretched chain length. These parameters, especially  $a_0$ , depend not only on the geometry, given by the van der Waals radii of the atoms, but are sensitive to the experimental conditions (salts, electrostatic interactions, nature of the oil, temperature, pH, etc.). For example, in the presence of polar oils, very different degrees of oil penetration can be observed varying from a localization in the hydrocarbon core of the surfactant assembly (oil-like behavior) to a localization in the surfactant palisade layer (surfactant-like palisade), as shown by Kanei et al.<sup>37</sup> Hence, the term “effective” packing parameter is more suitable.<sup>38,39</sup> The  $\nu$  and  $l_t$  quantities can be determined approximately by the Gruen<sup>40</sup> and Tanford<sup>31</sup> equations, respectively, and  $a_0$  can be estimated from either surface tension measurement or more precisely small angle neutron scattering (SANS). Spherical micelles preferred aggregation when  $P \leq 1/3$ , whereas, for  $P$  values between 1/3 and 1/2, cylindrical aggregates are formed; surfactants with  $P$  values in the range 1/2 to 1 always

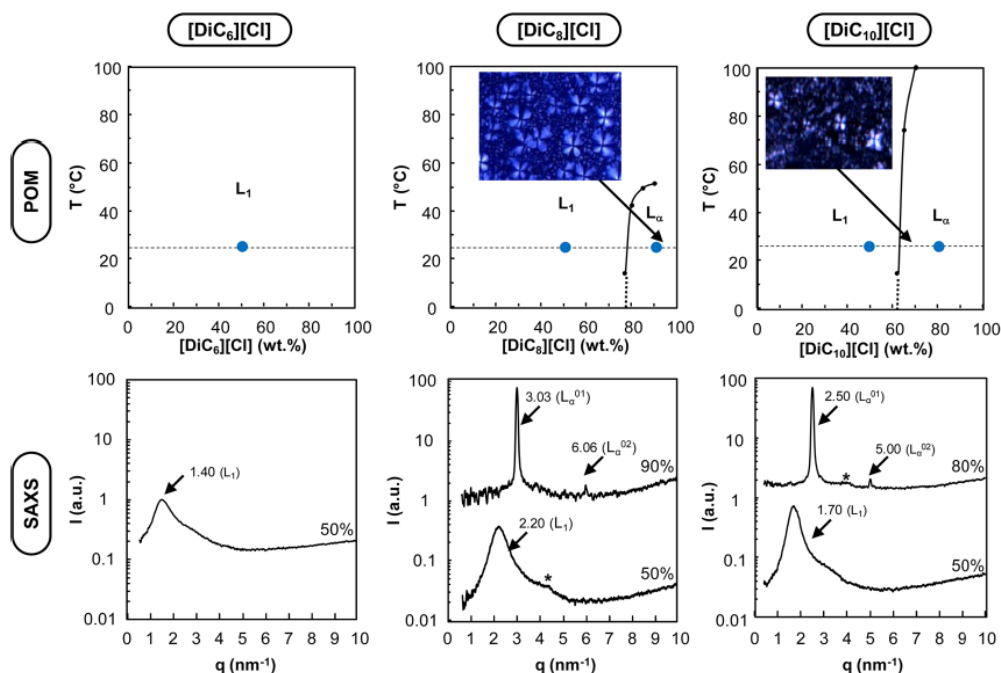


**Figure 3.** Schematic partial binary phase diagrams determined by polarized light optical microscopy of  $[\text{DiC}_n][\text{Cl}]$  ( $n = 6, 8, \text{ or } 10$ ).  $L_1$  = isotropic solution and  $L_\alpha$  = lamellar phase. Photomicrographs show the optical textures of the lamellar phase (with Maltese cross patterns). Typical SAXS curves obtained at 25 °C for various concentrations of  $[\text{DiC}_n][\text{Cl}]$  were also given. The broad peak marked with a star symbol (\*) at  $q \approx 4 \text{ nm}^{-1}$  corresponds to the scattering of the “Kapton” plastic film used as a container in the experiment.

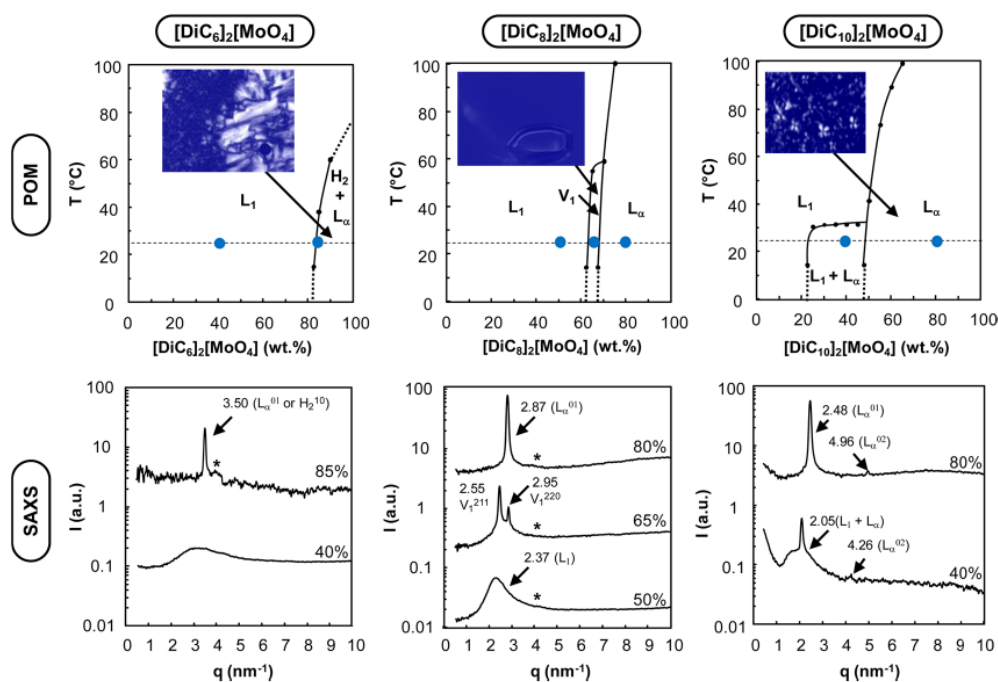


Figure 4. Schematic partial binary phase diagrams determined by polarized light optical microscopy of  $[\text{DiC}_n]_2[\text{MoO}_4]$  ( $n = 6, 8, \text{ or } 10$ ).  $L_1$  = isotropic solution,  $V_1$  = cubic phase,  $L_\alpha$  = lamellar phase, and  $H_2$  = reverse hexagonal phase. Photomicrographs show the optical textures of the lamellar phase (with Maltese cross patterns), the reverse hexagonal phase (“fan-like” texture), and faceted air bubbles in the cubic phase. Typical SAXS curves obtained at 25 °C for various concentrations of  $[\text{DiC}_n]_2[\text{MoO}_4]$  were also given. The broad peak marked with a star symbol (\*) at  $q \approx 4 \text{ nm}^{-1}$  corresponds to the scattering of the “Kapton” plastic film used as a container in the experiment.

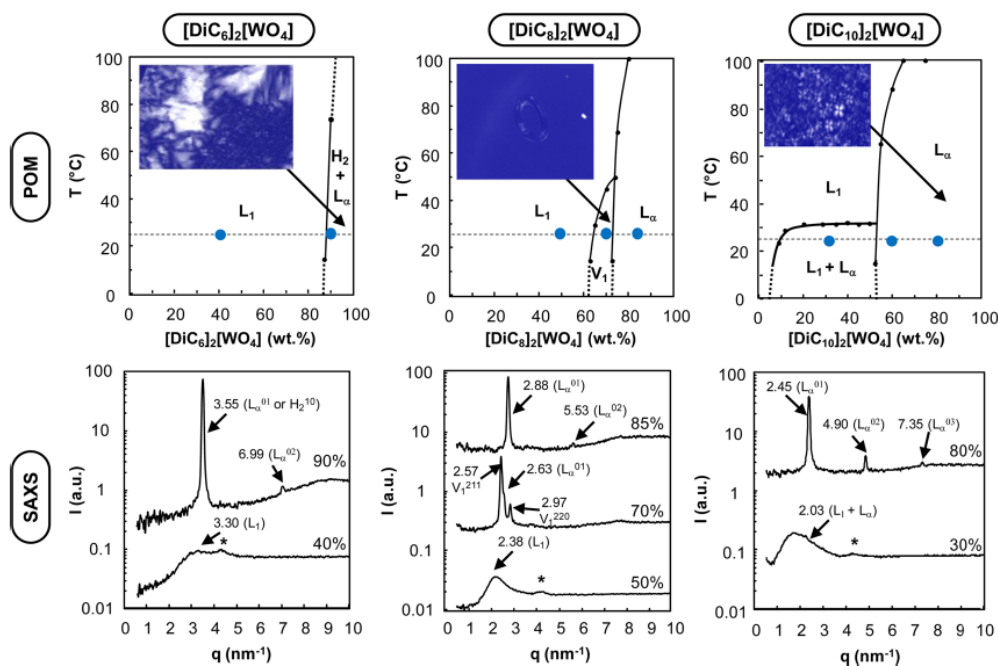


Figure 5. Schematic partial binary phase diagrams determined by polarized light optical microscopy of  $[\text{DiC}_n]_2[\text{WO}_4]$  ( $n = 6, 8, \text{ or } 10$ ).  $L_1$  = isotropic solution,  $V_1$  = cubic phase,  $L_\alpha$  = lamellar phase, and  $H_2$  = reverse hexagonal phase. Photomicrographs show the optical textures of the lamellar phase (with Maltese cross patterns), the reverse hexagonal phase (“fan-like” texture), and faceted air bubbles in the cubic phase. Typical SAXS curves obtained at 25 °C for various concentrations of  $[\text{DiC}_n]_2[\text{WO}_4]$  were also given. The broad peak marked with a star symbol (\*) at  $q \approx 4 \text{ nm}^{-1}$  corresponds to the scattering of the “Kapton” plastic film used as a container in the experiment.



spontaneously form bilayer structures, such as vesicles, disk-shape micelles, and liposomes.

For single-chain surfactants, due to the effective packing parameter ranging from 1/3 to 1/2, the binary phase diagram has a classical phase behavior pattern. In the dilute regime, micelles are formed, usually followed by an increase in the micelle size or a change in the micelle shape by increasing concentration. In the high concentration regime, lyotropic liquid crystals may form, with the classical evolution from hexagonal to cubic to lamellar phases.<sup>41</sup> On the other hand, the double-chain surfactants also exhibit a general sequence; the phase behavior evolves from an isotropic solution (vesicle, disk-like micelle, oblate micelle, etc.) and two phases (dispersed lamellae) to lamellar liquid crystals by increasing the concentration of surfactant in water.<sup>9,13,14,42</sup> Although sometimes the CMCs of the two different surfactants were similar, such as SDS and  $[\text{DiC}_8]_2[\text{MoO}_4]$ , the binary phase behavior also exhibited a great difference due to the different packing parameters.

The binary quaternary ammonium amphiphile/water diagrams of  $[\text{DiC}_n][\text{Cl}]$  and  $[\text{DiC}_n]_2[\text{MO}_4]$  (with  $M = \text{Mo}$  or  $\text{W}$  and  $n = 6, 8,$  and  $10$ ) have been investigated. The phase diagrams were preliminarily studied by polarized optical microscopy (POM) by gradually increasing the concentration of surfactant, which can discriminate isotropic phases from anisotropic phases. Then, the type of liquid crystals was distinguished by different textures and confirmed by SAXS experiments (Figures 3–5).<sup>43–46</sup>

As depicted in Figures 3–5, lamellar liquid crystal exhibits mosaic or “Maltese cross” textures. On the other hand, normal or reverse hexagonal phases show “fan-like” texture. The micelle solution and cubic phase are not birefringent, but the cubic phase is highly viscous compared to fluid micellar solution. Due to the high viscosity, the distorted bubbles trapped in the cubic phase were often encountered (see the insets in Figures 4 and 5).

It is noteworthy that  $[\text{DiC}_6][\text{Cl}]$  does not present birefringent solution whatever its concentration or temperature. In contrast, according to the chain length and the anion nature, various phases can be obtained, i.e., cubic and lamellar. The nature of the liquid crystal phase follows the global curvature of the surfactant which decreases by increasing surfactant concentration, i.e., in decreasing water and hydration of the polar head. Figures 3–5 clearly show that the increase of the chain length gives liquid crystal phases with less curved interface, i.e., lamellar phase. It is noteworthy that the transition from one phase to another mediated by the coexistence of the two is not always observed experimentally. Typical SAXS curves of different concentrations of  $[\text{DiC}_n][\text{Cl}]$  and  $[\text{DiC}_n]_2[\text{MO}_4]$  ( $M = \text{MoO}_4$  or  $\text{WO}_4$  and  $n = 6, 8,$  or  $10$ ) at 25 °C were also given in Figures 3–5.

SAXS experiments are used here to confirm the nature of the phases observed by POM. Bragg peaks are generally obtained for well organized surfactant liquid crystal structure, i.e., cubic, hexagonal, or lamellar phase. On the other hand,  $L_1$  isotropic solution exhibits a broad peak due to the low level of organization between surfactant aggregate.

For the  $[\text{DiC}_6]_2[\text{MoO}_4]$  and  $[\text{DiC}_6]_2[\text{WO}_4]$ , a biphasic region with lamellar  $L_\alpha$  and reverse hexagonal  $H_2$  phases is clearly observed in POM for the very high concentrations, >82 and >88%, respectively (see pictures in Figures 4 and 5).<sup>47</sup> A reverse hexagonal phase is common for double-chained surfactant like AOT<sup>48</sup> or lecithin<sup>49</sup> in water at high

concentrations (>80 wt %) and/or high temperature (>100 °C).

From the SAXS spectra, lamellar and reverse hexagonal phases are characterized by sharp Bragg reflections with  $q$  ratios respectively of 1:2:3 and  $1:\sqrt{3}:2$ . For  $[\text{DiC}_6]_2[\text{MoO}_4]$ , only one sharp reflection is observed which can be attributed to both lamellar or reverse hexagonal phase, as suggested by the POM pictures (presence of “fan-like” texture). On the other hand,  $[\text{DiC}_6]_2[\text{WO}_4]$  shows a “fan-like” texture in POM pictures as well as a second reflection  $L_\alpha^{02}$  that confirms the presence of a lamellar phase and suggests an equilibrium between a lamellar phase and a reverse hexagonal phase. The absence of  $H_2^{20}$  reflection can be explained by a rather low proportion of reverse hexagonal phase vs lamellar phase.

SAXS spectra of the cubic phase observed with  $[\text{DiC}_8]_2[\text{MoO}_4]$  and  $[\text{DiC}_8]_2[\text{WO}_4]$  show a main peak and a second order whose positions (the ratio of the peak position is around 1.1) can be described by the two reflection peaks (211 and 220) of bicontinuous cubic phase of the symmetry group  $Ia3d$ . The bicontinuous structures formed are well described by infinite periodic minimal surfaces (IPMS), i.e., surfaces whose mean curvature is zero at all points.<sup>50,51</sup> The group  $Ia3d$  is most commonly obtained in V1 phases.<sup>51</sup> In some of the SAXS 2D images, a 4-fold symmetry is observed; see Figure S1 in the Supporting Information, which is also typical of an  $Ia3d$  phase.<sup>52</sup>

The diagrams of  $[\text{DiC}_8][\text{Cl}]$  and  $[\text{DiC}_{10}][\text{Cl}]$  have similar patterns, but the  $[\text{DiC}_{10}][\text{Cl}]$ /water system has a larger and more stable lamellar liquid crystal region (see Figure 3). This is due to the longer chain and larger size of aggregates formed,<sup>13,27</sup> which means the interaction between aggregates is stronger for  $[\text{DiC}_{10}][\text{Cl}]$  than for  $[\text{DiC}_8][\text{Cl}]$ . These results also follow the trend already observed by Shinoda who reported the phase diagrams of dialkyl ( $\text{C}_{12}$ ,  $\text{C}_{14}$ , and  $\text{C}_{18}$ ) dimethylammonium chloride/water binary systems and anticipated that  $[\text{DiC}_{10}][\text{Cl}]$  and  $[\text{DiC}_8][\text{Cl}]$  do not have biphasic mixture regions at room temperature.<sup>13</sup>  $[\text{DiC}_8]_2[\text{MoO}_4]$  and  $[\text{DiC}_8]_2[\text{WO}_4]$  show similar binary phase behavior with, for both of them, a narrow bicontinuous cubic region between the isotropic solution and the lamellar phase.<sup>53</sup> Unlike  $[\text{DiC}_{10}][\text{Cl}]$ , the  $[\text{DiC}_{10}]_2[\text{MoO}_4]$  and  $[\text{DiC}_{10}]_2[\text{WO}_4]$  binary systems display in addition a large range of biphasic region before the formation of liquid crystal phases. According to a Monte Carlo simulation,<sup>54</sup> there is a significant attraction between the lamellae derived from the charge fluctuation for divalent counterions which cause lower swelling ability of this kind of amphiphile. This can lead to the phase demixing between  $L_\alpha$  and  $L_1$  phases.<sup>54</sup>

In the SAXS spectra, the position of the first reflection  $L_\alpha^{01}$ , here called  $q^*$ , can be correlated to the interlamellar spacing  $d^*$  with the relation  $d^* = 2\pi/q^*$ . For a homogeneous lamellar phase, the thickness of the lamella  $\delta$  can be calculated with  $\Phi = \delta/d^*$ , where  $\Phi$  is the surfactant volume fraction and  $\delta = 2l_c^n$ , with  $l_c^n$  being the lamella half-thickness for a given surfactant containing an alkyl chain with  $n$  carbons. At a given concentration, the surfactant length can be estimated by the maximal alkyl chain length given by Tanford's relation ( $l_c^n = 1.5 + 1.265n$  in nm).<sup>31</sup> All the surfactants in this study, except  $[\text{DiC}_6][\text{Cl}]$ , form a lamellar liquid crystal at  $\Phi=0.9$  with  $l_c^n \approx l_c^4$  which is typical for fluid bilayers:  $l_c^6 \approx 0.80$  nm ( $l_c^6 = 0.80$  nm),  $l_c^8 \approx 0.96$  nm ( $l_c^8 = 1.16$  nm), and  $l_c^{10} \approx 1.15$  nm ( $l_c^{10} = 1.41$  nm) for  $[\text{DiC}_6]$ ,  $[\text{DiC}_8]$ , and  $[\text{DiC}_{10}]$  series, respectively; see Table S1 in the Supporting Information. Careful observation of the  $l_c^n$



Table 2. Minimal Amounts Required to Obtain a WIH  $\mu\text{em}$  ( $\gamma_0$ ), a WIV  $\mu\text{em}$  ( $\gamma^*$ ), and “Optimal” Oil for the Dialkyldimethylammonium  $[\text{DiC}_n][\text{X}]$  with  $\text{X} = \text{Cl}$  or  $\text{Br}$  and  $[\text{DiC}_n]_2[\text{X}]$  with  $\text{X} = \text{MoO}_4$  or  $\text{WO}_4$  ( $n = 8$  and  $10$ )

X	$[\text{DiC}_8][\text{X}]$		$[\text{DiC}_8]_2[\text{X}]$		$[\text{DiC}_{10}]_2[\text{X}]$	
	Cl	Br	$\text{MoO}_4$	$\text{WO}_4$	$\text{MoO}_4$	$\text{WO}_4$
$\gamma_0$ (wt %)	11	2	2	2	2	2
$\gamma^*$ (wt %)	24.0	35.1	25.1	22.5	29.1	25.1
“optimal” oil	$\text{C}_{42}\text{Cl}_2^a$	$\text{C}_{72}\text{Cl}^b$	$\text{C}_{25}\text{Cl}_2^c$	$\text{C}_{24}\text{Cl}_2^d$	$\text{C}_{82}\text{Cl}^e$	$\text{C}_{54}\text{Cl}^f$

<sup>a</sup>0.8C<sub>4</sub>Cl<sub>2</sub>/0.2C<sub>5</sub>Cl<sub>2</sub>. <sup>b</sup>0.8C<sub>7</sub>Cl/0.2C<sub>8</sub>Cl. <sup>c</sup>0.5C<sub>2</sub>Cl<sub>2</sub>/0.5C<sub>3</sub>Cl<sub>2</sub>. <sup>d</sup>0.6C<sub>2</sub>Cl<sub>2</sub>/0.4C<sub>3</sub>Cl<sub>2</sub>. <sup>e</sup>0.8C<sub>8</sub>Cl/0.2C<sub>9</sub>Cl. <sup>f</sup>0.6C<sub>5</sub>Cl/0.4C<sub>6</sub>Cl.

evolution shows a deviation from Tanford's length from  $[\text{DiC}_6]$  to  $[\text{DiC}_8]$  and  $[\text{DiC}_{10}]$  which can be related to the disorder degree of the fluid alkyl chain in the lamellar phase: the longer the alkyl chain, the larger the chain disorder and the lower the measured length  $l_c^*$  compared to  $l_t^{55}$ . This effect is more pronounced for large numbers of carbon:  $l_c^* = 0.80$  nm vs  $l_t^* = 0.91$  nm for  $[\text{DiC}_6]_2[\text{MoO}_4]$  and  $l_c^{10} = 1.15$  nm vs  $l_t^{10} = 1.41$  nm for  $[\text{DiC}_{10}]_2[\text{MoO}_4]$ . In addition, a slight decrease in  $l_c^*$  is observed depending on the nature of the counterion from monovalent ( $[\text{Cl}]$ :  $l_c^{10} = 1.12$  nm) to divalent ( $[\text{MoO}_4]$ :  $l_c^{10} = 1.18$  nm). Divalent ion leads to lower repulsive interactions between the polar heads and reduces the available space for the alkyl chain and the chain disorder. This effect results in the increase in the lamella thickness.

It is noteworthy that cubic phases are only observed for  $[\text{DiC}_8]_2[\text{MoO}_4]$  and  $[\text{DiC}_8]_2[\text{WO}_4]$ , whereas the analogous  $[\text{DiC}_8][\text{Cl}]$  shows only a lamellar phase. The replacement of a monovalent counterion by a divalent counterion in a given system results in significant changes due to the variation of counterion hydration. In the literature, the hexadecyltrimethylammonium bromide does not give cubic phases at room temperature, whereas the substitution of bromide by sulfate allows the occurrence of a cubic phase at a concentration around 45%.<sup>56</sup> The ion hydration free energy,  $\Delta G_{\text{hydr}}$  which provides indirect measures of the ion–water interactions, is a relevant parameter of ionic properties.  $\Delta G_{\text{hydr}}$  values for many ions were carefully tabulated by Marcus.<sup>57</sup> However, some data are missing especially for  $[\text{WO}_4]$  and  $[\text{MoO}_4]$ .  $\Delta G_{\text{hydr}}$  can be predicted for all anions from PM6/SCF-MO calculation with MOPAC2009. The use of the COSMO method (conductor-like screening model) is useful for determining the stability of counterions in a water environment and for comparing this with the gas phase. For  $[\text{Br}]$ ,  $[\text{Cl}]$ ,  $[\text{WO}_4]$ ,  $[\text{MoO}_4]$ , and  $[\text{SO}_4]$ , the following  $\Delta G_{\text{hydr}}$  values were obtained: 76.2, 80.2, 224.2, 228.2, and 242.7 kcal·mol<sup>-1</sup> respectively. For  $[\text{Br}]$ ,  $[\text{Cl}]$ , and  $[\text{SO}_4]$ , the values are in good agreement with the ones tabulated by Marcus (75.3, 81.3, and 258.2 kcal·mol<sup>-1</sup>, respectively).<sup>57</sup> As  $\Delta G_{\text{hydr}}$  of  $[\text{Cl}]$  is close to  $[\text{Br}]$  and as  $[\text{WO}_4]$  and  $[\text{MoO}_4]$  are comparable to  $[\text{SO}_4]$ , in the sense that they are divalent oxo-anions, we can suppose that the apparition of the cubic phase is related to the high hydration of divalent oxo-anions compared with monovalent anions. In other words, the hydration of divalent anion acts as a promoter in the formation of the cubic phase. Moreover, the cubic melting of  $[\text{DiC}_8]_2[\text{MoO}_4]$  and  $[\text{DiC}_8]_2[\text{WO}_4]$  is different (respectively 60 and 50 °C, see Table 2). This temperature corresponds to cubic  $\rightarrow$  micellar solution transition. As the hydrogen bonds are disrupted by increasing temperature, thereby releasing weakly bound water, the cubic phase is destabilized in favor of the micellar solution. It is noteworthy that  $[\text{MoO}_4]$  shows a better resistance of the cubic phase by increasing temperature. This observation confirms the influence of the counterion hydration on the stability of the cubic phase.

As the packing parameter is clearly modified with the increase of the carbon number of the cationic moiety, the spontaneous curvature is then modified, resulting in the disappearance of the cubic phase in favor of the lamellar phase from  $[\text{DiC}_8]$  to  $[\text{DiC}_{10}]$ . On the other hand, for divalent anions, the decrease of the chain length leads to a simplification of the diagrams, i.e., a decrease of the number of phases. It is thus clearly shown that the surfactant chain length as well as the nature of the counterion act as key parameters on the nature of the liquid crystal phases in the dialkyldimethylammonium series. As mentioned in our previous work,<sup>27</sup>  $[\text{DiC}_8]_i[\text{X}]$  amphiphiles ( $i = 1$  or  $2$ ) present a dual behavior between hydrotropes ( $[\text{DiC}_6]_i[\text{X}]$ ) which do not show any liquid crystal phases (when  $i = 1$  and  $\text{X} = \text{Cl}$ ) or just lamellar phases (when  $i = 2$  and  $\text{X} = \text{WO}_4$  or  $\text{MoO}_4$ ) and true surfactants ( $[\text{DiC}_{10}]_i[\text{X}]$ ) which give only lamellar phases (when  $i = 1$  and  $\text{X} = \text{Cl}$ ) or a biphasic region  $L_1 + L_\alpha$  (when  $i = 2$  and  $\text{X} = \text{WO}_4$  or  $\text{MoO}_4$ ).

**Microemulsion Phase Diagrams and Amphiphile Classification.** Ionic surfactants with one single hydrocarbon chain are generally too hydrophilic to build up microemulsions alone, and phase inversion can take place only if an electrolyte and/or a cosurfactant is added to the mixture.<sup>28</sup> However, using double-chain ionic surfactants, such as the typical sodium-bis-ethylhexylsulfosuccinate (AOT) and didodecyl dimethyl ammonium bromide (DDAB), no cosurfactant is necessary to tune the mean curvature of the amphiphilic film from positive to negative.<sup>28</sup> The phase behavior of ternary di-*n*-alkyldimethylammonium bromides and their ability to form a one-phase microemulsion have been reported for different surfactant chain lengths ( $[\text{DiC}_n][\text{Br}]$  with  $n = 10$ –14 and asymmetric compounds  $[\text{DiC}_n\text{C}_m][\text{Br}]$  with  $n = 8$ ,  $m = 16$ ) in the presence of alkanes.<sup>6,12</sup> Another elegant experimental method to investigate the phase behavior of a surfactant/oil/water system consists of constructing the so-called fish diagram as introduced by Kahlweit for non-ionic surfactants in 1988.<sup>58</sup> Indeed, such diagrams are often preferred to ternary Gibbs diagrams due to their simplicity and the useful information they provide notably regarding the efficiency and the hydrophobic–lipophilic balance of the surfactant. We have thus examined the amphiphilic properties of the dichained quaternary ammonium amphiphiles by constructing their fish diagram at a constant water-to-oil ratio equal to 1. Such diagrams exhibit four types of Winsor  $\mu\text{em}$  systems depending on the value of the formulation variable (temperature, salinity, oil hydrophobicity) and the amount of amphiphile, i.e., the Winsor I (O/W  $\mu\text{em}$  in equilibrium with an excess oil phase), the Winsor II (W/O  $\mu\text{em}$  in equilibrium with an excess water phase), the Winsor III (bicontinuous  $\mu\text{em}$  in equilibrium with both excess oil and water phases), and the Winsor IV, a one-phase  $\mu\text{em}$  in which water and oil are completely cosolubilized.<sup>24,25,59,60</sup> The Winsor types of the  $\mu\text{em}$ 's are readily determined by simple visual inspection once the different phases reached equilibrium. In the present work, the formulation variable chosen for gradually

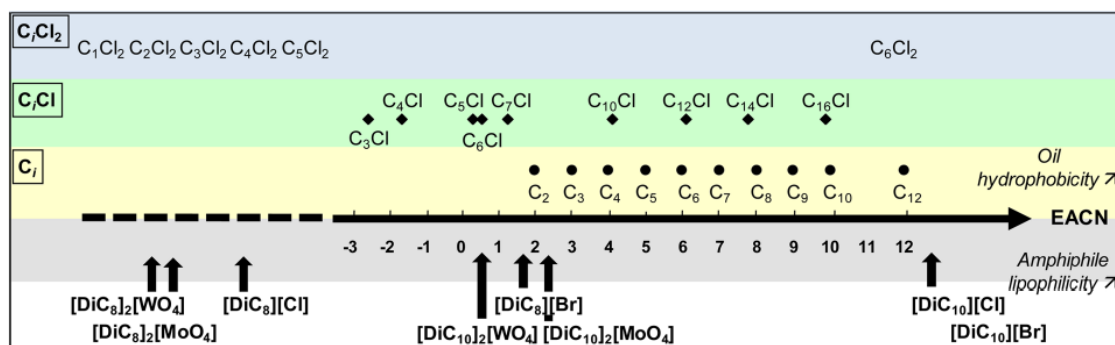


Figure 6. Range of EACN values accessible with three series of homologous oils: *n*-alkanes noted  $C_i$  with  $i = 6-16$  (●); 1-chloroalkanes noted  $C_i\text{Cl}$  with  $i = 3-16$  (◆); and  $\alpha,\omega$ -dichloroalkanes noted  $C_i\text{Cl}_2$  with  $i = 1-6$ . Classification of the quaternary ammonium amphiphiles according to the EACN scale.

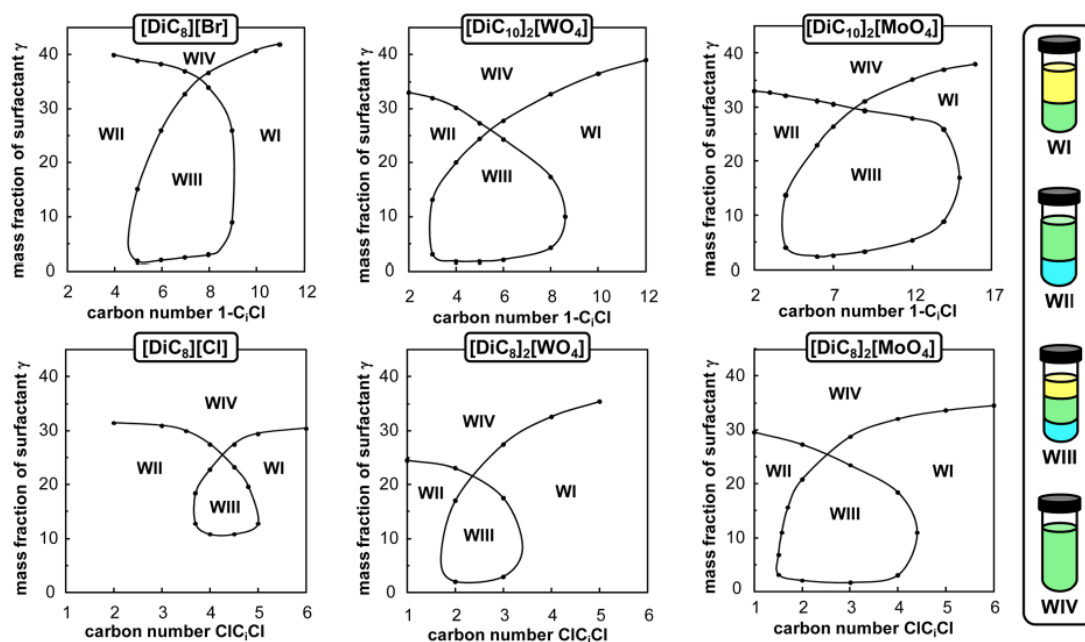


Figure 7. Fish diagrams of  $[\text{DiC}_8][\text{Cl}]$ ,  $[\text{DiC}_8][\text{Br}]$ ,  $[\text{DiC}_8]_2[\text{WO}_4]$ ,  $[\text{DiC}_8]_2[\text{MoO}_4]$ ,  $[\text{DiC}_{10}]_2[\text{WO}_4]$ , and  $[\text{DiC}_{10}]_2[\text{MoO}_4]$  determined by using 1-chloroalkane ( $1\text{-}C_i\text{Cl}$ ) or  $\alpha,\omega$ -dichloroalkane ( $C_i\text{Cl}_2$ ) solvents as scan variables. Tubes represent the different Winsor systems (water phase in blue, oily phase in yellow, and  $\mu\text{em}$  phase in green).

modifying the relative affinity of the amphiphile for the oil and aqueous phases was the hydrophobicity of the oil, as temperature has almost no effect on the ternary phase behavior of the ionic systems and salt tuning is forbidden since it would lead to an anion exchange between the added electrolyte and the quaternary ammonium salt. When the oil hydrophobicity is the scanning variable, the experiments are usually carried out with *n*-alkanes ranging from 6 to 19 carbon atoms. However, the polarity window afforded by *n*-alkanes is too limited and none of them is polar enough to provide the so-called “optimal formulation” with the cationic amphiphiles under study. We therefore resorted to two other homologous series of more polar oils, i.e., the 1-chloro- and  $\alpha,\omega$ -dichloro-*n*-alkanes, abbreviated respectively as  $C_i\text{Cl}$  ( $i = 2-16$ ) and  $C_i\text{Cl}_2$  ( $i = 1-6$ ).  $C_i\text{Cl}$  were used for  $[\text{DiC}_8][\text{Br}]$ ,  $[\text{DiC}_{10}]_2[\text{MoO}_4]$ , and  $[\text{DiC}_{10}]_2[\text{WO}_4]$ , whereas  $C_i\text{Cl}_2$  were more suitable for  $[\text{DiC}_8][\text{Cl}]$ ,  $[\text{DiC}_8]_2[\text{MoO}_4]$ , and  $[\text{DiC}_8]_2[\text{WO}_4]$ . The inter-

est of using homologous series of oils lies in the possibility to vary gradually their polarity by progressively incrementing the number of carbons of the alkyl chain. Moreover, the monochloroalkanes can be quantitatively classified according to a dimensionless number that reflects their hydrophobicity. This number is the equivalent alkane carbon number or EACN introduced by Wade et al. in 1977.<sup>61</sup> The EACN value of a given oil can be experimentally determined by comparing its phase behavior with that of a well-defined linear hydrocarbon. By definition, the EACN is equal to the number of carbons of the *n*-alkane exhibiting the same behavior. Typically,  $C_iE_j$ /water/*n*-alkane systems characterized by the “fish tail” temperature noted  $T^*$  are used for calibration. On the basis of their EACN, a classification of complex oils according to their “hydrophobicity” can be established. For example, such data have been reported by Queste et al.<sup>62</sup> and by Kunieda et al.<sup>63</sup> for alkylcyclohexanes and alkylbenzenes, by Bouton et al.<sup>38,64</sup>



for a series of fragrant mono- and sesquiterpenes, by Ontiveros et al. for ester oils,<sup>65</sup> and by Wormuth and Kaler for ethers.<sup>66</sup> Such an absolute oil scale can then further be used to classify amphiphiles according to the EACN of the oil, providing the optimal formulation at 25 °C of true ternary SOW systems without any further additive.<sup>28</sup> Thus, the oil (or the mixture of oils) giving a WIV system with a minimum amount of surfactant, i.e., at  $\gamma^*$ , is the “optimal oil”. The EACN values of the monochloroalkanes ( $C_iCl$  with  $i = 3-16$ ) have been determined by Queste,<sup>67</sup> but for the  $\alpha,\omega$ -dichloroalkanes, they could not be determined because of a loss of linearity in the calibration curve, especially for the very short chain ones which exhibit a high polarity and, hence, for which very low EACN values are expected. However, a partially quantitative scale may be defined (Figure 6).

The fish diagrams of the  $[DiC_8]$  series,  $[DiC_{10}]_2[MoO_4]$ , and  $[DiC_{10}]_2[WO_4]$  are shown in Figure 7. The  $[DiC_6]$  series is too hydrophilic to be studied with this method, since it always gives WI systems in the range of investigated oils.

It is interesting to note that each dialkyldimethylammonium amphiphile displays a characteristic fish diagram. When the amphiphile is gradually added to the biphasic water/oil mixture, a middle-phase appears at the “fish head” point characterized by a minimal mass fraction  $\gamma_0$ . When the concentration is further increased, the volume of the middle phase increases, and at the “fish tail” point ( $X$ -point), the three-phase body meets the monophasic region at  $\gamma^*$  which is the minimum amount of surfactant needed to form a one-phase  $\mu em$ . Hence,  $\gamma^*$  reflects the efficiency of the surfactant,<sup>60,68</sup> whereas the  $X$ -point corresponds to a precise “optimal” oil which is characteristic of the hydrophilic–lipophilic balance of the surfactant. This “optimal” oil is rarely a well-defined one but more often an appropriate mixture of two oils differing only in a single carbon so that it behaves as an ideal mixture. The values of  $\gamma_0$  and  $\gamma^*$  are reported in Table 2.

Depending on the EACN of the “optimal” oil, a classification of the cationic amphiphiles was established (see Figure 6). Indeed, at the “optimal” formulation, i.e., at the  $X$ -point, the amphiphile has the same affinity for water and oil. Accordingly, if its affinity for water increases, then, the oil should be more polar to compensate for and vice versa. The order found, besides the chain length, is mainly governed by the counter-anion and rationalized by its hydration degree, in agreement with the Hofmeister anion effect.<sup>69–71</sup> Though divalent anions are electrostatically associated with two dialkyl hydrophobic chains, molybdate and tungstate salts are highly hydrated (see above  $\Delta G_{hydr}$ ) and, thus, require more polar oils. Indeed, the process involved in the formation of bicontinuous microemulsions will be less energetically favorable: it must be dehydrated to make contact with the oil phase. On the other hand, the efficiency of the amphiphiles to form microemulsions is reflected by the value of  $\gamma^*$ . This parameter depends on two factors: (i) the chain length of the amphiphile, i.e., when it increases,  $\gamma^*$  decreases accordingly, and (ii) the polarity of the oil, i.e., when the EACN of the oil increases, then  $\gamma^*$  increases. To illustrate this, we can see that  $[DiC_8]_2[WO_4]$  is much more efficient than  $[DiC_8][Br]$ . Indeed, the oils providing the “optimal” formulation with the tungstate salt are much more polar than those required for the bromide salt which is also more hydrophobic. This might also explain the good efficiency of  $[DiC_8][Cl]$  for which  $\gamma^*$  is equal to 24 wt % for an optimal oil equivalent to a 0.8Cl<sub>4</sub>Cl/0.2Cl<sub>5</sub>Cl mixture.

The  $\gamma_0$  value, i.e., the minimum amount of surfactant needed to enter the three-phase region, characterizing the “fish head” position, is also relevant information. It is of ca. 2 wt % for all the amphiphiles except for  $[DiC_6][Cl]$  for which at least 11 wt % of amphiphile is required to form a WIII system. This might be accounted for by the unusual phase behavior of this peculiar amphiphile in dilute aqueous solution. Indeed, as already reported,<sup>27</sup> it forms dimers between 0.2 and 10 mM followed by bilayers at 10–30 mM, and finally, the first true “micelles” appear only above 30 mM, which is not detected by simple surface tension measurements, as it takes place in the bulk. Therefore, as the formation of micelles in the aqueous phase is a prerequisite for a microemulsion to form, a high value of the CMC leads to a high  $\gamma_0$ .

The fish diagrams also exhibit variable body shapes with a relatively larger body fish with molybdate salts. Finding an explanation is not trivial at all because the oil is used as a tuning parameter, thus changing the ternary system, and because the hydrophobicity of dichloroalkanes does not follow a linear variation according to the number of carbons. However, Strey and co-workers<sup>72</sup> have reported that, for a series of polyethoxylated alcohols  $C_iE_j$  and for the same  $n$ -alkanes, the extension of the three-phase body is low for the shortest ones, passes through a maximum for medium-chain ones, and decreases again for long-chain ones. The maximum in the temperature extension of the fish body indicates the frontier between weakly and strongly structured mixtures, also called the Lifshitz line.<sup>73</sup> In the present case, we are above this maximum that corresponds to  $C_6$  chain length. Hence, when the chain length increases, the fish body should be narrower but the phenomena are here more intricate, since we have to compare mono-, i.e., chloride and bromide, with divalent, i.e., molybdate and tungstate, anions.

All of these results demonstrate that several key parameters govern the ternary phase behavior of the dialkyldimethylammonium salts, notably the hydration degree and the valence of the counteranion, the chain length of the hydrophobic tail, and the polarity or EACN of the oil. Rationalization is not straightforward, as several effects overlapped but tendencies can be deduced affording amphiphile classification and ternary phase behavior prediction.

## CONCLUSION

The CACs, the binary diagrams, and the microemulsion phase behavior have been investigated for a series of double-chain quaternary ammonium molybdate and tungstate,  $[DiC_n]_2[MO_4]$  with  $M = W$  or  $Mo$  and  $n = 6, 8,$  and  $10$  in comparison with their chloride and bromide counterparts.  $[DiC_6]$  salts behave as hydrotropes and do not form well-defined aggregates in water. The evolution of the phase behavior from  $[DiC_{10}]$  to  $[DiC_6]$  was reflected by the binary phase diagrams. The boundary of isotropic solution and anisotropic phase moved to higher concentrations when the alkyl chain decreased. This was ascribed to the hydrophobic effects of the alkyl chain of the surfactant. The  $[DiC_{10}]_2[MoO_4]$  and  $[DiC_{10}]_2[WO_4]$  gave a wide range of biphasic mixture region, whereas the  $[DiC_{10}][Cl]$  did not, which was consistent with Monte Carlo simulation and the conclusion that there is a significant attraction between the lamellae derived from the charge fluctuation for divalent counterions. The micellar, cubic, and lamellar phases were clearly distinguished and identified with polarized optical microscopy and SAXS. From the fish diagrams of the  $H_2O-$

surfactant–chloroalkane systems, the hydrophilic–lipophilic balance of these amphiphiles could be assessed, at least qualitatively. The behavior of the  $[\text{DiC}_8]$  series with the four counteranions can be rationalized by the Hofmeister anion sequence. In the whole manuscript, the unusual behavior of the  $[\text{DiC}_8][\text{Cl}]$  and  $[\text{DiC}_8]_2[\text{MO}_4]$  ( $M = \text{W}$  or  $\text{Mo}$ ) is emphasized again. The particular behavior observed in diluted aqueous solution (previously reported)<sup>14</sup> is maintained to a great extent in the liquid crystal phase and ternary system.

## EXPERIMENTAL SECTION

**Materials.** All the surfactants were prepared according to the method previously reported, and the counterion exchange was carried out by using the exchange resin Amberlite IRA-400(Cl).<sup>24–27</sup> The high purity (>99.8%) was confirmed by  $^1\text{H}$  and  $^{13}\text{C}$  NMR. All the other reagents were purchased from Sigma-Aldrich or TCI chemicals and used as received. Chloropropane (1-ClC<sub>3</sub>) (98%), chloropentane (1-ClC<sub>5</sub>) (99%), chlorohexane (1-ClC<sub>6</sub>) (99%), chloroheptane (1-ClC<sub>7</sub>) (99%), chlorooctane (1-ClC<sub>8</sub>) (99%), chlorononane (1-ClC<sub>9</sub>) (98%), chlorodecane (1-ClC<sub>10</sub>) (98%), chlorotetradecane (1-ClC<sub>14</sub>) (98%), and dichlorobutane (C<sub>4</sub>Cl<sub>2</sub>) (99%) were from Aldrich. Chlorobutane (1-ClC<sub>4</sub>) (99.5%) was from Alfa Aesar. Chlorododecane (1-ClC<sub>12</sub>) (95%) was purchased from TCI. Dichloromethane (C<sub>1</sub>Cl<sub>2</sub>) (99%) and dichloroethane (C<sub>2</sub>Cl<sub>2</sub>) (98%) were from Prolabo. Dichloropropane (C<sub>3</sub>Cl<sub>2</sub>) (98%) was purchased from Fluka and dichloropentane (C<sub>5</sub>Cl<sub>2</sub>) (99%) from Acros Organics. The water used in all the experiments was purified by Millipore (18.2 M $\Omega$ /cm; Simplicity 185).  $^1\text{H}$  and  $^{13}\text{C}$  NMR spectra were recorded with a Bruker Avance AV 300 instrument.

**Methods. Surface Tension Measurements.** Surface tensions were measured with the tensiometer K11 (Krüss) using the Wilhelmy plate method. Ultrapure water (Millipore water,  $\sigma = 72.0 \text{ mN}\cdot\text{m}^{-1}$  at 25 °C) was used to prepare all concentrations. Surface tension was recorded after equilibration for each mixture. All equilibrium surface tension values were mean quantities of at least three measurements. The standard deviation of the mean never deviated  $\pm 1.5\%$  of the mean. The precision of the force transducer of the surface tension apparatus was  $0.1 \text{ mN}\cdot\text{m}^{-1}$ , and before each experiment, the platinum plate was cleaned in red/orange color flame. The temperature was stabilized at  $25 \pm 0.05$  °C with a thermostated bath Lauda RC6. The standard deviation was estimated at  $\pm 10\%$  for the CAC value.

**Polarized Light Optical Microscopy.** The phase penetration technique was first used for a rough estimate of the sequence of mesophases occurring.<sup>74</sup> A few milligrams of the surfactant powder (usually around 20 mg) was placed between a glass slide and a coverslip. When the powder could not be made sufficiently compact to obtain a well-defined interface, the sample might be heated until softening for homogenization and then cooled back to room temperature, in order to obtain a well-defined interface. The sample was then contacted with a distilled water drop, and diffusion of water by capillarity into the surfactant sample took place so that a concentration gradient from extremely dilute aqueous solution to pure surfactant was more or less quickly established. Identification of the different phases was based on visual observation through an optical polarizing microscope<sup>75,76</sup> Olympus BX60 (100 $\times$  magnification) equipped with a LTS120 Analyza Peltier temperature stage capable of controlling to  $\pm 0.1$  °C the temperature. After having established roughly the succession of

liquid crystalline phases from the penetration scan, the transition compositions were determined by preparing samples of given concentrations (from 5 to 95 wt % with 5 wt % intervals, so that the accuracy of the resulting diagrams was of about  $\pm 2.5\%$ ). Samples of 100 mg or more were prepared in glass tubes which were then sealed with a gas burner placed in a water bath at 80 °C for 2 h and were then centrifuged at 2500 rpm for 1 h at room temperature for homogenization. The rate used during the heating sequence was typically  $5$  °C $\cdot\text{min}^{-1}$ . The type of the phase was investigated by the birefringence of the mixture, and the texture was given by the liquid crystal type.

**Small Angle X-ray Scattering (SAXS) Experiments.** SAXS measurements using Mo radiation ( $\lambda = 0.71$  Å) were performed on a bench built by XENOCOS. The scattered beam was recorded using a large online scanner detector (diameter: 345 mm, from MAR Research). A large  $Q$  range ( $2.10^{-2}$ – $2.5$  Å $^{-1}$ ) was covered with an off-center detection. Preanalysis of data was performed using FIT2D software. The scattered intensities are expressed versus the magnitude of scattering vector  $Q = [(4\pi/\lambda) \sin(\theta/2)]$ , where  $\lambda$  is the wavelength of incident radiation and  $\theta$  the scattering angle. 2 mm quartz capillaries were used as sample containers for dilute and fluid solutions, i.e., isotropic micellar solutions. Usual corrections for background (empty cell and detector noise) subtractions and intensity normalization using Lupolen as a standard were applied. For the study of highly viscous lyotropic phases, a special home designed cell was used.

**Fish Diagrams.** Ternary amphiphile/oil/water systems were prepared in 2 mL test tubes with the studied compound and chosen oil. Equal amounts (in weight) of water and oil were first introduced, and increasing amounts of amphiphiles were added. After each addition, the test tubes were gently mixed and placed at 25 °C until the attainment of equilibrium, which generally required ca. 4 h for  $[\text{DiC}_8][\text{X}]$  and ca. 6 h for  $[\text{DiC}_{10}][\text{X}]$ . The types of Winsor systems (I–IV) were determined by visual observation.

## ASSOCIATED CONTENT

### Supporting Information

Experimental data and procedures. This material is available free of charge via the Internet at <http://pubs.acs.org>.

## AUTHOR INFORMATION

### Corresponding Authors

\*E-mail: pierre.bauduin@cea.fr.

\*E-mail: veronique.rataj@univ-lille1.fr. Phone: +33 (0)3-20-33-63-69.

### Notes

The authors declare no competing financial interest.

## ACKNOWLEDGMENTS

We are grateful to the Fonds Européens de Développement Régional (FEDER) and to the ANR (Project ANR-10-CD2I-01) for financial support.

## REFERENCES

- (1) Chantelle, M. B.; Lynne, A. O.; Wentz, M. Property Modifications of Finished Textiles by a Cationic Surfactant. *J. Am. Oil Chem. Soc.* 1990, 67, 689–697.
- (2) Ducker, W. A.; Pashley, R. M.; Ninham, B. W. The Flotation of Quartz Using a Double-chained Cationic Surfactant. *J. Colloid Interface Sci.* 1989, 128, 66–75.



- (3) Martins, L. M. S.; Mamizuka, E. M.; Carmona-Ribeiro, A. M. Cationic Vesicles as Bactericides. *Langmuir* 1997, 13, 5583–5587.
- (4) Campanha, M. T. N.; Mamizuka, E. M.; Carmona-Ribeiro, A. M. Interactions Between Cationic Vesicles and *Candida Albicans*. *J. Phys. Chem. B* 2001, 105, 8230–8236.
- (5) Hac-Wydro, K.; Wydro, P.; Dynarowicz-Latka, P. Interactions Between Dialkyldimethylammonium Bromides (DXDAB) and Sterols: A Monolayer Study. *J. Colloid Interface Sci.* 2005, 286, 504–510.
- (6) Liang, C.-H.; Chou, T.-H. Effect of Chain Length on Physicochemical Properties and Cytotoxicity of Cationic Vesicles Composed of Phosphatidylcholines and Dialkyldimethylammonium Bromides. *Chem. Phys. Lipids* 2009, 158, 81–90.
- (7) Puchta, R. Cationic Surfactants in Laundry Detergents and Laundry After treatment Aids. *J. Am. Oil Chem. Soc.* 1984, 61, 367–376.
- (8) Zhang, L.; Sun, X.; Song, Y.; Jiang, X.; Dong, S.; Wang, E. Didodecyldimethylammonium Bromide Lipid Bilayer-protected Gold Nanoparticles: Synthesis, Characterization, and Self-assembly. *Langmuir* 2006, 22, 2838–2843.
- (9) Gregory, G. W.; Sen, R.; Evans, D. F.; Trend, J. E. Microemulsion Formation and Phase Behavior of Dialkyldimethylammonium Bromide Surfactants. *J. Phys. Chem.* 1988, 92, 774–783.
- (10) Tucker, I.; Penfold, J.; Thomas, R. K.; Tildesley, D. J. Interplay between the Surface Adsorption and Solution-Phase Behavior in Dialkyl Chain Cationic-Nonionic Surfactant Mixtures. *Langmuir* 2009, 25, 3924–3931.
- (11) Reck, R. A.; Harwood, H. J.; Ralston, A. W. Solubilities of Dodecyl- and Octadecyl-Trimethyl-Ammonium Chlorides in Organic Solvents. *J. Org. Chem.* 1947, 12, 517–521.
- (12) Blum, F. D.; Pickup, S.; Ninham, B.; Chen, S. J.; Evans, D. F. Structure and Dynamics in Three-Component Microemulsions. *J. Phys. Chem.* 1985, 89, 711–713.
- (13) Kunieda, H.; Shinoda, K. Solution Behavior of Dialkyldimethylammonium Chloride in Water. Basic Properties of Antistatic Fabric Softeners. *J. Phys. Chem.* 1978, 82, 1710–1714.
- (14) Fontell, K.; Ceglie, A.; Lindman, B. Some Observations on Phase Diagrams and Structure in Binary and Ternary Systems of didodecyldimethylammonium Bromide. *Acta Chem. Scand., Ser. A* 1986, 40, 247–256.
- (15) Lianos, P.; Lang, J.; Zana, R. Fluorescence Probe Study of the Effect of Concentration on the State of Aggregation of Dodecylalkyldimethylammonium Bromides and Dialkyldimethylammonium Chlorides in Aqueous Solution. *J. Colloid Interface Sci.* 1983, 91, 276–279.
- (16) Warnheim, T.; Jonsson, A.; Sjöberg, M. Phase Diagrams for Cationic Surfactants in Polar Systems. *Prog. Colloid Polym. Sci.* 1990, 82, 271–279.
- (17) Khan, A.; Kang, C. Self-Assembly in Systems of Didodecyldimethylammonium Surfactants: Binary and Ternary Phase Equilibria and Phase Structures with Sulphate, Hydroxide, Acetate, and Chloride Counterions. *J. Colloid Interface Sci.* 1993, 156, 218–228.
- (18) Feitosa, E.; Jansson, J.; Lindman, B. The Effect of Chain Length on the Melting Temperature and Size of Dialkyldimethylammonium Bromide Vesicles. *Chem. Phys. Lipids* 2006, 142, 128–132.
- (19) Binks, B. P.; Espert, A.; Fletcher, P. D.; Soubiran, L. Phase Behaviour of Microemulsions Stabilised by Double Chain Cationic Surfactants and Alcohol Co-surfactants. *Colloids Surf., A* 2003, 212, 135–145.
- (20) Ralston, A. W.; Eggengerber, D. N.; Du Brow, P. L. Conductivities of Quaternary Ammonium Chlorides Containing Two Long-chain Alkyl Groups. *J. Am. Chem. Soc.* 1948, 70, 977–979.
- (21) Lang, J. Ultrasonic Relaxation and Carbon-13 NMR Studies of Dialkyldimethylammonium Chloride. Micelles. *J. Phys. Chem.* 1982, 86, 992–998.
- (22) Svitova, T. F.; Smirnova, Y. P.; Pisarev, S. A.; Berezina, N. A. Self-assembly in Double-tailed Surfactants in Dilute Aqueous Solutions. *Colloids Surf., A* 1995, 98, 107–115.
- (23) Hiramatsu, K.; Kameyama, K.; Ishiguro, R.; Mori, M.; Hayase, H. Properties of Dilute Aqueous Solutions of Double-Chain Surfactants, Alkyldodecyldimethylammonium Bromides with a Change in the Length of the Alkyl Chains. *Bull. Chem. Soc. Jpn.* 2003, 76, 1903–1910.
- (24) Nardello-Rataj, V.; Caron, L.; Borde, C.; Aubry, J. M. Oxidation in Three-liquid-phase Microemulsion Systems Using “Balanced Catalytic Surfactants”. *J. Am. Chem. Soc.* 2008, 130, 14914–14915.
- (25) Fressancourt-Collinet, M.; Hong, B.; Leclercq, L.; Alsters, P. L.; Aubry, J. M.; Nardello-Rataj, V. Acidic Three-Liquid-Phase Microemulsion Systems Based on Balanced Catalytic Surfactant for Epoxidation and Sulfide Oxidation under Mild Conditions. *Adv. Synth. Catal.* 2013, 355, 409–420.
- (26) Leclercq, L.; Nardello-Rataj, V.; Turmine, M.; Azaroual, N.; Aubry, J.-M. Stepwise Aggregation of Dimethyl-di-n-octylammonium Chloride in Aqueous Solutions: From Dimers to Vesicles. *Langmuir* 2010, 26, 1716–1723.
- (27) Collinet-Fressancourt, M.; Leclercq, L.; Bauduin, P.; Aubry, J. M.; Nardello-Rataj, V. Counter Anion Effect on the Self-Aggregation of Dimethyl-di-N-octylammonium Cation: A Dual Behavior between Hydrotropes and Surfactants. *J. Phys. Chem. B* 2011, 115, 11619–11630.
- (28) Stubenrauch, C. *Microemulsions: Background, New Concepts, Applications, Perspectives*, 1st ed.; Wiley-Blackwell publishing: Oxford, U.K., 2009; pp 92–101.
- (29) del Burgo, P.; Aicart, E.; Junquera, E. Mixed Vesicles and Mixed Micelles of the Cationic–Cationic Surfactant System: Didecyl-dimethylammonium Bromide/ Dodecylethyldimethylammonium Bromide/ Water. *Colloids Surf., A* 2007, 292, 165–172.
- (30) Chandler, D. Interfaces and the Driving Force of Hydrophobic Assembly. *Nature* 2005, 437, 640–647.
- (31) Tanford, C. *The hydrophobic Effect: Formation of Micelles and Biological Membranes*; John Wiley & Sons Inc.: New York, 1973.
- (32) Lindman, B.; Kamenka, N.; Puyal, M. C.; Brun, B.; Jonsson, B. Tracer Self-Diffusion Studies of Micelle Formation of a Short-Chain Ionic Surfactant, Sodium *n*-Octanoate. *J. Phys. Chem.* 1984, 88, 53–57.
- (33) Khan, A.; Mendonca, C. Solution Properties of a Short Double-Chain Cationic Surfactant System: Hexylammonium Hexanoate. *J. Colloid Interface Sci.* 1995, 169, 60–64.
- (34) Popova, M. V.; Tchernyshev, Y. S.; Michel, D. NMR Investigation of the Short-Chain Ionic Surfactant-Water Systems. *Langmuir* 2004, 20, 632–636.
- (35) Bauduin, P.; Renoncourt, A.; Kopft, A.; Touraud, K. D.; Kunz, W. Unified Concept of Solubilization in Water by Hydrotropes and Cosolvents. *Langmuir* 2005, 21, 6769–6775.
- (36) Israelachvili, J. N. *Intermolecular and Surface Forces*, 2nd ed.; Academic Press: San Diego, CA, 1992.
- (37) Kanei, N.; Tamura, Y.; Kuneida, H. Effect of Types of Perfume Compounds on the Hydrophile-Lipophile Balance Temperature. *J. Colloid Interface Sci.* 1999, 218, 13–22.
- (38) Bouton, F.; Durand, M.; Nardello-Rataj, V.; Borosy, A.; Quillet, C.; Aubry, J. M. A QSPR Model for the Prediction of the “Fish-Tail” Temperature of C<sub>12</sub>E<sub>4</sub>/Water/Polar Hydrocarbon Oil Systems. *Langmuir* 2010, 26, 7962–7970.
- (39) Testard, F.; Zemb, T. Excess of Solubilization and Curvature in Nonionic Microemulsions. *Colloids Surf., A* 1999, 219, 11–19.
- (40) Gruen, D. W. R. A Model for the Chains in Amphiphilic Aggregates. 1. Comparison with a Molecular Dynamics Simulation of a Bilayer. *J. Phys. Chem.* 1985, 89, 146–153.
- (41) McGrath, K. M. Phase Behavior of Dodecyltrimethylammonium Bromide Mixtures. *Langmuir* 1995, 11, 1835–1839.
- (42) Dubois, M.; Zemb, T. Phase Behavior and Scattering of Double-Chain Surfactants in Diluted Aqueous Solutions. *Langmuir* 1991, 7, 1352–1360.
- (43) Porod, G.; Glatter, O.; Kratky, O. *Small angle X-ray scattering*; Academic Press Inc: London, 1982.
- (44) Auvray, X.; Petipas, C.; Dupuy, C.; Louvet, S.; Anthore, R.; Rico-Lattes, A.; Lattes, I. Small-angle X-ray Diffraction Study of the Thermotropic and Lyotropic Phases of Five Alkyl Cyclic and Acyclic Disaccharides: Influence of the Linkage Between the Hydrophilic and Hydrophobic Moieties. *Eur. Phys. J. E* 2001, 4, 489–504.

- (45) Angelov, B.; Angelova, A.; Vainio, U.; Garamus, V. M.; Lesieur, S.; Willumeit, R.; Couvreur, P. Lon-living Intermediates During a Lamellar to a Diamond-cubic Lipid Phase Transition: a Small-angle X-ray Scattering Investigation. *Langmuir* 2009, 25, 3734–3742.
- (46) Ricoul, F.; Dubois, M.; Zemb, T.; Heck, M. P.; Vandais, A.; Plusquellec, D.; Rico-Lattes, I.; Diat, O. An Efficient Method to Determine Isothermal Ternary Phase Diagrams Using SAXS. *J. Phys. Chem. B* 1998, 102, 2769–2775.
- (47) Kelman, M.; Lavrentovich, O. D. *Soft Matter Physics: An Introduction*; Springer-Verlag Inc.: New York, 2003.
- (48) Coppola, L.; Muzzalupo, R.; Ranieri, G. A.; Terenzi, M. Characterization of the Lamellar Phase Aerosol OT/Tracer. System by NMR Diffusion Measurements. *Langmuir* 1995, 11, 1116–1121.
- (49) Bergenstfahl, B.; Fontell, K. Phase Equilibria in the System Soybean Lecithin/Water. *Prog. Colloid Polym. Sci.* 1983, 68, 48–52.
- (50) Andersson, S.; Hyde, S. T.; Larsson, K.; Lidin, S. Minimal Surfaces and Structures: From Inorganic and Metal Crystals to Cell Membranes and Biopolymers. *Chem. Rev.* 1988, 88, 221–242.
- (51) Larsson, K.; Tiberg, F. Periodic Minimal Surface Structures in Bicontinuous Lipid–Water Phases and Nanoparticles. *Curr. Opin. Colloid Interface Sci.* 2005, 9, 365–369.
- (52) Impéror-Clerc, M. Geometry of Interfaces: Topological Complexity in Biology and Materials. *Interface Focus* 2012, 2, S29–S38.
- (53) Seddon, J. M.; Hogan, J. L.; Warrender, N. A.; Pebay-Peyroula, E. Structural Studies of Phospholipid Cubic Phases. *Prog. Colloid Polym. Sci.* 1990, 81, 189–197.
- (54) Guldbbrand, L.; Joensson, B.; Wennerstroem, H.; Linse, P. Electrical Double-layer Forces: A Monte Carlo Study. *J. Chem. Phys.* 1984, 80, 2221–2228.
- (55) Holmberg, K., et al., Eds. *Handbook of applied surface and colloid chemistry*, Vol. 1; Wiley: Chichester, 2002.
- (56) Fontell, K.; Khan, A.; Lindström, B.; Maciejewska, D.; Puang-Ngern, S. Phase Equilibria and Structures in Ternary Systems of a Cationic Surfactant ( $C_{16}TABr$  or  $(C_{16}TA)_2SO_4$ ), Alcohol, and Water. *Colloid Polym. Sci.* 1991, 269, 727–742.
- (57) Marcus, Y. *Ion properties*; Marcel Dekker Inc.: New York, Basel, 1997.
- (58) Kahlweit, M. Microemulsions. *Science* 1988, 240 (4852), 617–621.
- (59) Marquez, N.; Anton, R. E.; Graciaa, A.; Lachaise, J.; Salager, J. L. Partitioning of Ethoxylated Alkylphenol Surfactants in Microemulsion-oil-water Systems. *Colloids Surf., A* 1995, 100, 225–231.
- (60) Bourrel, M.; Schechter, R. S. *Microemulsions and Related Systems*; Marcel Dekker: New York, 1988.
- (61) Wade, W. H.; Morgan, J. C.; Jacobson, J. K.; Schechter, R. S. Low Interfacial Tensions Involving Mixtures of Surfactants. *Soc. Pet. Eng. J.* 1977, 17, 122–128.
- (62) Queste, S.; Salager, J. L.; Strey, R.; Aubry, J. M. The EACN Scale for Oil Classification Revisited Thanks to Fish Diagrams. *J. Colloid Interface Sci.* 2007, 312, 98–107.
- (63) Kunieda, H.; Miyajima, A. The Effect of the Mixing of Oils on the Hydrophile-Lipophile-Balanced (HLB) Temperature in a Water/nonionic Surfactant/oil System. *J. Colloid Interface Sci.* 1989, 128, 605–607.
- (64) Bouton, F.; Durand, M.; Nardello-Rataj, V.; Serry, M.; Aubry, J. M. Classification of Terpene Oils Using the Fish Diagrams and the Equivalent Alkane Carbon (EACN) Scale. *Colloids Surf., A* 2009, 338, 142–147.
- (65) Ontiveros, J. F.; Pierlot, C.; Catte, M.; Molinier, V.; Pizzino, A.; Salager, J. L.; Aubry, J. M. Classification of Ester Oils According to Their Equivalent Alkane Carbon Number (EACN) and Asymmetry of Fish Diagrams of  $C_{10}E_4$ /ester oil/water Systems. *J. Colloid Interface Sci.* 2013, 403, 67–76.
- (66) Wormuth, K. R.; Kaler, E. W. Microemulsifying Polar Oils. *J. Phys. Chem.* 1989, 93, 4855–4861.
- (67) Queste, S. Classement absolu des huiles et des amphiphiles par la méthode de la formulation optimale. Université Lille1, France, 2006.
- (68) Marquez, N.; Graciaa, A.; Lachaise, J.; Salager, J. L. Partitioning of Ethoxylated Alkylphenol Surfactants in Microemulsion–Oil–Water Systems: Influence of Physicochemical Formulation Variables. *Langmuir* 2002, 18, 6021–6024.
- (69) Kunz, W. *Specific Ion Effects*; World Scientific Publishing: Singapore, 2010.
- (70) Leontidis, E. Hofmeister Anion Effects on Surfactant Self-assembly and the Formation of Mesoporous Solids. *Curr. Opin. Colloid Interface Sci.* 2002, 7, 81–91.
- (71) Collins, K. D.; Washabaugh, M. W. The Hofmeister Effect and the Behaviour of Water at Interfaces. *Q. Rev. Biophys.* 1985, 18, 323–422.
- (72) Koehler, R. D.; Schubert, K. V.; Strey, R.; Kaler, E. W. The Lifshitz Line in Binary Systems: Structures in Water/ $C_4E_1$  Mixtures. *J. Chem. Phys.* 1994, 101, 10843–10849.
- (73) D'Arrigo, G.; Giordano, R.; Teixeira, J. Small-angle Neutron Scattering Studies of Aqueous Solutions of Short-chain Amphiphiles. *Eur. Phys. J.* 2003, 10, 135–142.
- (74) Lawrence, A. S. C. In *Liquid Crystals*, Vol. 1; Brown, G. H., Ed.; Gordon & Breach: London, 1969; p 1.
- (75) Lawrence, A. *Surface Activity and Detergency*; Marcel Dekker: New York, 1961.
- (76) Rosevear, F. B. The Microscopy of the Liquid Crystalline Neat and Middle Phases of Soaps and Synthetic Detergents. *J. Am. Oil Chem. Soc.* 1954, 31, 628–639.